

# Advances

## in Clinical and Experimental Medicine

MONTHLY ISSN 1899-5276 (PRINT) ISSN 2451-2680 (ONLINE)

[advances.umw.edu.pl](http://advances.umw.edu.pl)

2024, Vol. 33, No. 8 (August)

Impact Factor (IF) – 2.1  
Ministry of Science and Higher Education – 70 pts  
Index Copernicus (ICV) – 161.11 pts



WROCLAW  
MEDICAL UNIVERSITY

Advances  
in Clinical and Experimental  
Medicine



# Advances in Clinical and Experimental Medicine

ISSN 1899-5276 (PRINT)

ISSN 2451-2680 (ONLINE)

advances.umw.edu.pl

**MONTHLY 2024**  
**Vol. 33, No. 8**  
**(August)**

Advances in Clinical and Experimental Medicine (*Adv Clin Exp Med*) publishes high-quality original articles, research-in-progress, research letters and systematic reviews and meta-analyses of recognized scientists that deal with all clinical and experimental medicine.

## Editorial Office

ul. Marcinkowskiego 2–6  
50-368 Wrocław, Poland  
Tel.: +48 71 784 12 05  
E-mail: redakcja@umw.edu.pl

## Editor-in-Chief

Prof. Donata Kurpas

## Deputy Editor

Prof. Wojciech Kosmala

## Managing Editor

Marek Misiak, MA

## Statistical Editors

Wojciech Bombała, MSc

Łucja Janek, MSc

Anna Kopszak, MSc

Dr. Krzysztof Kujawa

Jakub Wronowicz, MSc

## Manuscript editing

Marek Misiak, MA

Paulina Piątkowska, MA

## Publisher

Wrocław Medical University  
Wybrzeże L. Pasteura 1  
50-367 Wrocław, Poland

Online edition is the original version  
of the journal

## Scientific Committee

Prof. Sandra Maria Barbalho

Prof. Antonio Cano

Prof. Chong Chen

Prof. Breno Diniz

Prof. Erwan Donal

Prof. Chris Fox

Prof. Yuko Hakamata

Prof. Carol Holland

Prof. Sabine Bährer-Kohler

Prof. Markku Kurkinen

Prof. Christos Lionis

Prof. Raimundo Mateos

Prof. Zbigniew W. Raś

Prof. Jerzy W. Rozenblit

Prof. Silvina Santana

Prof. Sajee Sattayut

Prof. James Sharman

Prof. Jamil Shibli

Prof. Michał J. Toborek

Prof. László Vécsei

Prof. Cristiana Vitale

Prof. Hao Zhang

## Section Editors

### Basic Sciences

Prof. Iwona Bil-Lula

Prof. Bartosz Kempisty

Dr. Wiesława Kranc

Dr. Anna Lebedeva

### Clinical Anatomy, Legal Medicine, Innovative Technologies

Prof. Rafael Boscolo-Berto

### Dentistry

Prof. Marzena Dominiak

Prof. Tomasz Gedrange

Prof. Jamil Shibli

### Laser Dentistry

Assoc. Prof. Kinga Grzech-Leśniak

### Dermatology

Prof. Jacek Szepietowski

### Emergency Medicine, Innovative Technologies

Prof. Jacek Smereka

### Gynecology and Obstetrics

Prof. Olimpia Sipak-Szmigiel

### Histology and Embryology

Dr. Mateusz Olbromski

### Internal Medicine

#### Angiology

Dr. Angelika Chachaj

#### Cardiology

Prof. Wojciech Kosmala

Dr. Daniel Morris

#### Endocrinology

Prof. Marek Bolanowski

#### Gastroenterology

Assoc. Prof. Katarzyna Neubauer

### Hematology

Prof. Andrzej Deptała  
Prof. Dariusz Wołowicz

### Nephrology and Transplantology

Prof. Mirosław Banasik  
Prof. Krzysztof Letachowicz

### Pulmonology

Prof. Anna Brzecka

### Microbiology

Prof. Marzenna Bartoszewicz  
Assoc. Prof. Adam Junka

### Molecular Biology

Dr. Monika Bielecka

### Neurology

Assoc. Prof. Magdalena Koszewicz  
Assoc. Prof. Anna Pokryszko-Dragan  
Dr. Masaru Tanaka

### Neuroscience

Dr. Simone Battaglia  
Dr. Francesco Di Gregorio

### Oncology

Prof. Andrzej Deptała  
Prof. Adam Maciejczyk  
Prof. Hao Zhang

### Gynecological Oncology

Dr. Marcin Jędryka

### Ophthalmology

Dr. Małgorzata Gajdzis

### Orthopedics

Prof. Paweł Reichert

### Otolaryngology

Assoc. Prof. Tomasz Zatoński

### Pediatrics

### Pediatrics, Metabolic Pediatrics, Clinical Genetics, Neonatology, Rare Disorders

Prof. Robert Śmigiel

### Pediatric Nephrology

Prof. Katarzyna Kiliś-Pstrusińska

### Pediatric Oncology and Hematology

Assoc. Prof. Marek Ussowicz

### Pharmaceutical Sciences

Assoc. Prof. Marta Kepinska  
Prof. Adam Matkowski

### Pharmacoeconomics, Rheumatology

Dr. Sylwia Szafraniec-Buryło

### Psychiatry

Dr. Melike Küçükkarapınar  
Prof. Jerzy Leszek  
Assoc. Prof. Bartłomiej Stańczykiewicz

### Public Health

Prof. Monika Sawhney  
Prof. Izabella Uchmanowicz

### Qualitative Studies, Quality of Care

Prof. Ludmiła Marcinowicz

### Radiology

Prof. Marek Szaśniadek

### Rehabilitation

Dr. Elżbieta Rajkowska-Labon

### Surgery

Assoc. Prof. Mariusz Chabowski  
Assoc. Prof. Mirosław Kozłowski  
Prof. Renata Taboła

### Telemedicine, Geriatrics, Multimorbidity

Assoc. Prof. Maria Magdalena  
Bujnowska-Fedak

## Editorial Policy

Advances in Clinical and Experimental Medicine (Adv Clin Exp Med) is an independent multidisciplinary forum for exchange of scientific and clinical information, publishing original research and news encompassing all aspects of medicine, including molecular biology, biochemistry, genetics, biotechnology and other areas. During the review process, the Editorial Board conforms to the "Uniform Requirements for Manuscripts Submitted to Biomedical Journals: Writing and Editing for Biomedical Publication" approved by the International Committee of Medical Journal Editors ([www.ICMJE.org](http://www.ICMJE.org)). The journal publishes (in English only) original papers and reviews. Short works considered original, novel and significant are given priority. Experimental studies must include a statement that the experimental protocol and informed consent procedure were in compliance with the Helsinki Convention and were approved by an ethics committee.

For all subscription-related queries please contact our Editorial Office: [redakcja@umw.edu.pl](mailto:redakcja@umw.edu.pl)  
For more information visit the journal's website: [advances.umw.edu.pl](http://advances.umw.edu.pl)

Pursuant to the ordinance of the Rector of Wrocław Medical University No. 37/XVI R/2024, from March 1, 2024, authors are required to pay a fee for each manuscript accepted for publication in the journal Advances in Clinical and Experimental Medicine. The fee amounts to 1600 EUR for all types of papers.

Advances in Clinical and Experimental Medicine has received financial support from the resources of Ministry of Science and Higher Education within the "Social Responsibility of Science – Support for Academic Publishing" project based on agreement No. RCN/SP/0584/2021.



Ministry of Education and Science  
Republic of Poland

Czasopismo Advances in Clinical and Experimental Medicine korzysta ze wsparcia finansowego ze środków Ministerstwa Edukacji i Nauki w ramach programu „Społeczna Odpowiedzialność Nauki – Rozwój Czasopism Naukowych” na podstawie umowy nr RCN/SP/0584/2021.



Ministerstwo  
Edukacji i Nauki

Indexed in: MEDLINE, Science Citation Index Expanded, Journal Citation Reports/Science Edition, Scopus, EMBASE/Excerpta Medica, Ulrich's™ International Periodicals Directory, Index Copernicus

Typographic design: Piotr Gil, Monika Kołęda

DTP: Wydawnictwo UMW

Cover: Monika Kołęda

Printing and binding: PRINT PROFIT Sp. z o.o., Koźmin 27, 59-900 Zgorzelec

## Contents

### Editorials

- 767 Paolo Iovino, Izabella Uchmanowicz, Ercole Vellone  
**Self-care: An effective strategy to manage chronic diseases**

### Original papers

- 773 Veysel Tahiroğlu, Elif Uğur, Erkam Coşkun, Naci Ömer Alayunt, Gülşah Zorgör  
**Protective role of BDNF in Alzheimer's disease pathophysiology and its correlation with new biomarkers: Can the role of BDNF be re-discussed?**
- 781 Anna Wędrychowicz, Teresa Grzelak, Alicja Pietraszek, Maria Skrzyszowska, Mari Minasjan, Jerzy B. Starzyk  
**Affected brother as the highest risk factor of type 1 diabetes development in children and adolescents: One center data before implementing type 1 diabetes national screening**
- 791 Turan Poyraz, Özgül Vupa Çilengiroğlu  
**Blood biomarkers in acute ischemic stroke: The prognostic value of neutrophil-to-lymphocyte ratio and mean platelet volume**
- 805 Hasan Yasar, Durdu Altuner, Seval Bulut, Betül Cicek, Cebrail Gursul, Mehmet Kuzucu, Halis Suleyman  
**Taxifolin as a novel therapeutic agent for epileptic seizures induced by caffeine-induced oxidative stress in rats**
- 817 Jie Hu, Yan Zhou, Junhao Wang, Jianpeng Han, Jianyong Feng, Wenbin Chen, Kuo Guo, Yongzhang Li  
**Dihydroartemisinin ameliorated the inflammatory response and regulated miRNA-mRNA expression profile of chronic nonbacterial prostatitis**
- 831 Xueli Zhang, Xiaoyi Qin  
**CTRP3/AMPK pathway plays a key role in the anti-hypertrophic effects of cyanidin-3-O-glucoside by inhibiting the inflammatory response**
- 843 Guofu Zheng, Qingsong Jiang, Cai Jiang, Xingxin Zhu, Yongjie Wang  
**Identification and verification on prognostic index of glioblastoma immune-related lncRNAs**
- 857 Jiaqi Fan, Jianhong Liao, Yuwen Huang  
**Combined bioinformatics and machine learning methodologies reveal prognosis-related ceRNA network and propose ABCA8, CAT, and CXCL12 as independent protective factors against osteosarcoma**

### Reviews

- 869 Reem Hamoud Alrashoudi  
**Unleashing the power of anti-CD20 immunotherapy: Mitigating multiple sclerosis risk in Epstein–Barr virus latent infections**
- 881 Adam Bębenek, Bartosz Godlewski  
**Anterior cervical discectomy and fusion (ACDF) with and without plating: A comparison of radiological and clinical outcomes**

### Research letters

- 889 Li Deng, Bishun Deng, Ziling Zhao, Huijie Huang, Xiaowan Wang, Ruimin Tian, Guohua Li, Enyu Liang, Anping Peng, Peifeng Ke, Peng Xu, Min He  
**Expansion of T follicular helper cells is associated with disease progression in rat experimental membranous nephropathy model**



# Self-care: An effective strategy to manage chronic diseases

Paolo Iovino<sup>1,A,D,F</sup>, Izabella Uchmanowicz<sup>2,D–F</sup>, Ercole Vellone<sup>2,3,D–F</sup>

<sup>1</sup> Department of Health Sciences, University of Florence, Italy

<sup>2</sup> Department of Nursing and Obstetrics, Faculty of Health Sciences, Wrocław Medical University, Poland

<sup>3</sup> Department of Biomedicine and Prevention, Tor Vergata University of Rome, Italy

A – research concept and design; B – collection and/or assembly of data; C – data analysis and interpretation;

D – writing the article; E – critical revision of the article; F – final approval of the article

Advances in Clinical and Experimental Medicine, ISSN 1899–5276 (print), ISSN 2451–2680 (online)

*Adv Clin Exp Med.* 2024;33(8):767–771

## Address for correspondence

Izabella Uchmanowicz

E-mail: [izabella.uchmanowicz@umw.edu.pl](mailto:izabella.uchmanowicz@umw.edu.pl)

## Funding sources

None declared

## Conflict of interest

None declared

Received on February 25, 2024

Reviewed on May 12, 2024

Accepted on July 11, 2024

Published online on August 28, 2024

## Abstract

The increase in life expectancy and an aging demographic have led to a surge in chronic diseases, presenting substantial challenges to healthcare systems worldwide. Chronic conditions are characterized by their long-term nature, recurrence and incurability, necessitating effective management strategies. This paper aims to explore the concept of self-care as a pivotal element in chronic disease management, examining its evolution, components and the role of caregivers in facilitating self-care practices. It also seeks to review the development of instruments for measuring self-care and discuss recent experimental research on self-care interventions. Self-care is an essential strategy for managing chronic diseases, involving maintenance, monitoring and management practices influenced by various personal and environmental factors. Caregivers play a vital role in supporting self-care, especially within certain cultural contexts. The development of reliable and valid instruments to measure self-care is crucial for assessing the effectiveness of the interventions. Recent trials, such as those focusing on motivational interviewing and virtual reality, show promise in improving self-care behaviors and patient outcomes. This paper advocates for the design of tailored, evidence-based interventions and highlights the potential of artificial intelligence in advancing self-care research. Future studies should continue to explore the dyadic dynamics between patients and caregivers and include economic evaluations to inform clinical decision-making.

**Key words:** chronic diseases, self-care, Orem concept

## Cite as

Iovino P, Uchmanowicz I, Vellone E. Self-care: An effective strategy to manage chronic diseases. *Adv Clin Exp Med.* 2024;33(8):767–771. doi:10.17219/acem/191102

## DOI

10.17219/acem/191102

## Copyright

Copyright by Author(s)

This is an article distributed under the terms of the Creative Commons Attribution 3.0 Unported (CC BY 3.0) (<https://creativecommons.org/licenses/by/3.0/>)

## Introduction

With the increase in life expectancy and the aging of the population, we are facing a worrying increase in the number of people affected by chronic diseases. Currently, there is no uniform definition of chronic diseases, but the general literature agrees that they share the characteristics of incurability, persistence, recurrence, and duration in terms of months or years.<sup>1</sup> Cardiovascular and respiratory diseases, diabetes mellitus and cancer are examples of the major and common chronic diseases highly prevalent in Western countries.<sup>2</sup>

The harmful effects of chronic diseases are well known to health scientists thanks to the numerous qualitative and quantitative research papers published in the field. These long-term conditions have a significant impact on all aspects of the lives of those affected. For example, chronically ill patients often suffer from physical disability, pain, distress, depression, and a poor quality of life,<sup>3–5</sup> which inevitably leads to an increase in healthcare utilization and mortality.<sup>6,7</sup> This is the reason why, over the years, self-care has become so important in the management of chronic diseases.

## What is self-care?

Traditionally outlined in *Nursing* by Orem in 1959,<sup>8</sup> the concept of self-care has been expanded over the years, as a result of the shift from the traditional medical model to multidimensional patient-centered care. In 1979, Levin defined self-care as a broader process in which people take responsibility for health promotion, disease prevention and treatment.<sup>9</sup> An even more complete definition was given by the World Health Organization (WHO) in 2013, where self-care was defined as “the ability of individuals, families and communities to promote health, prevent disease, maintain health, and to cope with illness and disability with or without the support of a healthcare provider”.<sup>10</sup>

The authors of this editorial have adopted the definition of self-care derived from the Middle-Range Theory of Self-Care of Chronic Illness, in which it is “a process of maintaining health through health-promoting practices and managing illness”.<sup>11</sup> In this theory, self-care includes the 3 main concepts of self-care maintenance, self-care monitoring and self-care management. Self-care maintenance is a group of behaviors that patients with chronic conditions engage in to promote wellbeing and control their physical and emotional stability. Some examples include medication adherence, healthy eating and physical activity. Self-care monitoring refers to observing signs and symptoms of the disease, e.g., routinely measuring blood pressure or blood sugar. Self-care management refers to the behaviors that are put into practice whenever signs and symptoms of illness occur, such as consulting a healthcare provider or taking medication in cases of pain. The process of self-care requires making complex cognitive decisions and can

be influenced by a number of factors related to knowledge, self-efficacy, functional and cognitive skills, cultural beliefs, support from others, and access to care.<sup>11</sup>

## The role of caregivers in self-care

Many patients affected by chronic diseases face difficulties in performing self-care, particularly if they are older or belong to a culture that prioritizes familial ties over individualism. In this particular context, the caregiving role is essential. Caregivers are defined as those individuals within the family or friends’ network who assume most of the responsibility for providing informal care to their loved ones. This type of care can be measured using specific tools designed in the format of a traditional questionnaire, where caregivers are asked to self-report on the frequency with which they support or substitute the patients in carrying out specific self-care tasks.

The first instrument to measure caregiver contribution to self-care was developed for heart failure,<sup>12</sup> but over the years, other instruments have been developed for general chronic conditions,<sup>13</sup> pulmonary diseases<sup>14</sup> and ostomies.<sup>15</sup> Investigators are also developing instruments to measure caregiver contribution to self-care in diabetes, cancers, inflammatory bowel diseases, and strokes. A caregiver’s contribution to self-care was conceived with the identical 3 core concepts of (caregiver contribution to) self-care maintenance, self-care monitoring and self-care management, and numerous investigators have utilized this instrument as a landmark to develop their specific caregiver contribution instruments.

The items of the caregiver contribution to self-care measure the same aspects of self-care behaviors (e.g., physical activity), but the wording has been changed to be completed by caregivers. For example, while the item of the patient version of the instrument asks how often they have performed physical activity, in the caregiver version, they are asked how often they have recommended the patient to perform physical activity.

Regular assessment of caregiving contribution is particularly important in the context of chronic diseases. Caregivers often experience significant physical, emotional, social, and financial challenges while taking care of these patients. Scheduling periodic screenings can identify caregivers at risk and provide them with information and education, which are known to increase caregiving competence and promote wellbeing.<sup>16</sup>

## Dyadic approaches to study self-care

The possibility of measuring patient self-care and caregiver contributions to self-care has stimulated researchers to investigate the self-care process using a dyadic approach.



This is because patients are uniquely linked to their caregivers, and caregivers are also dependent on the patient's behaviors and attitudes. In the context of a chronic illness, these 2 members approach the health problem as a unit and become an interdependent team, making illness management a dyadic phenomenon.<sup>17</sup>

The existence of the dyad in the self-care process implies that patients and caregivers influence each other. This violates the assumption of statistical independence because their scores in the questionnaires are likely to be correlated. Adopting a dyadic approach in self-care research implies that the variables of both members are used in the models. For example, if we want to understand whether depression affects the patients' self-care behavior, one would be tempted to build a regression model with only patient-level variables (i.e., patient depression and self-care). However, according to the theory of dyadic illness management, patient self-care may be influenced not only by their levels of depression (actor effect) but also by the caregivers' level of depression (partner effect). This relationship can be bidirectional, i.e., depressed caregivers can provide poor contributions to self-care as a result of their own mental state (actor effect), and that of the patients (partner effect). These partner effects should be taken into account to avoid inaccurate test statistics and the inflation or absence of statistical significance of the hypothesized relationships.

The actor-partner interdependence model (APIM) is widely utilized for analyzing dyadic data in the social and health sciences. This statistical framework allows for the estimation of both actor and partner effects, enabling the investigation of various processes occurring within the members of the dyad. Notable contributions to the field of self-care research can be found in the work by Iovino et al.,<sup>18</sup> who explored the dyadic predictors of self-care in individuals with multiple chronic conditions. These findings revealed that caregivers, in comparison to other groups, were more inclined to provide support to patients who had a higher formal education. Additionally, it was observed that patients were more likely to engage in health-promoting behaviors when cared for by female caregivers. Iovino et al.<sup>19</sup> studied dyad members in the context of ostomy care; their findings revealed that, compared to the others, caregivers of more depressed patients were more likely to stimulate the health-promoting activities of their partners. Additionally, patients with more depressed caregivers were less likely to take action in case of signs and symptoms occurrence. For interested readers, all the contributions to self-care instruments can be viewed on the following website: <https://self-care-measures.com>.

## How to measure self-care

The authors of this editorial have devoted consistent efforts to the development and validation of theory-based instruments for measuring self-care in chronic illnesses.

These measures, which are based on the middle-range theory of self-care in chronic illness, can be condition-specific, such as the Self-Care of Heart Failure Index (SCHFI)<sup>20</sup> or the Self-Care of Diabetes Inventory (SCODI),<sup>21</sup> or generic, such as the Self-Care of Chronic Illness Inventory (SC-CII).<sup>22</sup> For interested readers, all the self-care instruments can be viewed on <https://self-care-measures.com>.

Self-care is, by definition, an ensemble of complex behaviors. Therefore, to measure this construct, the instruments must assess a wide range of behaviors. An important structural characteristic of these instruments is the formulation of their questions on a 5-point Likert scale. This format is important because it helps researchers and clinicians measure how often a behavior is performed in a given period. As in this case, Likert scales measure behaviors with greater precision and nuance than simple “yes” or “no” questions. For example, the reader can come up with a question to measure medication adherence. One instrument may ask patients whether they take prescribed medicines without missing a dose, with a “yes” or “no” response, and another asks how often or routinely they take the medicines. In the latter case, of course, the patient has the opportunity to give a more specific and precise answer.

Another requirement of self-care measures (and indeed for any other instrument) is that they must be psychometrically valid and reliable and adapted to the patient's cultural context.<sup>23</sup> This aspect is not surprising, considering that, as mentioned above, self-care behaviors are highly sensitive to the cultural context. It may be that a certain behavior is never performed or not performed as often as in other countries. For example, De Maria et al.<sup>24</sup> conducted a cross-cultural validity study of the Self-Care of Chronic Illness Inventory across Italian, Swedish and American patients, and found that people in the USA used comparatively higher scores when answering the items related to physical activity and diet. This is an example of bias that must be recognized when validating a scale, as scores on the scales can be seriously inflated when different types of populations are compared. Therefore, when there is a knowledge gap, validation of an instrument in specific countries and languages is mandatory before administration.

## Trials on self-care

Compared to the last decade, where the main efforts were to understand the deficits in self-care and its risk factors in chronically ill populations, we have recently approached the so-called experimental phase. This phase is about gathering evidence for the effectiveness of self-care interventions. One of these trials is the MOTIVATE-HF study, in which an intervention based on motivational interviewing demonstrated significant improvement in self-care maintenance behaviors, physical symptoms, quality of life, and mortality in patients with heart failure.<sup>25–28</sup>

A more recent study in the same population (the REMO-TIVATE-HF trial) is currently ongoing, in which a similar but more intensive intervention is being implemented remotely via video calls.<sup>29</sup> Other ongoing trials are looking at the effectiveness of virtual reality on rehabilitation adherence in patients with heart failure<sup>30</sup> and educational interventions for patients with ostomies.<sup>31</sup>

## Future trends for the study of self-care


We believe that the future of self-care sciences will be devoted to the design of interventions that could be highly effective for a number of important outcomes, including the quality of life of patients and their caregivers. To accomplish this, evidence is still needed to understand the power of specific behavior-change techniques; moreover, further studies should be invested in designing interventions that would adapt to the patients' and caregivers' needs. In this regard, it is important to highlight that certain populations face important barriers that impede their access to self-care interventions.<sup>32,33</sup> Such barriers include inherent beliefs (e.g., lack of trust in healthcare providers), psychosocial conditions (e.g., homelessness, poverty, loneliness, and migration), and structural barriers (excessive distance from the healthcare setting and a lack of transportation). Consequently, the focus of research will inevitably shift from individuals with high and medium socioeconomic status to individuals in disadvantaged and underserved communities.<sup>32</sup> The involvement of clinicians, researchers and policymakers is crucial in determining how these programs can be customized for disadvantaged people, whether they could help reduce the inequities, and ultimately improve their wellbeing. To accomplish this, a thorough multidimensional assessment of the patient-caregiver background is necessary to pinpoint contextual factors that may impede access and effectiveness of self-care interventions.<sup>32</sup>

We also foresee a step further to the evidence extracted from trials by including economic evaluations. With such information, we will help clinicians make more informed decisions about which types of interventions should be adopted to care for their patients.

An important role will be taken using artificial intelligence (AI) to study self-care. Artificial intelligence could be used to collect and analyze data collected by patients or by wearable devices and sensors, or it could be used to study how patients report their experience with chronic diseases on social media.<sup>34</sup> So far, there is evidence that AI-driven approaches offer substantial benefits in terms of higher frequency and duration of lifestyle choices, as well as decreased utilization of healthcare services.<sup>35</sup> Future studies could be performed by testing AI-powered chatbots, which can provide patients with personalized and motivated self-care guidance. Artificial

intelligence algorithms can also predict potential challenges patients may face in managing specific self-care behaviors (e.g., exercise). These are the only examples in which AI can be used. Other forthcoming trends will undoubtedly be the study of patient-caregiver dyads and, specifically, how their coactive relationship during the disease process could be mutually beneficial for both members.

### ORCID iDs

Paolo Iovino  <https://orcid.org/0000-0001-5952-881X>

Izabella Uchmanowicz  <https://orcid.org/0000-0001-5452-0210>

Ercle Vellone  <https://orcid.org/0000-0003-4673-7473>

### References

1. Goodman RA, Posner SF, Huang ES, Parekh AK, Koh HK. Defining and measuring chronic conditions: Imperatives for research, policy, program, and practice. *Prev Chronic Dis*. 2013;10:120239. doi:10.5888/pcd10.120239
2. Kopp W. How Western diet and lifestyle drive the pandemic of obesity and civilization diseases. *Diabetes Metab Syndr Obes*. 2019;12:2221–2236. doi:10.2147/DMSO.S216791
3. Siboni F, Alimoradi Z, Atashi V, Alipour M, Khatooni M. Quality of life in different chronic diseases and its related factors. *Int J Prev Med*. 2019;10(1):65. doi:10.4103/ijpvm.IJPVM\_429\_17
4. Chou CY, Chiu CJ, Chang CM, et al. Disease-related disability burden: A comparison of seven chronic conditions in middle-aged and older adults. *BMC Geriatr*. 2021;21(1):201. doi:10.1186/s12877-021-02137-6
5. Ma Y, Xiang Q, Yan C, Liao H, Wang J. Relationship between chronic diseases and depression: The mediating effect of pain. *BMC Psychiatry*. 2021;21(1):436. doi:10.1186/s12888-021-03428-3
6. Kim KY, Lee E, Cho J. Factors affecting healthcare utilization among patients with single and multiple chronic diseases. *Int J Public Health*. 2020;49(12):2367–2375. doi:10.18502/ijph.v49i12.4820
7. Martín-Lesende I, Recalde E, Viviane-Wunderling P, et al. Mortality in a cohort of complex patients with chronic illnesses and multimorbidity: A descriptive longitudinal study. *BMC Palliat Care*. 2016; 15(1):42. doi:10.1186/s12904-016-0111-x
8. Orem DE. *Guides for Developing Curricula for the Education of Practical Nurses*. Washington, D.C, USA: Department of Health, Education (DHEW), and Welfare, Office of Education; 1959:176. <https://files.eric.ed.gov/fulltext/ED013305.pdf>.
9. Levin LS. Self-care: New challenge to individual health. *J Am Coll Health Assoc*. 1979;28(2):117–120. doi:10.1080/01644300.1979.10392909
10. World Health Organization (WHO). *Economic and Financing Considerations of Self-Care Interventions for Sexual and Reproductive Health and Rights*. United Nations University Centre for Policy Research, 2–3 April 2019, New York, USA: Summary Report. New York, USA: World Health Organization (WHO); 2020:28. <https://iris.who.int/bitstream/handle/10665/331195/WHO-SRH-20.2-eng.pdf?sequence=1>.
11. Riegel B, Jaarsma T, Strömberg A. A middle-range theory of self-care of chronic illness. *Adv Nurs Sci*. 2012;35(3):194–204. doi:10.1097/ANS.0b013e318261b1ba
12. Vellone E, Barbaranelli C, Pucciarelli G, Zeffiro V, Alvaro R, Riegel B. Validity and reliability of the Caregiver Contribution to Self-Care of Heart Failure Index Version 2. *J Cardiovasc Nurs*. 2020;35(3):280–290. doi:10.1097/JCN.0000000000000655
13. Vellone E, Lorini S, Ausili D, et al. Psychometric characteristics of the caregiver contribution to self-care of chronic illness inventory. *J Adv Nurs*. 2020;76(9):2434–2445. doi:10.1111/jan.14448
14. Matarese M, Pondoni R, Ausili D, Vellone E, De Maria M. Validity and reliability of Caregiver Contribution to Self-Care of Chronic Obstructive Pulmonary Disease Inventory and Caregiver Self-Efficacy in Contributing to Self-Care Scale. *Eval Health Prof*. 2023;46(3):255–269. doi:10.1177/01632787221134712
15. Villa G, Vellone E, Sciarra S, et al. Two new tools for self-care in ostomy patients and their informal caregivers: Psychosocial, clinical, and operative aspects. *Int J Urol Nurs*. 2019;13(1):23–30. doi:10.1111/ijun.12177

16. Corry M, While A, Neenan K, Smith V. A systematic review of systematic reviews on interventions for caregivers of people with chronic conditions. *J Adv Nurs*. 2015;71(4):718–734. doi:10.1111/jan.12523
17. Lyons KS, Lee CS. The theory of dyadic illness management. *J Fam Nurs*. 2018;24(1):8–28. doi:10.1177/1074840717745669
18. Iovino P, Lyons KS, De Maria M, et al. Patient and caregiver contributions to self-care in multiple chronic conditions: A multilevel modelling analysis. *Int J Nurs Stud*. 2021;116:103574. doi:10.1016/j.ijnurstu.2020.103574
19. Iovino P, De Maria M, Corvese F, et al. The influence of patient and caregiver depression on patient self-care and caregiver contribution to self-care in ostomy: A dyadic analysis. *J Clin Nurs*. 2023;32(17–18):6441–6449. doi:10.1111/jocn.16676
20. Riegel B, Barbaranelli C, Carlson B, et al. Psychometric testing of the Revised Self-Care of Heart Failure Index. *J Cardiovasc Nurs*. 2019;34(2):183–192. doi:10.1097/JCN.0000000000000543
21. Ausili D, Barbaranelli C, Rossi E, et al. Development and psychometric testing of a theory-based tool to measure self-care in diabetes patients: The Self-Care of Diabetes Inventory. *BMC Endocr Disord*. 2017;17(1):66. doi:10.1186/s12902-017-0218-y
22. Riegel B, Barbaranelli C, Sethares KA, et al. Development and initial testing of the self-care of chronic illness inventory. *J Adv Nurs*. 2018;74(10):2465–2476. doi:10.1111/jan.13775
23. Matarese M, Barbaranelli C, Riegel B. Advancing knowledge of self-care instruments. *Heart Lung*. 2022;52:198–199. doi:10.1016/j.hrtlng.2021.12.002
24. De Maria M, Matarese M, Strömberg A, et al. Cross-cultural assessment of the Self-Care of Chronic Illness Inventory: A psychometric evaluation. *Int J Nurs Stud*. 2021;116:103422. doi:10.1016/j.ijnurstu.2019.103422
25. Iovino P, Rebora P, Occhino G, et al. Effectiveness of motivational interviewing on health-service use and mortality: A secondary outcome analysis of the MOTIVATE-HF trial. *ESC Heart Fail*. 2021;8(4):2920–2927. doi:10.1002/ehf2.13373
26. Caggianelli G, Iovino P, Rebora P, et al. A motivational interviewing intervention improves physical symptoms in patients with heart failure: A secondary outcome analysis of the Motivate-HF Randomized Controlled Trial. *J Pain Symptom Manage*. 2022;63(2):221–229.e1. doi:10.1016/j.jpainsymman.2021.09.006
27. Vellone E, Rebora P, Ausili D, et al. Motivational interviewing to improve self-care in heart failure patients (MOTIVATE-HF): A randomized controlled trial. *ESC Heart Fail*. 2020;7(3):1309–1318. doi:10.1002/ehf2.12733
28. Rebora P, Spedale V, Occhino G, et al. Effectiveness of motivational interviewing on anxiety, depression, sleep quality and quality of life in heart failure patients: Secondary analysis of the MOTIVATE-HF randomized controlled trial. *Qual Life Res*. 2021;30(7):1939–1949. doi:10.1007/s11136-021-02788-3
29. Vellone E, Rebora P, Iovino P, et al. Remote motivational interviewing to improve patient self-care and caregiver contribution to self-care in heart failure (REMOTIVATE-HF): Rationale, design, and methodology for a multicentre randomized controlled trial. *Res Nurs Health*. 2023;46(2):190–202. doi:10.1002/nur.22289
30. Micheluzzi V, Casu G, Sanna GD, et al. Improving adherence to rehabilitation for heart failure patients through immersive virtual reality (VIRTUAL-HF): A protocol for a randomized controlled trial. *Cont Clin Trials*. 2024;138:107463. doi:10.1016/j.cct.2024.107463
31. Iovino P, Vellone E, Campoli A, et al. Telehealth vs in-person education for enhancing self-care of ostomy patients (Self-Stoma): Protocol for a noninferiority, randomized, open-label, controlled trial. *PLoS ONE*. 2024;19(6):e0303015. doi:10.1371/journal.pone.0303015
32. World Health Organization (WHO). *WHO Guideline on Self-Care Interventions for Health and Well-Being, 2022 Revision: Executive Summary*. Geneva, Switzerland: World Health Organization (WHO); 2022:22. <https://iris.who.int/bitstream/handle/10665/357179/9789240052239-eng.pdf?sequence=1>.
33. Hopkins J, Narasimhan M. Access to self-care interventions can improve health outcomes for people experiencing homelessness. *BMJ*. 2022;376:e068700. doi:10.1136/bmj-2021-068700
34. Moscato S, Orlandi S, Di Gregorio F, et al. Feasibility interventional study investigating PAIN in neurorehabilitation through wearable SensorS (PAINLESS): A study protocol. *BMJ Open*. 2023;13(11):e073534. doi:10.1136/bmjopen-2023-073534
35. Ngiam KY, Khor IW. Big data and machine learning algorithms for health-care delivery. *Lancet Oncol*. 2019;20(5):e262–e273. doi:10.1016/S1470-2045(19)30149-4



# Protective role of BDNF in Alzheimer's disease pathophysiology and its correlation with new biomarkers: Can the role of BDNF be re-discussed?

Veysel Tahiroğlu<sup>1,A,C-F</sup>, Elif Uğur<sup>2,B-D,F</sup>, Erkam Coşkun<sup>3,C-F</sup>, Naci Ömer Alayunt<sup>4,A,D-F</sup>, Gülşah Zorgör<sup>2,B-F</sup>

<sup>1</sup> Department of Nursing, Faculty of Health Sciences, Şırnak University, Turkey

<sup>2</sup> Neurology Outpatient Clinic, Şırnak State Hospital, Turkey

<sup>3</sup> Clinic of Medical Biochemistry, Şırnak State Hospital, Turkey

<sup>4</sup> Department of Medical Biochemistry, Faculty of Medicine, Siirt University, Turkey

A – research concept and design; B – collection and/or assembly of data; C – data analysis and interpretation;

D – writing the article; E – critical revision of the article; F – final approval of the article

Advances in Clinical and Experimental Medicine, ISSN 1899–5276 (print), ISSN 2451–2680 (online)

*Adv Clin Exp Med.* 2024;33(8):773–779

## Address for correspondence

Veysel Tahiroğlu

E-mail: veysel.tahiroglu@sirnak.edu.tr

## Funding sources

This work was financially supported by Şırnak University Scientific Research Projects Coordination Unit (BAP); Project No. 2022.FNAP. 18.03.01.

## Conflict of interest

None declared

Received on July 11, 2023

Reviewed on August 21, 2023

Accepted on September 8, 2023

Published online on December 6, 2023

## Abstract

**Background.** The pathophysiology of Alzheimer's disease (AD) is not fully understood and that new biomarkers for the condition should be presented.

**Objectives.** Our study aimed to determine the blood levels of some biochemical molecules and peptide proteins in AD, which is accepted as the most common cause of dementia in the world, and to elucidate the relationship between them.

**Materials and methods.** The study consisted of 2 groups: 40 newly diagnosed AD patients and 40 healthy individuals. Plasma levels between the 2 groups and the correlation between them were statistically analyzed.

**Results.** The median brain-derived neurotrophic factor (BDNF) level in the AD group was found to be higher and statistically significant compared to the control group ( $p = 0.033$ ).

**Conclusions.** According to our literature review, this is the first article in which these molecules have been studied together in AD patients. In this study, we revealed the importance of these parameters and especially the instrumental role of BDNF in the form and function of the brain in AD patients. Interestingly, in the patient group, all parameters in our study showed a positive and significant positive relationship with one another ( $p < 0.001$ ).

**Key words:** BDNF, Alzheimer's disease, correlation, biomarkers

## Cite as

Tahiroğlu V, Uğur E, Coşkun E, Alayunt NÖ, Zorgör G.

Protective role of BDNF in Alzheimer's disease pathophysiology and its correlation with new biomarkers:

Can the role of BDNF be re-discussed? *Adv Clin Exp Med.*

2024;33(8):773–779. doi:10.17219/acem/172012

## DOI

10.17219/acem/172012

## Copyright

Copyright by Author(s)

This is an article distributed under the terms of the Creative Commons Attribution 3.0 Unported (CC BY 3.0)

(<https://creativecommons.org/licenses/by/3.0/>)

## Background

Alzheimer's disease (AD) is a chronic, progressive neurodegenerative disease characterized by cognitive impairment. It is the most common form of dementia in the elderly population, and its impact is increasing worldwide. Over 47 million people are thought to be affected by AD globally.<sup>1–3</sup> Age is the leading risk factor and research has shown that people over 60 are more likely to develop AD.<sup>4</sup> The primary pathology of AD consists of amyloid-(A) deposition and neurofibrillary tangles of hyperphosphorylated tau.<sup>5</sup> Moreover, it is believed that neuroinflammation, microglial activation, oxidative stress, lack of metabolic energy, and neuronal death are all intimately linked to the pathogenesis of AD.<sup>6</sup> Synaptic dysfunction and degeneration have recently been discovered to be more significantly linked to cognitive impairments than plaques or nodes.<sup>7</sup> Therefore, it has become essential to investigate various novel compounds that can serve as biomarkers for the pathophysiology of AD. Enzyme structure (spermidine synthase and agmatinase), factor structure such as brain-derived neurotrophic factor (BDNF), vascular endothelial growth factor (VEGF) and coagulation factor V (fV), and hormone structure such as heptapeptide angiotensin 1–7 (Ang-(1–7)) and peptide proteins (neurokinin B and amyloid A) may be effective biomarkers in the early diagnosis of AD. As we look at these molecules, we can see that spermidine impacts neuronal excitability, particularly ion channels, and is included in a number of processes in the mammalian nervous system. It has also been linked to better memory function in older people at risk for AD who take spermidine supplements. Spermidine may impair memory function in older people, although the precise methods by which it does are unclear.<sup>8,9</sup> L-arginine generated by arginine decarboxylase is decarboxylated to yield agmatine. The mammalian brain is predicted to use agmatine as a neuromodulator, but it has been reported that its functional importance and the mechanisms of A $\beta$ -stimulated changes in agmatine metabolism remain unclear. This is because A $\beta$  interacts with multiple receptors to participate in a variety of neuronal functions.<sup>10,11</sup> The plasticity of neurons is dependent on BDNF. It is well known that the cortex, hypothalamus and hippocampus are among the brain regions where it is significantly expressed. In the hippocampus, BDNF specifically helps support the long-term potentiation of glutamatergic neurons. As a result, it aids the long-term memory storage process and is known to promote dendritic cell development and remodeling in response to altered neuronal activity.<sup>12</sup> Coagulation factor V, unlike most other coagulation factors, is not enzymatically active but acts as a cofactor. It is known to shed light on the molecular mechanisms responsible for its physiological and pathological properties.<sup>13</sup> The vascular and neurological systems are supported by the intricate signaling molecule – VEGF. The AD neuropathological symptoms have been linked to impaired hippocampus volume and cognition, and have

previously been documented to have a positive relationship with VEGF in cerebrospinal fluid (CSF).<sup>14</sup> A recently discovered axis of the brain's renin–angiotensin system is the Ang-(1–7) axis. Angiotensin 1–7 is a heptapeptide that is created from Ang II by ACE2 and acts favorably by attaching to the MAS1 receptor. According to reports, Ang-(1–7) impacts the plasma levels of AD patients, and an Ang-(1–7) deficiency may contribute to the pathogenesis of AD.<sup>15,16</sup> Neurokinin B is a 10-residue neuropeptide containing histidine. It has been reported that neurokinin peptides have different potentials in many neurodegenerative diseases, especially in AD, and that the neuroprotective agent neurokinin B can shield neurons against the toxicity of A $\beta$  peptides. The mechanisms by which neurokinin B affects the inhibition of A $\beta$  aggregation are still unknown.<sup>17,18</sup> Amyloid A is actively included in the pathological processes of rheumatoid arthritis, cancer, atherosclerosis, and AD by its collection. The apolipoprotein family includes the highly conserved protein amyloid A, which is mostly produced by the liver. Its role in the pathophysiology of AD is still debated.<sup>19</sup> In this study, BDNF has attracted the most attention due to its potential therapeutic value and possible role in the development of neurological and psychiatric disorders, such as protein synthesis, axonal growth, dendritic cell formation, and synaptic plasticity, which are critical for learning.<sup>20</sup> In the definition of BDNF-related metabolic processes, the determination and comparison of some parameters were important in the evaluation of AD levels.

## Objectives

This research aims to elucidate the relationship between AD patients and various molecules (spermidine synthase, agmatinase, BDNF, coagulation fV, VEGF, Ang (1–7), neurokinin B, and amyloid A). It is also aimed to reconsider the role of BDNF.

## Materials and methods

### Study design

This research was conducted in line with the recommendations of the Declaration of Helsinki. The Siirt University Non-Interventional Clinical Research Ethics Committee approval was obtained before the study commencement (approval No. 2022/04.06 issued on May 30, 2022). A total of 80 people participated in this study. The study's patient group comprised 40 newly diagnosed volunteer patients with AD and a control group of 40 volunteers without AD or other neurological diseases. The diagnosis was made by neurologists working in the neurology outpatient clinics of the Şırnak State Hospital (Turkey). The Diagnostic and Statistical Manual of Mental Disorders-Fifth Edition (DSM-V) was used according to the criteria established

by the National Institute of Neurological and Communication Disorders and Stroke and the AD and Related Disorders Association (NINCDS-ADRDA).<sup>21,22</sup> For each patient to be involved in the study, the age range of 45–90 was chosen as the inclusion criterion. Those with neurological and/or psychiatric diseases other than AD, clinical depression, brain tumors, subdural hematomas, chronic alcoholism, cognitive impairment caused by heavy exercise, use of antioxidant supplements, and those who quit voluntarily were not included in the study. Informed consent was obtained from all individuals included in this study.

## Sample collection

After an overnight fast, fasting venous blood samples were taken from the participants voluntarily for the study, after an average of 10 h of fasting from the arm veins using tubes without anticoagulant (SST Vacusera, 5 mL, 235305; Disera A.Ş, İzmir, Turkey) and tubes with anticoagulant (K3 EDTA, 2 mL, 70697; sodium-citrate 3.2%, 2.7 mL; Ayset, Adana, Turkey). The tubes were gently inverted several times. Blood samples in tubes without anticoagulant and samples with sodium citrate were centrifuged at 4°C for 10 min at 4000 rpm. Complete blood count (XN 1000; Sysmex Company, Kobe, Japan), biochemical (c8000; Abbott, Abbott Park, USA) and hormonal assays (Roche Cobas 6000 c601; Roche Diagnostics, Mannheim, Germany) were carried out at Şırnak State Hospital Medical Biochemistry Laboratory. To measure the plasma levels of other molecules, the obtained plasma samples were divided into portions, placed in Eppendorf tubes and labeled. Prior to analysis, Eppendorf tubes were stored at –80°C.

## Measurement of plasma levels of molecules

The BDNF, neurokinin B, agmatinase, VEGF, spermidine synthase, Ang-(1–7), serum amyloid A, and coagulation fV levels were measured in the plasma samples using human enzyme-linked immunosorbent assay (ELISA) kits (catalog No. 201-12-1303, 201-12-8627, 201-12-) 3110, 201-12-0081, 201-12-4979, 201-12-2828, 201-12-1226, 201-12-6817; SunRed Biological Technology, Shanghai, China). Absorption was measured at 450 nm with ELISA microplate reader (Thermo Scientific Multiskan GO, SN: 1510-02723; Thermo Fisher Scientific, Waltham, USA) using an antibody-coated 96-well plate. Thermo Scientific Wellwash, SN:888-3023A (Thermo Fisher Scientific) was used as the automatic washer for plate washing. Intra-test

and inter-assay coefficient variables (%CV) in all kits were below 10%. All ELISA analyses for this research were done in the laboratory of the Siirt University Science and Technology Application and Research Center.

## Statistical analyses

IBM SPSS v. 21.0 (IBM Corp., Armonk, USA) was utilized for statistical analysis. Shapiro–Wilk and Kolmogorov–Smirnov tests and graphs were used to evaluate whether the data in all groups, including age, were normally distributed. According to Shapiro–Wilk and Kolmogorov–Smirnov tests, the data were not distributed normally. The normality results of the tables and graphs have been presented in the Supplementary material. The Mann–Whitney U test was employed to compare plasma median values between groups using non-normally distributed data. The scatterplots were inspected visually to check for monotonicity between the variables. Since there were monotonic relationships between the variables, Spearman's correlation analysis was employed to measure the strength of these relationships. Descriptive statistics were used for numerical variables, group median values, minimum and maximum values, and interquartile range (IQR) data. In addition, z-values and Mann–Whitney U and effect size values are presented in Table 1 and Table 2. A value of  $p < 0.05$  was considered significant.

## Results

A total of 80 people, 40 healthy controls (male/female ratio: 14/26) and 40 AD patients (male/female ratio: 15/25), participated in this study. The mean age of the patient group ( $79.88 \pm 7.57$  years) was found to be higher than of the control group ( $76.43 \pm 10.75$  years), but the difference between the groups was not statistically significant ( $p = 0.225$ ; Table 1). When the levels of BDNF, VEGF, spermidine synthase, Ang-(1–7), serum amyloid A, and coagulation fV were examined between the groups, increases were seen in the group with AD ( $1.67 \pm 0.50$  ng/mL,  $1290.38 \pm 472.51$  ng/L,  $22.59 \pm 8.38$  ng/mL,  $216.50 \pm 83.69$  ng/L,  $5.71 \pm 2.06$  µg/mL, and  $39.11 \pm 19.21$  ng/mL) compared to the control group ( $1.29 \pm 0.49$  ng/mL,  $1198.60 \pm 357.81$  ng/L,  $18.99 \pm 6.37$  ng/mL,  $176.19 \pm 47.31$  ng/L,  $5.32 \pm 1.89$  µg/mL, and  $31.94 \pm 7.26$  ng/mL),  $p = 0.033$  for BDNF,  $p = 0.613$  for VEGF,  $p = 0.073$  for spermidine synthase,  $p = 0.056$  for Ang-(1–7),  $p = 0.371$  for amyloid A, and  $p = 0.485$  for coagulation fV, neurokinin B and agmatinase decreased in the group with

Table 1. Age compared between groups

Variable	Control (n = 40)				AD patients (n = 40)				Z-value	p-value
	IQR	min	max	median	IQR	min	max	median		
Age [years]	15.25	49	89	79	15	65	90	79	–1.214	0.225

The comparison was made using the Mann–Whitney U test; IQR – interquartile range; Min – minimum; Max – maximum; AD – Alzheimer's disease.

**Table 2.** Plasma levels of molecules compared between groups

Variables	Control (n = 40)				AD patients (n = 40)				Z-value	Effect size	p-value
	IQR	min	max	median	IQR	min	max	median			
BDNF [ng/mL]	0.71	0.01	2.30	1.24	1.17	0.69	3.48	1.49	-2.132	0.058	0.033*
Neurokinin B [ng/L]	102	93.08	398.66	257.46	142	121.21	445.67	238.85	-0.427	0.002	0.669
Agmatinase [ng/mL]	4.86	6.19	22.11	11.83	6.42	4.58	23.26	10.76	-0.846	0.009	0.397
VEGF [ng/L]	593.19	245.11	1870.67	1158.39	692.79	475.72	2565.56	1126.30	-0.505	0.003	0.613
Spermidine synthase [ng/mL]	9.52	3.94	34.51	17.63	13.72	10.24	45.92	20.02	-1.791	0.041	0.073
Angiotensin 1-7 [ng/L]	62.29	75.85	282.89	173.77	126.18	97.48	443.16	191.84	-1.911	0.046	0.056
Serum amyloid A [ $\mu$ g/mL]	2.74	0.60	9.71	5.11	3.36	2.34	11.30	5.78	-0.894	0.010	0.371
Coagulation factor V [ng/mL]	11.23	20.00	52.18	31.30	29.32	11.01	77.62	31.51	-0.698	0.006	0.485

The comparison was made using the Mann-Whitney U test; IQR – interquartile range; Min – minimum; Max – maximum; BDNF – brain-derived neurotrophic factor; VEGF – vascular endothelial growth factor; \* statistically significant group; AD – Alzheimer's disease.

**Table 3.** Correlation analysis results of the control group

Variables	Neurokinin B [ng/L]	Agmatinase [ng/mL]	VEGF [ng/L]	Spermidine synthase [ng/mL]	Angiotensin 1-7 [ng/L]	Serum amyloid A [ $\mu$ g/mL]	Coagulation factor V [ng/mL]
BDNF (ng/mL)	r = 0.651** p < 0.001	r = 0.528** p < 0.001	r = 0.692** p < 0.001	r = 0.719** p < 0.001	r = 0.536** p < 0.001	r = 0.794** p < 0.001	r = 0.493** p = 0.001
Neurokinin B [ng/L]	–	r = 0.555** p < 0.001	r = 0.682** p < 0.001	r = 0.760** p < 0.001	r = 0.567** p < 0.001	r = 0.740** p < 0.001	r = 0.665** p < 0.001
Agmatinase [ng/mL]	–	–	r = 0.454** p = 0.003	r = 0.525** p < 0.001	r = 0.307 p = 0.054	r = 0.484** p = 0.002	r = 0.601** p < 0.001
VEGF [ng/L]	–	–	–	r = 0.746** p < 0.001	r = 0.611** p < 0.001	r = 0.809** p < 0.001	r = 0.567** p < 0.001
Spermidine synthase [ng/mL]	–	–	–	–	r = 0.617** p < 0.001	r = 0.742** p < 0.001	r = 0.683** p < 0.001
Angiotensin 1-7 [ng/L]	–	–	–	–	–	r = 0.587** p < 0.001	r = 0.435** p = 0.005
Serum amyloid A [ $\mu$ g/mL]	–	–	–	–	–	–	r = 0.548** p < 0.001

\*\*Correlation is significant at the 0.001 level (two-tailed); r – correlation coefficient; BDNF – brain-derived neurotrophic factor; VEGF – vascular endothelial growth factor.

AD compared with the control group (267.85  $\pm$  82.45 ng/L, 11.86  $\pm$  4.24 ng/mL), respectively (270.03  $\pm$  77.89 ng/L, 12.57  $\pm$  3.59) (neurokinin B, p = 0.669, for agmatinase p = 0.397). The increase in BDNF levels in the patient group was statistically significant (p = 0.033 for BDNF; Table 2). The control evaluation of the correlation is given in Table 3 and the patient evaluation is presented in Table 4. Interestingly, the parameters in the patient group showed a positive and significant relationship with each other (p < 0.001).

## Discussion

Health expenditures in the world and new medical treatments prolong life expectancy in old age and increase the share of the elderly population in the total population. The world's demographic is changing to include a larger elderly population. Alzheimer's disease is a chronic disease seen in advanced age, affecting millions of people worldwide, and is the most prevalent reason for primary neurodegenerative dementia. It progresses in stages in many

people who have not yet developed advanced dementia, and can reach a level that affects the daily life of the patient, with memory difficulties during the middle stage.<sup>23,24</sup> There is a need for strategies to combat this devastating disease, whose prevalence rises with age. Perhaps the most significant of these strategies is to detect AD as early as possible. The depicted pathological properties of AD are amyloid- $\beta$  (A $\beta$ ) and tau pathology.<sup>25</sup> It is a neurodegenerative, pathogenic and chronic disease of enzymes (spermidine synthase and agmatinase), factor structures (BDNF, coagulation fV, VEGF), peptide structures (neurokinin B, amyloid A), and hormone structure heptapeptide (Ang-(1-7)) proteins. We examined whether they could be effective biomarkers for the early diagnosis of AD. Interestingly, the parameters in the patient group in our study showed a positive and significant relationship with each other (p < 0.001, Table 4). The AD patient's brain tissue develops A $\beta$  oligomers, which have a direct effect on the disease's development. One of the primary causes of neurotoxicity, A $\beta$  oligomers, are known to produce intracellular Ca<sup>2+</sup> excess and neuronal death, both of which can be avoided



Table 4. Correlation analysis results of the patient group

Variables	Neurokinin B [ng/L]	Agmatinase [ng/mL]	VEGF [ng/L]	Spermidine synthase [ng/mL]	Angiotensin 1–7 [ng/L]	Serum amyloid A [μg/mL]	Coagulation factor V [ng/mL]
BDNF [ng/mL]	r = 0.749** p < 0.001	r = 0.800** p < 0.001	r = 0.717** p < 0.001	r = 0.771** p < 0.001	r = 0.720** p < 0.001	r = 0.683** p < 0.001	r = 0.622** p < 0.001
Neurokinin B [ng/L]	–	r = 0.788** p < 0.001	r = 0.840** p < 0.001	r = 0.778** p < 0.001	r = 0.645** p < 0.001	r = 0.678** p < 0.001	r = 0.589** p < 0.001
Agmatinase [ng/mL]	–	–	r = 0.830** p < 0.001	r = 0.838** p < 0.001	r = 0.643** p < 0.001	r = 0.746** p < 0.001	r = 0.610** p < 0.001
VEGF [ng/L]	–	–	–	r = 0.793** p < 0.001	r = 0.714** p < 0.001	r = 0.732** p < 0.001	r = 0.630** p < 0.001
Spermidine synthase [ng/mL]	–	–	–	–	r = 0.721** p < 0.001	r = 0.812** p < 0.001	r = 0.665** p < 0.001
Angiotensin 1–7 [ng/L]	–	–	–	–	–	r = 0.622** p < 0.001	r = 0.539** p < 0.001
Serum amyloid A [μg/mL]	–	–	–	–	–	–	r = 0.769** p < 0.001

\*\*Correlation is significant at the 0.001 level (two-tailed); r – correlation coefficient; BDNF – brain-derived neurotrophic factor; VEGF – vascular endothelial growth factor.

because of the action of N-methyl-D-aspartate (NMDA) receptor antagonists.<sup>26</sup> According to reports, Aβ oligomers rapidly activate NMDA receptors, and medications that inhibit the action of these receptors can stop Aβ from damaging neurons in AD.<sup>27</sup> Nitric oxide synthase (NOS), which helps to produce NO, is inhibited by polyamines such as agmatine and spermidine.<sup>26</sup> It has inhibitory effects on glutamatergic NMDA receptors in rat hippocampal neurons.<sup>27</sup> Nevertheless, it is uncertain where exactly NMDA receptor antagonist drugs interact.<sup>28</sup> From this perspective, it can be deduced that polyamines such as agmatine and spermidine, which are NMDA receptor antagonists, contribute to the pathogenesis of AD. According to our knowledge, the effect of polyamines such as agmatine and spermidine on NMDA receptor blockade in AD, which accumulates Aβ, has not yet been clarified in this mechanism in which agmatine synthase and spermidine synthase enzymes are directly involved. In our study, agmatinase enzyme levels were discovered to decrease in AD patients compared to controls. In AD, patients' spermidine synthase enzyme levels were higher than in the control group. A statistically significant decrease in agmatinase enzyme levels ( $p = 0.397$ ) and a rise in spermidine synthase enzyme levels ( $p = 0.073$ ) was observed; considering the short half-life in the metabolic pathway of agmatine degraded from L-arginine, the relationship between agmatine over-release or high agmatine concentrations and AD is related to the brain, CSF or AD. Agmatine levels in blood can be interpreted as affecting NMDA receptor blockade. The increase in spermidine synthase enzyme due to the spermidine step released from agmatine and ornithine may also be the source of NMDA receptor blockade. All these interpretations may explain the source of NMDA receptor blockade in the pathogenesis of AD by accumulated Aβ oligomers. Agmatine reduction, which was also observed in our AD study, can have negative consequences,

including depression-like symptoms, reduced cognitive abilities and memory loss. Agmatine's multi-receptor affinity and various physiological functions and its antagonism of NMDA receptors are significant in elucidating the pathogenesis of AD. Polyamine pathway and imidazoline receptor agents restoring BDNF in β-amyloid-induced AD provide insufficient information on how they affect BDNF levels in the hippocampus. The BDNF expression, which plays a significant role in neuronal development besides the pathogenesis of AD, is a matter of considerable interest in the brains of patients with AD. In our study, BDNF levels in AD patients were detected to be higher than in controls (Table 2). The BDNF, which exhibits a statistically significant rise in blood levels ( $p = 0.033$ ), is crucial to understand the pathophysiology of AD. According to one study, agmatine's antidepressant-like effects in AD are linked to decreased levels of pro-inflammatory cytokines (interleukin(IL)-6 and tumor necrosis factor alpha (TNF-α)) and elevated levels of BDNF in the hippocampus.<sup>29</sup> Studying the pathogenicity suggests that the VEGF system controls synapse function mechanisms which toxic soluble Aβ oligomers disrupt in the early stages of AD. Growing evidence suggests that Aβ targets excitatory synapses through a particular dendritic area and binds to a subset of neurons.<sup>30</sup> Because of the putative neuroprotective function of VEGF in AD, higher VEGF levels have been linked to reduced cognitive loss in studies employing AD biomarkers.<sup>31</sup> Compared to the control group, a drop was seen in our AD group, though this decrease was not statistically significant ( $p = 0.613$ ). Abnormal levels of VEGF have been associated with Aβ deposition in AD. One of the most studied receptors among neurokinin receptors is the neurokinin 1 receptor. We also included the neurokinin B parameter from the neuropeptide family, which we think provides protection against the neurotoxic processes of AD in multiple ways. In our study, a decrease

was observed in neurokinin B levels in the AD group compared to the control group, but this decrease was not statistically significant ( $p = 0.669$ ). We observed a slight, but not significant, decrease in the activity of neuropeptides and thus an increase in the metabolic half-life of the neurokinin 1 receptor substance. Neurokinin 1 receptor antagonists reduce the level of neurokinin 1 receptor substance in the cortex, hippocampus and striatum in AD and animal models where neuroinflammation-mediated changes in neural circuits were significant.<sup>32,33</sup>

One potential mechanism underpinning the pathogenesis of AD is potassium channel malfunction. The neuroprotective effects brought about by the neurokinin 1 receptor are mediated by a few voltage-gated potassium channels. Administration of neurokinin 1 receptors inhibits A $\beta$ -induced disturbance of cognitive functions by inhibiting A $\beta$ -induced upregulation of potassium channel subunits and A $\beta$ -type K<sup>+</sup> currents.<sup>34,35</sup> Serum amyloid A, the precursor protein synthesized in the liver, whose physiological role has not been fully elucidated, is an acute phase reactant whose blood level increases in response to various diseases. Inflammation in the brain in AD is demonstrated by the proteins involved in the complement cascade and the presence of  $\alpha$ -1-antichymotrypsin (ACT). However, although local inflammation is strongly involved in the pathogenesis of AD, studies that mention the presence of amyloid-A in the AD brain have not been found. In our study, there was an increase in serum amyloid-A levels in the AD group; however, it was not statistically significant ( $p = 0.371$ ). Large-scale studies are needed to explain this mechanism. A potential biomarker of AD is the Ang-(1–7) heptapeptide. Angiotensin 1–7 is said to be beneficial for facilitating neuronal functioning and reducing apoptosis in memory-related brain structures in AD patients.<sup>36</sup> In our study, Ang-(1–7) levels increased in the AD group compared to the control group, but this increase was not statistically significant ( $p = 0.056$ ). Therefore, evaluating these effects may be a promising strategy for the discovery of therapeutics or biomarkers for AD, as upregulation of these pathways is expected to have a significant effect on AD pathogenesis.<sup>37</sup>

In AD, BDNF levels tend to decrease in regions where memory and cognitive functions are regulated, especially in the hippocampus and cortex of nerve cells. This can lead to less exposure of nerve cells to BDNF, and thus a decrease in supporting factors important for cell survival, growth and communication. Decreased BDNF levels can contribute to nerve cell damage and death. Therefore, increasing or maintaining BDNF levels may be an important target for the treatment and prevention of AD. Research on this topic shows that strategies such as BDNF-boosting drugs or lifestyle changes can help reduce the effects of AD by increasing the survival and function of nerve cells. However, research in this area is still ongoing, and the exact mechanism of the BDNF effect on AD and its therapeutic potential need to be better understood. In our

study, we found a significant increase in BDNF profile. However, AD, which is a neurological disease, has been associated with low levels of BDNF. A systematic review and meta-analysis concluded that in 15 analyzed studies, 2067 AD patients had significantly lower serum BDNF levels than healthy controls.<sup>38</sup> While discussing the effects of all parameters that could be biomarkers in the AD pathophysiology, we noticed the increased levels of BDNF. The role of BDNF in relation to AD, which has not yet been fully elucidated, is important because of its effects on the pathophysiology of the disease and neuroplasticity. Due to the small number of study patients we cannot draw any definitive conclusions, but a larger-scale study may support our hypothesis in the future.

## Limitations

The limitation of this study is the small number of patients. Different results could be obtained if the study was conducted with a larger number of patients.

## Conclusions

We concluded that BDNF may be increased as a result of the effect of agmatine reduction on  $\beta$ -amyloid-induced AD in neuroinflammation by activating imidazoline receptors. Exactly how BDNF is effective in AD is not yet clear and research is ongoing. It is observed that the studies conducted in this area show promising results – the regulation of BDNF levels or drugs that interact with BDNF may have the potential to slow the progress of the disease. However, it is important to remember that AD is a complex condition, and a single molecule is not sufficient to cure the disease. Further studies and clinical trials can help develop potential new methods and drugs for the treatment of AD. Large-scale studies are needed to elucidate the mechanisms of this disease. While BDNF levels are observed to decrease in AD patients, we saw an interesting BDNF increase in our study. We think that the reason for this may be the high level of protein-containing nutrition in the region and the use of plant-based appetizers with meals that may have affected BDNF levels. Finally, we believe that experiments using AD models should use these parameters to clarify their function in disease identification and management.

## Supplementary data

The Supplementary materials are available at <https://doi.org/10.5281/zenodo.8406302>. The package comprises of the following files:

- Supplementary Table 1. Normality test results for age.
- Supplementary Table 2. Parameters normality test results.
- Supplementary Table 3. Control grubuna ait scatterplots.
- Supplementary Table 4. patient grubuna ait scatterplots.

## ORCID iDs

Veysel Tahiroğlu  <https://orcid.org/0000-0003-3516-5561>  
 Elif Uğur  <https://orcid.org/0000-0003-0006-850X>  
 Erkam Coşkun  <https://orcid.org/0000-0001-5471-8606>  
 Naci Ömer Alayunt  <https://orcid.org/0000-0003-2215-0934>  
 Gülşah Zоргör  <https://orcid.org/0000-0003-2071-5276>

## References

- Lane CA, Hardy J, Schott JM. Alzheimer's disease. *Eur J Neurol*. 2018; 25(1):59–70. doi:10.1111/ene.13439
- Dos Santos Picanco LC, Ozela PF, De Fatima De Brito Brito M, et al. Alzheimer's disease: A review from the pathophysiology to diagnosis, new perspectives for pharmacological treatment. *Curr Med Chem*. 2018;25(26):3141–3159. doi:10.2174/0929867323666161213101126
- Tanaka M, Török N, Vécsei L. Novel pharmaceutical approaches in dementia. In: Riederer P, Laux G, Nagatsu T, Le W, Riederer C, eds. *NeuroPsychopharmacotherapy*. Cham, Switzerland: Springer International Publishing; 2021:1–18. doi:10.1007/978-3-319-56015-1\_444-1
- Adali A, YiRün A, Koçer-Gümüşel B, Erkekoğlu P. Possible effects of biological agents on the development of Alzheimer's disease [in Turkish]. *Ankara Üniversitesi Eczacılık Fakültesi Dergisi*. 2020;44(1):167–187. doi:10.33483/jfpau.523804
- Rajmohan R, Reddy PH. Amyloid-beta and phosphorylated tau accumulations cause abnormalities at synapses of Alzheimer's disease neurons. *J Alzheimers Dis*. 2017;57(4):975–999. doi:10.3233/JAD-160612
- Jin Y, Sumsuzzman D, Choi J, Kang H, Lee SR, Hong Y. Molecular and functional interaction of the myokine irisin with physical exercise and Alzheimer's disease. *Molecules*. 2018;23(12):3229. doi:10.3390/molecules23123229
- Wang L; Alzheimer's Disease Neuroimaging Initiative. Association of cerebrospinal fluid Neurogranin with Alzheimer's disease. *Ageing Clin Exp Res*. 2019;31(2):185–191. doi:10.1007/s40520-018-0948-3
- Wirth M, Schwarz C, Benson G, et al. Effects of spermidine supplementation on cognition and biomarkers in older adults with subjective cognitive decline (SmartAge): Study protocol for a randomized controlled trial. *Alzheimers Res Ther*. 2019;11(1):36. doi:10.1186/s13195-019-0484-1
- Wright JW, Harding JW. Contributions by the brain renin-angiotensin system to memory, cognition, and Alzheimer's disease. *J Alzheimers Dis*. 2019;67(2):469–480. doi:10.3233/JAD-181035
- Dixit MP, Rahmatkar SN, Raut P, Umekar MJ, Taksande BG, Kotagale NR. Evidences for agmatine alterations in Aβ1-42induced memory impairment in mice. *Neurosci Lett*. 2021;740:135447. doi:10.1016/j.neulet.2020.135447
- Gül F, Pelit T, Terzioğlu B, Ekinci O, Gören M. Effects of agmatine on the survival rate in rats bled to hemorrhage. *Arzneimittelforschung*. 2011;61(4):229–233. doi:10.1055/s-0031-1296192
- Amidfar M, De Oliveira J, Kucharska E, Budni J, Kim YK. The role of CREB and BDNF in neurobiology and treatment of Alzheimer's disease. *Life Sci*. 2020;257:118020. doi:10.1016/j.lfs.2020.118020
- Duga S, Asselta R, Tenchini ML. Coagulation factor V. *Int J Biochem Cell Biol*. 2004;36(8):1393–1399. doi:10.1016/j.biocel.2003.08.002
- Tubi MA, Kothapalli D, Hapenny M, et al. Regional relationships between CSF VEGF levels and Alzheimer's disease brain biomarkers and cognition. *Neurobiol Aging*. 2021;105:241–251. doi:10.1016/j.neurobiolaging.2021.04.025
- Ribeiro VT, De Souza LC, Simões E Silva AC. Renin-angiotensin system and Alzheimer's disease pathophysiology: From the potential interactions to therapeutic perspectives. *Protein Pept Lett*. 2020;27(6):484–511. doi:10.2174/0929866527666191230103739
- Duan R, Wang SY, Wei B, et al. Angiotensin-(1–7) analogue AVE0991 modulates astrocyte-mediated neuroinflammation via lncRNA SNHG14/miR-223-3p/NLRP3 pathway and offers neuroprotection in a transgenic mouse model of Alzheimer's disease. *J Inflamm Res*. 2021;14:7007–7019. doi:10.2147/JIR.S343575
- Press-Sandler O, Miller Y. Assessments of the effect of neurokinin B on toxic Aβ aggregates in Alzheimer's disease with the molecular mechanisms' action. *ACS Chem Neurosci*. 2020;11(20):3418–3429. doi:10.1021/acchemneuro.0c00535
- Shahzad R, Jones MR, Viles JH, Jones CE. Endocytosis of the tachykinin neuropeptide, neurokinin B, in astrocytes and its role in cellular copper uptake. *J Inorg Biochem*. 2016;162:319–325. doi:10.1016/j.jinorgbio.2016.02.027
- Maszota-Zieleniak M, Danielsson A, Samsonov SA. The potential role of glycosaminoglycans in serum amyloid A fibril formation by in silico approaches. *Matrix Biol Plus*. 2021;12:100080. doi:10.1016/j.mbplus.2021.100080
- Numakawa T, Odaka H, Adachi N. Actions of brain-derived neurotrophin factor in the neurogenesis and neuronal function, and its involvement in the pathophysiology of brain diseases. *Int J Mol Sci*. 2018;19(11):3650. doi:10.3390/ijms19113650
- Black DW, Grant JE. *DSM-5 Guidebook: The Essential Companion to the Diagnostic and Statistical Manual of Mental Disorders, Fifth Edition*. Washington, DC, USA: American Psychiatric Publishing; 2014. ISBN:978-1-58562-465-2.
- McKhann GM, Knopman DS, Chertkow H, et al. The diagnosis of dementia due to Alzheimer's disease: Recommendations from the National Institute on Aging-Alzheimer's Association workgroups on diagnostic guidelines for Alzheimer's disease. *Alzheimers Dement*. 2011;7(3):263–269. doi:10.1016/j.jalz.2011.03.005
- Cummings JL, Benson DF. *Dementia: A Clinical Approach*. 2<sup>nd</sup> ed. Boston, USA: Butterworth-Heinemann; 1992. ISBN:978-0-7506-9065-2.
- Gurvit H, Emre M, Tinaz S, et al. The prevalence of dementia in an urban Turkish population. *Am J Alzheimers Dis Other Demen*. 2008; 23(1):67–76. doi:10.1177/1533317507310570
- Texidó L, Martín-Satué M, Alberdi E, Solsona C, Matute C. Amyloid β peptide oligomers directly activate NMDA receptors. *Cell Calcium*. 2011;49(3):184–190. doi:10.1016/j.ceca.2011.02.001
- Galea E, Regunathan S, Eliopoulos V, Feinstein DL, Reis DJ. Inhibition of mammalian nitric oxide synthases by agmatine, an endogenous polyamine formed by decarboxylation of arginine. *Biochem J*. 1996;316(1):247–249. doi:10.1042/bj3160247
- Yang XC, Reis DJ. Agmatine selectively blocks the N-methyl-D-aspartate subclass of glutamate receptor channels in rat hippocampal neurons. *J Pharmacol Exp Ther*. 1999;288(2):544–549. PMID:9918557.
- Gibson DA, Harris BR, Rogers DT, Littleton JM. Radioligand binding studies reveal agmatine is a more selective antagonist for a polyamine-site on the NMDA receptor than arcaine or ifenprodil. *Brain Res*. 2002;952(1):71–77. doi:10.1016/S0006-8993(02)03198-0
- Kotagale N, Deshmukh R, Dixit M, Fating R, Umekar M, Taksande B. Agmatine ameliorates manifestation of depression-like behavior and hippocampal neuroinflammation in mouse model of Alzheimer's disease. *Brain Res Bull*. 2020;160:56–64. doi:10.1016/j.brainresbull.2020.04.013
- Lacor PN, Buniel MC, Chang L, et al. Synaptic targeting by Alzheimer's-related amyloid β oligomers. *J Neurosci*. 2004;24(45):10191–10200. doi:10.1523/JNEUROSCI.3432-04.2004
- Hohman TJ, Bell SP, Jefferson AL. The role of vascular endothelial growth factor in neurodegeneration and cognitive decline: Exploring interactions with biomarkers of Alzheimer disease. *JAMA Neurol*. 2015;72(5):520. doi:10.1001/jamaneurol.2014.4761
- Mantyh PW. Neurobiology of substance P and the NK1 receptor. *J Clin Psychiatry*. 2002;63(Suppl 11):6–10. PMID:12562137.
- Ahmed MM, Hoshino H, Chikuma T, Yamada M, Kato T. Effect of memantine on the levels of glial cells, neuropeptides, and peptide-degrading enzymes in rat brain regions of ibotenic acid-treated Alzheimer's disease model. *Neuroscience*. 2004;126(3):639–649. doi:10.1016/j.neuroscience.2004.04.024
- Campolongo P, Ratano P, Ciotti MT, et al. Systemic administration of substance P recovers beta amyloid-induced cognitive deficits in rat: Involvement of Kv potassium channels. *PLoS One*. 2013;8(11):e78036. doi:10.1371/journal.pone.0078036
- Pieri M, Amadoro G, Carunchio I, et al. SP protects cerebellar granule cells against β-amyloid-induced apoptosis by down-regulation and reduced activity of Kv4 potassium channels. *Neuropharmacology*. 2010;58(1):268–276. doi:10.1016/j.neuropharm.2009.06.029
- Gouveia F, Camins A, Ettcheto M, et al. Targeting brain renin-angiotensin system for the prevention and treatment of Alzheimer's disease: Past, present and future. *Ageing Res Rev*. 2022;77:101612. doi:10.1016/j.arr.2022.101612
- Alpat İ, Ersoy G. Alzheimer Hastalığında Koruyucu ve Tedavi Edici Bir Müdahale Olarak Egzersiz. *Geratrik Bilimler Dergisi*. 2022;5(3):90–96. doi:10.47141/geriatrik.1169599
- Ng T, Ho C, Tam W, Kua E, Ho R. Decreased serum brain-derived neurotrophic factor (BDNF) levels in patients with Alzheimer's disease (AD): A systematic review and meta-analysis. *Int J Mol Sci*. 2019; 20(2):257. doi:10.3390/ijms20020257



# Affected brother as the highest risk factor of type 1 diabetes development in children and adolescents: One center data before implementing type 1 diabetes national screening

Anna Wędrychowicz<sup>1,2,A–F</sup>, Teresa Grzelak<sup>3,B–D,F</sup>, Alicja Pietraszek<sup>4,A–C,F</sup>,  
Maria Skrzyszowska<sup>4,A–C,F</sup>, Mari Minasjan<sup>4,B,C,F</sup>, Jerzy B. Starzyk<sup>1,2,A,F</sup>

<sup>1</sup> Department of Pediatric and Adolescent Endocrinology, Pediatric Institute, Jagiellonian University Medical College, Kraków, Poland

<sup>2</sup> Department of Pediatric and Adolescent Endocrinology, University Children's Hospital, Kraków, Poland

<sup>3</sup> Department of Physiology, Poznan University of Medical Sciences, Poland

<sup>4</sup> Students' Scientific Society at the Department of Pediatric and Adolescent Endocrinology, Pediatric Institute, Jagiellonian University Medical College, Kraków, Poland

A – research concept and design; B – collection and/or assembly of data; C – data analysis and interpretation;

D – writing the article; E – critical revision of the article; F – final approval of the article

Advances in Clinical and Experimental Medicine, ISSN 1899–5276 (print), ISSN 2451–2680 (online)

*Adv Clin Exp Med.* 2024;33(8):781–790

## Address for correspondence

Anna Wędrychowicz  
E-mail: anna.wedrychowicz@uj.edu.pl

## Funding sources

None declared

## Conflict of interest

None declared

Received on July 3, 2023

Reviewed on July 27, 2023

Accepted on September 18, 2023

Published online on November 24, 2023

## Cite as

Wędrychowicz A, Grzelak T, Pietraszek A, Skrzyszowska M, Minasjan M, Starzyk JB. Affected brother as the highest risk factor of type 1 diabetes development in children and adolescents: One center data before implementing type 1 diabetes national screening. *Adv Clin Exp Med.* 2024;33(8):781–790. doi:10.17219/acem/172446

## DOI

10.17219/acem/172446

## Copyright

Copyright by Author(s)

This is an article distributed under the terms of the Creative Commons Attribution 3.0 Unported (CC BY 3.0) (<https://creativecommons.org/licenses/by/3.0/>)

## Abstract

**Background.** There is an increased risk for childhood type 1 diabetes (T1D) when T1D and type 2 diabetes (T2D) are reported in relatives.

**Objectives.** Our objective was to evaluate current family risk factors for T1D development before implementing a national screening program for T1D.

**Materials and methods.** A population of 879 Caucasian children and adolescents with T1D and 286 healthy controls were enrolled in the study. All participants completed the same questionnaire, which collected information about family history of diabetes over 3 generations. In statistical analyses, frequency tables and  $\chi^2$  tests evaluated possible multicollinearity among risk factors that were significantly associated with the outcomes.

**Results.** Family history of diabetes was more frequent in controls ( $n = 75$ , 26.2%) than in patients with T1D ( $n = 146$ , 16.6%, odds ratio (OR) = 1.785, 95% confidence interval (95% CI): 1.299–2.452, degrees of freedom (df) = 12.976,  $p = 0.004$ ), especially with a family history of T2D ( $n = 62$ , 21.7% compared to  $n = 79$ , 9.0%, respectively, OR = 2.803, 95% CI: 1.948–4.034, df = 32.669,  $p < 0.001$ ). Also, there was a tendency for the nuclear family of T1D patients to be more frequently affected by T1D ( $n = 74$ , 8.4%) than the controls ( $n = 15$ , 5.2%, OR = 1.605, 95% CI: 0.937–2.751, df = 3.081,  $p = 0.079$ ). The risk of T1D was associated with the closest family members being affected and accelerated over generations. Indeed, it was highest in siblings, especially brothers (OR = 12.985, 95% CI: 0.782–215.743, Fisher's test:  $p < 0.001$ ). A positive family history of T2D burden among second-degree relatives was 2.728 times more frequent in the control group than in the T1D group (OR = 2.728; 95% CI: 1.880–3.962,  $p < 0.001$ ). Furthermore, a positive family history of T1D among first-degree relatives was less frequent in the controls than in the T1D group (OR = 0.124; 95% CI: 0.030–0.516,  $p = 0.004$ ).

**Conclusions.** A family history of T1D, but not T2D, is a significant risk factor for T1D development. Indeed, the priority in screening for T1D should be given to first-degree relatives of T1D patients, starting from siblings.

**Key words:** type 2 diabetes mellitus, siblings, type 1 diabetes mellitus, first-degree relatives, family history of diabetes

## Background

Type 1 diabetes (T1D) develops from interactions between several combinations of susceptibility genes and environmental exposures. Numerous studies have found an increased risk of T1D in children whose relatives have both type 1 and type 2 diabetes (T2D).<sup>1–3</sup> Previous studies demonstrated that individuals with first-degree relatives with T1D have an approx. 15-fold higher relative lifetime risk of developing T1D than the general population, and the prevalence of T1D by the age of 20 is around 5% compared to approx. 0.3% in the general population, making screening an effective approach to recruiting for preventive screening. However, over 85% of newly diagnosed patients have no family history.<sup>4–6</sup> Moreover, it is well established that the prevalence of autoimmunity and T1D in individuals with certain human leukocyte antigen (HLA) loci varies significantly, with a gradient that includes a range of highly susceptible protective loci.<sup>7,8</sup> Indeed, over 70 T1D genetic variants have been identified in genome-wide association studies.<sup>9</sup> Around half of them are HLA-DR and HLA-DQ loci. First-degree relatives who carry HLA-DR3-DQ2/DR4-DQ8 have an elevated risk of islet autoimmunity and T1D, which increases by about 20%.<sup>10,11</sup> In families living together, similar environmental risk factors for diabetes may also explain this observation.

Type 1 diabetes often occurs in combination with several endocrine and non-endocrine autoimmune disorders. Recent studies have shown a strong cluster of T1D and autoimmune diseases in patients and their first-degree relatives.<sup>12</sup> Annual serological and subsequent functional screening for autoimmune disorders in T1D patients and their first-degree relatives is recommended. Screening for T1D autoantibodies has positive clinical consequences, including reduced diabetic ketoacidosis events, improved glycemic control, and a positive impact on short-term and long-term complications.<sup>13</sup> In some regions of Poland, screening for T1D antibodies in first-degree relatives of patients with T1D has been conducted.<sup>14</sup> According to the International Society for Pediatric and Adolescent Diabetes (ISPAD) recommendations, routine screening for family members as part of clinical care has been proposed as an intermediate step toward general population screening.<sup>15</sup> Such an approach would be highly recommended if effective immunotherapies that delay progression and preserve  $\beta$ -cell function are approved by regulatory bodies and the cost/benefit ratio related to screening is optimized.<sup>16</sup>

## Objectives

This study aimed to assess T1D risk in children and adolescents with a positive family history of diabetes at our center prior to the implementation of a national T1D screening program.

## Materials and methods

Our cohort study was conducted between 2017 and 2018 and involved 879 Caucasian children and adolescents with T1D and 286 healthy Caucasian children and adolescents. The T1D patients constituted an unselected group of patients and included 90% of all patients treated in our department, with a median age of 12.8 (9.2; 15.5) years. The T1D diagnosis was made according to the 2017 criteria of the Polish Diabetes Society.<sup>17</sup> The control group consisted of children and adolescents from public schools, representative of the general population.

The Ethics Committee of Jagiellonian University approved the study (approval No. 1072.6120.206.2017). All parents/legal guardians of the study participants gave their written informed consent by completing a family interview questionnaire. All participants completed the same questionnaire, which was prepared by the authors of the study. Family history collected information about diabetes over 3 generations (defined as grandparents, i.e., both of the parent's parents, parents, siblings of parents, i.e., aunts and uncles, and the children of parents' siblings, i.e., cousins and siblings). Data on the number of relatives with diabetes, the age of disease onset, and the use of insulin in those diagnosed with diabetes were obtained. The questionnaire used the term latent autoimmune diabetes in adults (LADA) for T1D diagnosed in adults according to the then valid classification. In addition, we asked about autoimmune diseases in diabetic family members, specifically celiac disease, autoimmune thyroiditis, including Graves' disease, and non-celiac autoimmune bowel diseases, to minimize the risk of T1D overdiagnosis among diabetic relatives treated with insulin. The interviewers were medical students from a scientific group working in our department. Data on study participants were mostly obtained from their parents (predominantly from mothers).

## Statistical analyses

All statistical analyses employed IBM SPSS v. 25 (IBM Corp., Armonk, USA) and Statistica v. 13 with the medical kit (StatSoft, Tulsa, USA). Results are presented as medians with upper and lower quartiles. The normality of data distribution was assessed using the Shapiro–Wilk test (for a relatively small sample size <50) and the Kolmogorov–Smirnov test (for a large sample size). Due to interval data with non-parametric distribution in parameters such as age and the T1D diagnosed age, which occurred in at least 1 of the 2 examined groups of children (Table 1,2), the Mann–Whitney U test for 2 independent samples was used. Frequency tables and  $\chi^2$  tests assessed possible collinearity among risk factors that were significantly associated with the outcomes.

For subsets of data with smaller numbers, the  $\chi^2$  test with Yates' correction and Fisher's exact test of independence were used. The chi-square automatic interaction detection (CHAID) decision tree algorithm proposed by Kass

**Table 1.** Values of normality tests for age in the entire examined population (n = 1165), the group of children with T1D (n = 879) and control group (n = 286), taking gender into account

Groups	D statistics (D) and p-values in the Kolmogorov–Smirnov tests	W statistics (W) and p-values in the Shapiro–Wilk tests
Entire examined population (n = 1165)	D = 0.073827 p < 0.001	W = 0.968583 p < 0.001
Group of children with T1D (n = 879)	D = 0.081427 p < 0.001	W = 0.954083 p < 0.001
Control group (n = 286)	D = 0.137104 p < 0.001	W = 0.47486 p < 0.001
Entire examined boy population (n = 588)	D = 0.081074 p < 0.001	W = 0.964077 p < 0.001
Entire examined girl population (n = 570)	D = 0.070772 p = 0.006	W = 0.971673 p < 0.001
Group of boys with T1D (n = 451)	D = 0.084905 p = 0.003	W = 0.949227 p < 0.001
Group of girls with T1D (n = 428)	D = 0.086927 p = 0.003	W = 0.957016 p < 0.001
Boys in the control group (n = 137)	D = 0.157911 p = 0.002	W = 0.936828 p < 0.001
Girls in the control group (n = 142)	D = 0.132553 p = 0.013	W = 0.950827 p < 0.001

T1D – type 1 diabetes; T2D – type 2 diabetes; n – number of children.

**Table 2.** Values of normality tests for age at diagnosis of T1D in the group of children with T1D (n = 879) depending on family history of T1D and T2D, taking gender into account

Groups	D statistics (D) and p-values in the Kolmogorov–Smirnov test	W statistics (W) and p-values in the Shapiro–Wilk test
Group of children with T1D (n = 879)	D = 0.081427 p < 0.001	W = 0.954083 p < 0.001
Group of boys with T1D (n = 451)	D = 0.097346 p < 0.001	W = 0.954009 p < 0.001
Group of girls with T1D (n = 428)	D = 0.053759 p = 0.162	W = 0.944326 p < 0.001
Group of children with T1D with a positive family history of T2D (n = 79)	D = 0.0661 p = 0.858	W = 0.980561 p = 0.271
Group of children with T1D with a negative family history of T2D (n = 800)	D = 0.073228 p < 0.001	W = 0.949314 p < 0.001
Group of children with T1D with a positive family history of T2D burden among second-degree relatives (n = 76)	D = 0.069974 p = 0.825	W = 0.978839 p = 0.235
Group of children with T1D with a negative family history of T2D among second-degree relatives (n = 803)	D = 0.072574 p < 0.001	W = 0.949625 p < 0.001
Group of children with T1D with a positive family history of T2D burden among grandparents (n = 73)	D = 0.081854 p = 0.681	W = 0.974688 p = 0.149
Group of children with T1D with a negative family history of T2D burden among grandparents (n = 806)	D = 0.072066 p < 0.001	W = 0.949656 p < 0.001

T1D – type 1 diabetes; T2D – type 2 diabetes; n – number of children.

identified the main determinants of T1D at younger ages (84 months and below). These decision trees operate through a series of steps, including merging, splitting and retaining, based on user-specified criteria, and split the data into more homogeneous groups.<sup>18</sup> Multivariate logistic regression models determined the odds of avoiding T1D. A 95% confidence interval (95% CI) was used to estimate the precision of the odds ratio (OR). A two-tailed p-value <0.05 was considered statistically significant.

## Results

The study included 879 children with T1D, among them 451 (51%) boys and 428 (49%) girls (Fig. 1). The median age in the male subgroup with T1D amounted to 154 months (110.5; 187) and did not differ from the female subgroup (149 months (109;185.5); U = 94804, p = 0.346). In the group of children with T1D, the median age at T1D diagnosis was 84 months (49; 124), which did not differ

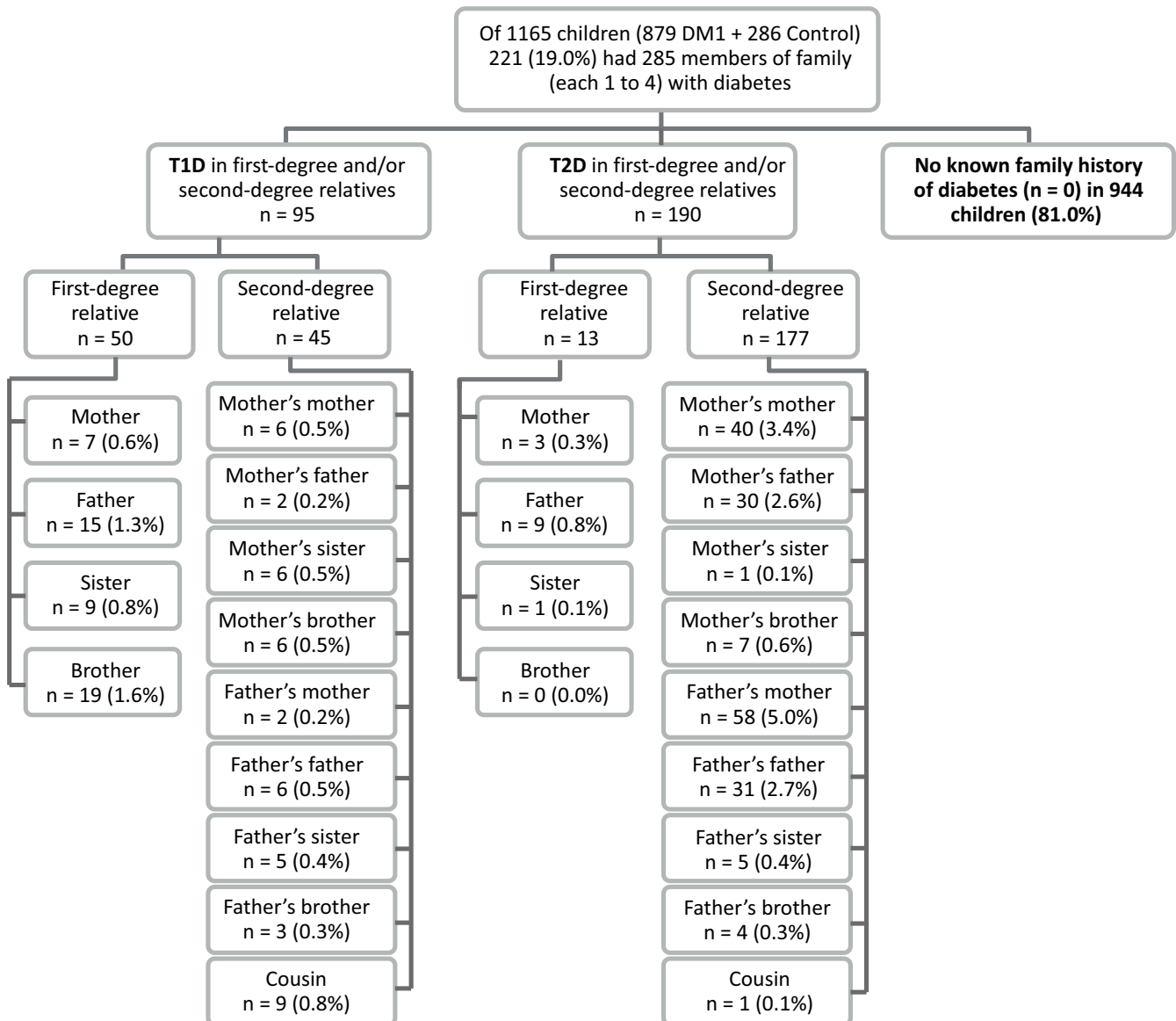


Fig. 1. Flowchart presenting the numbers (n) and proportions of participants with relatives affected by type 1 diabetes (T1D) and type 2 diabetes (T2D) in the total cohort of 1165 children

between genders ( $U = 91937$ ,  $p = 0.224$ ). The 286 healthy individuals in the control group consisted of 137 boys (48%) and 142 girls (50%), with gender not specified in 7 (2%) questionnaires. The gender distribution (boys compared to girls) was similar in the control group compared to the T1D group (degrees of freedom (df) = 0.412,  $p = 0.521$ ).

### Family history of diabetes mellitus

Of the 879 children with T1D, 109 (12.4%) had 1 family member (first- or second-degree relative) with diabetes (all types) (Fig. 2), 30 (3.4%) had 2 family members, 6 (0.7%) had 3 family members and only 1 (0.1%) had 4 family members with diabetes. In summary, 16.6% ( $n = 146$ ) of children with T1D had at least 1 family member (first- or second-degree relative) affected by diabetes. Of the 286 control children,

58 (20.3%) had 1 family member (first- or second-degree relative) with diabetes (all types) (Fig. 3), 15 (5.2%) had 2 affected members and only 2 (0.7%) had 3 family members with diabetes. To sum up, 26.2% ( $n = 75$ ) of children from the control group had at least 1 family member (first- or second-degree relative) with diabetes.

### Family history of diabetes mellitus type 1

Of the 879 children with T1D, 69 (7.8%) had 1 family member (first- or second-degree relative) affected by T1D (Fig. 2), 4 (0.5%) had 2 such family members and only 1 (0.1%) had 3 family members affected by T1D. Overall, 8.4% ( $n = 74$ ) of children with T1D had at least 1 family member (first- or second-degree relative) affected by T1D. Of the 286 children in the control group, 15 (5.2%) had 1 family member (first- or second-degree relative) affected by T1D.



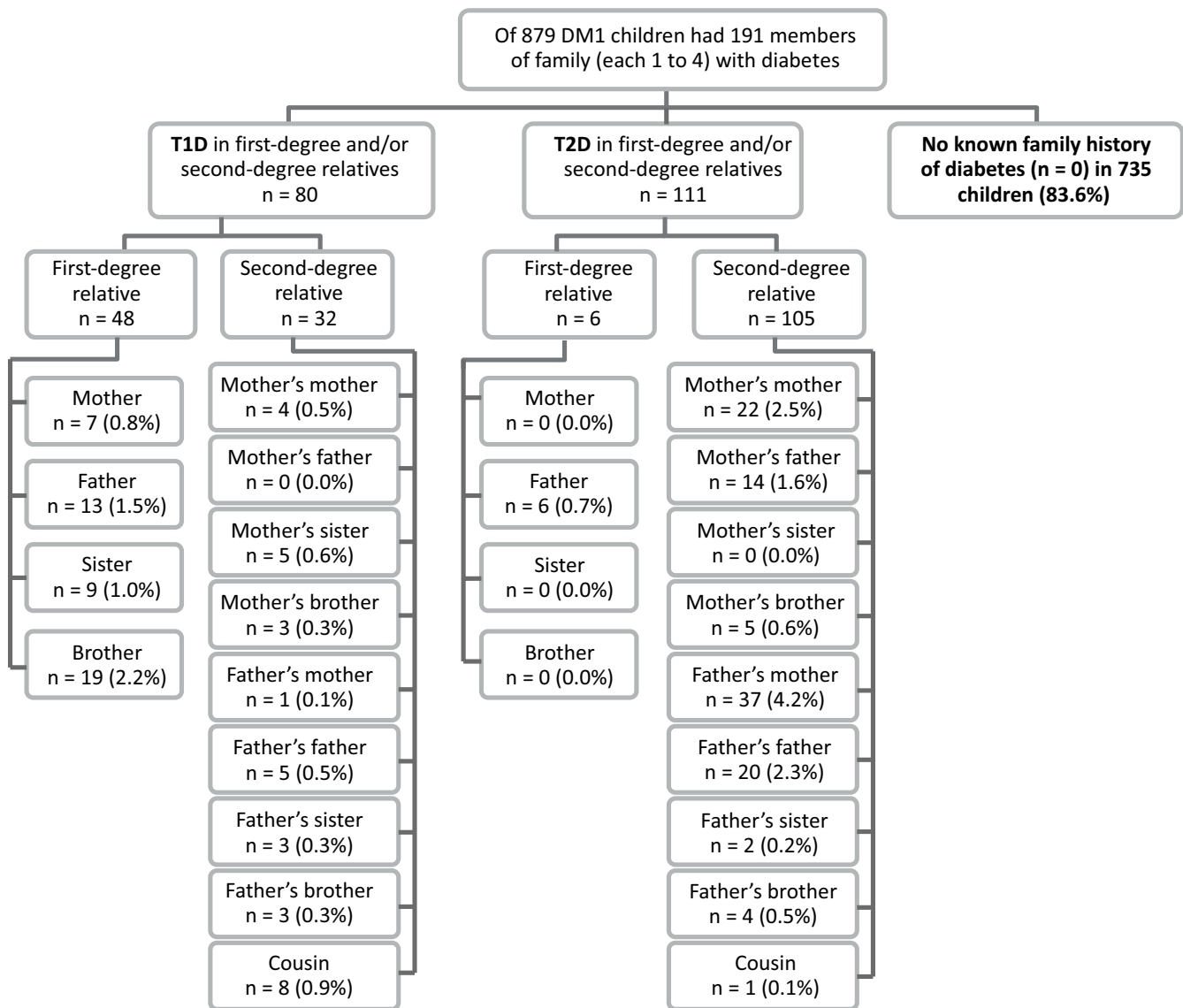


Fig. 2. Flowchart presenting the numbers (n) and proportions of participants with relatives affected by type 1 diabetes (T1D) and type 2 diabetes (T2D) in a group of 879 children diagnosed with T1D

Of the 879 T1D patients, 13 (1.5%) had a T1D father and 7 (0.8%) had an affected mother. In addition, 19 patients (2.2%) had a brother with T1D and 9 (1.0%) had an affected sister. Of the 286 children in the control group, 2 (0.7%) had a father with T1D (Fig. 3). There were no cases of affected mothers or affected siblings in this group. The incidence of T1D in first- and second-degree relatives is detailed in Fig. 2 and Fig. 3.

We observed a tendency for the nuclear family of patients with T1D to be more frequently affected by T1D (n = 74, 8.4%) than the control group (n = 15, 5.2%, OR = 1.605, 95% CI: 0.937–2.751, df = 3.081, p = 0.079). Children with T1D had parents with T1D more often (OR = 4.070, 95% CI: 1.900–8.733) than they had grandparents with T1D (df = 15.173, p < 0.001). In the control group, the numbers of parents and grandparents with T1D were similar (OR = 0.665, 95% CI: 0.065–3.747; Fisher's exact test, p = 0.726). A positive family history of T1D

among first-degree relatives was more frequent (n = 48, 5.4%, OR = 8.202, 95% CI: 1.981–33.963) in the T1D group (Fisher's exact test, p < 0.001) than in the control group (n = 2, 0.7%). A positive family history of T1D among second-degree relatives was as common in the T1D group (n = 27, 3.1%, df = 1.414, p = 0.234) as it was in the control group (n = 13, 4.5%).

A positive family history of T1D among siblings was more frequent (n = 28, 19.0%, OR = 19.173, 95% CI: 1.167–315.137) in the T1D group (Fisher's exact test, p < 0.001) than in the control group (n = 0, 0%). A positive family history of T1D among brothers was more frequent (n = 19, 2.2%, OR = 12.985, 95% CI: 0.782–215.743) in the T1D group (Fisher's exact test, p = 0.006) than in controls (n = 0, 0%).

Parental family history of T1D was similar between the T1D group (Fisher's exact test, p = 0.130) and the control group, although there was a tendency for male family members of T1D children to have a more frequent positive

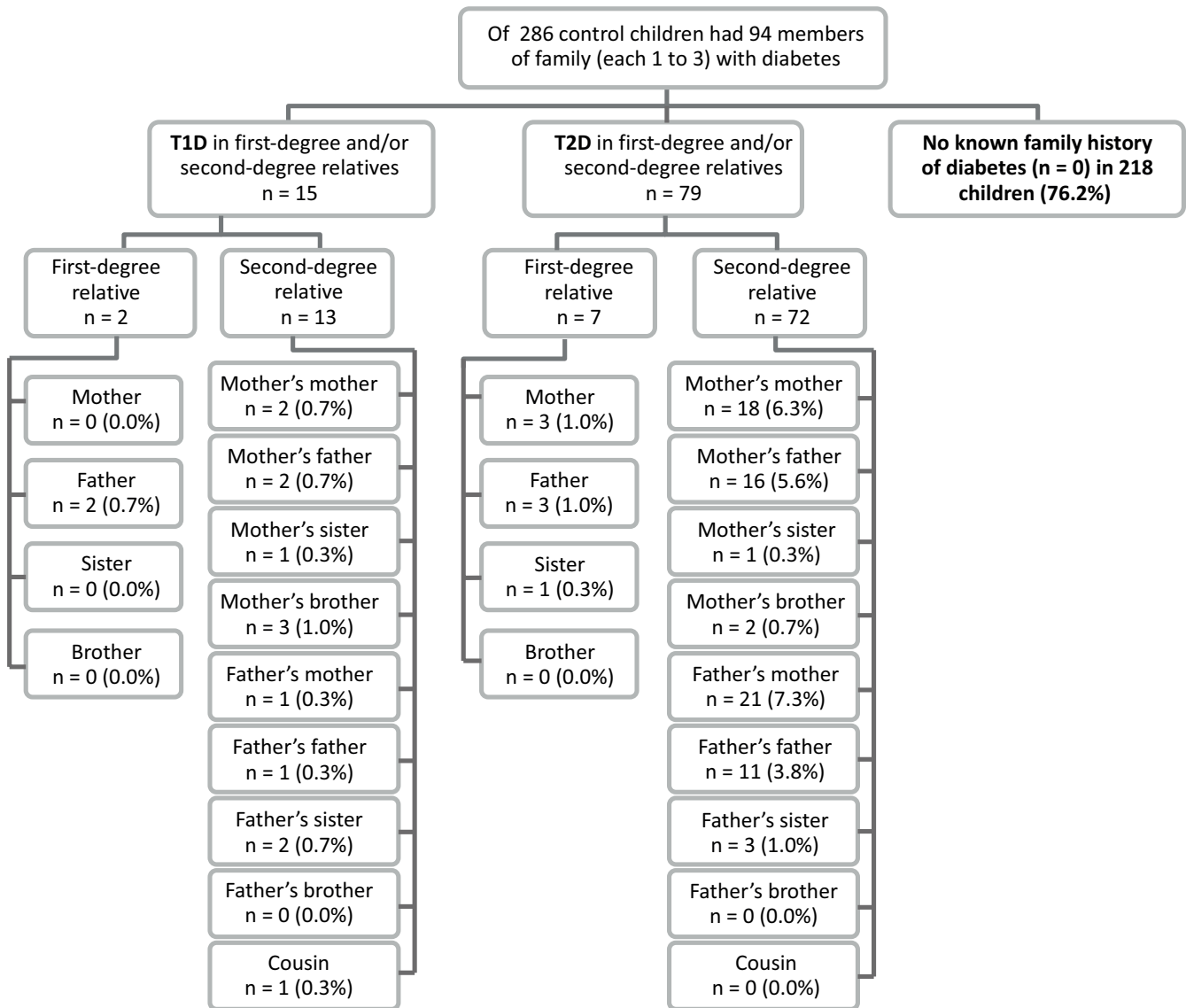


Fig. 3. Flowchart presenting the numbers (n) and proportions of participants with relatives affected by type 1 diabetes (T1D) and type 2 diabetes (T2D) in the control group (286 children).

history of T1D ( $df = 2.900$ ,  $p = 0.089$ ). A family history of T1D in aunts, uncles and cousins was similar in the T1D and control groups.

### Family history of diabetes mellitus type 2

Among the 879 children with T1D, 53 (6.0%) had 1 family member (first- or second-degree relative) affected by T2D (Fig. 2), 21 (2.4%) had 2 such members, 4 (0.5%) had 3 members, and only 1 (0.1%) had 4 family members affected by T2D. Overall, 9.0% ( $n = 79$ ) of children with T1D had at least 1 family member (first- or second-degree relative) affected by T2D. Of the 286 control children, 47 (16.4%) had 1 family member (first- or second-degree relative) affected by T2D (Fig. 3), 13 (4.5%) had 2 such family members and only 2 children (0.7%) had 3 family members affected by T2D. Overall, 21.7% ( $n = 62$ ) of the children in the control group had at least 1 family member (first- or second-degree relative) affected by T2D.

Family history of T2D was more frequent in the control group (OR = 2.803, 95% CI: 1.948–4.034,  $df = 32.669$ ,  $p < 0.001$ ) than T1D. Grandparents with T2D were statistically more frequent than parents with T2D in both groups (OR = 5.143; 95% CI: 2.213–11.947,  $df = 17.903$ ,  $p < 0.001$  for the T1D group and OR = 11.956; 95% CI: 5.067–28.211,  $df = 47.971$ ,  $p < 0.001$  for the control group). In patients with T1D and a positive family history of T2D burden among grandparents, T1D was diagnosed later ( $U = 24505$ ,  $p = 0.018$ , median age (25; 75%): 107 months (77; 127)) than in patients with a negative family history of T2D (81 months (48; 124)). This finding corresponded with, among other things, decision tree (CHAID) results, which showed that the children with a positive family history of T2D among grandparents were more frequent (OR = 2.342; 95% CI: 1.153–4.755) in the older T1D diagnosis group ( $df = 8.785$ ,  $p = 0.003$ ) than in the younger group (84 months and below).

## Family history of diabetes mellitus: comparison of diabetes types

In children with a positive family history of T2D, T1D was diagnosed later ( $U = 26469$ ,  $p = 0.018$ , median age of 103 months (73.5; 126.5),  $n = 79$ ) than in the group with a negative history (81 months (48; 124)). In cases with a family history of T1D, there were no such observations ( $U = 27512$ ,  $p = 0.278$ ; median age of 97 (49.25; 137) compared to 84 (49; 124) months).

The logistic regression model showed a significant impact of T2D scores on the chances of second-degree relatives avoiding T1D in the entire study population ( $F = 27.133$ ,  $p < 0.001$ ). In order to describe this phenomenon more precisely, the model included an additional T1D variable in the family member(s) burden among first-degree relatives ( $F = 42.867$ ,  $p < 0.001$ ; Table 2). After using a least absolute shrinkage and selection operator (LASSO) logistic regression model, the full logistic regression model included 2 variables (T2D in family member(s) burden among second-degree relatives and T1D in family member(s) burden among first-degree relatives) to assess the chance of avoiding T1D in the entire study population (Table 3,4). In the final model, children with a positive family history of T2D burden among second-degree relatives were classified more frequently by an average of 2.727 times ( $OR = 2.728$ ; 95% CI: 1.880–3.962,  $p < 0.001$ ) in the control group than in the T1D group, but children with a positive family history of T1D burden among first-degree relatives were classified less frequently ( $OR = 0.124$ ; 95% CI: 0.030–0.516,  $p = 0.004$ ) in the control group than in the T1D group.

## Discussion

The results of our study confirm that a positive family history of T1D in first-degree relatives is more common in children with T1D than in healthy controls ( $p < 0.001$ ). Our data show that 5.4% of children with T1D had at least 1 first-degree relative affected by T1D, which was statistically significantly higher than in the control group (0.7%). In the USA, data from the SEARCH study suggest that the risk of developing T1D in a child is 1.54 per 1000, or 0.154%.<sup>19</sup> The risk of developing T1D in a child is higher if one of the parents has T1D, and the risk of T1D in siblings is 6%.<sup>20</sup> When analyzing the immediate family members in our T1D group, 1.5% had a father with T1D, 0.8% had a mother with T1D, 2.2% had a brother with T1D, and 1.0% had a sister with T1D. It is worth emphasizing that children with a negative family history of T1D among brothers were more frequent in the control group than in the T1D group ( $p = 0.005$ ). Interestingly, T1D parents were statistically more common than T1D grandparents ( $p < 0.001$ ), but in the control group, the number of T1D parents and T1D grandparents was similar ( $p = 0.726$ ); perhaps this is the effect of the epigenetic phenomenon of acceleration in subsequent generations.

Interestingly, male family members carry a higher risk of developing T1D. In previous studies, the risk of developing familial T1D has been reported to be more than 2 times higher in the offspring of affected fathers than in those of affected mothers. Familial T1D characteristics in first-degree relatives were investigated in children diagnosed before the age of 15 using data from an international

**Table 3.** Comparison of the 2 logistic regression models explaining the chance of avoiding T1D in the entire examined population ( $n = 1165$ ) – before and after adding a new variable (T1D in member(s) family) to the basic model, which includes 1 variable: T2D in member(s) family burden among first-degree relatives ( $\chi^2$  test: 15.733;  $p = 0.001$ )

Statistical parameters	Model including 1 variable: T2D in member(s) family burden among second-degree relatives	Extended model with a new variable: T1D in member(s) family burden among first-degree relatives
F	27.133	42.867
p-value	<0.001	<0.001
df	1	2
R <sup>2</sup> Nagelkerke (goodness-of-fit measure)	0.034	0.054

T1D – type 1 diabetes; T2D – type 2 diabetes;  $n$  – number of children;  $F$  – F statistic;  $df$  – degrees of freedom.

**Table 4.** Restricted model in logistic regression explaining the chance of avoiding T1D in the entire examined population ( $n = 1165$ )

Parameters	B	SE(B)	95% CI for B		Wald statistic	p-value	Exp(B)	95% CI for Exp(B)	
			lower	upper				lower	upper
T2D in member(s) of the family burden among second-degree relatives	1.010	0.189	0.640	1.381	28.5407	<0.001	2.746	1.896	3.978
Constant	1.263	0.075	-1.411	-1.116	282.482	<0.001	0.283	0.244	0.328

B – regression coefficient in Wald statistic; SE(B) – standard error in Wald statistic; Exp(B) – odds ratio; 95% CI – 95% confidence interval; T2D – type 2 diabetes.

population registries network and a case-control study, and showed a positive association between the population-based incidence rate of T1D and the incidence of T1D in fathers of affected children.<sup>21</sup> Pooled results from all centers showed that a higher proportion of fathers (3.4%) of affected children had T1D than mothers, giving a hazard ratio (HR) of 1.8. These data are consistent with our observations (HR of 1.86 in children with T1D), although we only noticed a trend towards a higher positive history of T1D in male family members of children with T1D. The hypothesis was built suggesting that index children with an affected father may have a more aggressive disease process at diagnosis than those with other affected first-degree relatives. Moreover, the hypothesis stated that maternal insulin treatment protects against T1D. A Finnish group reported that the index children with an affected father or mother were younger than those with an affected sibling.<sup>22</sup> After age- and sex-adjusted analyses, index children with an affected father presented more often with ketoacidosis and exhibited more weight loss before diagnosis than those with an affected mother.

Recent data from an international study report that the risk of developing multiple autoantibodies was lower in children with maternal T1D. For the whole group, the risk of developing multiple autoantibodies was independent of birthweight but was greater in those with increased height velocity during the first 2 years of life. However, the risk associated with paternal T1D diabetes was not linked to differences in birthweight or early growth.<sup>23</sup> Also, Verge et al. reported that the offspring of a father with T1D were more likely to seroconvert to positivity for diabetes-related autoantibodies than the offspring of an affected mother.<sup>24</sup> Similarly, the risk of developing multiple islet autoantibody positivity tended to be higher in the offspring of affected fathers compared with affected mothers in the BABYDIAB study.<sup>25</sup> In a German study, compared with the reference population, individuals with T1D had significantly fewer children and were more often childless, and more men (51.1%) than women (35.7%,  $p < 0.001$ ) were childless.<sup>26</sup> This report refutes the hypothesis that affected fathers bring T1D risk to offspring more frequently because women with T1D decide not to have children due to fears over pregnancy, its complications and defects in their offspring.

The beneficial effects of estrogen with regard to insulin action and secretion in healthy women are well known.<sup>27</sup> However, there is no direct data that suggest that estrogens protect against autoimmune insulinitis. Moreover, estrogen's action could not explain why young, especially prepubertal male members of the family carry a higher risk of developing T1D. Rather, some genes on the Y chromosome increase the risk of T1D development. Azulay et al. demonstrated that the predominance of the HLA-DRB1\*03 and DRB1\*04 alleles in conferring an increased risk in a Brazilian population and being more frequently related to the ancestry of the European Y chromosome suggests that, in this

population, the risk of T1D can be transmitted by European ancestors through miscegenation.<sup>28</sup>

Finnish data from 2013 indicate that 12.2% of T1D patients had a first-degree relative with T1D (6.2% father, 3.2% mother and 4.8% sibling) and 11.9% had a second-degree relative affected. Given an extended family history of T1D, the rate of sporadic diabetes can be reduced to less than 80%. In this cited study, a positive family history of T1D was associated with less severe metabolic decompensation at diagnosis, even if only second-degree relatives were affected. Autoantibody profiles were similar in familial and sporadic T1D diabetes, suggesting similar pathogenetic mechanisms.<sup>29</sup> We did not analyze the associations between a positive family history and the metabolic status of our patients at the time of diagnosis of T1D, but certainly, knowledge about the disease could help avoid metabolic decompensation when diagnosed in subsequent family members. This is the most important premise for the planned introduction of T1D screening tests in our country. Even screening for T1D among close relatives of children with T1D would play an important role, although the latest Finnish data from 2019 indicate that all clinical and metabolic variables were significantly worse in children with sporadic diabetes than familial diabetes.<sup>22</sup> Also, an Italian study found that children whose first- or second-degree relatives were affected by T1D had earlier disease onset and showed lower glycated hemoglobin (HbA1C) levels that were negatively associated with a positive family history of T1D, fasting C-peptide levels and some autoantibody levels. Milder metabolic decompensation in children with a positive family history of T1D is probably explained by families' awareness of early T1D symptoms, while younger age of onset and higher levels of autoantibodies may suggest greater genetic susceptibility associated with a more aggressive autoimmune process.<sup>30</sup> However, the latest data from the literature indicate that T1D in non-nuclear relatives is an important risk factor for islet autoimmunity and progression to clinical disease in HLA-susceptible children.<sup>31</sup> Therefore, national screening is important for all.

Our results are at odds with previous reports of an increased positive family history of T2D in T1D patients. In our study, 9% of children with T1D had at least 1 family member (first- or second-degree relative) affected by T2D, while 21.7% of control children had at least 1 family member affected by T2D. A 2021 Finnish study found that characteristics associated with T2D, such as increased weight, older age at diagnosis and lack of autoantibodies, are more likely to be present at T1D diagnosis in children with a positive family history of T2D. Considering the cited report, one should be aware of the clinical picture of T1D in obese children.<sup>32</sup> This observation is difficult to explain. Recent evidence indicates that both T1D and T2D represent a model of an immunological continuum of endotypes lying between the 2 extremes, "insulin-resistant" and "autoimmune  $\beta$ -cell targeting," shaped by environmental and genetic factors that contribute to determining specific immune-conditioned

outcomes.<sup>33</sup> However, T2D is rather associated with insulin resistance. In our study, children with a positive family history of T2D among second-degree relatives were diagnosed with T1D later than those with a negative family history ( $p = 0.028$ ), which may suggest that insulin resistance delays the onset of autoimmune  $\beta$ -cell destruction. Another explanation would be that a positive family history of diabetes implies a reduction in family intake of simple carbohydrates, which may prolong the time to T1D symptom onset. This is partly in line with Wilkin's accelerator hypothesis, which assumes that the pathogenesis of both types of diabetes is related to the interaction between insulin resistance (including, i.a., an abnormal lifestyle) and genetic determinants (which are connected, especially in T1D, with autoimmune  $\beta$ -cell destruction).<sup>34</sup> However, there is no objective clinical data to support our hypothesis. The observation of a much later onset of T1D associated with a maternal history of T1D and T2D was reported by Holstein et al.<sup>26</sup>

## Limitations

The strength of our study is the cohort of a homogenous Caucasian population of participants, almost all of whom lived within nuclear families with the same environmental risk factors of developing T1D. Compared to other studies, the weaknesses are the lack of verification of data obtained from parents/legal guardians based on medical documents.

## Conclusions

Our research has shown that a family history of T1D, but not T2D, is a significant risk factor for developing T1D. The risk of T1D is associated with affected members of the immediate family and accelerates from generation to generation. It is greatest in siblings, and therefore first-degree relatives of T1D patients, especially siblings, should have priority in T1D screening. An interesting finding worthy of further studies is that male family members carry a higher risk of developing T1D.

## ORCID iDs

Anna Wędrychowicz  <https://orcid.org/0000-0003-0864-6810>  
 Teresa Grzelak  <https://orcid.org/0000-0002-2815-0372>  
 Alicja Pietraszek  <https://orcid.org/0000-0001-6892-2923>  
 Maria Skrzyszowska  <https://orcid.org/0000-0002-8095-9849>  
 Mari Minasjan  <https://orcid.org/0000-0001-9382-6896>  
 Jerzy B. Starzyk  <https://orcid.org/0000-0002-4086-6525>

## References

- Dahlquist G, Blom L, Holmgren G, et al. The epidemiology of diabetes in Swedish children 0–14 years: A six-year prospective study. *Diabetologia*. 1985;28(11):802–808. doi:10.1007/BF00291068
- Allen C, Palta M, D'Alessio DJ. Risk of diabetes in siblings and other relatives of IDDM subjects. *Diabetes*. 1991;40(7):831–836. doi:10.2337/diab.40.7.831
- Ziegler AG, Kick K, Bonifacio E, et al. Yield of a public health screening of children for islet autoantibodies in Bavaria, Germany. *JAMA*. 2020;323(4):339. doi:10.1001/jama.2019.21565
- Cernea S, Dobreanu M, Raz I. Prevention of type 1 diabetes: Today and tomorrow. *Diabetes Metab Res Rev*. 2010;26(8):602–605. doi:10.1002/dmrr.1138
- Huber A, Menconi F, Corathers S, Jacobson EM, Tomer Y. Joint genetic susceptibility to type 1 diabetes and autoimmune thyroiditis: From epidemiology to mechanisms. *Endocr Rev*. 2008;29(6):697–725. doi:10.1210/er.2008-0015
- Besser REJ, Ng SM, Gregory JW, Dayan CM, Randell T, Barrett T. General population screening for childhood type 1 diabetes: Is it time for a UK strategy? *Arch Dis Child*. 2022;107(9):790–795. doi:10.1136/archdischild-2021-321864
- Stankov K, Benc D, Draskovic D. Genetic and epigenetic factors in etiology of diabetes mellitus type 1. *Pediatrics*. 2013;132(6):1112–1122. doi:10.1542/peds.2013-1652
- Pociot F, Lernmark Å. Genetic risk factors for type 1 diabetes. *Lancet*. 2016;387(10035):2331–2339. doi:10.1016/S0140-6736(16)30582-7
- Robertson CC, Inshaw JRJ, Onengut-Gumuscu S, et al. Fine-mapping, trans-ancestral and genomic analyses identify causal variants, cells, genes and drug targets for type 1 diabetes. *Nat Genet*. 2021;53(7):962–971. doi:10.1038/s41588-021-00880-5
- Hippich M, Beyerlein A, Hagopian WA, et al. Genetic contribution to the divergence in type 1 diabetes risk between children from the general population and children from affected families. *Diabetes*. 2019;68(4):847–857. doi:10.2337/db18-0882
- Aly TA, Ide A, Jahromi MM, et al. Extreme genetic risk for type 1A diabetes. *Proc Natl Acad Sci U S A*. 2006;103(38):14074–14079. doi:10.1073/pnas.0606349103
- Frommer L, Kahaly GJ. Type 1 diabetes and associated autoimmune diseases. *World J Diabetes*. 2020;11(11):527–539. doi:10.4239/wjdv.11.111.527
- Peters A. Screening for autoantibodies in type 1 diabetes: A call to action. *J Family Pract*. 2021;70(6 Suppl):S47–S52. doi:10.12788/jfp.0223
- Noiszewska K, Bossowski A, Zasim A, et al. 3 Screen ICA TM Elisa: A new tool for identifying pre-clinical diabetes in first-degree relatives of patients with type 1 diabetes (Pre-D1Abetes Study). In: *60th Annual Meeting of the European Society for Paediatric Endocrinology (ESPE)*. Vol. 95. Rome, Italy-Basel, Switzerland: S. Karger AG; 2022:1–241. doi:10.1159/000525606
- Greenbaum CJ. A key to T1D prevention: Screening and monitoring relatives as part of clinical care. *Diabetes*. 2021;70(5):1029–1037. doi:10.2337/db20-1112
- Craig ME, Codner E, Mahmud FH, et al. ISPAD Clinical Practice Consensus Guidelines 2022: Editorial. *Pediatr Diabetes*. 2022;23(8):1157–1159. doi:10.1111/pedi.13441
- Diabetes Poland. 2017 Guidelines on the management of diabetic patients: A position of Diabetes Poland. *Clin Diabetol*. 2017;6(A):1–80. doi:10.5603/DK.2017.0001
- Kass GV. An exploratory technique for investigating large quantities of categorical data. *Applied Statistics*. 1980;29(2):119. doi:10.2307/2986296
- Liese A, D'Agostino Jr RB, Hamman R, et al. The burden of diabetes mellitus among US youth: Prevalence estimates from the SEARCH for Diabetes in Youth Study. *Pediatrics*. 2006;118(4):1510–1518. doi:10.1542/peds.2006-0690
- Mehers KL, Gillespie KM. The genetic basis for type 1 diabetes. *Br Med Bull*. 2008;88(1):115–129. doi:10.1093/bmb/ldn045
- EURODIAB ACE Study Group; EURODIAB ACE substudy 2 study Group. Familial risk of type I diabetes in European children. *Diabetologia*. 1998;41(10):1151–1156. doi:10.1007/s001250051044
- Turtinen M, Härkönen T, Parkkola A, Ilonen J, Knip M. Characteristics of familial type 1 diabetes: Effects of the relationship to the affected family member on phenotype and genotype at diagnosis. *Diabetologia*. 2019;62(11):2025–2039. doi:10.1007/s00125-019-4952-8
- Pacaud D, Nucci AM, Cuthbertson D, et al. Association between family history, early growth and the risk of beta cell autoimmunity in children at risk for type 1 diabetes. *Diabetologia*. 2021;64(1):119–128. doi:10.1007/s00125-020-05287-1
- Verge CF, Gianani R, Kawasaki E, et al. Prediction of type I diabetes in first-degree relatives using a combination of insulin, GAD, and ICA512bdc/IA-2 autoantibodies. *Diabetes*. 1996;45(7):926–933. doi:10.2337/diab.45.7.926

25. Bonifacio E, Hummel M, Walter M, Schmid S, Ziegler AG. *IDDM1* and multiple family history of type 1 diabetes combine to identify neonates at high risk for type 1 diabetes. *Diabetes Care*. 2004;27(11):2695–2700. doi:10.2337/diacare.27.11.2695
26. Holstein A, Patzer O, Tiemann T, Vortherms J, Kovacs P. Number and sex ratio of children and impact of parental diabetes in individuals with type 1 diabetes. *Diabet Med*. 2012;29(10):1268–1271. doi:10.1111/j.1464-5491.2012.03618.x
27. Codner E. Estrogen and type 1 diabetes mellitus. *Pediatr Endocrinol Rev*. 2008;6(2):228–234. PMID:19202509.
28. Azulay RSDS, Porto LC, Silva DA, et al. Genetic ancestry inferred from autosomal and Y chromosome markers and HLA genotypes in type 1 diabetes from an admixed Brazilian population. *Sci Rep*. 2021;11(1):14157. doi:10.1038/s41598-021-93691-x
29. Parkkola A, Härkönen T, Ryhänen SJ, Ilonen J, Knip M; Finnish Pediatric Diabetes Register. Extended family history of type 1 diabetes and phenotype and genotype of newly diagnosed children. *Diabetes Care*. 2013;36(2):348–354. doi:10.2337/dc12-0445
30. Bizzarri C, Paladini A, Benevento D, Fierabracci A, Cappa M. Family history and ethnicity influencing clinical presentation of type 1 diabetes in childhood. *J Endocrinol Invest*. 2015;38(10):1141–1143. doi:10.1007/s40618-015-0317-4
31. Kuusela S, Keskinen P, Pokka T, et al. Extended family history of type 1 diabetes in HLA-predisposed children with and without islet autoantibodies. *Pediatr Diabetes*. 2020;21(8):1447–1456. doi:10.1111/pedi.13122
32. Parkkola A, Turtinen M, Härkönen T, Ilonen J, Knip M; Finnish Pediatric Diabetes Register. Family history of type 2 diabetes and characteristics of children with newly diagnosed type 1 diabetes. *Diabetologia*. 2021;64(3):581–590. doi:10.1007/s00125-020-05342-x
33. Petrelli A, Giovanzana A, Insalaco V, Phillips BE, Pietropaolo M, Giannoukakis N. Autoimmune inflammation and insulin resistance: Hallmarks so far and yet so close to explain diabetes endotypes. *Curr Diab Rep*. 2021;21(12):54. doi:10.1007/s11892-021-01430-3
34. Wilkin T. The convergence of type 1 and type 2 diabetes in childhood: The accelerator hypothesis. *Pediatr Diabetes*. 2012;13(4):334–339. doi:10.1111/j.1399-5448.2011.00831.x

# Blood biomarkers in acute ischemic stroke: The prognostic value of neutrophil-to-lymphocyte ratio and mean platelet volume

Turan Poyraz<sup>1,A–F</sup>, Özgül Vupa Çilengiroğlu<sup>2,A–D</sup>

<sup>1</sup> Department of Elderly Care, Vocational Schools of Health Services, Izmir University of Economics, Turkey

<sup>2</sup> Department of Statistics, Faculty of Science, Dokuz Eylül University, Izmir, Turkey

A – research concept and design; B – collection and/or assembly of data; C – data analysis and interpretation; D – writing the article; E – critical revision of the article; F – final approval of the article

Advances in Clinical and Experimental Medicine, ISSN 1899–5276 (print), ISSN 2451–2680 (online)

*Adv Clin Exp Med.* 2024;33(8):791–803

## Address for correspondence

Turan Poyraz

E-mail: turanpoyraz@gmail.com

## Funding sources

None declared

## Conflict of interest

None declared

Received on May 26, 2023

Reviewed on August 21, 2023

Accepted on September 13, 2023

Published online on December 20, 2023

## Cite as

Poyraz T, Vupa Çilengiroğlu Ö. Blood biomarkers in acute ischemic stroke: The prognostic value of neutrophil-to-lymphocyte ratio and mean platelet volume.

*Adv Clin Exp Med.* 2024;33(8):791–803.

doi:10.17219/acem/172239

## DOI

10.17219/acem/172239

## Copyright

Copyright by Author(s)

This is an article distributed under the terms of the Creative Commons Attribution 3.0 Unported (CC BY 3.0) (<https://creativecommons.org/licenses/by/3.0/>)

## Abstract

**Background.** The neutrophil-to-lymphocyte ratio (NLR) and mean platelet volume (MPV) reflect systemic inflammation, which plays an important role in the process of treating ischemic strokes. Few studies have evaluated the association between blood biomarkers and clinical outcomes in ischemic strokes in intensive care units (ICUs).

**Objectives.** This retrospective study aims to explore the relationship between blood biomarkers and the clinical outcomes of acute ischemic stroke (AIS) patients.

**Materials and methods.** Basic descriptive statistics of the patients admitted to the ICU with the diagnosis of AIS according to sociodemographic, clinical and laboratory findings were collected. Receiver operating characteristic (ROC) curve analysis was used to determine the cutoff point for NLR and MPV variables based on the diagnosis in statistical analyses and crosstab analyses of variables. The  $\chi^2$  and Fisher's exact tests were used to assess the statistical relationship between categorical variables. In addition, the odds ratio (OR) was utilized to show the strength of the relationship between the categorical NLR, MPV and modified Rankin Scale (mRS) variables. Finally, the Mann–Whitney U test was used to compare the medians of 2 independent groups.

**Results.** A total of 1,379 records were identified in the database search. Eighty-seven patients who met the inclusion criteria and were hospitalized in the ICU were included in the study. The optimal cutoff point was determined to be 4.0 for NLR and 9.0 for the MPV. A statistically significant relationship was found between high medians of the NLR and the MPV and unfavorable functional outcomes using a 5% significance level ( $p < 0.001$  and  $p < 0.001$ , respectively).

**Conclusions.** We showed that the NLR and MPV are associated with stroke severity, unfavorable functional outcomes and mortality in AIS. These findings provide new insights into the mechanisms and treatment strategies of AIS. The results show that these accessible values can be used as independent predictive biomarkers.

**Key words:** inflammation, prognosis, acute ischemic stroke, mean platelet volume, neutrophil-to-lymphocyte ratio

## Background

Our immune system carries out its defense function against harmful endogenous or exogenous factors with the functional cooperation of 2 main cell groups, collectively called leukocytes. Granulocytes and lymphocytes (agranulocytes) constitute the immune system's 2 cell groups. Granulocytes mainly include neutrophils, eosinophils, basophils, mast cells, dendritic cells, monocyte-macrophages, and phagocytes. Lymphocytes, on the other hand, consist of natural killer cells and some specialized cells in the T and B lymphocyte groups. Granulocytes directly inactivate pathogens. During these granulocyte functions, unlike lymphocytes, there is no need for mediator molecules or antigen presentation. Thanks to these features, they can actively display their functions from the first moments of life. Therefore, this innate immune response is called innate immunity. Lymphocytes, on the other hand, have acquired functional abilities, such as recognizing pathogenic structures and target molecules, keeping them in memory and synthesizing some specialized molecules to use when the time comes. Thus, they form the acquired immune system.<sup>1</sup> In situations that cause damage to our body, some cytokines, such as eicosanoids and leukotrienes, are secreted in the damaged areas, causing inflammation. This inflammation causes neutrophils to be directed to the area. Consequently, an inflammatory response develops in reaction to neutrophils, cytokines, dead pathogens, and cellular elements in the damaged tissue or site. In general, neutrophil counts do not increase in viral infections, while systemic infections or systemic inflammatory responses cause an increase in neutrophil counts in the blood.<sup>2</sup> Another inflammatory marker is the mean platelet volume (MPV), a measure of the mean platelet size that is used to determine the rate of platelet production and destruction in the bone marrow. Mean platelet volume is accepted as a marker of subclinical inflammation and inflammatory disease activity because platelets become active in the presence of inflammation and secrete pro-inflammatory and thrombotic factors. In the literature, many studies have shown a positive association between MPV, inflammation and coronary artery disease (CAD).<sup>3,4</sup>

Stroke is the 2<sup>nd</sup> leading cause of death and a major cause of disability worldwide.<sup>5</sup> Recovery from a stroke can take a very long time, and despite adequate treatment, this does not always result in a full recovery. Some studies have been conducted regarding the ability of various biomarkers to predict stroke prognosis. Fibrinogen levels have been associated with neurological deterioration in patients with acute ischemic stroke (AIS).<sup>6,7</sup> Interleukin-6 (IL-6) levels have been shown to be associated with stroke severity and functional outcomes during the first year of stroke.<sup>8</sup>

Post-stroke inflammation plays an important role in the pathogenesis of brain injury.<sup>9</sup> Inflammatory biomarkers have been associated with stroke severity and

clinical outcomes. For example, elevated neutrophil counts have been associated with larger infarct volumes,<sup>10</sup> and elevated leukocyte counts have been associated with higher initial stroke severity and worse short- and long-term clinical outcomes.<sup>11,12</sup> In addition, increased serum concentrations of high-sensitivity C-reactive protein (hsCRP) have been found to be associated with the risk of stroke recurrence and worse functional outcomes.<sup>13</sup> A number of neural substrates play an essential role in the pathophysiology of stroke and its relationship with immune responses. An important consideration is the delicate balance between pro-inflammatory and anti-inflammatory responses during AIS. Understanding the interaction between these 2 types of responses and the complex mechanisms that regulate this balance can offer valuable insights into potential therapeutic interventions aimed at modulating immune responses to optimize stroke recovery. The synergistic relationships between various inflammatory markers such as hsCRP and interleukins are highly suggestive of their contribution to the overall inflammatory environment in these complex processes, and, hence, the impact of the immune response on the ischemic environment of the brain. In ischemic stroke patients with elevated hsCRP levels, there is a significant association between high platelet counts and unfavorable functional outcomes. In contrast, this was not the case in AIS patients with low hsCRP levels. Therefore, co-administration of antiplatelet and anti-inflammatory therapy in patients with AIS with high hsCRP levels may be a rational approach.<sup>14</sup>

An inflammatory condition plays a vital role at all stages of the ischemic cascade. The energy deficit caused by the loss of the neurons' ability to synthesize adenosine triphosphate (ATP) is the main mechanism of cell death in the region of cerebral ischemia. Disruption of ATP synthesis also causes a decrease in glutamate reuptake and an increase in its extracellular amount. Excessive activation of glutamate receptors causes excitotoxicity and accumulation of Ca<sup>2+</sup> ions, leading to mitochondrial failure and apoptosis. The influx of Ca<sup>2+</sup> ions activates catabolic enzymes by producing arachidonic acid and increasing the production of reactive oxygen species (ROS), mainly in neurons. The excitotoxicity and growth of ROS activate microglia and astrocytes that secrete cytokines, chemokines and matrix metalloproteinases (MMPs).<sup>15,16</sup> These inflammatory mediators induce the expression of endothelial cell adhesion molecules such as P-selectin, E-selectin, endothelial leukocyte adhesion molecule-1 (ELAM-1), and intercellular cell adhesion molecule-1 (ICAM-1), so that the neutrophils infiltrate into the ischemic areas of the brain.<sup>17</sup> As a result of cell damage in the hypoxic and/or necrotic brain, damage-associated molecular patterns (DAMPs) and high-mobility group box 1 (HMGB-1) are released into the environment, activating astrocytes and microglia. The DAMP-HMGB-1s stimulate pattern recognition receptors (PRRs) such as TLRs in the blood-brain barrier (BBB), leading to extravasation of leukocytes



(primarily neutrophils, macrophages and lymphocytes). The activation of TLR leads to inflammation, MMP activation, blood–brain barrier (BBB) breakdown, and leukocyte extravasation.<sup>18</sup> These mediators increase the expression of adhesion molecules on cerebral endothelial cells, which promotes adhesion and infiltration of the blood-derived leukocytes (neutrophils, macrophages and lymphocytes) into ischemic brain tissues. Activated M1 microglial cells release various pro-inflammatory mediators such as TNF- $\alpha$ , IL-1 $\beta$  and IL-6, contributing to the permeability of many immune cells and resulting in BBB disruption. Further reduced blood flow decreases ATP levels and increases the levels of Ca<sup>2+</sup> and nitric oxide (NO), promoting free radical generation (ROS) and mitochondrial failure, which leads to cell death. Meanwhile, activated microglia/macrophages and infiltrated T cells also secrete some neuroprotective factors (e.g., IL-10 and TGF- $\beta$ ) that could suppress post-ischemic inflammation.<sup>19</sup> In this complex process, neutrophils infiltrating the ischemic/hypoxic tissue from the permeable BBB play a dominant role (Fig. 1).

The role of specific neuropharmacological adjuvants involved in neurochemical synaptic transmission and acting on brain plasticity processes in stroke may determine both our future therapeutic approach and the role of noninvasive brain stimulation techniques. One of the important questions in the coming years will be how modulation of neuronal substrates, such as the glutamatergic, noradrenergic and endocannabinoid systems, will have a curative effect on stroke in humans and, in particular, on the elimination of fear learning and anxiety disorders.<sup>20</sup> Understanding neurochemical synaptic transmission and brain plasticity processes, especially behavioral problems that may occur after stroke, may contribute to the correction of our abilities related to sensory perception inputs such as visuospatial attention, metacognitive abilities and objective performance gain. Regulation of neuronal substrates with neuromodulation techniques during attentional deployment is very important for understanding the effect of sensory input on objective performance and its atypical perceptual consequences.<sup>21</sup> The neurophysiological models developed regarding the shift of visual-spatial perception towards the right hemifield and deficiencies in perceiving left contralesional stimuli, especially in patients with stroke-related left hemispatial neglect. The regulation of neuronal substrates and their psychophysiological correlates were investigated using structural equation models calculated with discriminative electroencephalogram (EEG) measurements.<sup>22</sup>

Even with thrombolytic therapy in AIS, neuronal damage may not be prevented due to exaggerated inflammatory responses. Similar to peripheral molecular mimicry mechanisms, microglial activation may also be altered during ischemic stroke processes.<sup>23</sup> Increased astroglia and oligodendrocyte reactivity may reduce potential regenerative mechanisms of plasticity patterns, such as axonal growth, synaptic remodeling, remyelination, cortical remodeling, and reattachment of neural networks to healthy intact

tissue. Attenuation of the pro-inflammatory effects and strengthening of the anti-inflammatory effects after stroke may guide our future treatment strategies. In particular, antagonists of cascades driven by pro-inflammatory chemokines and allosteric agonists of cascades driven by anti-inflammatory chemokines can alter neuronal plasticity by affecting GABAergic neurotransmission.<sup>24</sup> Concerning the C-X-C chemokine ligand 12 (CXCL12)/C-X-C chemokine receptor type 4 (CXCR4)/C-X-C chemokine receptor type 7 (CXCR7) chemokine pathway, rats subjected to transient middle cerebral artery occlusion (tMCAO) have been shown to improve functional outcomes after the administration of an experimental molecule, a CXCR4 receptor antagonist and allosteric CXCR7 agonist.<sup>25</sup> In addition, similar effects have been confirmed after the exogenous administration of C-X-C chemokine ligand 1 (CX3CL1)/C-X-C chemokine receptor type 1 (CX3CR1) chemokines to wild-type mice.<sup>26</sup>

In summary, brain-resident immune cells such as microglia and astrocytes are activated to respond to injury. Subsequently, peripheral immune cells are activated and recruited to the brain to assist in the immune response. The constant influx of leukocytes leads to lymphocytopenia. This immunosuppression has an important contribution to increase the risk of post-stroke infections. The extent of these local and peripheral immune responses to a stroke is variable and plays an important role in determining patient outcomes and overall functional recovery in the acute and chronic phases after stroke.<sup>27</sup> Anxiety, depression and emotional disorders associated with stress have significant effects on both mental and physical health. The altered neurohormonal balance in AIS provides a controlled environment for examining the mechanisms underlying these disorders by identifying potential drug targets and treatment strategies within the framework of preclinical models. Therefore, understanding the biological mechanisms of neurobehavioral problems in both pre-ischemic and post-ischemic stroke may allow researchers to develop and test new therapeutic interventions.<sup>28</sup>

Another important research topic for AIS is reperfusion therapy. Reperfusion therapy aims to restore the blood flow of occluded blood vessels. However, successful recanalization is often associated with disruption of the BBB, leading to reperfusion injury. Delay in recanalization increases the risk of severe reperfusion injury, particularly cerebral edema and hemorrhage. With a better understanding of blood biomarkers and the biological mechanisms of stroke, the transient receptor potential melastatin-like subfamily member 4 (TRPM4) has emerged as an important drug target for the treatment of stroke and other autoimmune diseases. The TRPM4-blocking antibodies have been shown to ameliorate reperfusion injury and improve functional outcomes in animal models of early stroke reperfusion.<sup>29</sup>

Analyzing patient datasets and bioinformatic databases with artificial intelligence and machine learning will allow us to develop smart drugs on a molecular basis, to better

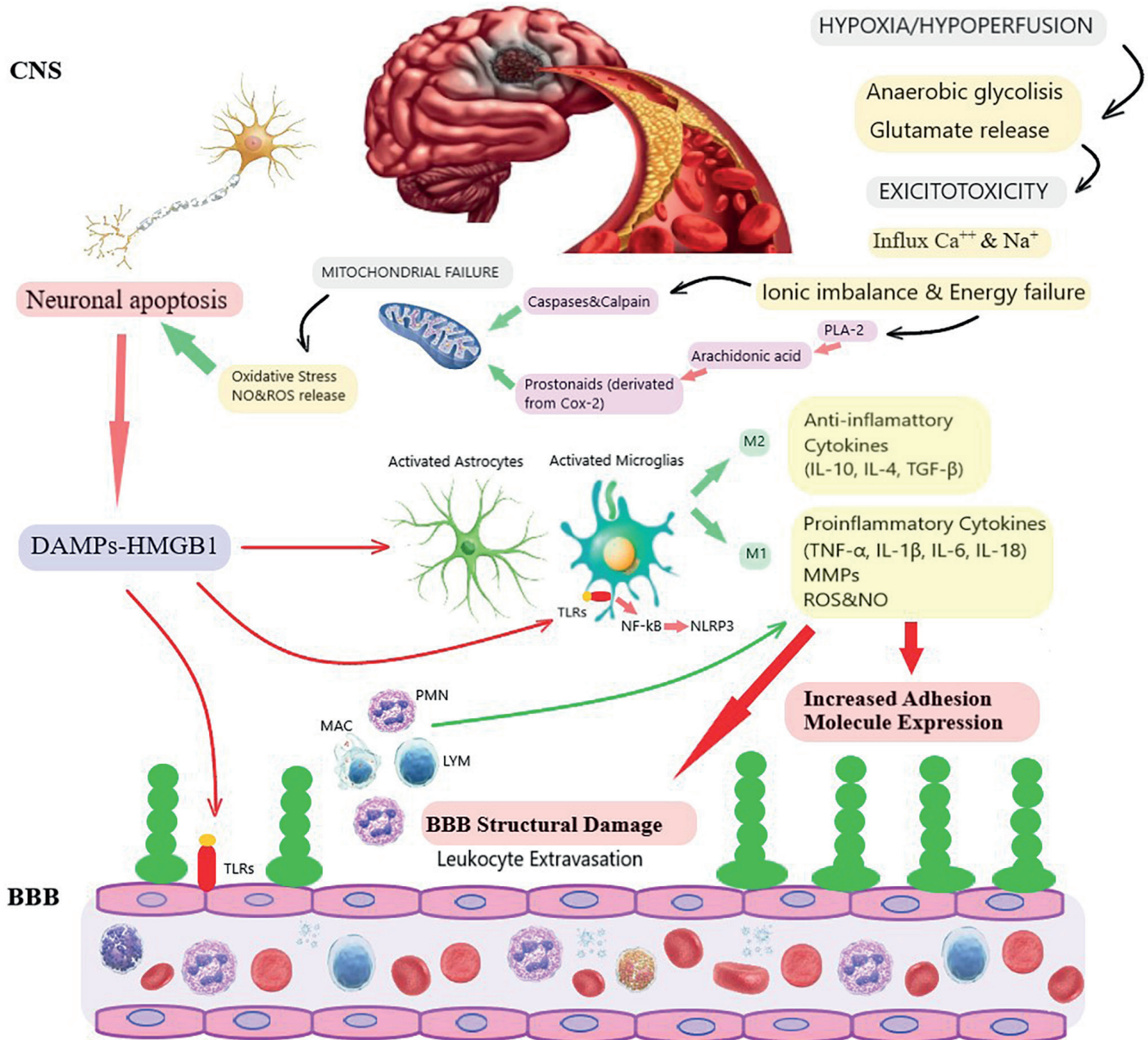


**Fig. 1.** Due to hypoxia, the deterioration in adenosine triphosphate (ATP) synthesis as a result of anaerobic glycolysis increases the reuptake of glutamate and its extracellular levels. With the overstimulation of glutamate receptors, excitotoxicity begins, and intracellular calcium ( $Ca^{2+}$ ) influx develops. The increase of  $Ca^{2+}$  ions leads to ionic imbalance and energy failure. Thus, it leads to arachidonic acid from phospholipase A-2 (PLA-2) activity and, consequently, to an increase in the level of prostanoids derived from cyclooxygenase-2 (Cox-2). Through the simultaneous caspase and calpain enzymatic system, intracellular free radical generation or reactive oxygen species (ROS) production is increased, resulting in mitochondrial failure. Mitochondrial failure leads to oxidative stress, nitric oxide (NO) synthesis, and ROS release, resulting in cellular damage (neuronal apoptosis). As a result of cell damage, damage-associated molecular patterns (DAMPs) and high-mobility group box 1 (HMGB-1) are released into the environment, activating astrocytes and microglia. The DAMP-HMGB-1s stimulate pattern recognition receptors (PRRs) such as TLRs in the blood-brain barrier (BBB), leading to extravasation of leukocytes (primarily neutrophils, macrophages and lymphocytes). By stimulating M1 microglia again via TLRs, pro-inflammatory cytokines such as tumor necrosis factor alpha (TNF- $\alpha$ ), interleukin (IL)-1 $\beta$ , IL-6, and IL-18 are released from nuclear factor kappa-light-chain-enhancer of activated B cells (NF-kB) via the nod-like receptor protein-3 (NLRP3) inflammasome, and the synthesis of matrix metalloproteases (MMPs), ROS, and NO is increased. These pro-inflammatory factors lead to structural damage and increase the expression of adhesion molecules such as P-selectin, E-selectin, endothelial leukocyte adhesion molecule (ELAM-1), and intercellular cell adhesion molecules-1 (ICAM-1) on cerebral endothelial cells causing the influx of blood-derived inflammatory cells such as neutrophils, macrophages and lymphocytes to the ischemic area. Extravasated PMLs from the peripheral circulation also trigger the pro-inflammatory process. T regulatory lymphocytes (Treg) and M2-activated microglia secrete anti-inflammatory cytokines such as IL-10, IL-4, and TGF- $\beta$ .

understand the pathogenesis and to discover new treatments for neuropsychiatric disorders. Interdisciplinary, synthesizable research models and their integration with biomechanics will be a milestone for our future treatment strategies.<sup>30</sup>

Stress and associated inflammation have been related to the activation of the metabolic system of tryptophan (Trp)-kynurenine (KYN), which visibly contributes to the development of pathological conditions, including neurological and psychiatric disorders. Mitochondria,

which are multifunctional organelles related to cellular energy, homeostasis, intracellular and intercellular signaling, and gene expression, and which are seen as the source of our life in a way, are structurally impaired in emotional disorders or biomechanical problems such as ischemia.<sup>31</sup> A number of gene polymorphisms have been found to contribute to laboratory aspirin resistance (AR), which is measured by platelet aggregation with arachidonic acid (AA) and adenosine diphosphate (ADP) in ischemic stroke patients. The effect of prostanoids, such as the AA pathway, in the pathogenesis of mitochondrial failure is well known.<sup>32</sup> The Trp–KYN metabolic system is closely linked to glutamate excitotoxicity, and blockade of this system can alleviate neuroinflammation by modifying microglia activation. As a result, there may be a therapeutic target for the treatment of neuroinflammatory conditions such as AIS, migraine and neuropathic pain.<sup>33</sup>

Rehabilitation of motor deficits after AIS is difficult. A series of impulses, such as mental practices and observation tasks, are believed to temporarily activate networks of neurons in the brain, known as mirror neurons and mentalization systems, to support healing. Understanding the effects of blood biomarkers on recovery, especially the change in rehabilitation level, may be the subject of further investigations.<sup>34</sup>

Experimental animal studies have also been conducted on the potential of xenografts, known as human umbilical mesenchymal stem cells (HUMSCs), in reducing inflammation and preventing tissue damage in chronic stroke patients, apart from treatment with rehabilitation or supportive interventions.<sup>35</sup>

The neutrophil-to-lymphocyte ratio (NLR) in whole blood analysis is accepted as a determinant of clinical/subclinical inflammation. In neurological diseases, studies on the prognostic value of NLR have been carried out, especially in diseases such as the spectrum of demyelinating diseases and ischemic stroke.<sup>36,37</sup> However, there is no consensus yet on what are the normal values of NLR, taking into account variables such as age, gender and ethnicity. A higher NLR has been associated with stroke severity and short-term mortality,<sup>38</sup> unfavorable functional outcomes, many post-stroke complications, including risk of intracerebral hemorrhage, and an increased risk of recurrent ischemic stroke.<sup>39–41</sup>

Until now, the studies have shown that NLR is associated with the severity of AIS and short-term functional outcomes; previous assessments of functional outcomes have been limited. In addition, there is no study in which easily measurable MPV values are compared with NLR and their prognostic value is analyzed. Determining the predictive value of these blood biomarkers, their interrelationships and their effects on the prognosis forms the basis of this study. Therefore, we conducted a single-center cross-sectional study to examine the relationship between blood biomarkers and stroke severity and to investigate the prognostic values of NLR and MPV in AIS patients.

## Objectives

The neuroinflammatory response has been shown to play an important role in the pathophysiology of ischemic stroke. The NLR has recently been reported as a potential novel biomarker for baseline inflammatory processes. However, data on MPV are insufficient. Appropriate clinical decision-making tools and models are required to take advantage of the predictive value of NLR and MPV, which can be useful in identifying and monitoring high-risk patients to guide early treatment and achieve better outcomes. Our knowledge about the role of NLR and MPV in the immunopathogenesis of AIS and their impact on clinical practice is also insufficient. Biomarkers that may reliably predict post-stroke outcomes are necessary to plan appropriate interventions and treatment modalities. Given the limited availability, temporal constraints and problems associated with technical infrastructure standardization of advanced neuroimaging, simple, routinely collected blood-based biomarkers are of enormous clinical and translational importance. This article aimed to provide a comprehensive overview of the role of NLR and MPV in AIS patients admitted to the intensive care unit (ICU), to compare them with clinical tests such as the modified Rankin Scale (mRS) and the National Institutes of Health Stroke Scale (NIHSS), and to provide perspectives on future research areas in order to better understand the role of these blood biomarkers in the prognosis, treatment options and classification of patients.

## Materials and methods

### Patients

Patients who were admitted to the Medifema Hospital Level 3 Neurology ICU with the diagnosis of AIS between 2013 and 2020 and were hospitalized within the first 24 h from the onset of symptoms were included in the study. The inclusion criteria were as follows:

1. No active infection or fever at the time of application;
2. No history of major surgery or trauma in the last 3 months;
3. No history of stroke in the last 6 months;
4. No known autoimmune/inflammatory disease or malignancy;
5. Hemorrhage was excluded using computed tomography (CT) or magnetic resonance imaging (MRI);
6. Not under immunosuppressive therapy; and
7. Patients whose data could be accessed from the information file were included. The flowchart of the study is shown in Fig. 2.

### Study data

In this retrospective study, sociodemographic and clinical characteristics used for database research were

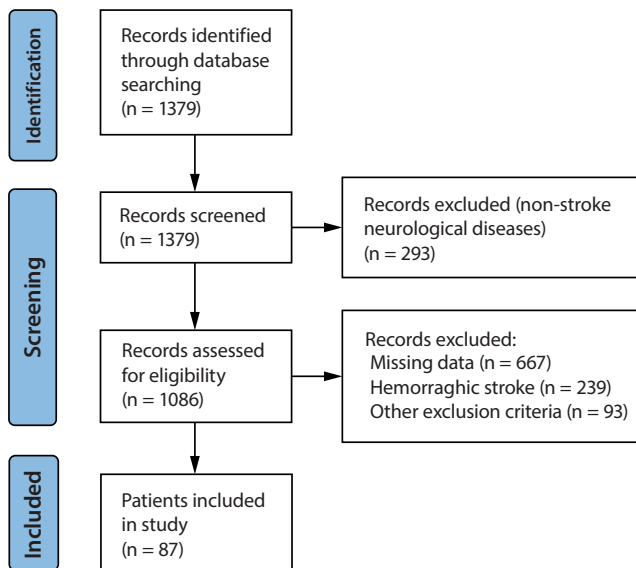


Fig. 2. Flowchart of the study

recorded using a data collection form. Data obtained from all patients at the time of admission and discharged from the ICU (or death of a patient) were taken into account. Demographic characteristics such as age, gender, medication history, medical history, comorbid diseases, and social habits (such as smoking and alcohol use) were recorded. The entrance hemogram and lipid profile of the patients in our hospital as well as the control hemogram values obtained at discharge were recorded as study data. The NLR and MPV values were reported according to hemogram results. Considering these characteristics, a total of 1,379 records were identified in the database search. Due to non-stroke diseases, 293 records were excluded. Additional 667 patients were excluded due to missing data, 239 patients due to hemorrhagic stroke, and 93 patients due to other exclusion criteria. Eighty-seven patients who met the inclusion criteria and were hospitalized in the ICU were included in the study.

## Clinical tests

The neurological evaluations of the patients were evaluated with NIHSS, and their stroke-related disabilities were evaluated with mRS. All patients were evaluated by the same neurologist throughout the study. A mRS score of 0–2 was considered a favorable functional result and a score >3 an unfavorable functional result. Patients were categorized according to NIHSS severity in mild (1–4), moderate (5–15), moderate to severe (16–20), and severe stroke (21–42).

## Classification of patients

The patients were classified into 3 subcategories according to the Bamford classification: anterior circulation,

posterior circulation and lacunar infarcts.<sup>42</sup> Although the results of cerebral brain imaging were not required for classification, they were confirmed radiologically (with CT and MRI).

## Statistical analyses

The sample size was calculated using G\*Power v. 3.1 (<https://www.psychologie.hhu.de/arbeitsgruppen/allgemeine-psychologie-und-arbeitspsychologie/gpower>). At 80% statistical power and an  $\alpha$ -value of 0.05 (significance level), the smallest sample size required to determine a 0.25 Cohen's *f* effect size was calculated as a total of 85 participants with one-way analysis of variance (ANOVA).<sup>43</sup> We included 87 patients in the final sample. Alpha indicates a type 1 error, in which probability of finding a significant effect when there is no significant effect. A smaller level of significance increases the sample size. The study data were analyzed using IBM SPSS (Windows, v. 26.0) software (IBM Corp., Armonk, USA). Descriptive statistics (mean (M), standard deviation (SD), median) were used for continuous variables, and frequency and percentage values were used for categorical variables. It is more appropriate to use the median without the M when the data distribution is not normal and to use the M with SD when the data distribution is normal. Usually, normally distributed data are expressed as  $M \pm SD$ . The receiver operating characteristic (ROC) curve analysis was used to determine the cutoff point for NLR and MPV variables, based on the diagnosis in statistical analyses and crosstab analyses of variables. With this analysis, continuous NLR and MPV variables were made categorically using statistical criteria such as sensitivity and specificity, and then used in relationship tests with other categorical variables. The  $\chi^2$  and Fisher's exact tests were used to find the statistical relationship between 2 categorical variables. In the  $R \times C$  tables for the  $\chi^2$  test statistic, the expected frequencies should not be less than 1. The expected frequencies in  $2 \times 2$  tables should be greater than 5. Otherwise, Fisher's exact test should be used. Another use of Fisher's exact test is when more than 20% of the expected frequencies are less than 5 in  $2 \times 2$  tables. In this study, demographic, clinical and laboratory findings based on the diagnosis were obtained with the  $\chi^2$  relationship test. In addition, Fisher's exact and  $\chi^2$  tests were used to evaluate the relationship between risk factors of mortality and demographic characteristics. Under the assumption of normal distribution, the t-test is used to compare the means of 2 independent groups. If the assumption cannot be met, nonparametric tests are used to compare medians. In this study, the Mann–Whitney U test (M–W) was used to compare the medians of 2 independent groups. The odds ratio (OR) is a statistic that shows the strength of the relationship between 2 categorical variables. The OR value can range from 0 to infinity. If the OR is less than 1, this variable is interpreted as a protective factor, if it is greater than 1, this variable is a risk factor, and if it is equal to 1, it is interpreted as having no effect. In this

study, OR statistics were used to show the strength of the association of NLR and MPV risk factors on mRS variables. A  $p$ -value  $<0.05$  was considered statistically significant.

## Ethics

This study was conducted in accordance with the World Medical Association Declaration of Helsinki. The study was approved by the İzmir Bakırçay University Non-Interventional Transactions Ethics Committee (approval No. 860/840, January 25, 2023).

## Results

In this study, the data of 87 patients who met the criteria and were hospitalized in the ICU were examined. Thirty (34.5%) female and 57 (65.5%) male patients were included, with a mean age of  $77.59 \pm 11.82$  (23–96). Eleven (12.6%) patients died during follow-up. The stroke type was anterior circulation in 54 (62.1%) patients, posterior circulation in 21 (24.1%) and lacunar stroke in 12 (13.8%). Clinical, demographic and medical history characteristics are summarized in Table 1. While mRS was evaluated in 2 classes as favorable (0–2) and unfavorable (3–6) functional outcomes, stroke severity was also evaluated using the NIHSS. The normality test of the continuous variables (Anderson–Darling) was performed within the scope of the study. According to this test, while low density lipoprotein (LDL) and high density lipoprotein (HDL) variables were normally distributed ( $p > 0.05$ ), other demographic, clinical and laboratory findings were non-normally distributed ( $p < 0.05$ ). Appropriate descriptive statistics (median or  $M \pm SD$ ) for these variables are summarized in Table 2. The NLR and MPV cutoff values for unfavorable functional outcomes (mRS: 3 and above) were determined separately with a ROC curve. The area under the ROC curve (AUC) provides an aggregated measure of performance across all possible classification thresholds. The AUC value ranges from 0 to 1. A model with 100% incorrect predictions has an AUC of 0, and a model with 100% correct predictions has an AUC of 1. The AUC for NLR was determined to be 94.7%. In addition, when the ROC curve was examined, it was decided that the optimal cutoff value was approx. 4, as the point where the highest sensitivity and specificity values were reached was between 3.33 and 4.37 on the ROC curve. For the value of 3.33, the sensitivity is 95% and the specificity is 89%, while for the value of 4.37, the sensitivity is 83% and the specificity is 99% (Fig. 3). With the selected value of 4, the sensitivity value will be between 83% and 95% and the specificity value will be between 89% and 99%. It is categorized as “0” for values below the cutoff point and “1” for values above the cut-off point for NLR to be used in crosstabs for statistical analysis. According to the results of the  $\chi^2$  test for the relationship between

**Table 1.** Frequency and percentage of patients according to clinical, demographic and medical history characteristics

	Variable	Frequency (f)	Percentage (%)
Gender	female	30	34.5
	male	57	65.5
Comorbidity	stroke	25	28.7
	diabetes mellitus	44	50.6
	cardiovascular diseases	29	33.3
	hypertension	70	80.5
	hyperlipidemia	46	52.9
	chronic renal failure	12	13.8
	obesity	10	11.5
Bamford classification	anterior infarct	54	62.1
	posterior infarct	21	24.1
	lacunar infarct	12	13.8
mRS	2	9	10.3
	3	31	35.6
	4	25	28.7
	5	11	12.6
	6	11	12.6
Habitation	smoking (active smoker)	12	13.8
	smoking (ex-smoker)	54	62.1
	never smoked	21	24.1
	alcohol (actively consuming)	6	6.69
	alcohol (consumed in the past)	31	35.6
	never consume	50	57.5
Medication	warfarin	4	4.6
	new oral anticoagulant	21	24.1
	antiaggregant	42	48.3
	antihypertensive	59	67.8
	statin	32	36.8
	insulin/oral anti-diabetic	19	21.8
Carotid stenosis	$<50$	35	40.2
	$\geq 50$	52	59.8
Posterior circulation disorder		18	20.7
Exitus		11	12.6

mRS – modified Rankin Scale.

diagnosis and NLR, the relationship between these 2 variables was determined at a 5% significance level ( $p < 0.05$ ). It was also observed that a NLR value above 4 was higher in those diagnosed with anterior ischemia (96.3%) and posterior ischemia (85.7%, Table 3).

In the ROC curve analysis performed for the cutoff value for MPV, the AUC was determined to be 84.9%. In addition, when the ROC curve was examined, it was decided that the optimal cutoff value was approx. 9, since the point where the highest sensitivity and specificity values were reached was between 8.80 and 9.05 on the ROC curve. For

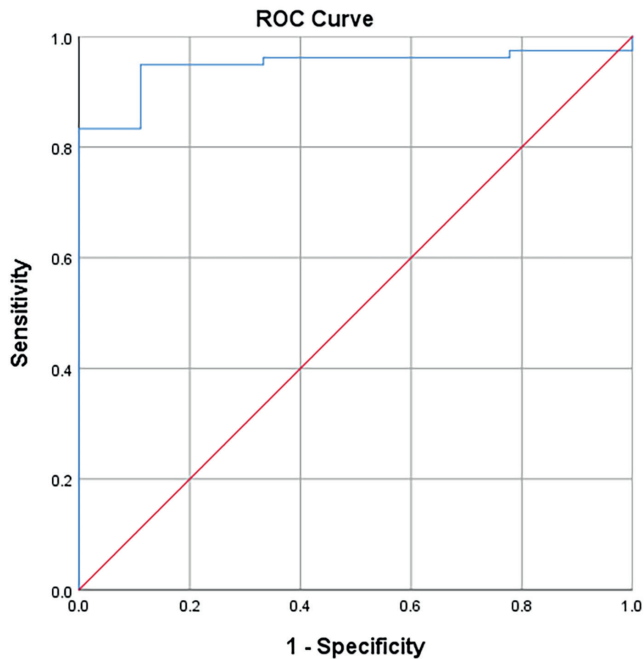


Fig. 3. Receiver operating characteristic (ROC) curve analysis for the neutrophil-to-lymphocyte ratio (NLR) to predict unfavorable functional outcomes (mRS  $\geq 3$ ) in acute ischemic stroke (AIS) patients. The area under the ROC curve (AUC) for NLR is 94.7. The ROC curve analysis in this study showed the optimal cutoff of 3.33 with a 95% sensitivity and 89% specificity, and the optimal cutoff 4.37 with a 83% sensitivity and 99% specificity

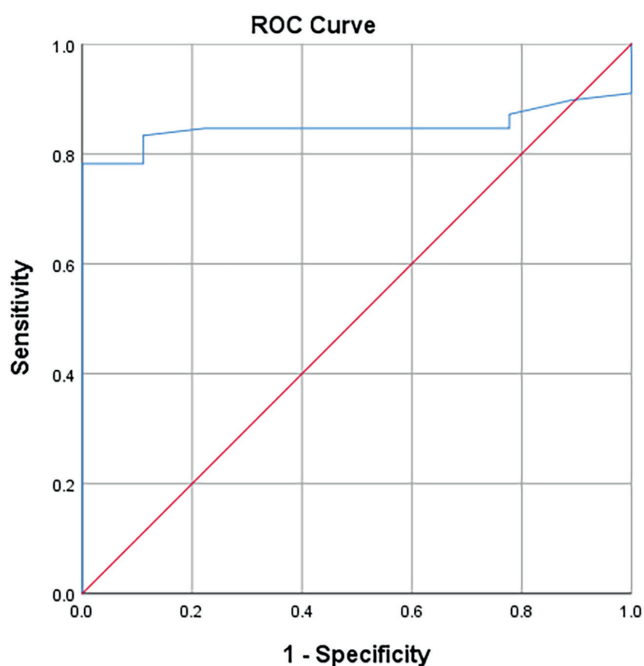


Fig. 4. Receiver operating characteristic (ROC) curve analysis for mean platelet volume (MPV) to predict unfavorable functional outcomes (mRS  $\geq 3$ ) in acute ischemic stroke (AIS) patients. The area under the ROC curve (AUC) for MPV is 84.9%. The ROC curve analysis in this study showed the optimal cutoff of 8.80 with a 83% sensitivity and 89% specificity and the optimal cutoff of 9.05 with a 78% sensitivity and 99% specificity

Table 2. Descriptive statistics of patients according to demographic, clinical and laboratory findings

Variable	Anderson-Darling p-value	Median or M $\pm$ SD	Min-max
Age	0.005*	78.5	23.00–96.00
NLR	0.048*	7.3	1.36–14.60
MPV	0.005*	11.6	5.90–17.90
LDL	0.877	145.28 $\pm$ 29.55	75.00–224.00
Triglycerides	0.005*	162.5	95.00–480.00
HDL	0.543	39.40 $\pm$ 8.99	16.00–63.00
NIHSS_Admission	0.005*	14.5	7.00–36.00
NIHSS_Exit	0.005*	8.5	3.00–40.00

\*  $p < 0.05$  (a statistically significant value, non-normal distribution); HDL – high density lipoprotein; LDL – low density lipoprotein; MPV – mean platelet volume; NIHSS – National Institute of Health Sciences Score; NLR – neutrophil-to-lymphocyte ratio; M  $\pm$ SD – mean  $\pm$  standard deviation.

the value of 8.80, the sensitivity is 83% and the specificity is 89%, while for the value of 9.05, the sensitivity is 78% and the specificity is 99% (Fig. 4). With the selected value of 9, the sensitivity value will be between 78% and 83%, and the specificity value will be between 89% and 99%. It is categorized as “0” for values below the cutoff point and “1” for values above the cutoff point for MPV to be used in crosstabs for statistical analysis. According to the results of the  $\chi^2$  test for the relationship between diagnosis and MPV, MPV value has a strong relationship with the diagnosis at a 5% significance level ( $p < 0.05$ ). It was also observed that a MPV value above 9 was higher in those diagnosed with anterior ischemia (90.7%) and posterior ischemia (71.4%, Table 3). In addition, the frequency table and  $\chi^2$  relationship test results between diagnosis and other variables such as gender, mRS, comorbidity, habits, drugs, rate of carotid and vertebral artery stenosis, and exitus are given in Table 3.

In the mRS data, it was determined that 78 patients (89.7%) had a severe stroke (mRS  $\geq 3$ ) compared to unfavorable functional outcomes, and this rate was also very high. At the same time, since the NLR and MPV variables were not normally distributed, the M–W test was used to assess the statistical difference between the medians of these variables in the mRS classes. Considering the small number of observations in the mRS class (mRS  $< 3$ ), it was decided that the distributions of these variables were approximately similar based on the histograms and central tendency measures (mode  $<$  median = M). According to this approach, a statistically significant difference was found between the NLR and MPV medians of the mRS groups with a 5% significance level ( $p = 0.000$  and  $p = 0.001$ , respectively). Based on these data, a statistically significant association was established between high medians of NLR and MPV and unfavorable functional outcomes (Table 4).

**Table 3.** The  $\chi^2$  relationship test results between diagnosis and demographic, clinical and laboratory findings

Demographic, clinical and laboratory findings		Diagnosis frequency						$\chi^2$	p-value
		anterior infarct		posterior infarct		lacunar infarct			
		f	(%)	f	(%)	f	(%)		
Gender	female	21	38.9	6	28.6	3	34.5	1.266	0.531
	male	33	61.1	15	71.4	9	75.0		
NLR	0	2	3.7	3	14.3	7	58.3	24.648	<0.001
	1	52	96.3	18	85.7	5	41.7		
MPV	0	5	9.3	6	28.6	10	83.3	29.717	<0.001
	1	49	90.7	15	71.4	2	16.7		
MRS	3+	52	96.3	20	95.2	6	50.0	23.620	<0.001
	1–2	2	3.7	1	4.8	6	50.0		
Stroke	absence	30	55.6	20	95.2	12	100	17.240	<0.001
	presence	24	44.4	1	4.8	0	0		
Hypertension	absence	4	7.4	11	52.4	2	16.7	19.525	<0.001
	presence	50	92.6	10	47.6	10	83.3		
Diabetes mellitus	absence	24	44.4	8	38.1	11	91.7	10.180	0.006*
	presence	30	55.6	13	61.9	1	8.3		
Hyperlipidemia	absence	15	27.8	17	81.0	9	75.0	21.498	<0.001
	presence	39	72.2	4	19.0	3	25.0		
Obesity	absence	46	85.2	19	90.5	12	100	2.224	0.329
	presence	8	14.8	2	9.5	0	0		
CRF	absence	43	79.6	20	95.2	12	100	5.325	0.070
	presence	11	20.4	1	4.8	0	0		
Cardiovascular disease	absence	31	57.4	16	76.2	11	91.7	6.315	0.043*
	presence	23	42.6	5	23.8	1	8.3		
Carotid stenosis	absence	32	59.3	3	14.3	0	0	22.088	<0.001
	presence	22	40.7	18	85.7	12	100		
Vertebral artery stenosis	absence	37	68.5	20	95.2	12	100	10.210	0.006*
	presence	17	31.5	1	4.8	0	0		
Exitus	no	43	79.6	21	100	12	100	7.695	0.021*
	yes	11	20.4	0	0	0	0		
Smoking	active smoker	2	3.7	2	9.5	8	66.7	35.225	<0.001
	ex-smoker	36	66.7	16	76.2	2	16.7		
	never smoked	16	29.6	3	14.3	2	16.7		
Insulin	absence	40	74.1	16	76.2	12	100	3.929	0.140
	presence	14	25.9	5	23.8	0	0		
Antiaggregant	absence	24	44.4	14	66.7	7	58.3	3.234	0.199
	presence	30	55.6	7	33.3	5	41.7		
Antihypertensive	absence	11	20.4	14	66.7	3	25.0	15.177	<0.001
	presence	43	79.6	7	33.3	9	75.0		
Statin	absence	26	48.1	19	90.5	10	83.3	14.072	<0.001
	presence	28	51.9	2	9.5	2	16.7		
NOAC	absence	37	68.5	17	81.0	12	100	5.706	0.058
	presence	17	31.5	4	19.0	0	0		

\* p < 0.05 (a statistically significant value, there is a relationship between variables); CRF – chronic renal failure; MPV – mean platelet volume; NLR – neutrophil-to-lymphocyte ratio; NOAC – new oral anticoagulant; f – frequency.

**Table 4.** Mann–Whitney U test results for the neutrophil-to-lymphocyte ratio (NLR) and mean platelet volume (MPV) variables according to the modified Rankin Scale (mRS) for a cutoff point of 3

Variable	mRS ≥ 3 (f = 78)		mRS < 3 (f = 9)		M–W	p-value
	median	mean rank	median	mean rank		
NLR	7.45	48.03	2.77	9.11	37.0	<0.001*
MPV	12.30	47.14	8.35	16.78	106.0	<0.001*

\* p < 0.05 (a statistically significant value, different medians); mRS ≥ 3 (an unfavorable functional outcome); mRS < 3 (a favorable functional outcome); M–W – Mann–Whitney U test.

**Table 5.** Fisher's exact test results for the relationship between unfavorable functional outcome and neutrophil-to-lymphocyte ratio (NLR) and mean platelet volume (MPV)

Variable		mRS ≥ 3	mRS < 3	OR (95% CI)	p-value
NLR	0	4 (5.1)	8 (88.9)	reference	
	1 (≥4)	74 (94.9)	1 (11.1)	148 (14.70–1490.31)	<0.001*
MPV	0	13 (16.7)	8 (88.9)	reference	
	1 (≥9)	65 (83.3)	1 (11.1)	40 (4.60–347.70)	<0.001*

\* p < 0.05 (a statistically significant value, different medians); mRS ≥ 3 (an unfavorable functional outcome); mRS < 3 (a favorable functional outcome); mRS – modified Rankin Scale; OR – odds ratio; 95% CI – 95% confidence interval.

**Table 6.** Mann–Whitney U test results of neutrophil-to-lymphocyte ratio (NLR) and mean platelet volume (MPV) variables according to the modified Rankin Scale (mRS) for a cutoff point of 6

Variable	mRS ≥ 6 (f = 11)		mRS < 6 (f = 76)		MW	p-value
	median	mean rank	median	mean rank		
NLR	9.6	74.77	6.45	39.55	79.5	<0.001*
MPV	15.35	73.91	11.20	39.67	89.0	<0.001*

\* p < 0.05 (a statistically significant value, different medians); M–W – Mann–Whitney U test.

The categorical values for NLR and MPV were cross-tabulated. The categorical values separated as mRS ≥ 3 (an unfavorable functional outcome) and mRS < 3 (a favorable functional outcome) were evaluated according to the cut-points of NLR and MPV, and a statistically significant relationship was found with a 5% significance level according to the Fisher's exact test (p = 0.000). According to this result, it can be determined that there is a significant relationship between unfavorable functional outcomes and high NLR and MPV values. The categorical relationship between unfavorable functional outcomes and cut-points of NLR and MPV values is summarized in Table 5.

Considering the small number of observations in the mRS class (mRS = 6), it was decided by looking at the histograms and central tendency measures that the distributions of these variables were approximately similar (mode < median = M). According to this approach, when the relationship between the median NLR and MPV values of patients who died (mRS = 6) and did not die (mRS < 6) during intensive care follow-up was examined, a statistically significant difference was found between the NLR medians of the mRS and the MPV medians with 95% confidence intervals (95% CIs) compared to the M–W test (p < 0.000 and p = 0.001, respectively). Based on these data, a relationship between stroke-related mortality and high NLR and MPV values can be confirmed (Table 6).

To summarize the results, both NLR and MPV variables were separately associated with unfavorable functional outcomes and mortality. In addition, the severity of stroke and clinical worsening increased as the levels of NLR and MPV increased.

## Discussion

The ischemic stroke injury is caused by a complex neuro-inflammatory process. Detailed analysis and correct understanding of this process are very important for the formation of current and reliable data on the natural history, severity, progression, and, ultimately, the treatment of the disease. In addition to determining the prognosis of the disease, the detection of easy and accessible blood biomarkers will enable the development of future-focused therapeutic strategies.

In this study, we particularly focused on the early and relatively easily detectable responses of this neuroinflammation. In particular, extravasation of neutrophils by the stimulation of PRRs by DAMPs, which occurs with BBB disruption and glial damage, was evaluated as an early neuroinflammatory response. However, since confirming this situation with another blood biomarker will provide a better understanding of the process, it was planned to evaluate the increased platelet volume in the circulation



simultaneously with the increase in neutrophils, to understand their effects on the prognosis, and as a result, to develop future-focused treatment strategies for this cascade.

Ischemic stroke is a life-threatening disease with high mortality and morbidity rates. There are several studies on the role of neuroinflammation in ischemic stroke.<sup>44</sup> Early determination of stroke severity is critical for disease management, follow-up and prognostic evaluation of patients. Studies have shown that parameters such as NLR, MPV, neutrophil, leukocyte, and platelet counts are significantly associated with survival.<sup>45</sup> The NLR and MPV have been reported as novel biomarkers, especially showing the initial inflammatory response, and are considered to be potential predictors of prognosis in patients with ischemic stroke.<sup>39</sup> The NLR is an easy, available, inexpensive, and practical indicator that can be calculated using complete blood count data. Studies have been conducted to show that the NLR can be used as a predictive marker not only for ischemic stroke but also for CAD,<sup>46</sup> colorectal cancer<sup>47</sup> and multiple sclerosis.<sup>48</sup>

In the pathogenesis of ischemic stroke, the first response to damaged tissue is the migration of neutrophils to the site. In this inflammatory reaction, which results in liquefactive necrosis, the released cytokines, eicosanoids and adhesion molecules regulate the migration of leukocytes. As a result of neutrophil activity in this region, it is thought that several proteolytic enzymes, such as acid phosphatase, cause damage not only in the core area of the infarct but also in the penumbra. Therefore, it is assumed that there is a correlation between neutrophil density and the severity of the injury. Although there are opinions to the contrary, several cytokines and growth factors secreted by T lymphocytes are suggested to be involved in the repair of inflamed tissue by modulating microglial activation.<sup>49</sup> Therefore, an increase in the NLR rate can be linked to a poor prognosis. It has been shown that the NLR hemogram values taken within the first 24 h in AIS patients with a mRS  $\geq 3$  or NIHSS  $\geq 15$ , which are considered unfavorable functional outcomes, are in line with the literature. The NLR has also been shown to be an independent risk factor for mortality, similar to unfavorable functional outcomes. It was thought that both the decrease in neutrophils and the increase in lymphocytes were effective in causing the relative decrease in the NLR values obtained from the hemograms of patients during the first week.

While some studies report the NLR cutoff values for unfavorable functional outcomes in AIS as 4.0,<sup>50</sup> 3.3<sup>40</sup> and 3.51,<sup>51</sup> some studies propose cutoff values such as 4.1 for the estimation of mortality in stroke patients.<sup>52</sup>

In our study, the NLR and MPV cutoff values for unfavorable functional outcomes were found to be 4.0 and 9.0, respectively, with the ROC curve. The MPV is an accurate measurement of volume-based platelet sizes calculated using hematology analyzers during routine hemogram testing. Significantly developed or abnormal thrombocytopoiesis, the result of activating factors on platelets, can lead

to changes in the ratios between MPV and platelet count (PLT). Therefore, possible applications of these parameters in the diagnosis of certain diseases have been proposed. In addition, MPV is associated with platelet activation and is therefore considered a marker of platelet activity.<sup>53</sup> High MPV values are observed in patients with acute cerebrovascular ischemia, as well as in some inflammatory diseases such as ischemic heart disease,<sup>54</sup> some respiratory diseases and rheumatoid arthritis.<sup>55</sup> Individuals with high MPV values are at greater risk of acute stroke than those with normal MPV values. Studies have shown a decrease in platelet values along with an increase in MPV values.<sup>56</sup> Although no significant correlation was observed between 6-month survival and the evaluation of prognosis, higher mortality rates were reported in patients with high MPV values. Therefore, the use of MPV as a prognostic marker has been suggested.<sup>57</sup> In our study, it was observed that MPV values were high in patients with unfavorable functional outcomes (mRS  $\geq 3$ ). This risk was found to be more pronounced in patients with an MPV value  $\geq 9$ . It was found that high MPV was associated with unfavorable functional outcomes and mortality.

In our study, a statistically significant relationship was found between the diagnosis (anterior, posterior and lacunar) and risk factors such as stroke, hypertension, diabetes mellitus, hyperlipidemia, chronic renal failure (CRF), carotid stenosis, vertebral artery stenosis, exitus, smoking, antihypertensive therapy, and statin therapy. In addition, a statistical relationship was found between mRS and NLR and between mRS and MPV variables.

In addition to the use of existing stroke risk factors, NLR and MPV have the potential to be used as an easy, accessible and low-cost prognostic scale. While clinical assessment scales such as the NIHSS and mRS are of great prognostic importance, simple laboratory markers can guide the course and severity of the disease. In ICUs, where prognostic assessment is of greater importance, there may be some confusing factors that determine the prognosis of the disease, including nosocomial infections, electrolyte disorders and organ failures.<sup>58</sup> However, when these conditions are excluded, independent clinical laboratory tests that can be clinically correlated with stroke severity and an unfavorable functional outcome can guide clinicians in establishing a global decision-making framework.

## Limitations

The fact that this study was conducted in stroke patients admitted to the ICU increased the likelihood of certain infections that could affect neutrophil and lymphocyte counts. However, other clinical and laboratory parameters related to infection were strictly controlled for in all patients, and these processes were excluded. However, it should be kept in mind that the length of stay in the ICU may be prolonged, and therefore the risk of infections may increase. The limitations of our study include its


retrospective nature, very strict exclusion criteria for the reliability of the file data, the selection of participants from only one institution, and the relatively small sample size. With larger sample sizes, prospective follow-up studies and multicenter measurements, possible estimations can be made more powerful.

## Conclusions

The results demonstrate the importance of the inflammatory response in the pathophysiology of both mortality and stroke severity. Increasing evidence has shown that the inflammatory response can provoke cell death following ischemic cerebral injury, as well as play a beneficial role by serving a complex function in the pathophysiologic process. As the molecular-based pathogenesis of ischemic stroke is understood, our future-focused treatment strategies will be updated. Therefore, it is necessary to investigate the experimental drugs that support the anti-inflammatory process and suppress the pro-inflammatory response.

### ORCID iDs

Turan Poyraz  <https://orcid.org/0000-0002-5928-8614>

Özgül Vupa Çilengiroğlu  <https://orcid.org/0000-0003-0181-8376>

### References

- Artis D, Spits H. The biology of innate lymphoid cells. *Nature*. 2015; 517(7534):293–301. doi:10.1038/nature14189
- Liew PX, Kubes P. The neutrophil's role during health and disease. *Physiol Rev*. 2019;99(2):1223–1248. doi:10.1152/physrev.00012.2018
- Korniluk A, Koper-Lenkiewicz OM, Kamińska J, Kemon H, Dymicka-Piekarska V. Mean platelet volume (MPV): New perspectives for an old marker in the course and prognosis of inflammatory conditions. *Mediators Inflamm*. 2019;2019:9213074. doi:10.1155/2019/9213074
- Gasparyan YA, Ayzvayan L, Mikhailidis PD, Kitis DG. Mean platelet volume: A link between thrombosis and inflammation? *Curr Pharm Des*. 2011;17(1):47–58. doi:10.2174/138161211795049804
- Donkor ES. Stroke in the 21<sup>st</sup> century: A snapshot of the burden, epidemiology, and quality of life. *Stroke Res Treat*. 2018;2018:3238165. doi:10.1155/2018/3238165
- Katan M, Luft A. Global burden of stroke. *Semin Neurol*. 2018;38(2): 208–211. doi:10.1055/s-0038-1649503
- Lee SJ, Hong JM, Lee SE, et al. Association of fibrinogen level with early neurological deterioration among acute ischemic stroke patients with diabetes. *BMC Neurol*. 2017;17(1):101. doi:10.1186/s12883-017-0865-7
- Shaafi S, Sharifipour E, Rahmanifar R, et al. Interleukin-6, a reliable prognostic factor for ischemic stroke. *Iran J Neurol*. 2014;13(2):70–76. PMID:25295149. PMCID:PMC4187333.
- Jin R, Yang G, Li G. Inflammatory mechanisms in ischemic stroke: Role of inflammatory cells. *J Leukoc Biol*. 2010;87(5):779–789. doi:10.1189/jlb.1109766
- Buck BH, Liebeskind DS, Saver JL, et al. Early neutrophilia is associated with volume of ischemic tissue in acute stroke. *Stroke*. 2008;39(2): 355–360. doi:10.1161/STROKEAHA.107.490128
- Kammersgaard LP, Jørgensen HS, Nakayama H, Reith J, Raaschou HO, Olsen TS. Leukocytosis in acute stroke: Relation to initial stroke severity, infarct size, and outcome (The Copenhagen Stroke Study). *J Stroke Cerebrovasc Dis*. 1999;8(4):259–263. doi:10.1016/S1052-3057(99)80076-7
- Quan K, Wang A, Zhang X, Wang Y. Leukocyte count and adverse clinical outcomes in acute ischemic stroke patients. *Front Neurol*. 2019;10:1240. doi:10.3389/fneur.2019.01240
- Li J, Zhao X, Meng X, et al. High-sensitive C-reactive protein predicts recurrent stroke and poor functional outcome: Subanalysis of the clopidogrel in high-risk patients with acute non-disabling cerebrovascular events trial. *Stroke*. 2016;47(8):2025–2030. doi:10.1161/STROKEAHA.116.012901
- Liu F, Yang P, Wang Y, et al. HS-CRP modifies the prognostic value of platelet count for clinical outcomes after ischemic stroke. *J Am Heart Assoc*. 2023;12(14):e030007. doi:10.1161/JAHA.123.030007
- Simats A, Garcia-Berrococo T, Montaner J. Neuroinflammatory biomarkers: From stroke diagnosis and prognosis to therapy. *Biochim Biophys Acta Mol Basis Dis*. 2016;1862(3):411–424. doi:10.1016/j.bbdis.2015.10.025
- Pawluk H, Woźniak A, Grzešek G, et al. The role of selected pro-inflammatory cytokines in pathogenesis of ischemic stroke. *Clin Interv Aging*. 2020;15:469–484. doi:10.2147/CIA.S233909
- Ramiro L, Simats A, Garcia-Berrococo T, Montaner J. Inflammatory molecules might become both biomarkers and therapeutic targets for stroke management. *Ther Adv Neurol Disord*. 2018;11:1756286418789340. doi:10.1177/1756286418789340
- Gülke E, Gelderblom M, Magnus T. Danger signals in stroke and their role on microglia activation after ischemia. *Ther Adv Neurol Disord*. 2018;11:175628641877425. doi:10.1177/1756286418774254
- Thapa K, Shivam K, Khan H, et al. Emerging targets for modulation of immune response and inflammation in stroke. *Neurochem Res*. 2023;48(6):1663–1690. doi:10.1007/s11064-023-03875-2
- Battaglia S, Di Fazio C, Vicario CM, Avenanti A. Neuropharmacological modulation of N-methyl-D-aspartate, noradrenaline and endocannabinoid receptors in fear extinction learning: Synaptic transmission and plasticity. *Int J Mol Sci*. 2023;24(6):5926. doi:10.3390/ijms24065926
- Trajkovic J, Di Gregorio F, Avenanti A, Thut G, Romei V. Two oscillatory correlates of attention control in the alpha-band with distinct consequences on perceptual gain and metacognition. *J Neurosci*. 2023;43(19):3548–3556. doi:10.1523/JNEUROSCI.1827-22.2023
- Di Gregorio F, Petrone V, Casanova E, et al. Hierarchical psychophysiological pathways subtend perceptual asymmetries in neglect. *Neuroimage*. 2023;270:119942. doi:10.1016/j.neuroimage.2023.119942
- Poyraz T. Miller–Fisher syndrome associated with COVID-19: A history of molecular mimicry and an up-to-date review of the literature. *Cureus*. 2023;15(8):e43111. doi:10.7759/cureus.43111
- Caleo M. Rehabilitation and plasticity following stroke: Insights from rodent models. *Neuroscience*. 2015;311:180–194. doi:10.1016/j.neuroscience.2015.10.029
- Michalettos G, Walter HL, Antunes ARP, Wieloch T, Talhada D, Ruscher K. Effect of anti-inflammatory treatment with AMD3100 and CX3CR1 deficiency on GABAA receptor subunit and expression of glutamate decarboxylase isoforms after stroke. *Mol Neurobiol*. 2021;58(11): 5876–5889. doi:10.1007/s12035-021-02510-x
- Ruscher K, Kuric E, Liu Y, et al. Inhibition of CXCL12 signaling attenuates the post-ischemic immune response and improves functional recovery after stroke. *J Cereb Blood Flow Metab*. 2013;33(8):1225–1234. doi:10.1038/jcbfm.2013.71
- Zera KA, Buckwalter MS. The local and peripheral immune responses to stroke: Implications for therapeutic development. *Neurotherapeutics*. 2020;17(2):414–435. doi:10.1007/s13311-020-00844-3
- Tanaka M, Szabó Á, Vécsei L. Preclinical modeling in depression and anxiety: Current challenges and future research directions. *Adv Clin Exp Med*. 2023;32(5):505–509. doi:10.17219/acem/165944
- Chen B, Wei S, Low SW, et al. TRPM4 blocking antibody protects cerebral vasculature in delayed stroke reperfusion. *Biomedicines*. 2023;11(5):1480. doi:10.3390/biomedicines11051480
- Tanaka M, Szabó Á, Vécsei L. Integrating armchair, bench, and bedside research for behavioral neurology and neuropsychiatry: Editorial. *Biomedicines*. 2022;10(12):2999. doi:10.3390/biomedicines10122999
- Tanaka M, Szabó Á, Spekker E, Polyák H, Tóth F, Vécsei L. Mitochondrial impairment: A common motif in neuropsychiatric presentation? The link to the tryptophan–kynurenine metabolic system. *Cells*. 2022;11(16):2607. doi:10.3390/cells11162607
- Ikonnikova A, Anisimova A, Galkin S, et al. Genetic association study and machine learning to investigate differences in platelet reactivity in patients with acute ischemic stroke treated with aspirin. *Biomedicines*. 2022;10(10):2564. doi:10.3390/biomedicines10102564

33. Tajti J, Szok D, Csáti A, Szabó Á, Tanaka M, Vécsei L. Exploring novel therapeutic targets in the common pathogenic factors in migraine and neuropathic pain. *Int J Mol Sci.* 2023;24(4):4114. doi:10.3390/ijms24044114
34. Abdullahi A, Wong TWL, Ng SSM. Rehabilitation of severe impairment in motor function after stroke: Suggestions for harnessing the potentials of mirror neurons and the mentalizing systems to stimulate recovery. *Brain Sci.* 2022;12(10):1311. doi:10.3390/brainsci12101311
35. Fu YS, Yeh CC, Chu PM, Chang WH, Lin MYA, Lin YY. Xenograft of human umbilical mesenchymal stem cells promotes recovery from chronic ischemic stroke in rats. *Int J Mol Sci.* 2022;23(6):3149. doi:10.3390/ijms23063149
36. Demirci S, Demirci S, Kutluhan S, Koyuncuoglu HR, Yurekli VA. The clinical significance of the neutrophil-to-lymphocyte ratio in multiple sclerosis. *Int J Neurosci.* 2015;126(8):700–706. doi:10.3109/00207454.2015.1050492
37. Zahorec R. Neutrophil-to-lymphocyte ratio, past, present and future perspectives. *Bratisl Med J.* 2021;122(07):474–488. doi:10.4149/BLL\_2021\_078
38. Tokgoz S, Keskin S, Kayrak M, Seyithanoglu A, Ogmegul A. Is neutrophil/lymphocyte ratio predict to short-term mortality in acute cerebral infarct independently from infarct volume? *J Stroke Cerebrovasc Dis.* 2014;23(8):2163–2168. doi:10.1016/j.jstrokecerebrovasdis.2014.04.007
39. Xue J, Huang W, Chen X, et al. Neutrophil-to-lymphocyte ratio is a prognostic marker in acute ischemic stroke. *J Stroke Cerebrovasc Dis.* 2017;26(3):650–657. doi:10.1016/j.jstrokecerebrovasdis.2016.11.010
40. Giede-Jeppe A, Madžar D, Sembill JA, et al. Increased neutrophil-to-lymphocyte ratio is associated with unfavorable functional outcome in acute ischemic stroke. *Neurocrit Care.* 2020;33(1):97–104. doi:10.1007/s12028-019-00859-5
41. Światońska M, Piekus-Słomka N, Słomka A, Sokal P, Żekanowska E, Lattanzi S. Neutrophil-to-lymphocyte ratio and symptomatic hemorrhagic transformation in ischemic stroke patients undergoing revascularization. *Brain Sci.* 2020;10(11):771. doi:10.3390/brainsci10110771
42. Bamford J, Sandercock P, Dennis M, et al. A prospective study of acute cerebrovascular disease in the community: The Oxfordshire Community Stroke Project 1981–86. 1. Methodology, demography and incident cases of first-ever stroke. *J Neurol Neurosurg Psychiatry.* 1988;51(11):1373–1380. doi:10.1136/jnnp.51.11.1373
43. Feng J, Lu X, Li H, Wang S. High neutrophil-to-lymphocyte ratio is a significant predictor of depressive symptoms in maintenance hemodialysis patients: A cross-sectional study. *BMC Psychiatry.* 2022;22(1):313. doi:10.1186/s12888-022-03963-7
44. Stoll G, Nieswandt B. Thrombo-inflammation in acute ischaemic stroke: Implications for treatment. *Nat Rev Neurol.* 2019;15(8):473–481. doi:10.1038/s41582-019-0221-1
45. Adiguzel A, Arsava EM, Topcuoglu MA. Temporal course of peripheral inflammation markers and indexes following acute ischemic stroke: Prediction of mortality, functional outcome, and stroke-associated pneumonia. *Neurol Res.* 2022;44(3):224–231. doi:10.1080/01616412.2021.1975222
46. Fang YN, Tong MS, Sung PH, et al. Higher neutrophil counts and neutrophil-to-lymphocyte ratio predict prognostic outcomes in patients after non-atrial fibrillation-caused ischemic stroke. *Biomed J.* 2017;40(3):154–162. doi:10.1016/j.bj.2017.03.002
47. Walsh SR, Cook EJ, Goulder F, Justin TA, Keeling NJ. Neutrophil-lymphocyte ratio as a prognostic factor in colorectal cancer. *J Surg Oncol.* 2005;91(3):181–184. doi:10.1002/jso.20329
48. Hasselbalch I, Søndergaard H, Koch-Henriksen N, et al. The neutrophil-to-lymphocyte ratio is associated with multiple sclerosis. *Mult Scler J Exp Transl Clin.* 2018;4(4):205521731881318. doi:10.1177/2055217318813183
49. Zhao L, Dai Q, Chen X, et al. Neutrophil-to-lymphocyte ratio predicts length of stay and acute hospital cost in patients with acute ischemic stroke. *J Stroke Cerebrovasc Dis.* 2016;25(4):739–744. doi:10.1016/j.jstrokecerebrovasdis.2015.11.012
50. Boz PB, Boz M, Acar D, Şanlı ZS, Evlice A, Giray S. The effect of neutrophil to lymphocyte and neutrophil to platelet ratios on prognosis in stroke patients. *Dicle Tıp Dergisi.* 2022;49(4):558–564. doi:10.5798/dicletip.1220732
51. Chen C, Gu L, Chen L, et al. Neutrophil-to-lymphocyte ratio and platelet-to-lymphocyte ratio as potential predictors of prognosis in acute ischemic stroke. *Front Neurol.* 2021;11:525621. doi:10.3389/fneur.2020.525621
52. Celikbilek A, Ismailogullari S, Zararsiz G. Neutrophil to lymphocyte ratio predicts poor prognosis in ischemic cerebrovascular disease: Neutrophil to lymphocyte ratio in ischemic stroke. *J Clin Lab Anal.* 2014;28(1):27–31. doi:10.1002/jcla.21639
53. Ntoliou P, Papanas N, Nena E, et al. Mean platelet volume as a surrogate marker for platelet activation in patients with idiopathic pulmonary fibrosis. *Clin Appl Thromb Hemost.* 2016;22(4):346–350. doi:10.1177/1076029615618023
54. Slavka G, Perkmann T, Haslacher H, et al. Mean platelet volume may represent a predictive parameter for overall vascular mortality and ischemic heart disease. *Arterioscler Thromb Vasc Biol.* 2011;31(5):1215–1218. doi:10.1161/ATVBAHA.110.221788
55. Şahin A, Yetişgin A, Şahin M, Durmaz Y, Cengiz A. Can mean platelet volume be a surrogate marker of inflammation in rheumatic diseases? *West Indian Med J.* 2015;65(1):165–169. doi:10.7727/wimj.2014.202
56. Greisenegger S, Endler G, Hsieh K, Tentschert S, Mannhalter C, Lalouschek W. Is elevated mean platelet volume associated with a worse outcome in patients with acute ischemic cerebrovascular events? *Stroke.* 2004;35(7):1688–1691. doi:10.1161/01.STR.0000130512.81212.a2
57. O'Malley T, Langhorne P, Elton RA, Stewart C. Platelet size in stroke patients. *Stroke.* 1995;26(6):995–999. doi:10.1161/01.STR.26.6.995
58. Christensen H, Boysen G. C-reactive protein and white blood cell count increases in the first 24 hours after acute stroke. *Cerebrovasc Dis.* 2004;18(3):214–219. doi:10.1159/000079944



# Taxifolin as a novel therapeutic agent for epileptic seizures induced by caffeine-induced oxidative stress in rats

Hasan Yasar<sup>1,A,D–F</sup>, Durdu Altuner<sup>2,C,E,F</sup>, Seval Bulut<sup>2,C,E,F</sup>, Betül Cicek<sup>3,D,F</sup>,  
Cebrail Gursul<sup>3,E,F</sup>, Mehmet Kuzucu<sup>4,B,F</sup>, Halis Suleyman<sup>2,A,D–F</sup>

<sup>1</sup> Department of Neurology, Faculty of Medicine, Erzincan Binali Yıldırım University, Turkey

<sup>2</sup> Department of Pharmacology, Faculty of Medicine, Erzincan Binali Yıldırım University, Turkey

<sup>3</sup> Department of Physiology, Faculty of Medicine, Erzincan Binali Yıldırım University, Turkey

<sup>4</sup> Department of Molecular Biology, Faculty of Arts and Sciences, Erzincan Binali Yıldırım University, Turkey

A – research concept and design; B – collection and/or assembly of data; C – data analysis and interpretation;

D – writing the article; E – critical revision of the article; F – final approval of the article

Advances in Clinical and Experimental Medicine, ISSN 1899–5276 (print), ISSN 2451–2680 (online)

*Adv Clin Exp Med.* 2024;33(8):805–815

## Address for correspondence

Halis Suleyman

E-mail: halis.suleyman@gmail.com

## Funding sources

None declared

## Conflict of interest

None declared

Received on December 18, 2022

Reviewed on April 12, 2023

Accepted on September 18, 2023

Published online on November 14, 2023

## Abstract

**Background.** Epilepsy is a severe neurological disease that results from excessive and/or synchronized neuronal activity in the brain, and oxidative stress plays a role in its pathogenesis. Taxifolin is a flavonoid that exhibits antioxidant activity.

**Objectives.** To investigate the effects of taxifolin on caffeine-induced epileptic seizures in rats and reveal the role of antioxidant activity in antiepileptic therapy.

**Materials and methods.** Forty rats were divided into 4 groups (n = 6/group): caffeine 300 mg/kg group (CG), taxifolin 50 mg/kg + caffeine 300 mg/kg group (TCG), 2 mg/kg diazepam + 300 mg/kg caffeine group (DCG), and a healthy group (HG). Taxifolin was given to the TCG, and diazepam was given to the DCG orally. One hour later, caffeine was injected intraperitoneally into the CG, TCG and DCG rats. The time between the caffeine injection and the contractions (the latency period) was determined. Animals were euthanized 1 h after caffeine injection, and brain tissues were biochemically examined for oxidants and antioxidants.

**Results.** Taxifolin and diazepam prolonged the latency period to a similar extent (p = 0.549), while taxifolin was more successful in preventing mortality. Taxifolin suppressed the caffeine-induced increase in myeloperoxidase, total oxidant status and oxidative stress index, and decreased total glutathione, superoxide dismutase and total antioxidant status more effectively than diazepam (p < 0.05).

**Conclusions.** We showed the relationship between antioxidant activity and epilepsy treatment, and demonstrated that taxifolin may be useful for treating epilepsy.

**Key words:** antioxidants, diazepam, epilepsy, taxifolin, oxidative stress

## Cite as

Yasar H, Altuner D, Bulut S, et al. Taxifolin as a novel therapeutic agent for epileptic seizures induced by caffeine-induced oxidative stress in rats. *Adv Clin Exp Med.* 2024;33(8):805–815. doi:10.17219/acem/172448

## DOI

10.17219/acem/172448

## Copyright

Copyright by Author(s)

This is an article distributed under the terms of the Creative Commons Attribution 3.0 Unported (CC BY 3.0) (<https://creativecommons.org/licenses/by/3.0/>)

## Background

The International League Against Epilepsy (ILAE) defines epileptic seizures as abnormal excessive and/or synchronized neuronal activity that occurs transiently in the brain.<sup>1</sup> Epilepsy is a severe neurological disorder with a 1% global prevalence<sup>2</sup> and is categorized by the ILAE as focal onset, generalized onset, unknown onset, and unclassified onset.<sup>3</sup> Experimental seizure models preferred today are generalized tonic-clonic seizures, generalized absence seizures and status epilepticus,<sup>4</sup> which are created using various chemicals, with systemically administered substances demonstrated to cause generalized tonic-clonic seizures.<sup>5</sup> The systemic administration of caffeine, as a methylxanthine derivative, has been used in a generalized tonic-clonic seizure model.<sup>6</sup>

The pathogenesis of epilepsy has yet to be fully clarified. However, an increase in reactive oxygen species (ROS) in epilepsy is thought to cause nerve cell mitochondrial dysfunction and oxidative damage.<sup>7</sup> Mitochondria are organelles that play vital roles in the maintenance and regulation of all brain functions, including neuroinflammation, neuroplasticity, oxidative stress, and apoptosis.<sup>8</sup> Most ROS, mainly superoxide anions, are products of mitochondrial respiration produced during electron flow in the mitochondrial electron transfer chain. The superoxide anion concentration in the mitochondrial matrix is 5–10 times higher than in the cytosol and the nucleus.<sup>9</sup> Therefore, mitochondria are vulnerable to oxidative damage.<sup>10</sup>

Mitochondrial dysfunction can cause many health issues, including psychiatric problems such as epileptic seizures, neurodegenerative diseases, anxiety, and depression.<sup>11,12</sup> In a study on rats, anxiety-like behaviors were linked to mitochondrial dysfunction in the nucleus accumbens. Mitochondrial function in the nucleus accumbens is crucial for social hierarchy establishment, and high anxiety results in low social competition.<sup>11,12</sup> Currently, there is no cure for mitochondrial diseases. Among the treatment strategies under investigation is oxidative stress modulation.<sup>11</sup>

Under normal conditions, the body produces ROS during aerobic metabolism, and a balance exists between ROS production and elimination.<sup>13</sup> Oxidative stress occurs when the amount of ROS exceeds the antioxidant capacity. The increase in ROS causes oxidative damage to macromolecules such as proteins, membrane lipids and deoxyribonucleic acid (DNA).<sup>11,14</sup> Reactive oxygen species maintained at low levels play a physiological role in intracellular signaling pathways; however, when overproduced, they cause cell and tissue damage.<sup>9</sup> The brain has more mitochondria, highly oxidizable lipids, a higher energy requirement, and less antioxidant capacity than other tissues; therefore, it is vulnerable to oxidative stress, which contributes to the formation of epileptic seizures.<sup>10</sup> On the other hand, there is a consensus that seizure activity induces ROS production, and this contributes to seizure-induced cell death, with the literature indicating that there is an affinity between ROS levels and seizure frequency.<sup>15</sup>

Malondialdehyde (MDA), a product of ROS-induced lipid peroxidation (LPO), has been shown to increase in chronic epilepsy.<sup>16</sup> Supporting this information, Turan et al. revealed an increase in MDA and myeloperoxidase (MPO) levels and a decrease in total glutathione (tGSH) and superoxide dismutase (SOD) activities. Such measurements represent the total endogenous antioxidants in the brain tissue of animals used to model epileptic seizures through the intraperitoneal administration of caffeine.<sup>6</sup> These findings suggest that epileptic seizures may be related to oxidative stress.

Epileptic seizures can cause cognitive and psychiatric problems, with reports that frequent seizures originating from the bilateral ventromedial prefrontal cortex (vmPFC) cause prefrontal dysfunction due to tissue damage, and antisocial personality disorder may develop in affected patients.<sup>17</sup> In addition, studies show that vmPFC lesions can cause cognitive and behavioral disorders.<sup>18</sup> Furthermore, temporal lobe epilepsy causes depression and anxiety, which is associated with cell loss.<sup>15</sup> Both antisocial personality disorder and depression are alleviated in patients who have undergone resective epilepsy surgery.<sup>17,19</sup> Based on the literature, it can be stated that epilepsy is not only a neurological problem but also a social issue. Therefore, studies on epilepsy pathogenesis and new strategies for epilepsy prevention and treatment are vital.

Taxifolin (dihydroquercetin) is a flavonoid approved by the U.S. Food and Drug Administration (FDA) and is abundant in various plants, such as grapes, citrus fruits and green tea.<sup>20,21</sup> Studies have shown that the oral bioavailability of taxifolin is low compared to the intravenous use.<sup>22,23</sup> The literature also shows that gastric taxifolin absorption is better than small intestine uptake. In addition, taxifolin undergoes biotransformation by the intestinal microflora, and while some of the formed metabolites are absorbed, some are excreted in the feces.<sup>24</sup> Absorbed taxifolin is primarily metabolized in enterocytes and hepatocytes, generally through phase II reactions. The metabolites are then transported to the organs through the bloodstream,<sup>25</sup> and taxifolin is eliminated from the body through urine and feces.<sup>25</sup> Almost 200 taxifolin metabolites have been identified, and the drug and its metabolites have been detected in many tissues.<sup>25,26</sup> After reviewing the literature, no information was found on the transfer mechanism of taxifolin to the brain. However, studies have shown that taxifolin can cross the blood–brain barrier and has been found in brain tissue, albeit at relatively low concentrations.<sup>25</sup>

Many studies have demonstrated the neuroprotective properties of taxifolin,<sup>23</sup> with a recent double-blind placebo-controlled clinical trial finding that consuming taxifolin-rich foods improved brain activity and mental fatigue in healthy young adults.<sup>27</sup> Furthermore, taxifolin can affect gene expression that regulates the balance between cell survival and cell death and exhibits rapid neuroprotection by suppressing ROS production in inhibitory gamma-aminobutyric acid

(GABA) neurons.<sup>21</sup> Dok-Go et al. correlated the neuroprotective effects of taxifolin in rat cortical cells with its antioxidant activity via radical scavenging and LPO inhibition.<sup>28</sup> Taxifolin has also been shown to attenuate ROS production, tGSH depletion and cell death.<sup>29</sup> The literature on taxifolin indicates that it may be useful for preventing caffeine-related oxidative stress-induced epileptic seizures.

## Objectives

No studies investigating the effects of taxifolin in caffeine-induced epileptic seizures were found when reviewing the literature. As such, this study was designed to assess the impact of taxifolin on caffeine-induced epileptic seizures in rats. Our primary aim was to determine the relationship between epileptic activity and antioxidant activity by evaluating oxidative stress, which is involved in the pathogenesis of epilepsy, by measuring oxidant and antioxidant parameters in brain tissue.

## Materials and methods

The current study created a caffeine-induced epilepsy model in Albino Wistar rats to assess the effects of taxifolin on epileptic seizures and compared the effect of taxifolin to diazepam. To investigate taxifolin effects, oxidant and antioxidant levels were measured in the brain tissues of the animals, and the latent period between epilepsy induction and seizure development was recorded. To determine whether or not taxifolin was effective, results were compared to a seizure group and a diazepam group.

### Animals

The experiments used 40 male Albino Wistar rats (210–220 g) procured from the Erzincan Binali Yildirim University Experimental Animals Application and Research Center (Erzincan, Turkey). Before the experiment, the animals were housed and fed at standard room temperature (22°C) for 1 week in a laboratory environment. The Animal Experiments Local Ethics Committee Experimental approved the procedures (approval No. 2022-11/56).

### Chemicals

Thiopental sodium was procured from IE Ulagay (Istanbul, Turkey), diazepam from Deva (Istanbul, Turkey), caffeine from Sigma-Aldrich (Darmstadt, Germany), and taxifolin from Evalar (Moscow, Russia).

### Animal groups

The animals were split into 4 groups, including a 300 mg/kg caffeine group (CG), 50 mg/kg taxifolin +

300 mg/kg caffeine group (TCG), 2 mg/kg diazepam + 300 mg/kg caffeine group (DCG), and healthy control group (HG).

## Experimental procedure

Taxifolin (25 mg/tablet, CAS No. 480-18-2) and diazepam (2 mg/tablet, CAS No. 439-14-5) were crushed into a powder and dissolved in distilled water. Solutions of 2.5 mg/mL of taxifolin and 0.1 mg/mL of diazepam were prepared. Caffeine (100 g bottle, powder, CAS No. 58-08-2) was dissolved in distilled water to obtain a 30 mg/mL solution. In the experimental application, 50 mg/kg taxifolin<sup>30</sup> was given to the TCG (n = 10) and 2 mg/kg diazepam to the DCG (n = 10) via oral gavage. Distilled water was administered orally at the same volume to the CG (n = 10) and HG (n = 10). One hour after administering taxifolin, diazepam, distilled water or 300 mg/kg caffeine<sup>6</sup> was injected intraperitoneally (ip.) into the CG, TCG and DCG. The same volume of distilled water was also injected ip. into the HG. Immediately after the caffeine injection, the animals were placed in groups in a plexiglass box (30 × 30 × 40 cm), and the caffeine injection time was recorded. The onset of tonic-clonic contractions was recorded as seizure onset. After the caffeine injection, the time until the onset of tonic-clonic contractions was measured with a stopwatch, and latency was recorded in minutes.<sup>6</sup> One hour after the caffeine injection, the animals were euthanized with 50 mg/kg thiopental sodium (0.5 g/20 mL vial, CAS No. 76-75-5), and the levels of MDA, MPO, tGSH, SOD, total oxidant status (TOS), and total antioxidant status (TAS), were measured in excised brain tissue.

### Sample preparation

To determine MDA levels, brain tissue was homogenized in a 1.15% potassium chloride solution in an icy environment and topped up to 2 mL using phosphate-buffered saline (PBS; pH 7.5) for other measurements. The solution was then centrifuged (10,000 rpm for 15 min at 4°C) and the supernatant was collected for analysis.

### Malondialdehyde analysis

The method of Ohkawa et al. was adopted for MDA measurement.<sup>31</sup> The method is based on the spectrophotometric measurement of the absorbance (532 nm) of a pink complex created by thiobarbituric acid (TBA) and MDA at high temperature (95°C). Homogenates were centrifuged at 5000 g for 20 min, and the supernatants used to determine the amount of MDA by preparing a solution containing 250 µL of homogenate, 100 µL of 8% sodium dodecyl sulfate (SDS), 750 µL of 20% acetic acid, 750 µL of 0.08% TBA, and 150 µL of distilled water, which was pipetted into capped test tubes and vortexed. After the mixture was incubated for 60 min at 100°C, 2.5 mL

of n-butanol was added and measured spectrophotometrically. The amount of red color formed was read using 3-mL cuvettes at 532 nm, and the amount of MDA in the samples was determined using the standard curve created using the previously prepared MDA stock solution, with consideration of dilution coefficients.

## Myeloperoxidase analysis

For determining the activity of MPO, an MPO-mediated oxidation reaction with hydrogen peroxide (H<sub>2</sub>O<sub>2</sub>) containing a 4-amino antipyrine/phenol solution as the substrate was used.<sup>32</sup>

## tGSH analysis

The amount of GSH in brain tissue homogenates was determined using the method described by Sedlak and Lindsay.<sup>33</sup> Samples were weighed and homogenized in 2 mL of 50 mmol/L Tris–HCl buffer containing 20 mmol/L ethylenediaminetetraacetic acid (EDTA) and 0.2 mmol/L sucrose at pH 7.5. Homogenates were immediately precipitated with 0.1 mL of 25% trichloroacetic acid, the precipitate was removed after centrifugation at 4200 rpm for 40 min at 4°C, and the supernatant was used to determine tGSH. A total of 1500 µL measurement buffer (200 mmol/L Tris–HCl buffer containing 0.2 mmol/L EDTA at pH 7.5), 500 µL supernatant, 100 µL 5,5-dithio-bis-(2-nitrobenzoic acid) (DTNB) (10 mmol/L), and 7900 µL methanol were added to the tube and vortexed and incubated for 30 min at 37°C. The DTNB was used as the chromogen, and it created a yellow-colored complex with sulfhydryl groups. The absorbance was measured at 412 nm using a Beckman DU 500 spectrophotometer (Beckman Coulter, Gaithersburg, USA). The standard curve was obtained using reduced GSH.

## SOD analysis

The measurements were performed using the method of Sun et al.,<sup>34</sup> with SOD formed when xanthine was converted into uric acid with xanthine oxidase. When a nitro blue tetrazolium (NBT) dye is added to this reaction, it reacts with SOD to form a purple-colored formazan dye. Samples were weighed and homogenized in 2 mL of 20 mmol/L PBS with 10 mmol/L EDTA (pH 7).<sup>8</sup> Samples were then centrifuged at 6000 rpm for 10 min, and the supernatant was used as the assay sample. The measurement mixture, containing 2450 µL of measurement mixture (0.3 mmol/L xanthine, 0.6 mmol/L EDTA, 150 µmol/L NBT, 0.4 mol/L Na<sub>2</sub>CO<sub>3</sub>, and 1 g/L bovine serum albumin), 500 µL supernatant, and 50 µL xanthine oxidase (167 U/L), was vortexed and incubated for 10 min. Formazan developed at the end of the reaction. The absorbance of the purple-colored formazan was measured at 560 nm. Less of the superoxide radical reacted with NBT when more of the enzyme was present.

## TOS and TAS status measurement

The TOS and TAS levels of the samples were determined using an automated measurement method created by Erel and commercial kits (Rel Assay Diagnostics, Gaziantep, Turkey).<sup>35,36</sup> The TAS method was based on bleaching the characteristic color of the more stable 2,2'-azino-bis (3-ethylbenzothiazoline-6-sulfonic acid) (ABTS) radical cation by antioxidants, and the measurements were taken at 660 nm. The results were given as nmol of H<sub>2</sub>O<sub>2</sub> equivalent/L. For the TOS method, the oxidants in the sample oxidized the iron ion-o-dianisidine complex to a ferric ion. The iron ion produced a colored complex with xylenol orange in an acidic environment. The color intensity was measured spectrophotometrically at 530 nm and was associated with the total amount of oxidant molecules in the sample. The results were indicated as µmol trolox equivalent/L. The percentage of TOS to TAS was used as the oxidative stress index (OSI) and calculated according to the formula: OSI = TOS/TAS\*0.1.<sup>37</sup>

## Statistical analyses

Statistical analyses employed IBM SPSS Statistics 22.0 (IBM Corp., Armonk, USA). A Shapiro–Wilk test determined if the data were normally distributed, and Levene's test assessed homogeneity of variance. Data with a normal distribution were analyzed using one-way analysis of variance (ANOVA) with Bonferroni's correction and are presented as mean ± standard deviation (M ± SD) and 95% confidence intervals (95% CIs). Meanwhile, data with a non-normal distribution were analyzed using the Kruskal–Wallis (K–W) test followed by Dunn's test, with the results expressed as median (1<sup>st</sup>–3<sup>rd</sup> quartile (Q1–Q3)). Performing all analyses on the same data set increased the probability of type 1 error. To prevent this situation, the level of significance was determined as 0.00625. This value was obtained by dividing 0.05 by the comparison number of eight.

## Results

### Latent period results

The period elapsed until seizure onset, after the caffeine-driven induction of an epileptic attack, was calculated in minutes as the latent period. There was a difference in the variable latent period between groups with respect to the variable group (H [2] = 20.066, *p* < 0.001). As shown in Fig. 1, Table 1 and Table 2, the latent period for the CG was higher than for the TCG (*p* = 0.004) and DCG (*p* < 0.001), while latency was similar in the taxifolin and diazepam groups (*p* = 1.000). All animals in the CG, TCG and DCG had epileptic seizures. All animals that had a seizure in the CG died (100%), while the number of animals that died in TCG and DCG was 3 (30%) and 9 (90%), respectively.



**Table 1.** Analysis results of the data obtained from the study

Biochemical parameters	Contents	Shapiro–Wilk				Levene's test	One-way ANOVA				
		CG	TCG	DCG	HG		sum of squares	df	mean square	f	sig.
MDA	statistic	0.977	0.908	0.949	0.929	8.070	8135.814	3	2711.938	865.927	0.000
	df	10	10	10	10	3/36	112.746	36	3.132	–	–
	sig.	0.945	0.270	0.662	0.439	0.000	8248.560	39	–	–	–
MPO	statistic	0.965	0.969	0.908	0.910	12.697	2196.455	3	732.152	253.522	0.000
	df	10	10	10	10	3/36	103.965	36	2.888	–	–
	sig.	0.837	0.877	0.268	0.283	0.000	2300.420	39	–	–	–
tGSH	statistic	0.932	0.964	0.849	0.952	0.999	405.690	3	135.230	1837.087	0.000
	df	10	10	10	10	3/36	2.650	36	0.074	–	–
	sig.	0.473	0.826	0.057	0.693	0.404	408.340	39	–	–	–
SOD	statistic	0.960	0.991	0.973	0.976	6.937	2109.204	3	703.068	210.255	0.000
	df	10	10	10	10	3/36	120.380	36	3.344	–	–
	sig.	0.783	0.998	0.915	0.941	0.001	2229.584	39	–	–	–
TOS	statistic	0.988	0.914	0.945	0.949	15.237	2362.577	3	787.526	429.338	0.000
	df	10	10	10	10	3/36	66.034	36	1.834	–	–
	sig.	0.994	0.313	0.605	0.653	0.000	2428.611	39	–	–	–
TAS	statistic	0.982	0.869	0.859	0.918	9.926	343.047	3	114.349	251.577	0.000
	df	10	10	10	10	3/36	16.363	36	0.455	–	–
	sig.	0.974	0.098	0.075	0.342	0.000	359.410	39	–	–	–
OSI	statistic	0.895	0.967	0.789	0.945	Kruskal–Wallis test	34.077	–	–	–	–
	df	10	10	10	10		3	–	–	–	–
	sig.	0.192	0.862	0.011	0.613		0.000	–	–	–	–
Latent period	statistic	0.889	0.935	0.805	–		20.066	–	–	–	–
	df	10	10	10	–		2	–	–	–	–
	sig.	0.166	0.499	0.017	–	0.000	–	–	–	–	

CG – 300 mg/kg caffeine-administered group; TCG – 50 mg/kg taxifolin + 300 mg/kg caffeine-administered group; DCG – 2 mg/kg diazepam + 300 mg/kg caffeine-administered group; HG – healthy group; MDA – malondialdehyde; MPO – myeloperoxidase; tGSH – total glutathione; SOD – superoxide dismutase; TOS – total oxidant status; TAS – total antioxidant status; OSI – oxidative stress index; df – degrees of freedom; df1 – number of groups; df2 – total number of samples; number of groups; sig. – significance; f – (largest variance)<sup>2</sup>/(smallest variance)<sup>2</sup>.

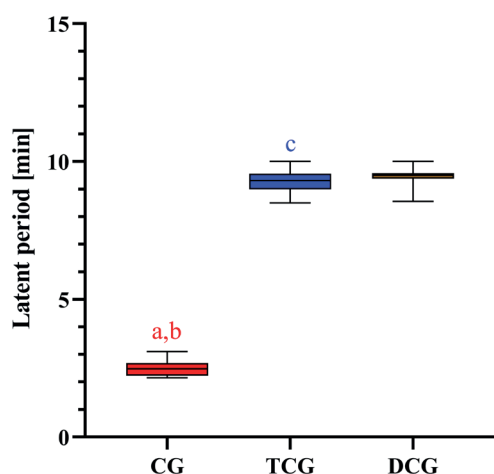


**Fig. 1.** Comparison of latency period data of the CG, TCG and DCG. Data are presented as median and Q1–Q3 percentile (horizontal line = median; bottom line of the box = Q1 (25<sup>th</sup>); top line of the box = Q3 (75<sup>th</sup>))

CG – 300 mg/kg caffeine-administered group; TCG – 50 mg/kg taxifolin + 300 mg/kg caffeine-administered group; DCG – 2 mg/kg diazepam + 300 mg/kg caffeine-administered group; (a). p = 0.04 compared to the TCG; (b). p < 0.001 compared to the DCG; (c). p = 1.000 compared to the DCG.

**Table 2.** Analysis of experimental groups in terms of latent period

Parameters	Contents	Latent period [min]
Median (Q1–Q3)	CG (n = 10)	2.48 (2.23–2.69)
	TCG (n = 10)	9.30 (8.98–9.56)
	DCG (n = 10)	9.51 (9.37–9.57)
Kruskal–Wallis test	H	20.066
	p-value	<0.001
Post hoc test p-values	CG vs. TCG	0.004
	CG vs. DCG	<0.001
	TCG vs. DCG	1.000

CG – 300 mg/kg caffeine-administered group; TCG – 50 mg/kg taxifolin + 300 mg/kg caffeine-administered group; DCG – 2 mg/kg diazepam + 300 mg/kg caffeine-administered group. Statistical analysis was performed with Kruskal–Wallis test, followed by Dunn's test.

## MDA and MPO analysis results

There was a difference in MDA ( $F[3,36] = 865.927$ ,  $p < 0.001$ ) and MPO ( $F[3,36] = 253.522$ ,  $p < 0.001$ ) with respect to the variable group. As seen in Fig. 2, Table 1 and Table 3, MDA and MPO levels in the brain tissues of rats in the CG were higher than those in the TCG, DCG and HG ( $p < 0.001$ ). While taxifolin and diazepam inhibited the increase in MDA at the same level ( $p = 1.000$ ), taxifolin suppressed the MPO increase better than diazepam ( $p < 0.001$ ).

## tGSH and SOD analysis results

There was a group difference in tGSH ( $F[3,36] = 1837.087$ ,  $p < 0.001$ ) and SOD ( $F[3,36] = 210.255$ ,  $p < 0.001$ ) with respect to the variable group. The tGSH and SOD levels in the CG were lower than those in the TCG, DCG and HG ( $p < 0.001$ ). Taxifolin inhibited this decrease in tGSH and SOD levels better than diazepam ( $p < 0.001$ ) (Fig. 3, Table 1 and Table 3).

## TOS, TAS and OSI analysis results

There were group differences in TOS ( $F[3,36] = 429.338$ ,  $p < 0.001$ ) and OSI ( $H[3] = 34.077$ ,  $p < 0.001$ ) with respect to the variable group. As shown in Fig. 4, Table 1 and Table 3, the CG had the highest TOS and OSI values, and there was a statistically significant difference between

the other groups ( $p < 0.001$ ). While TOS values were similar in the TCG and DCG, OSI values were lower ( $p = 1.000$  and  $p < 0.001$ , respectively). The OSI values in the TCG were similar to the HG ( $p = 1.000$ ). Furthermore, there was a group difference in TAS with respect to the variable group ( $F[3,36] = 251.577$ ,  $p < 0.001$ ). The TAS levels were lower in the CG than in the other groups ( $p < 0.001$ ). Taxifolin inhibited the decrease in TAS levels better than diazepam ( $p < 0.001$ ). There was no statistically significant difference in TAS levels between the TCG and HG ( $p = 1.000$ ).

The latent period data for the CG were higher than for the TCG and DCG. All animals in the CG, TCG and DCG had epileptic seizures. All animals who had a seizure in the CG died, while the number of animals that died in the TCG and DCG was 3 and 9, respectively. The MDA and MPO were higher in the CG than in the TCG, DCG and HG. While taxifolin and diazepam inhibited the MDA increase to the same extent, taxifolin suppressed the MPO increase better than diazepam. The SOD and tGSH were lower in the CG than in the TCG, DCG and HG. Taxifolin inhibited this decrease in tGSH and SOD better than diazepam. While TOS values were similar in the TCG compared to the DCG, OSI scores were lower. Oxidative stress index was similar for the TCG and HG. Meanwhile, TAS was lower in the CG than in the other groups. Taxifolin inhibited the decrease in TAS better than diazepam. There was no difference in TAS levels between the TCG and the HG.

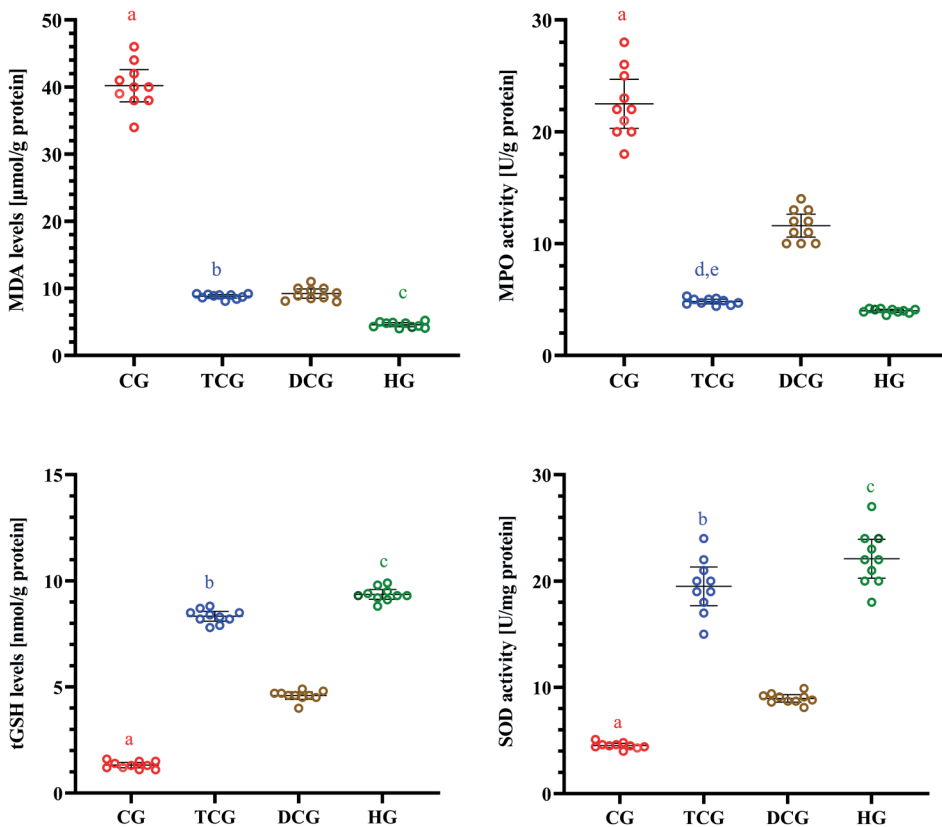


**Fig. 2.** Comparative analysis of MDA and MPO levels obtained from experimental groups. Data were presented as mean with 95% confidence intervals

(a).  $p < 0.001$  compared to the TCG, DCG and HG; (b).  $p = 1.000$  compared to the DCG; (c).  $p < 0.001$  compared to the CG, TCG and DCG; (d).  $p < 0.001$  compared to the DCG; (e).  $p = 1.000$  compared to the HG; MDA – malondialdehyde; MPO – myeloperoxidase; CG – 300 mg/kg caffeine-administered group; TCG – 50 mg/kg taxifolin + 300 mg/kg caffeine-administered group; DCG – 2 mg/kg diazepam + 300 mg/kg caffeine-administered group; HG – healthy group.

**Fig. 3.** Comparative analysis of tGSH and SOD levels obtained from experimental groups. Data were presented as mean with 95% confidence intervals

(a).  $p < 0.001$  compared to the TCG, DCG and HG; (b).  $p < 0.001$  compared to the DCG; (c).  $p < 0.001$  compared to the CG, TCG and DCG; tGSH – total glutathione; SOD – superoxide dismutase; CG – 300 mg/kg caffeine-administered group; TCG – 50 mg/kg taxifolin + 300 mg/kg caffeine-administered group; DCG – 2 mg/kg diazepam + 300 mg/kg caffeine-administered group; HG – healthy group.

**Table 3.** Statistical analysis of biochemical data obtained from experimental groups

Parameters	Contents	MDA	MPO	tGSH	SOD	TOS	TAS	OSI
X ±SD or median (Q1–Q3)	CG (n = 10)	40.20 ±3.36	22.50 ±3.06	1.32 ±0.18	4.52 ±0.29	25.50 ±2.64	3.19 ±0.32	0.84 (0.68–0.86)
	TCG (n = 10)	8.82 ±0.37	4.82 ±0.30	8.33 ±0.32	19.50 ±0.55	7.70 ±0.34	9.97 ±0.60	0.08 (0.07–0.08)
	DCG (n = 10)	9.21 ±0.96	11.60 ±1.43	4.59 ±0.24	8.96 ±0.50	7.15 ±0.39	5.81 ±0.38	0.12 (0.12–0.13)
	HG (n = 10)	4.57 ±0.42	3.99 ±0.19	9.36 ±0.32	22.10 ±2.56	8.51 ±0.35	10.14 ±1.10	0.08 (0.08–0.09)
95% CI for the mean change	CG lower–upper	37.97–42.60	20.31–24.69	1.20–1.45	4.31–4.73	23.62–27.39	2.96–3.42	–
	TCG lower–upper	8.56–9.08	4.62–5.03	8.10–8.56	17.68–21.32	7.46–7.95	9.54–10.40	–
	DCG lower–upper	8.52–9.90	10.58–12.62	4.42–4.76	8.61–9.31	6.87–7.43	5.54–6.08	–
	HG lower–upper	4.27–4.87	3.85–4.13	9.13–9.59	20.27–23.93	8.26–8.76	9.35–10.93	–
ANOVA or K–W	F (3.36) or H	865.927	253.522	1837.087	210.255	429.338	251.577	34.077
	p-values	<0.001	<0.001	<0.001	<0.001	<0.001	<0.001	<0.001
Post hoc test p-values	HG vs. TCG	<0.001	1.000	<0.001	0.018	1.000	1.000	1.000
	HG vs. DCG	<0.001	<0.001	<0.001	<0.001	0.186	<0.001	0.118
	HG vs. CG	<0.001	<0.001	<0.001	<0.001	<0.001	<0.001	<0.001
	TCG vs. DCG	1.000	<0.001	<0.001	<0.001	1.000	<0.001	0.004
	TCG vs. CG	<0.001	<0.001	<0.001	<0.001	<0.001	<0.001	<0.001
	DCG vs. CG	<0.001	<0.001	<0.001	<0.001	<0.001	<0.001	0.335

CG – 300 mg/kg caffeine-administered group; TCG – 50 mg/kg taxifolin + 300 mg/kg caffeine-administered group; DCG – 2 mg/kg diazepam + 300 mg/kg caffeine-administered group; HG – healthy group; MDA – malondialdehyde; MPO – myeloperoxidase; tGSH – total glutathione; SOD – superoxide dismutase; TOS – total oxidant status; TAS – total antioxidant status; OSI – oxidative stress index. Statistical analysis was performed with one-way analysis of variance (ANOVA) or the Kruskal–Wallis (K–W) test. One-way ANOVA was preferred for statistical analysis of MDA, MPO, tGSH, SOD, TOS, and TAS. Bonferroni correction was then applied. Statistical analysis for OSI was done using the K–W test and post hoc Dunn’s test was applied.

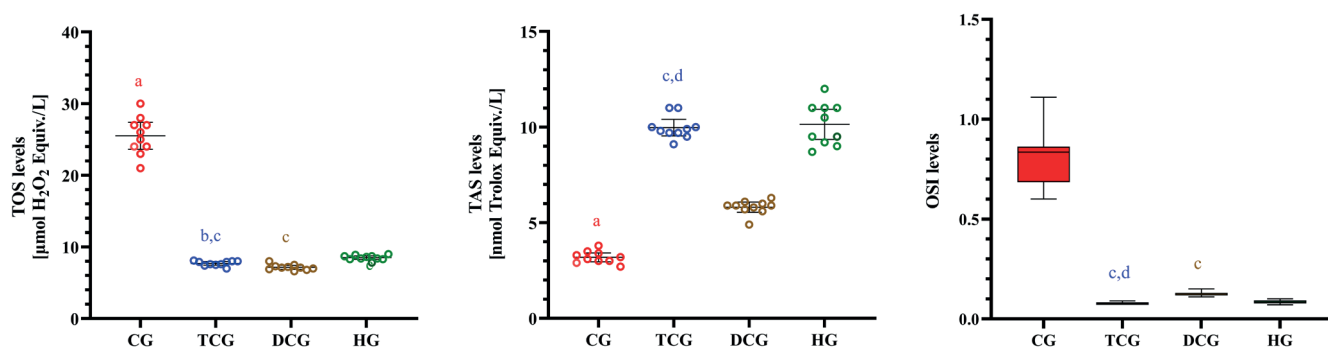


**Fig. 4.** Comparative analysis of TOS, TAS and OSI levels obtained from experimental groups. Data were presented as mean with 95% confidence intervals for TAS and TOS, and as median and Q1–Q3 percentile for OSI (horizontal line = median; bottom line of the box = Q1 (25<sup>th</sup>); top line of the box = Q3 (75<sup>th</sup>))

(a). p < 0.001 compared to the TCG, DCG and HG; (b). p = 1.000 compared to the DCG; (c). p > 0.05 compared to the HG; (d). p < 0.05 compared to the DCG; TOS – total oxidant status; TAS – total antioxidant status; OSI – oxidative stress index; CG – 300 mg/kg caffeine-administered group; TCG – 50 mg/kg taxifolin + 300 mg/kg caffeine-administered group; DCG – 2 mg/kg diazepam + 300 mg/kg caffeine-administered group; HG – healthy group.

## Discussion

An epileptic seizure results from abnormal synchronized neuronal activity in the brain and causes transient clinical signs or symptoms. The incidence is increasing, especially in developing countries.<sup>3</sup> The literature states that approx. 30% of epilepsy patients are resistant to current treatments. As such, new treatment options are needed to successfully control seizures and improve patient quality of life.<sup>38</sup> Although the pathogenesis of epilepsy has not been fully elucidated, oxidative stress is thought to play a role.<sup>7</sup> Therefore, this study investigated the effects of taxifolin

on caffeine-induced epileptiform activity in rats and analyzed its relationship with oxidative stress.

In this study, the latent period was significantly longer in the taxifolin and diazepam groups compared to the epilepsy group. Also, all animals were followed up clinically after the episode, and mortality rates were determined. While all rats in the epilepsy group died from seizures, the death rate was 30% in the taxifolin group and 90% in the diazepam group. Compared to the HG, the CG had higher MDA, MPO, TOS, and OSI values, and lower tGSH, SOD and TAS values. While taxifolin and diazepam inhibited the MDA and TOS increase at a similar level,

taxifolin was more successful than diazepam in suppressing the changes in MPO, tGSH, SOD, TAS, and OSI.

Previous studies reported that increased ROS production caused oxidative stress, disrupting the antioxidant balance and causing epilepsy-induced neuronal death.<sup>39</sup> Lipid peroxidation, due to increased ROS, can produce large amounts of MDA,<sup>13</sup> which is an important parameter used to analyze oxidative damage associated with an epileptic event.<sup>40,41</sup> Moreover, LPO causes impaired cell membrane permeability, decreased membrane potential and cell damage, with the latter exacerbated by MDA formation.<sup>42</sup> Turan et al. revealed that MDA levels in the brain tissue of rats increased significantly in a caffeine-induced epileptic seizure model.<sup>6</sup> Furthermore, previous studies using experimental epileptic episode models reported increased MDA levels in tissues and damaged neuronal cells.<sup>6,40,41,43</sup> Obtaining high MDA levels in the epilepsy group in the current study indicates that our experimental results are in line with the literature.

In the current study, TOS measurement was performed to analyze oxidative stress in more detail. The experimental results revealed that TOS and OSI levels were also high in the epilepsy group alongside high MDA levels. As is well known, there are various types of oxidant molecules, and measuring these oxidants separately increases costs. However, it is possible to determine the levels of all ROS using TOS analysis.<sup>36</sup> In the current literature, there were no studies analyzing the TOS level in the brain tissue of rats subjected to caffeine-induced epilepsy. Nonetheless, a study reported increased TOS and OSI values in parallel with elevated MDA levels in a rat model of pentetazol-induced epilepsy.<sup>44</sup> Consistent with the literature, our findings showed high MDA, TOS and OSI levels in the epilepsy group.

The accumulation of ROS in brain regions is a cellular threat that can cause significant neuronal damage if not appropriately prevented by local and systemic antioxidants.<sup>45</sup> Measuring changes in antioxidant levels is one of the most frequently used methods for clarifying the mechanisms of brain damage induced by ROS in epilepsy.<sup>46</sup> Therefore, SOD and tGSH levels, known as the endogenous antioxidants, were measured in brain tissue. Superoxide dismutase oxidizes one superoxide radical to oxygen and catalyzes the reduction of another superoxide radical to H<sub>2</sub>O<sub>2</sub>, which is a less reactive molecule.<sup>46,47</sup> On the other hand, GSH reacts with H<sub>2</sub>O<sub>2</sub> and organic peroxides catalyzed by active glutathione peroxidase, detoxifies them and protects the cells from ROS damage.<sup>46,48,49</sup> Our findings showed a significant decrease in SOD and tGSH levels in the brain tissue of rats as a result of caffeine treatment, which is in agreement with a previous study demonstrating that decreased SOD and tGSH levels were associated with brain damage in the caffeine-induced epileptic seizure rat model.<sup>6</sup> In our study, TAS level was measured to analyze the effects of caffeine on SOD, tGSH, and other antioxidants. Total antioxidant status is used

to measure the cumulative antioxidative effects of all antioxidants in organisms.<sup>35</sup> We found that the TAS level decreased in parallel with decreased SOD and tGSH levels in brain tissue. However, no studies investigating the level of TAS in caffeine-induced epilepsy models were found in the literature. Nonetheless, studies reported that TAS levels decreased and neuronal oxidative damage developed in experimental epilepsy models.<sup>50,51</sup>

Clinical and experimental evidence suggests that inflammatory processes in the brain play an important role in the pathophysiology of seizures and epilepsy. There is also evidence that inflammation may be a consequence as well as a cause of epilepsy.<sup>52</sup> Indeed, various experimental epilepsy models have reported that the overproduction of ROS triggers an increase in inflammation in neurons.<sup>53</sup> Myeloperoxidase is an enzyme abundant in neutrophil granules, and its secretion increases after neutrophil activation,<sup>54</sup> which generates hypochlorous acid from H<sub>2</sub>O<sub>2</sub> in the environment using chloride ions. Hypochlorous acid is a strong oxidant that reacts readily with biological molecules and causes neuronal damage.<sup>54,55</sup> Previous studies reported that increased MPO levels in experimental epilepsy models were associated with increased inflammation and oxidative stress, and this caused epileptic-induced neuronal cell death.<sup>6,39,56</sup> In the current study, a significant increase in MPO level was found in parallel with the increasing oxidative stress parameters and decreasing antioxidant parameters in the caffeine-induced epilepsy model, which is in line with the literature.

Taxifolin, analyzed in terms of its effect against caffeine-induced epileptic activity, significantly decreased the caffeine-induced increase in MDA and TOS levels in brain tissue. There was no information indicating the possible effects of taxifolin against the oxidative damage caused by epilepsy in the brain in the literature. However, Okkay et al. reported that increased MDA levels in the brain tissue of rats with hepatic encephalopathy were suppressed by taxifolin and revealed a neuroprotective effect.<sup>57</sup> Another study by Akagunduz et al. demonstrated that increased MDA and TOS levels in a rat model of pazopanib-induced oxidative liver injury were significantly decreased by taxifolin treatment.<sup>30</sup> Our experimental results and information obtained from the literature suggest that taxifolin has an antioxidant effect on ROS. Indeed, we demonstrated an oxidant/antioxidant balance change in favor of oxidants in the epilepsy group, whereas this balance was maintained in the taxifolin group, with the predominance of antioxidants. Turovskaya et al. reported that taxifolin protected neurons against ischemic damage by activating antioxidant systems.<sup>58</sup> Furthermore, other studies show that taxifolin prevented thioacetamide-associated GSH reduction in the hippocampus and protected the central nervous system from oxidative damage.<sup>57</sup>

It was determined that increased MPO levels due to epileptic activity-induced brain damage decreased significantly as a result of taxifolin treatment. Low MPO levels

in the taxifolin group rather than in the epilepsy group indicate that it antagonized caffeine-induced neuroinflammation. No previous studies have investigated the effects of taxifolin on MPO levels in caffeine-induced epileptic activity. However, Unver et al. reported that taxifolin significantly reduced the increase in MPO in extra-brain tissues and protected against inflammation-induced damage.<sup>59</sup>

The positive effects of taxifolin on epileptic seizures may be associated with oxidative stress, which is involved in the pathogenesis of epilepsy. Sun et al. determined that, in an epilepsy model induced by lithium chloride-pilocarpine in rats, ROS and MDA levels increased in the epilepsy group, while SOD and mitochondrial membrane potential decreased.<sup>60</sup> They also reported that GSH decreased with increasing MDA and ROS levels in brain tissues after epileptic seizures induced by pentylentetrazole in rats.<sup>61</sup> Previous studies show that epileptic seizures occur with similar pathology, although they are induced in different ways, which suggests that taxifolin may also be effective in epileptic seizures induced by various means.

Numerous clinical studies in adults have revealed that melatonin and cannabidiol added to antiepileptic treatment reduce the frequency and severity of seizures and increase the quality of life, and these results were associated with the antioxidant and anti-inflammatory properties of the agents used.<sup>62,63</sup> Therefore, it is not surprising that taxifolin, which has shown antioxidative<sup>57</sup> and anti-inflammatory properties,<sup>59</sup> has a neuroprotective effect in caffeine-induced epileptic seizures.

## Limitations

Objective measurement methods that could assess the effect of taxifolin on the epileptic seizure model, such as electroencephalography and histopathological examination, were excluded due to technical constraints. Also, brain tissue, cerebrospinal fluid and blood concentrations of caffeine and taxifolin could not be measured for technical reasons. Furthermore, additional groups could have been added to assess the effects of using taxifolin in combination with existing antiepileptics.

## Conclusions

The current study investigated the effects of taxifolin on caffeine-induced epileptiform activity in rats and analyzed its relationship with oxidative stress. Taxifolin prolonged the latency period of caffeine-induced epilepsy-like convulsions and reduced the severity of tonic-clonic seizures. In addition, taxifolin prevented a decrease in antioxidant capacity and an increase in oxidant and inflammatory markers in brain tissue after caffeine administration. Our experimental results showed that taxifolin may be useful for treating epilepsy and epilepsy-like convulsions. Based on our findings, using taxifolin, which has

antioxidant and anti-inflammatory effects, either alone or in combination with existing antiepileptics or a reduced dose of antiepileptic drugs, could be a new treatment strategy. Since no side effects have been found for taxifolin in human studies,<sup>23</sup> it could be used as a food supplement or to treat various diseases. In addition, this study may lead to further studies on the effects of other antioxidant and anti-inflammatory agents for epilepsy treatment.

## Supplementary data


The Supplementary materials are available at <https://doi.org/10.5281/zenodo.8354869>. The package consists of the following files:


Supplementary Table 1. Normality assumption test results for latent period.


Supplementary Table 2. Normality assumption test results for biochemical data.


Supplementary Table 3. Homogeneity of variances assumption test results for MDA, MPO, tGSH, SOD, TOS and TAS.


## ORCID iDs


Hasan Yasar  <https://orcid.org/0000-0003-1115-8359>


Durdu Altuner  <https://orcid.org/0000-0002-5756-3459>

Seval Bulut  <https://orcid.org/0000-0003-4992-1241>

Betul Cicek  <https://orcid.org/0000-0003-1395-1326>

Cebrail Gursul  <https://orcid.org/0000-0001-6521-6169>

Mehmet Kuzucu  <https://orcid.org/0000-0002-7786-7687>

Halis Suleyman  <https://orcid.org/0000-0002-9239-4099>

## References

- Seino M. Classification criteria of epileptic seizures and syndromes. *Epilepsy Res.* 2006;70:27–33. doi:10.1016/j.epilepsyres.2006.01.016
- Zupec-Kania BA, Spellman E. An overview of the ketogenic diet for pediatric epilepsy. *Nutr Clin Pract.* 2008;23(6):589–596. doi:10.1177/0884533608326138
- Falco-Walter J. Epilepsy: Definition, classification, pathophysiology, and epidemiology. *Semin Neurol.* 2020;40(6):617–623. doi:10.1055/s-0040-1718719
- Fisher RS. Animal models of the epilepsies. *Brain Res Rev.* 1989;14(3):245–278. doi:10.1016/0165-0173(89)90003-9
- Kandratavicius L, Balista P, Lopes-Aguiar C, et al. Animal models of epilepsy: Use and limitations. *Neuropsychiatr Dis Treat.* 2014;10:1693–1705. doi:10.2147/NDT.S50371
- Turan MI, Tan H, Cetin N, Suleyman H, Cayir A. Effects of thiamine and thiamine pyrophosphate on epileptic episode model established with caffeine in rats. *Epilepsy Res.* 2014;108(3):405–410. doi:10.1016/j.epilepsyres.2013.12.006
- Yang N, Guan QW, Chen FH, et al. Antioxidants targeting mitochondrial oxidative stress: Promising neuroprotectants for epilepsy. *Oxid Med Cell Longev.* 2020;2020:6687185. doi:10.1155/2020/6687185
- Fišar Z, Hroudová J, Zvěřová M, Jiráček R, Raboch J, Kitzlerová E. Age-dependent alterations in platelet mitochondrial respiration. *Biomedicines.* 2023;11(6):1564. doi:10.3390/biomedicines11061564
- Kowalczyk P, Sulejczak D, Kleczkowska P, et al. Mitochondrial oxidative stress: A causative factor and therapeutic target in many diseases. *Int J Mol Sci.* 2021;22(24):13384. doi:10.3390/ijms222413384
- Waldbaum S, Patel M. Mitochondria, oxidative stress, and temporal lobe epilepsy. *Epilepsy Res.* 2010;88(1):23–45. doi:10.1016/j.epilepsyres.2009.09.020
- Tanaka M, Szabó Á, Spekker E, Polyák H, Tóth F, Vécsei L. Mitochondrial impairment: A common motif in neuropsychiatric presentation? The link to the tryptophan–kynurenine metabolic system. *Cells.* 2022;11(16):2607. doi:10.3390/cells11162607

12. Hollis F, Van Der Kooij MA, Zanoletti O, Lozano L, Cantó C, Sandi C. Mitochondrial function in the brain links anxiety with social subordination. *Proc Natl Acad Sci U S A*. 2015;112(50):15486–15491. doi:10.1073/pnas.1512653112
13. Huang Y, Zhang X, Chen L, Ren BX, Tang FR. *Lycium barbarum* ameliorates neural damage induced by experimental ischemic stroke and radiation exposure. *Front Biosci (Landmark Ed)*. 2023;28(2):38. doi:10.31083/j.fbl2802038
14. Patel MN. Oxidative stress, mitochondrial dysfunction, and epilepsy. *Free Radic Res*. 2002;36(11):1139–1146. doi:10.1080/1071576021000016391
15. Maes M, Supasitthumrong T, Limotai C, et al. Increased oxidative stress toxicity and lowered antioxidant defenses in temporal lobe epilepsy and mesial temporal sclerosis: Associations with psychiatric comorbidities. *Mol Neurobiol*. 2020;57(8):3334–3348. doi:10.1007/s12035-020-01949-8
16. Kovac S, Dinkova-Kostova AT, Abramov A. The role of reactive oxygen species in epilepsy. *React Oxyg Species*. 2016;1(1):38–52. <https://rosj.org/index.php/ros/article/view/19>. Accessed June 15, 2023.
17. Trebuchon A, Bartolomei F, McGonigal A, Laguitton V, Chauvel P. Reversible antisocial behavior in ventromedial prefrontal lobe epilepsy. *Epilepsy Behav*. 2013;29(2):367–373. doi:10.1016/j.yebeh.2013.08.007
18. Battaglia S, Garofalo S, Di Pellegrino G, Starita F. Revaluing the role of vmPFC in the acquisition of Pavlovian threat conditioning in humans. *J Neurosci*. 2020;40(44):8491–8500. doi:10.1523/JNEUROSCI.0304-20.2020
19. Radaelli G, Majolo F, Leal-Conceição E, et al. Left hemisphere lateralization of epileptic focus can be more frequent in temporal lobe epilepsy surgical patients with no consensus associated with depression lateralization. *Dev Neurosci*. 2021;43(1):1–8. doi:10.1159/000513537
20. Saito S, Tanaka M, Satoh-Asahara N, Carare RO, Ihara M. Taxifolin: A potential therapeutic agent for cerebral amyloid angiopathy. *Front Pharmacol*. 2021;12:643357. doi:10.3389/fphar.2021.643357
21. Varlamova EG, Khabatova VV, Gudkov SV, Plotnikov EY, Turovsky EA. Cytoprotective properties of a new nanocomplex of selenium with taxifolin in the cells of the cerebral cortex exposed to ischemia/reoxygenation. *Pharmaceutics*. 2022;14(11):2477. doi:10.3390/pharmaceutics14112477
22. Zu Y, Wu W, Zhao X, et al. Enhancement of solubility, antioxidant ability and bioavailability of taxifolin nanoparticles by liquid antisolvent precipitation technique. *Int J Pharm*. 2014;471(1–2):366–376. doi:10.1016/j.ijpharm.2014.05.049
23. Das A, Baidya R, Chakraborty T, Samanta AK, Roy S. Pharmacological basis and new insights of taxifolin: A comprehensive review. *Biomed Pharmacother*. 2021;142:112004. doi:10.1016/j.biopha.2021.112004
24. Stenger Moura FC, Peroli L, Pagano C, et al. Chitosan composite microparticles: A promising gastroadhesive system for taxifolin. *Carbohydr Polym*. 2019;218:343–354. doi:10.1016/j.carbpol.2019.04.075
25. Li Y, Su H, Yin ZP, Li JE, Yuan E, Zhang QF. Metabolism, tissue distribution and excretion of taxifolin in rat. *Biomed Pharmacother*. 2022;150:112959. doi:10.1016/j.biopha.2022.112959
26. Yang P, Xu F, Li HF, et al. Detection of 191 taxifolin metabolites and their distribution in rats using HPLC-ESI-IT-TOF-MSn. *Molecules*. 2016;21(9):1209. doi:10.3390/molecules21091209
27. Shinozaki F, Kamei A, Shimada K, et al. Ingestion of taxifolin-rich foods affects brain activity, mental fatigue, and the whole blood transcriptome in healthy young adults: A randomized, double-blind, placebo-controlled, crossover study. *Food Funct*. 2023;14(8):3600–3612. doi:10.1039/D2FO03151E
28. Dok-Go H, Lee KH, Kim HJ, et al. Neuroprotective effects of antioxidative flavonoids, quercetin, (+)-dihydroquercetin and quercetin 3-methyl ether, isolated from *Opuntia ficus-indica* var. *saboten*. *Brain Res*. 2003;965(1–2):130–136. doi:10.1016/S0006-8993(02)04150-1
29. Kim A, Nam YJ, Lee CS. Taxifolin reduces the cholesterol oxidation product-induced neuronal apoptosis by suppressing the Akt and NF- $\kappa$ B activation-mediated cell death. *Brain Res Bull*. 2017;134:63–71. doi:10.1016/j.brainresbull.2017.07.008
30. Akagunduz B, Ozer M, Ozcicek F, et al. Protective effects of taxifolin on pazopanib-induced liver toxicity: An experimental rat model. *Exp Anim*. 2021;70(2):169–176. doi:10.1538/expanim.20-0103
31. Ohkawa H, Ohishi N, Yagi K. Assay for lipid peroxides in animal tissues by thiobarbituric acid reaction. *Anal Biochem*. 1979;95(2):351–358. doi:10.1016/0003-2697(79)90738-3
32. Bradley PP, Priebe DA, Christensen RD, Rothstein G. Measurement of cutaneous inflammation: Estimation of neutrophil content with an enzyme marker. *J Invest Dermatol*. 1982;78(3):206–209. doi:10.1111/1523-1747.ep12506462
33. Sedlak J, Lindsay RH. Estimation of total, protein-bound, and nonprotein sulfhydryl groups in tissue with Ellman's reagent. *Anal Biochem*. 1968;25:192–205. doi:10.1016/0003-2697(68)90092-4
34. Sun Y, Oberley LW, Li Y. A simple method for clinical assay of superoxide dismutase. *Clin Chem*. 1988;34(3):497–500. PMID:3349599.
35. Erel O. A novel automated method to measure total antioxidant response against potent free radical reactions. *Clin Biochem*. 2004;37(2):112–119. doi:10.1016/j.clinbiochem.2003.10.014
36. Erel O. A new automated colorimetric method for measuring total oxidant status. *Clin Biochem*. 2005;38(12):1103–1111. doi:10.1016/j.clinbiochem.2005.08.008
37. Icel E, Icel A, Uçak T, et al. The effects of lycopene on alloxan induced diabetic optic neuropathy. *Cutan Ocul Toxicol*. 2019;38(1):88–92. doi:10.1080/15569527.2018.1530258
38. Fattorusso A, Matricardi S, Mencaroni E, et al. The pharmacoresistant epilepsy: An overview on existent and new emerging therapies. *Front Neurol*. 2021;12:674483. doi:10.3389/fneur.2021.674483
39. Kim JH, Jang BG, Choi BY, et al. Post-treatment of an NADPH oxidase inhibitor prevents seizure-induced neuronal death. *Brain Res*. 2013;1499:163–172. doi:10.1016/j.brainres.2013.01.007
40. Zhao C, Yang F, Wei X, Zhang J. miR-139-5p upregulation alleviated spontaneous recurrent epileptiform discharge-induced oxidative stress and apoptosis in rat hippocampal neurons via regulating the Notch pathway. *Cell Biol Int*. 2021;45(2):463–476. doi:10.1002/cbin.11509
41. Mahmoudi T, Lorigooini Z, Rafieian-Kopaei M, et al. Effect of curcuma zedoaria hydro-alcoholic extract on learning, memory deficits and oxidative damage of brain tissue following seizures induced by pentylenetetrazole in rat. *Behav Brain Funct*. 2020;16(1):7. doi:10.1186/s12993-020-00169-3
42. Lin TK, Chen SD, Lin KJ, Chuang YC. Seizure-induced oxidative stress in status epilepticus: Is antioxidant beneficial? *Antioxidants*. 2020;9(11):1029. doi:10.3390/antiox9111029
43. Zhao F, Xiao K, Wu C. Glucose-PEG2000-DSPE modified carbamazepine nano system alleviated cell apoptosis and oxidative stress in epilepsy. *Nucleosides Nucleotides Nucleic Acids*. 2022;41(7):671–683. doi:10.1080/15257770.2022.2061714
44. Ergul Ercek O, Arihan O, Kara M, et al. Effects of *Leontice leontopetalum* and *Bongardia chrysogonum* on oxidative stress and neuroprotection in PTZ kindling epilepsy in rats. *Cell Mol Biol (Noisy-le-grand)*. 2018;64(15):71–77. PMID:30672439.
45. Baliellas DEM, Barros MP, Vardaris CV, et al. Propentofylline improves thiol-based antioxidant defenses and limits lipid peroxidation following gliotoxic injury in the rat brainstem. *Biomedicines*. 2023;11(6):1652. doi:10.3390/biomedicines11061652
46. Borowicz-Reutt KK, Czuczwar SJ. Role of oxidative stress in epileptogenesis and potential implications for therapy. *Pharmacol Rep*. 2020;72(5):1218–1226. doi:10.1007/s43440-020-00143-w
47. Olowe R, Sandouka S, Saadi A, Shekh-Ahmad T. Approaches for reactive oxygen species and oxidative stress quantification in epilepsy. *Antioxidants*. 2020;9(10):990. doi:10.3390/antiox9100990
48. Puttachary S, Sharma S, Stark S, Thippeswamy T. Seizure-induced oxidative stress in temporal lobe epilepsy. *Biomed Res Int*. 2015;2015:745613. doi:10.1155/2015/745613
49. Cárdenas-Rodríguez N, Coballase-Urrutia E, Pérez-Cruz C, et al. Relevance of the glutathione system in temporal lobe epilepsy: Evidence in human and experimental models. *Oxid Med Cell Longev*. 2014;2014:759293. doi:10.1155/2014/759293
50. Filiz AK, Gumus E, Karabulut S, Tastemur Y, Taskiran AS. Protective effects of lamotrigine and vitamin B12 on pentylenetetrazole-induced epileptogenesis in rats. *Epilepsy Behav*. 2021;118:107915. doi:10.1016/j.yebeh.2021.107915
51. Akkaya R, Gümüş E, Akkaya B, et al. Wi-Fi decreases melatonin protective effect and increases hippocampal neuronal damage in pentylenetetrazole induced model seizures in rats. *Pathophysiology*. 2019;26(3–4):375–379. doi:10.1016/j.pathophys.2019.11.003
52. Vezzani A, French J, Bartfai T, Baram TZ. The role of inflammation in epilepsy. *Nat Rev Neurol*. 2011;7(1):31–40. doi:10.1038/nrneurol.2010.178

53. Terrone G, Balosso S, Pauletti A, Ravizza T, Vezzani A. Inflammation and reactive oxygen species as disease modifiers in epilepsy. *Neuropharmacology*. 2020;167:107742. doi:10.1016/j.neuropharm.2019.107742
54. Khan A, Alsahli M, Rahmani A. Myeloperoxidase as an active disease biomarker: Recent biochemical and pathological perspectives. *Med Sci (Basel)*. 2018;6(2):33. doi:10.3390/medsci6020033
55. Lavelli V, Peri C, Rizzolo A. Antioxidant activity of tomato products as studied by model reactions using xanthine oxidase, myeloperoxidase, and copper-induced lipid peroxidation. *J Agric Food Chem*. 2000;48(5):1442–1448. doi:10.1021/jf990782j
56. Koyuncuoğlu T, Vızdıklar C, Üren D, et al. Obestatin improves oxidative brain damage and memory dysfunction in rats induced with an epileptic seizure. *Peptides*. 2017;90:37–47. doi:10.1016/j.peptides.2017.02.005
57. Okkay U, Ferah Okkay I, Cicek B, Aydin IC, Ozkaraca M. Hepatoprotective and neuroprotective effect of taxifolin on hepatic encephalopathy in rats. *Metab Brain Dis*. 2022;37(5):1541–1556. doi:10.1007/s11011-022-00952-3
58. Turovskaya MV, Gaidin SG, Mal'tseva VN, Zinchenko VP, Turovsky EA. Taxifolin protects neurons against ischemic injury in vitro via the activation of antioxidant systems and signal transduction pathways of GABAergic neurons. *Mol Cell Neurosci*. 2019;96:10–24. doi:10.1016/j.mcn.2019.01.005
59. Unver E, Tosun M, Olmez H, Kuzucu M, Cimen FK, Suleyman Z. The effect of taxifolin on cisplatin-induced pulmonary damage in rats: A biochemical and histopathological evaluation. *Mediators Inflamm*. 2019;2019:3740867. doi:10.1155/2019/3740867
60. Sun X, Kong L, Zhou L. Protective effect of *Fructus corni* polysaccharide on hippocampal tissues and its relevant mechanism in epileptic rats induced by lithium chloride-pilocarpine. *Exp Ther Med*. 2018;16(1):445–451. doi:10.3892/etm.2018.6142
61. Ata Yaseen Abdulqader Y, Abdel Kawy HS, Mohammed Alkreathy H, Abdullah Rajeh N. The potential antiepileptic activity of astaxanthin in epileptic rats treated with valproic acid. *Saudi Pharm J*. 2021;29(5):418–426. doi:10.1016/j.jsps.2021.04.002
62. Verma N, Maiti R, Mishra BR, Jha M, Jena M, Mishra A. Effect of add-on melatonin on seizure outcome, neuronal damage, oxidative stress, and quality of life in generalized epilepsy with generalized onset motor seizures in adults: A randomized controlled trial. *J Neurosci Res*. 2021;99(6):1618–1631. doi:10.1002/jnr.24820
63. Silvestro S, Mammana S, Cavalli E, Bramanti P, Mazzon E. Use of cannabidiol in the treatment of epilepsy: Efficacy and security in clinical trials. *Molecules*. 2019;24(8):1459. doi:10.3390/molecules24081459





# Dihydroartemisinin ameliorated the inflammatory response and regulated miRNA-mRNA expression profile of chronic nonbacterial prostatitis

Jie Hu<sup>1,A,D</sup>, Yan Zhou<sup>2,B</sup>, Junhao Wang<sup>2,B</sup>, Jianpeng Han<sup>2,B</sup>, Jianyong Feng<sup>2,B</sup>, Wenbin Chen<sup>2,C</sup>, Kuo Guo<sup>2,C</sup>, Yongzhang Li<sup>2,A,E,F</sup>

<sup>1</sup> Department of Urology, Langfang People's Hospital, China

<sup>2</sup> Department of Urology, Hebei Province Hospital of Chinese Medicine, Shijiazhuang, China

A – research concept and design; B – collection and/or assembly of data; C – data analysis and interpretation;

D – writing the article; E – critical revision of the article; F – final approval of the article

Advances in Clinical and Experimental Medicine, ISSN 1899–5276 (print), ISSN 2451–2680 (online)

*Adv Clin Exp Med.* 2024;33(8):817–829

## Address for correspondence

Yongzhang Li  
E-mail: liyz@hebcm.edu.cn

## Funding sources

This study was funded by the grant from the Natural Science Foundation of Hebei Province (No. H2021423018), Hebei Provincial Health Care Commission (No. 20210302), and Hebei Provincial Administration of Traditional Chinese Medicine (No. 2022040).

## Conflict of interest

None declared

Received on March 10, 2023

Reviewed on May 7, 2023

Accepted on September 15, 2023

Published online on November 28, 2023

## Abstract

**Background.** Chronic nonbacterial prostatitis (CNP) is a chronic inflammatory disease. Patients often have trouble urinating, experience painful and frequent urination, and pelvic floor pain, which seriously affects their quality of life. Dihydroartemisinin (DHA) is the most important artemisinin derivative with good anti-inflammatory effects. However, the mechanism of DHA for CNP has not been fully elucidated.

**Objectives.** To examine the protective effect of DHA on CNP in mice model and to explore the potential mechanisms from the perspective of microRNAs (miRNAs).

**Materials and methods.** The CNP mouse model was induced using a prostate protein extract solution and complete Freund's adjuvant. The pain threshold was determined using von Frey filaments. Hematoxylin and eosin (H&E) staining, TUNEL staining, western blot, real-time polymerase chain reaction (PCR), and small RNA sequencing were used to evaluate the effect of DHA on CNP.

**Results.** Dihydroartemisinin significantly alleviated prostate tissue damage in CNP mice, reduced the pain threshold, improved the prostate index, and reduced cell apoptosis. It also reduced the expressions of interleukin-1 $\beta$  (IL-1 $\beta$ ), interleukin-6 (IL-6), tumor necrosis factor- $\alpha$  (TNF- $\alpha$ ), and macrophage chemoattractant protein-1 (MCP-1). Furthermore, after screening 48 differentially expressed genes, we found 4 miRNAs significantly downregulated and 2 miRNAs upregulated in the model group, which were later significantly reversed by DHA treatment. These results indicate that DHA treatment of CNP involves several signaling pathways.

**Conclusions.** Dihydroartemisinin can improve the pathological state and inflammatory response in a CNP mouse model, which may be related to the regulation of miRNAs.

**Key words:** inflammation, dihydroartemisinin, chronic nonbacterial prostatitis, small RNA sequencing

## Cite as

Hu J, Zhou Y, Wang J, et al. Dihydroartemisinin ameliorated the inflammatory response and regulated miRNA-mRNA expression profile of chronic nonbacterial prostatitis. *Adv Clin Exp Med.* 2024;33(8):817–829. doi:10.17219/acem/172386

## DOI

10.17219/acem/172386

## Copyright

Copyright by Author(s)

This is an article distributed under the terms of the Creative Commons Attribution 3.0 Unported (CC BY 3.0) (<https://creativecommons.org/licenses/by/3.0/>)

## Background

Chronic prostatitis is a chronic inflammation that affects approx. 8–11.5% of men worldwide,<sup>1,2</sup> and more than 90% of chronic prostatitis are caused by chronic nonbacterial prostatitis (CNP).<sup>3,4</sup> Patients often experience difficulty urinating, painful and frequent urination, and pelvic floor pain, which seriously affects their quality of life.<sup>5</sup> Due to the multifactorial and complex pathogenesis of CNP, its mechanism has long been debated. However, at present, it remains not fully elucidated. Most researchers believe it is caused by a combination of etiological infection, inflammation, abnormal neuromuscular activity in the pelvic floor, and immune abnormalities.<sup>6</sup> Notably, inflammation plays a key role in the pathogenesis of many diseases.<sup>7–10</sup> Antibiotics, botanicals, alpha-blockers, and non-steroidal anti-inflammatory analgesics are common treatment methods for CNP.<sup>11</sup> However, chemicals are not appropriate as permanent therapeutics because they are prone to adverse reactions. Antibiotics are unlikely to help unless combined with alpha-blockers, and they are prone to dependence.<sup>12</sup> Surprisingly, the therapeutic role of traditional Chinese medicine (TCM) and some botanical ingredients in the treatment of chronic prostatitis has received increasing attention in recent years.<sup>13,14</sup> Therefore, the search for a safe, efficient and well-absorbed botanical component is of great importance for the treatment of CNP.

Recently, there has been remarkable advancement in TCM research. Some natural products have significant anti-inflammatory activity and promising applications for treating prostate diseases. Artemisinin is a special sesquiterpene lactone containing a peroxide bond extracted from the annual Compositae family member *Artemisia annua* L., which is an effective antimalarial component.<sup>15,16</sup> Dihydroartemisinin (DHA) is the most important artemisinin derivative, created by the oxidation of artemisinin with sodium tetrahydroborate.<sup>17</sup> As the first-generation derivative of artemisinin, DHA has better water solubility and stability, high efficiency, low toxicity, and strong activity.<sup>18</sup> In recent years, some studies have confirmed that DHA has anti-inflammatory, anti-tumor, antibacterial, and immunomodulatory characteristics, in addition to antimalarial properties.<sup>15,19–21</sup> Moreover, studies have reported that DHA improved the symptoms of systemic lupus erythematosus in mice and regulated the secretion of the pro-inflammatory mediator tumor necrosis factor- $\alpha$  (TNF- $\alpha$ ). It was thought that the possible mechanism was via the inhibition of NF- $\kappa$ B-induced inflammatory cascade by affecting NF- $\kappa$ B activation and translocation to the nucleus.<sup>22</sup> Previously, we investigated the protective effect of DHA on hyperglycemia-induced vascular smooth muscle cell (VSMC) proliferation and associated inflammation. Dihydroartemisinin dramatically lowered the mRNA levels of interleukin-1 $\beta$  (IL-1 $\beta$ ) and TNF- $\alpha$ , and this mechanism may play a protective role in VSMC proliferation and

inflammation via suppressing the *miR-376b-3p/KLF15* axis.<sup>23</sup> Previous research has demonstrated that DHA can lower the generation of inflammatory factors in prostatitis tissues and alleviate prostatitis and the inflammatory response by inhibiting the E2F7/HIF1 $\alpha$  pathway.<sup>24</sup>

However, little attention has been paid to gene regulation. MicroRNAs (miRNAs) have been extensively studied in many diseases, and their expression can be modulated by many different compounds.<sup>25</sup> To identify CNP-specific differentially expressed miRNAs (DEMs) and mRNAs, we used a bioinformatics approach to investigate candidate miRNA-mRNA expression profiles of DHA involved in the CNP pathogenesis.

## Objectives

In this study, we investigated the therapeutic impact of DHA on CNP mice from pharmacogenetic point of view and examined the underlying mechanisms responsible for this effect. The effect of DHA on miRNA-mRNA expression profile in the prostate tissue of CNP model mice was investigated by small RNA sequencing, which laid the foundation for the study on CNP.

## Materials and methods

### Animal experiments

#### Animals and drugs

Male nonobese diabetic (NOD) mice (6–8 weeks old, 20–22 g), supplied from Beijing Zhongke Zesheng Biotechnology Co., Ltd. (Beijing, China), were used in all experiments. Before experimental manipulation, all animals were exposed to 12 h of light and dark cycle and constantly supplied with food and drink for at least 7 days. The mice were fed a general experimental animal diet provided by Chengdu Dossy Experimental Animal Co., Ltd. (Chengdu, China). The composition of the animal diet was as follows: corn, soybeans, bone flour, wheat, fish flour, sodium chloride, and vitamin complex. All animal procedures were approved by the Laboratory Animal Ethical and Welfare Committee of Hebei Medical University (approval No. IACUC-Hebmu-P2021075). Dihydroartemisinin was purchased from Shanghai Yuanye Biotechnology Co., Ltd (batch No. B21182, purity  $\geq$ 98%).

#### Experimental autoimmune prostatitis

Prostate tissue was harvested from Sprague–Dawley rats under aseptic conditions, washed with saline, and added to a saline solution containing 0.5% Triton X-100. The prostate tissue was homogenized on ice prior to centrifugation to obtain the supernatant. The biconchonic acid (BCA)

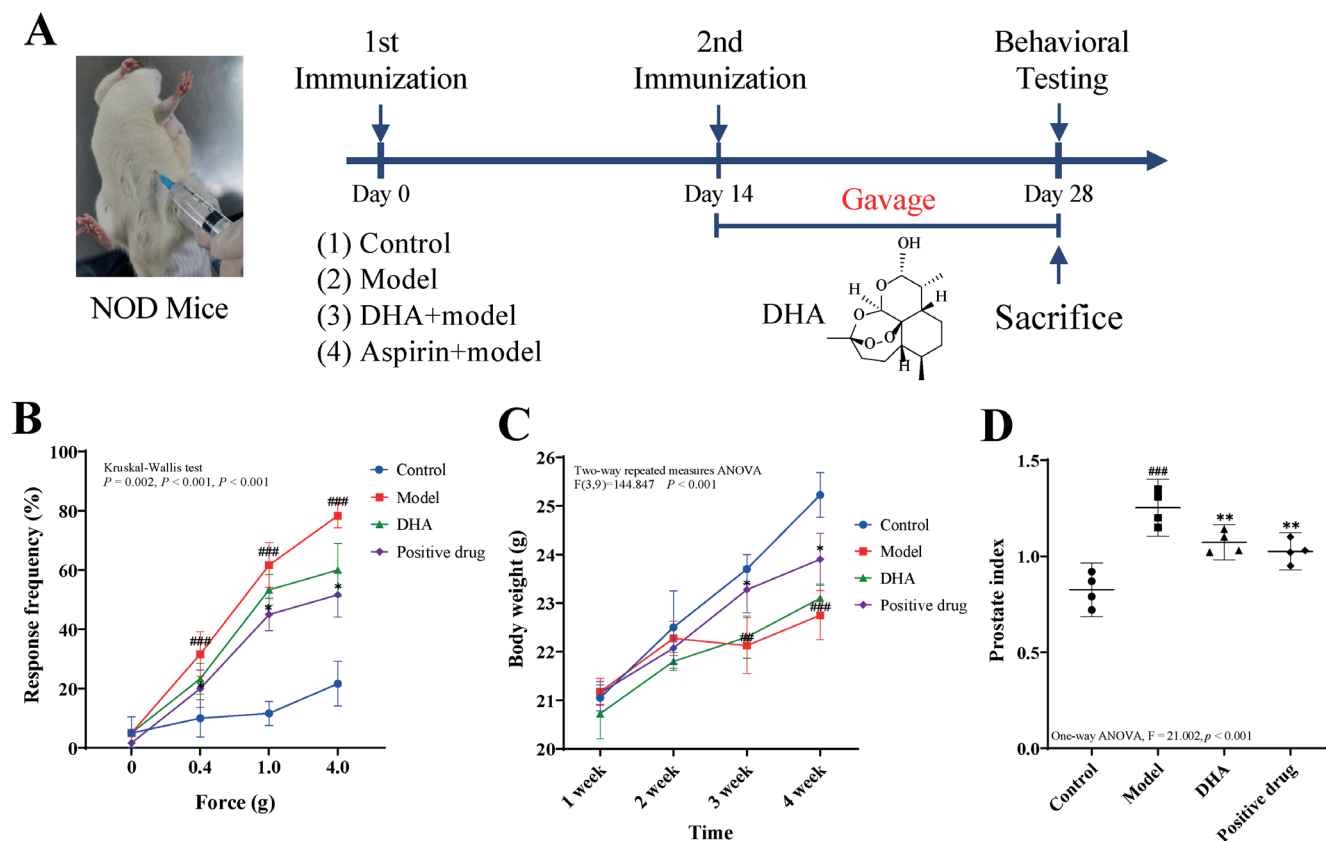


Fig. 1. Dihydroartemisinin improved nociceptive sensitivity in chronic nonbacterial prostatitis (CNP) mice. A. The experimental method is depicted in a timeline diagram; B. Nonobese diabetic (NOD) mice responded to mechanical abdominal stimulation using von Frey filaments at forces of 0, 0.4, 1.0, and 4.0 g. Response frequency was analyzed by the Kruskal–Wallis test ( $n = 6$ ); C. Body weight changes of mice; p-value calculated for the difference between groups by two-way repeated measures analysis of variance (ANOVA) ( $n = 6$ ); D. DHA significantly decreased the prostate index compared with the model group. The prostate index was analyzed by one-way ANOVA ( $n = 4$ ). Data are presented as the means and 95% confidence interval (95% CI) whiskers

## $p < 0.01$ ; ### $p < 0.001$  vs control group; \* $p < 0.05$ ; \*\* $p < 0.01$  compared with the model group; DHA – dihydroartemisinin group.

protein concentration assay kit was used to determine the protein concentration in the supernatant, which was adjusted to 20 mg/mL. Subsequently, the rat prostate protein purification solution was combined with an equivalent volume of complete Freund’s adjuvant via ultrasound to make a suspension.

Nonobese diabetic mice ( $n = 24$ ) were randomized into control, model, DHA (150 mg/kg), and positive drug (aspirin tablets, 150 mg/kg) groups ( $n = 6$ ). Each mouse in the control group was injected subcutaneously with phosphate buffer saline (PBS) + complete Freund’s adjuvant (0.1 mL). In the experimental autoimmune prostatitis (EAP) model group, DHA group and positive drug group, each mouse was injected subcutaneously with 0.1 mL of purified prostate protein solution and complete Freund’s adjuvant. A second immunization was performed after 14 days to establish a mouse model of chronic nonbacterial prostatitis, EAP. The DHA and positive drug groups were administered by gavage starting with the second immunization and repeated every 2 weeks until 28 days of harvesting. The pain thresholds were measured using von Frey fiber filaments on day 28. All mice were sedated with ip. pentobarbital (5%, 50 mg/kg), and the prostate

tissue was immediately isolated and weighed to calculate the prostate index. Prostate index = prostate weight (mg)/body weight (g). The tissues were stored in a  $-80^{\circ}\text{C}$  environment for later analysis. The detailed experimental procedure is shown in Fig. 1A.

### Behavioral nociception measurement

The pain threshold of NOD mice was determined using von Frey filaments, and the skin abnormalities were assessed on day 28 after immunization.<sup>26</sup> The test was performed in a transparent plastic chamber with a stainless-steel grid floor. Mice were placed in the experimental room for at least 30 min to acclimatize to the environment before the behavioral tests began. Von Frey filaments were then used to measure the tactile abnormal discomfort and hyperalgesia in each mouse at forces of 0, 0.4, 1.0, and 4.0 g, respectively. Von Frey filaments were administered on the abdomen for 1–2 s, 10 times, with 2 min between each stimulation. To prevent desensitization, stimulation was limited to the lower abdomen and varied areas within this area were stimulated. Positive reactions to filament stimulation were classified into 3 types, namely 1) abrupt abdominal retraction; 2) quick

licking or scratching; or 3) jumping.<sup>27</sup> The percentage reaction frequency was calculated as [(the number of positive responses/10 trials) × 100 = percentage response frequency].

## Hematoxylin and eosin staining

The prostate tissue was fixed, dehydrated and embedded in paraffin before being cut into sections and stained as follows.<sup>28</sup> The prostate tissue sections were first dewaxed, and then stained with hematoxylin for 20 min. Next, after being separated by HCl/95% alcohol for 10 s, they were put into a weak ammonia solution at 50°C to return to a blue color. The slides were then stained with eosin for 5 min. Sections then underwent a soaking process in graded concentrations of alcohol, followed by treatment with xylene to achieve transparency. They were then sealed with neutral gum and examined under a microscope (Zeiss AxioVision, Oberkochen, Germany).

## TUNEL staining

TUNEL staining was performed in the previous study.<sup>29</sup> To prepare the tissue sections, they were first deparaffinized and rehydrated, and then soaked in water for 5 min. Antigen retrieval was performed with a microwave, heating the samples for 8 min, followed by 3 washes with PBS (5 min per wash). Next, a TUNEL reaction mixture consisting of 50 µL TDT and 450 µL fluorescein-labeled dUTP solution was added to each slice, which was then incubated at 37°C for 1 h. Then, the sections were rinsed with PBS for 5 min × 3 times. DAPI nuclear staining was performed for 5 min, followed by rinsing with PBS and mounting the sections with 50% glycerol. The samples were stored at -20°C for microscopic examination (Nikon, Tokyo, Japan). The TUNEL analysis was assessed as 10 visual fields per mouse, and the apoptosis rate of each mouse was calculated.

## Western blotting

The tissues were first frozen and subsequently ground to a powder. The resulting powder was then lysed using RIPA lysate while kept on ice for 15 min. The lysed samples were then centrifuged at 12,000 rpm at 4°C for 10 min, and the resulting supernatant was collected. The protein concentration of the supernatant was determined using a BCA protein assay kit. To denature proteins, they were heated at 95°C for 5 min before being stored at a low temperature (-80°C) for subsequent analysis. Next, the samples were separated on 8–10% sodium dodecyl-sulfate polyacrylamide gel electrophoresis (SDS-PAGE) gels and transferred onto polyvinylidene fluoride (PVDF) membranes (Millipore, Billerica, USA). The membranes were blocked with 5% skim milk and left in a shaker for 2 h at 37°C. Then, primary antibodies (anti-IL-1β, No. A1112, 1:2000; anti-IL-6, No. A0286, 1:2000; anti-TNF-α, No. A11534, 1:2000;

MCP-1, No. A22744, 1:2000; β-actin, No. AC026, 1:100,000; all from Abclonal, Woburn, USA) were added and incubated overnight at 4°C. After washing with PBS, they were incubated with secondary antibodies (goat anti-rabbit IgG (H + L), No. s0001, 1:5000; Affinity, Changzhou, China) for 2 h, then washed with Tris-buffered saline with Tween (TBST) 3 times and colored by enhanced chemiluminescence (ECL) (Bio-Rad, Foster City, USA). Finally, the images were scanned and analyzed by a gel image analysis system.

## Small RNA sequencing

The total RNA extraction reagent Trizol was used to obtain the total RNA. An Agilent Bioanalyzer 2100 (Agilent Technologies, Santa Clara, USA) was used to evaluate sample concentration and integrity, which served as a reference for the library building and bioinformatic analysis. Polyacrylamide gel electrophoresis (PAGE) was used to separate the RNA fragments, and short RNAs with lengths of 18–30 nt were obtained. The Illumina TruSeq Small RNA Sample Prep kit (New England Biolabs, Inc., Ipswich, USA) was used to create small RNA libraries. Then, enriched libraries were amplified by polymerase chain reaction (PCR) to enrich cDNA with both 3' and 5' connectors. After cDNA amplification, the small RNA libraries were further purified by electrophoresis. The quality of the library was identified using an Agilent 2100 Bioanalyzer and an Agilent High Sensitivity DNA Kit (Agilent Technologies, Foster City, USA), with the criterion of the qualified libraries showing only a single peak and no junction. The libraries were then measured using the Quan-iT PicoGreen dsDNA assay kit (Thermo Fisher Scientific, Waltham, USA), and the Illumina platform was used for RNA sequencing. Single-stranded cDNA was used as a template for PCR amplification and sequencing by annealing a sequencing primer. The target genes of these miRNAs were classified after the identification of DEMs using sequencing. Finally, the miRNA targets were subjected to Gene Ontology (GO) and Kyoto Encyclopedia of Genes and Genomes (KEGG) pathway analyses.

## miRNA qPCR analysis

Total RNA was extracted using the Molpure® cell/tissue total RNA kit (No. 19221ES50; Yeasen Biotechnology Co., Ltd., Shanghai, China) according to the manufacturer's instructions. Reverse transcription (RT) reactions were performed using Bulge-Loop™ miRNA RT primers (No. R10031.7; RiboBio, Guangzhou, China) and Bulge-Loop™ miRNA qRT-PCR starter kit (No. R11067.2; RiboBio). The RT reaction procedure was performed at 42°C for 60 min and at 70°C for 10 min. Real-time PCR reactions were performed using 2X SYBR Green Mix, Bulge-Loop™ miRNA Forward Primer, and Bulge-Loop™ Reverse Primer. The reaction conditions

were as follows; pre-denaturation, 95°C, 10 min; denaturation, 95°C, 2 s; annealing, 60°C, 2 s; extension, 70°C, 10 s. All data were analyzed by a QuantStudio TM3 instrument (Thermo Fisher Scientific).

## Data analysis and statistical methods

GraphPad Prism 8.0 (GraphPad Software, San Diego, USA) and IBM SPSS 25.0 statistical software (IBM SPSS, Armonk, USA) were used for statistical analysis. The Shapiro–Wilk method was first used to test for normal distribution, and these were expressed as mean  $\pm$  standard deviation (SD), and non-normally distributed data were expressed as median and percentiles (25<sup>th</sup> percentile (P25) and 75<sup>th</sup> percentile (P75)). For data obeying normal distribution, one-way ANOVA was used for comparison between multiple groups, Levene's test was used for homogeneity of variance analysis, the LSD test for data with homogeneity of variance, and Tamhane's T2 test for data with unequal variance. Repeated measures were analyzed using a two-way repeated measures ANOVA followed by Bonferroni's multiple comparison test. Comparisons of non-normally distributed data were analyzed by non-parametric tests using the Kruskal–Wallis method. All data are presented as the means and 95% confidence interval whiskers. The value of  $p < 0.05$  was considered statistically significant. In addition, Spearman's correlation analysis was utilized to compare 2 genes, with  $p < 0.05$  representing statistical significance.

## Results

### DHA improved nociceptive sensitivity in the CNP model mice

The pain threshold of NOD mice was evaluated by von Frey filaments on day 28 after immunization to evaluate the effect of DHA on chronic pelvic pain in the CNP mice. The response frequency to tactile hypersensitivity was considerably greater in the model group compared with the control group (Kruskal–Wallis,  $F = 20.205$ ,  $p < 0.001$ ), and the response frequency was higher after the second vaccination compared to the first, indicating that CNP can directly produce pain in mice. The response frequency was lower in the DHA and positive drug groups compared with the model group under the forces of 0.4 g, 1.0 g and 4.0 g, respectively (Fig. 1B, Supplementary Table 1). To varying degrees, continuous daily doses of DHA and aspirin reduced the frequency of CNP-induced responses, suggesting that DHA has a pain-relieving effect on CNP mice.

Four weeks later, the average body weight of mice treated with rat prostate protein + Freund's adjuvant decreased sharply ( $F(3.9) = 144.847$ ,  $p < 0.001$ ). However, body weight increased after DHA administration, although it remained significantly lower than in the control group

(Fig. 1C, Supplementary Table 1). We also investigated how DHA affected benign prostatic hyperplasia (BPH). The prostate index, which is the ratio of prostate weight to body weight, can be used to indicate BPH. Our results revealed that the prostate index was raised in the model group (one-way ANOVA,  $F = 21.002$ ,  $p < 0.001$ ) but was lowered by DHA treatment (one-way ANOVA,  $F = 21.002$ ,  $p = 0.006$ ) (Fig. 1D, Supplementary Table 1). The difference in prostate index between the DHA and model group may be due to DHA reducing the inflammatory congestion and edema of the prostate tissue in mice.

### DHA ameliorated histopathological damage and apoptosis of prostate tissue in the CNP model mice

Next, we evaluated the effect of DHA on prostate tissue using pathological staining. Hematoxylin and eosin staining of prostate tissues showed that the control group contained normal structures without histopathological changes. The prostate tissue framework in the control group was integrated and transparent and exhibited an enlarged gland cavity with many folds. Moreover, the prostate gland exhibited a monolayer of flattened, cuboidal, columnar, or pseudostratified columnar glandular epithelium, which was neatly arranged and without showing obvious degeneration and necrosis. The model group's prostate tissue structure was considerably deteriorated as compared to the control group. It was obvious that some of the glandular ducts in the tissue were obscured, epithelial cells displayed degeneration and necrosis, were relatively flat with surrounding interstitial edema and inflammatory cell infiltration, and a large number of lymphocytes were observed. Surprisingly, the prostate tissue improved markedly after DHA therapy. However, edema with inflammatory cell infiltration, lymphocytes, plasma cells, neutrophils and mast cells could still be observed in the interstitium surrounding the glandular duct (Fig. 2A).

The principle of the TUNEL technique is that apoptosis is detected by labeling the 3'-OH site of DNA with fluorescein-conjugated nucleotides in the presence of deoxyribonuclease (TdT). Nuclei were stained with DAPI, and yellow cells were considered apoptotic. The results of TUNEL staining showed that DHA ameliorated cell apoptosis in the prostate tissue (Fig. 2B). Freund's adjuvant stimulation significantly increased apoptosis in prostate cells (one-way ANOVA,  $F = 271.622$ ,  $p < 0.001$ ), although the significant increase of apoptosis level in the model group was suppressed by DHA (one-way ANOVA,  $F = 271.622$ ,  $p < 0.001$ ) (Fig. 2C, Supplementary Table 2).

### DHA reduced inflammatory factors of prostate tissue in the CNP model mice

We used western blot analysis to identify the expression of numerous common inflammatory markers, including

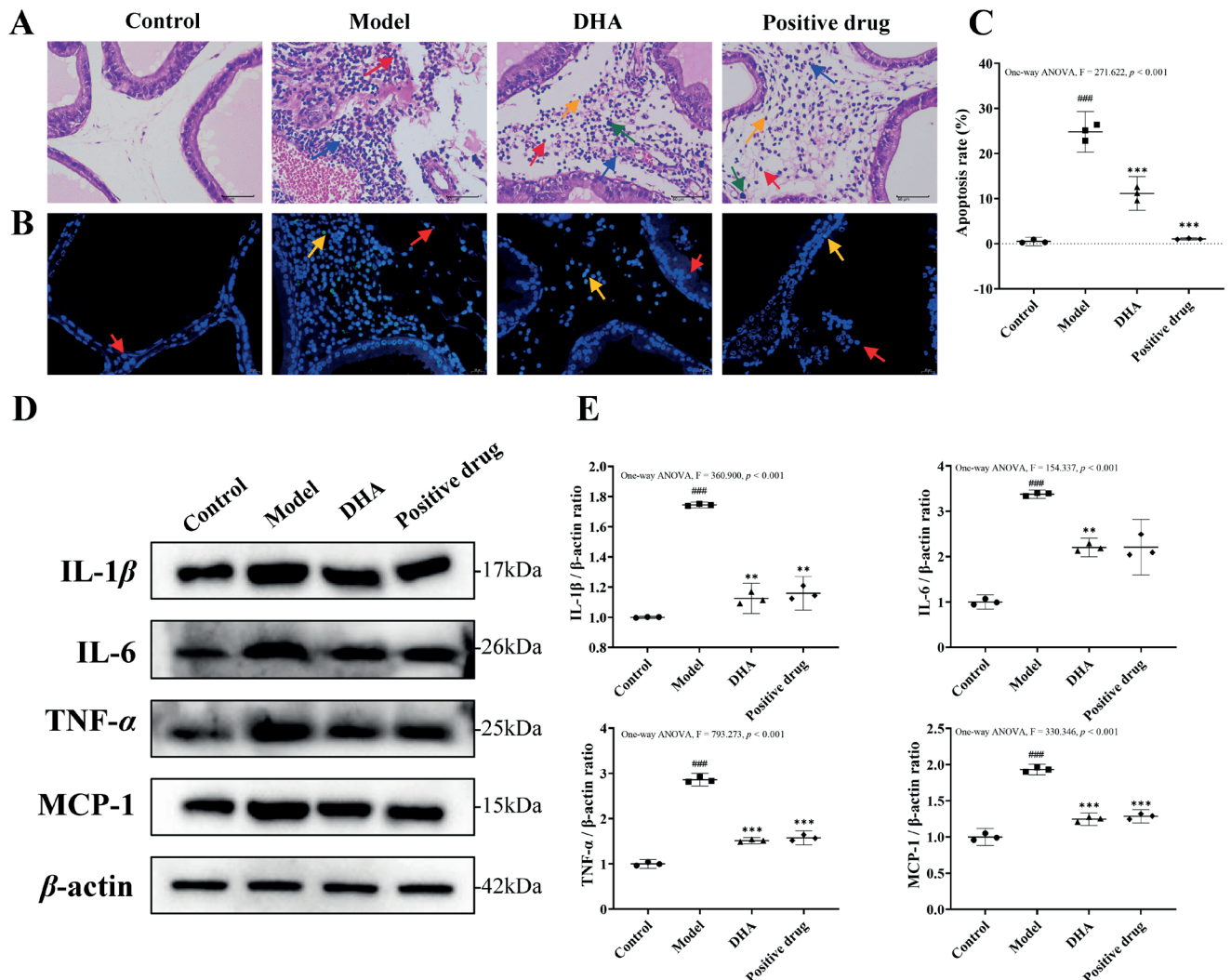


**Fig. 2.** Dihydroartemisinin ameliorated histopathological damage, apoptosis and inflammatory response in prostate tissue of chronic nonbacterial prostatitis (CNP) mice. **A.** Hematoxylin and eosin (H&E) staining of prostate tissues. All images are exhibited at the same magnification,  $\times 400$ , scale bar =  $50\ \mu\text{m}$ ; **B.** Representative TUNEL images show that DHA ameliorated apoptosis in prostate cells. Blue represents nuclear staining (red arrow), and green represents TUNEL staining (yellow arrow), scale bar =  $20\ \mu\text{m}$ ; **C.** The apoptosis rate of prostate cells; **D.** The protein expression of IL-1 $\beta$ , IL-6, TNF- $\alpha$ , and MCP-1 in the prostate tissues was detected using western blotting; **E.** Densitometric analysis of IL-1 $\beta$ , IL-6, TNF- $\alpha$ , and MCP-1 protein expression normalized to  $\beta$ -actin content ( $n = 3$ ). Data are presented as the means and 95% confidence interval (95% CI) whiskers. Statistical analysis of the data was performed using one-way analysis of variance (ANOVA)

### $p < 0.001$  compared with the control group; \*\* $p < 0.01$ ; \*\*\* $p < 0.001$  compared with the model group; DHA – dihydroartemisinin group.

IL-1 $\beta$ , interleukin-6 (IL-6), TNF- $\alpha$ , and macrophage chemoattractant protein-1 (MCP-1), in prostate tissues to better understand how DHA inhibits CNP by reducing inflammation. According to the findings, IL-1 $\beta$ , IL-6, TNF- $\alpha$ , and MCP-1 levels in the CNP mice were significantly elevated ( $F = 360.900$ ,  $p < 0.001$ ;  $F = 154.337$ ,  $p < 0.001$ ;  $F = 793.273$ ,  $p < 0.001$ ;  $F = 330.346$ ,  $p < 0.001$ ), whereas DHA dramatically decreased these proteins' expression ( $F = 360.900$ ,  $p = 0.006$ ;  $F = 154.337$ ,  $p = 0.002$ ;  $F = 793.273$ ,  $p < 0.001$ ;  $F = 330.346$ ,  $p < 0.001$ ) (Fig. 2D,E, Supplementary Table 2). Overall, these findings displayed that DHA could attenuate CNP and antagonize the inflammatory response.

## DHA affected the miRNA-mRNA expression profile of prostate tissue in the CNP mouse model

### Data filtering and small RNA sorting

Small RNA sequencing was performed on the control group, model group and DHA group, producing a total of 201,337,093 raw reads and 197,003,650 clean reads ( $\geq 18$  nt) from 9 samples (3 samples per group). We discarded sequences with average sequencing quality below 20 and then filtered them for subsequent analysis. The average clean rate was 97.83%, which indicated that the quality control of sequencing data was reliable (Table 1). We then summarized the annotation of all small RNAs compared to various types of RNAs (Fig. 3A).

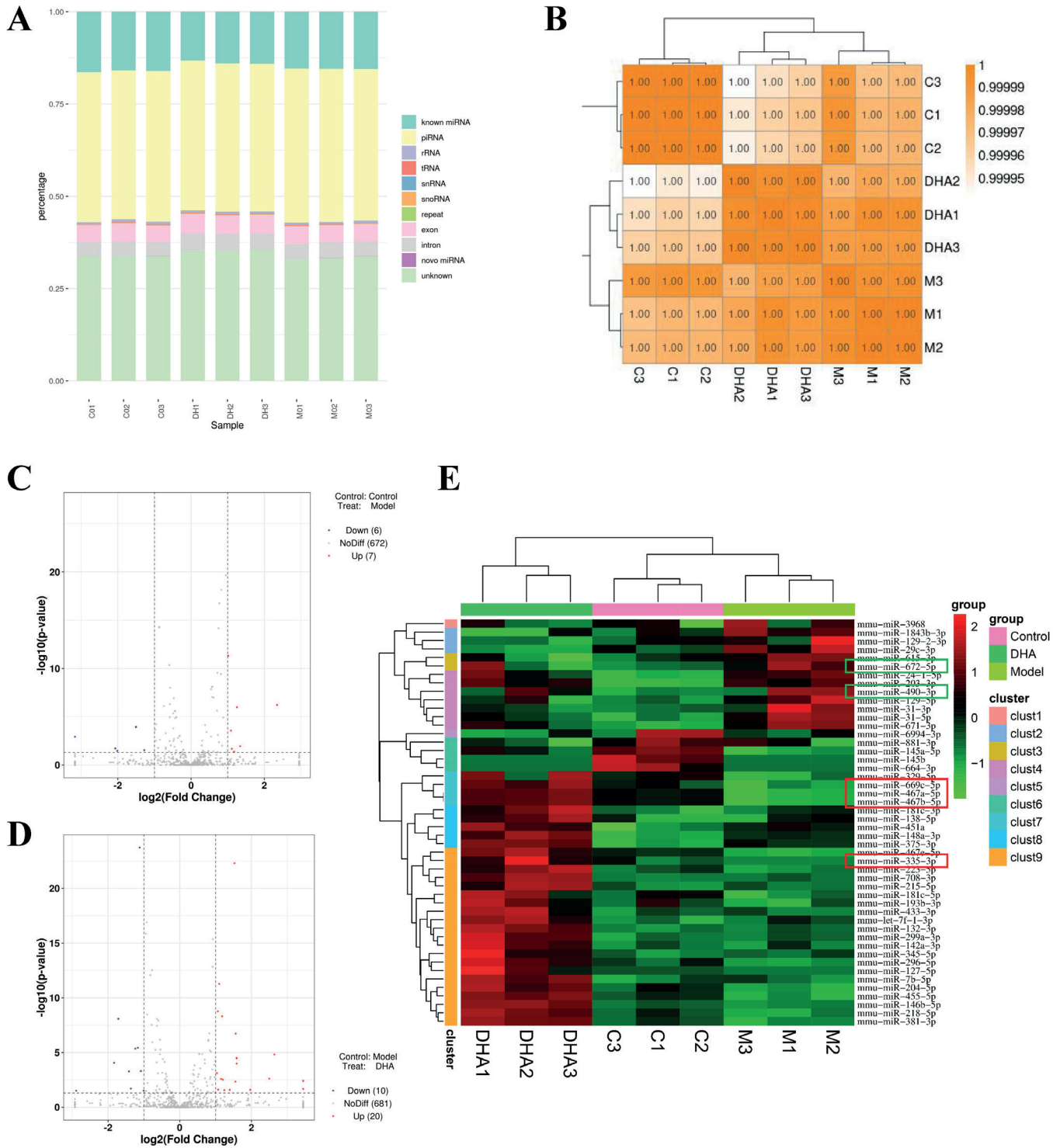


**Fig. 3.** Dihydroartemisinin affected miRNA-mRNA expression profile of prostate tissue in the chronic nonbacterial prostatitis (CNP) mice. **A.** Small RNA classification statistics chart. The horizontal coordinate is the sample name, and the vertical coordinate is the proportion of de-duplicated sequences annotated to various RNAs to the total de-duplicated sequences; **B.** Pearson correlation coefficient for a sample test. The left and the top are the sample clustering cases, the right and the bottom are the sample names, and the squares of different colors represent the high or low correlation between the 2 samples. Volcano map of differentially expressed genes (DEGs) in the control vs model group (**C**) and the model vs DHA group (**D**). Red dots represent upregulated genes, blue dots represent downregulated genes, and gray dots represent non-significant DEGs (fold change  $\geq 2$ ,  $p \leq 0.05$ ); **E.** Heatmap of DEMs in each sample based on hierarchical clustering analysis. The distance was calculated using the Euclidean method, and hierarchical clustering was applied. MiRNA with the most similar expression patterns are grouped together. Clustering was accomplished through the usage of complete linkage. Green denotes low expression, whereas red denotes strong expression

C – control group; M – model group; DHA – dihydroartemisinin group.

Table 1. Sequencing data volume statistics for 9 samples

Sample	Raw reads	Clean reads	Clean rate (%)
C1	22,999,745	22,549,376	98.04
C2	24,645,074	24,130,473	97.91
C3	23,197,912	22,677,066	97.75
DHA1	19,053,157	18,560,325	97.41
DHA2	18,479,443	18,042,214	97.63
DHA3	21,294,151	20,808,361	97.72
M1	22,018,657	21,606,038	98.13
M2	24,522,043	23,972,182	97.76
M3	25,126,911	24,657,615	98.13

Clean reads ( $\geq 18$  nt) – number of filtered sequences (nucleotide length  $\geq 18$  nt); C – control group; M – model group; DHA – dihydroartemisinin group.

### Screening and analysis of differentially expressed miRNAs

We conducted a Pearson correlation coefficient analysis to find any correlation between miRNA expressions (Fig. 3B). The Pearson correlation coefficient was 0.99, indicating that the samples were extremely strongly correlated with each other. Next, we analyzed the differences in miRNA expression levels by DESeq (the criteria are

based on  $|\log_2(\text{fold-change})| \geq 1$  and  $p < 0.05$ ). The findings revealed that 13 miRNAs were significantly modified in the model group ( $p < 0.05$ ), with 7 miRNAs upregulated and 6 miRNAs downregulated (Fig. 3C). A total of 30 miRNAs were notably expressed in the DHA group ( $p < 0.05$ ), with 20 miRNAs being upregulated and 10 miRNAs being downregulated (Fig. 3D). Next, we performed bidirectional clustering analysis of all miRNAs and samples, which revealed differences in 48 differentially expressed genes in each sample (Fig. 3E). Four miRNAs (*miR-467a-5p*, *miR-467b-5p*, *miR-335-3p*, *miR-669c-5p*) were downregulated in the CNP mice and upregulated after DHA treatment, while 2 miRNAs (*miR-490-3p*, *miR-672-5p*) were upregulated in the CNP mice and downregulated after DHA treatment (Table 2). Subsequently, we detected 6 differentially expressed miRNAs in prostatitis tissues using real-time quantitative PCR (Fig. 4A–F, Supplementary Table 3), and statistical analysis was performed using one-way ANOVA and Kruskal–Wallis test. Although there was no significant difference in the expression of *miR-669c-5p* (one-way ANOVA,  $F = 12.930$ ,  $p = 0.134$ ), *miR-467a-5p*, *miR-467b-5p* and *miR-335-3p* displayed reduced expression in the model group compared to the control group ( $F = 6.006$ ,  $p = 0.017$ ;  $F = 25.987$ ,  $p < 0.001$ ;  $F = 6.030$ ,  $p = 0.015$ ), and the expression levels of *miR-467b-5p* and

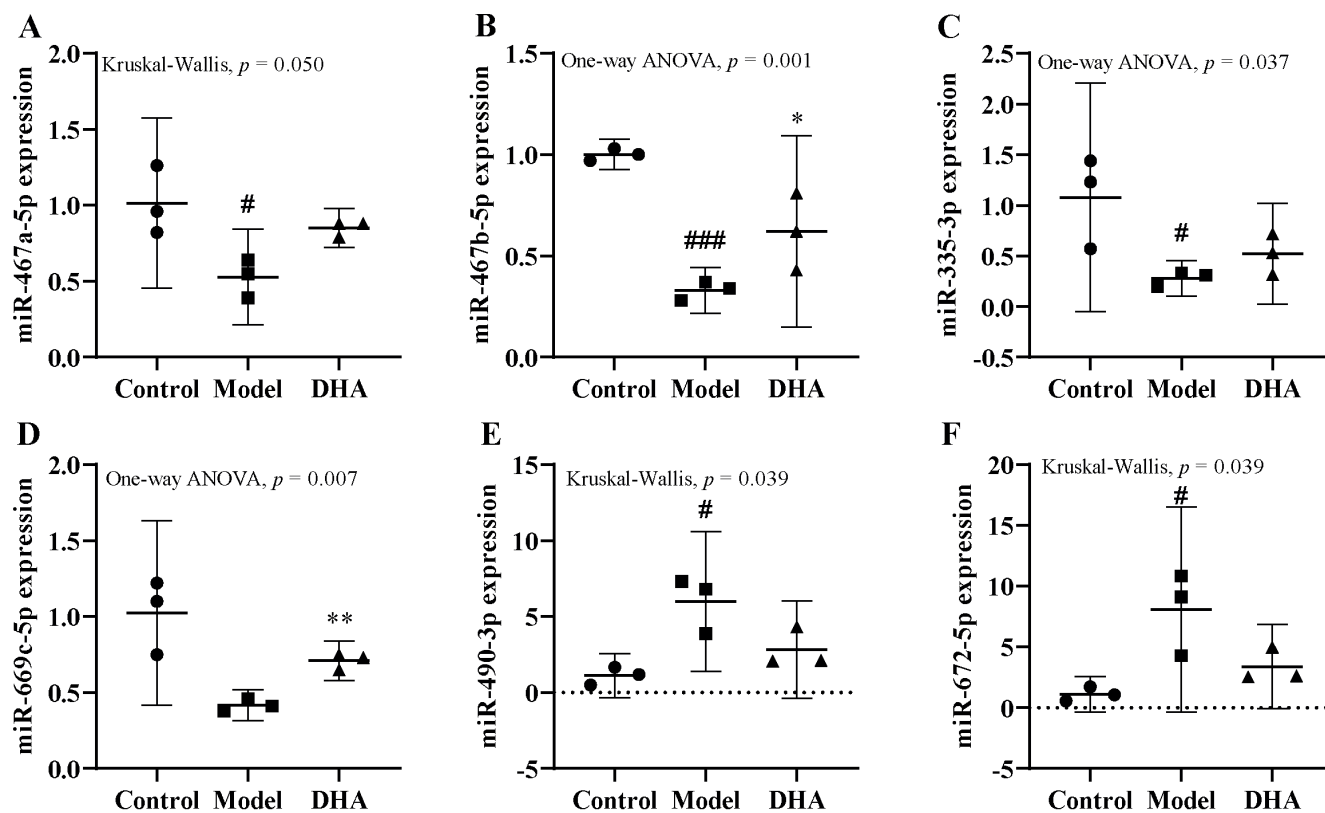


Fig. 4. Identification of 6 differentially expressed miRNAs in prostatitis tissues. The expressions of *miR-467a-5p* (A), *miR-467b-5p* (B), *miR-335-3p* (C), *miR-669c-5p* (D), *miR-490-3p* (E), and *miR-672-5p* (F) in prostatitis tissues were detected using real-time quantitative polymerase chain reaction (PCR) ( $n = 3$ ). Data are presented as the means and 95% confidence interval (95% CI) whiskers. Statistical analysis of the data was performed using one-way analysis of variance (ANOVA) and Kruskal–Wallis test

# $p < 0.05$ ; ### $p < 0.001$  compared with the control group; \* $p < 0.05$ ; \*\* $p < 0.01$  compared with the model group; DHA – dihydroartemisinin group.



**Table 2.** Differentially expressed miRNAs responding to dihydroartemisinin (DHA) treatment

miRNA	FoldChange (model/control)	log2FoldChange	p-value	Regulate	FoldChange (DHA/model)	log2FoldChange	p-value	Regulate
<i>miR-467a-5p</i>	0.353	-1.504	1.147E-04	down	3.006	1.588	3.204E-05	up
<i>miR-467b-5p</i>	0.353	-1.504	1.147E-04	down	3.006	1.588	3.204E-05	up
<i>miR-335-3p</i>	0.248	-2.014	3.394E-02	down	5.646	2.497	2.418E-03	up
<i>miR-669c-5p</i>	0.412	-1.278	2.889E-02	down	2.937	1.554	4.501E-03	up
<i>miR-490-3p</i>	2.381	1.252	1.011E-06	up	0.445	-1.169	3.630E-06	down
<i>miR-672-5p</i>	2.257	1.174	4.113E-02	up	0.389	-1.363	1.936E-02	down

FoldChange represents the differential multiples of gene expression between the control group and the model group, or the model group and the DHA group;  $p < 0.05$ .

*miR-669c-5p* were higher after DHA treatment compared to the model group before treatment ( $F = 25.987$ ,  $p = 0.021$ ;  $F = 12.930$ ,  $p = 0.006$ ). In contrast, *miR-490-3p* and *miR-672-5p* levels were higher in the model group when compared to the control group ( $F = 6.489$ ,  $p = 0.011$ ;  $F = 6.489$ ,  $p = 0.011$ ), while *miR-490-3p* and *miR-672-5p* levels were lower in the DHA group relative to the model group. However, this final result did not reach statistical significance, which was consistent with the sequencing data.

#### miRNA target gene prediction and bioinformatics analysis

We performed target gene prediction on differentially expressed miRNA sequences. A total of 48 miRNAs were analyzed, resulting in 15,689 predicted target genes, and 73,083 predicted target sites. To investigate the function and mechanisms of miRNA target genes, GO and KEGG pathway enrichment studies were carried out. Gene Ontology enrichment analysis of the control compared to the model group showed that there were 1887 statistically significant GO term entries in the total differential genome ( $p < 0.05$ ). The top 20 enriched GO terms of control vs model groups are shown in Fig. 5A. The biological processing (BP) contained “regulation of cellular process”, “regulation of biological process”, “signaling”, etc. For the cellular components (CC), terms related to “membrane” and “cell periphery” were enriched, while the molecular function (MF) included olfactory receptor activity. In the control vs model group, there were 2,631 statistically significant GO term entries in the total differential genome ( $p < 0.05$ ). The top 20 enriched GO terms of model vs DHA groups were involved in BP (cellular process, biological regulation, regulation biological process, regulation of the cellular process, etc.) and CC (cell periphery, membrane, intracellular, etc.) (Fig. 5B).

Further KEGG pathway analysis of the control vs model group showed that 27 pathways were enriched ( $p < 0.05$ ), including 5 major categories, namely “organismal systems”, “human diseases”, “environmental information processing”, “cellular processes”, and “metabolism”. Correspondingly, pathways were also involved in cancer (breast cancer,

microRNAs in cancer), glycan biosynthesis and metabolism, signal transduction (phosphatidylinositol signaling system, Wnt, MAPK, Rap1, and sphingolipid signaling pathway), lipid metabolism (biosynthesis of unsaturated fatty acids), and infectious disease: bacterial (yersinia infection), among others. Detailed information is shown in Fig. 5C. In the model vs DHA group, there were 94 statistically significant KEGG pathways in the total differential genome ( $p < 0.05$ ). The top 20 signaling pathways were divided into 4 major categories, “cellular processes”, “human diseases”, “organismal systems”, and “environmental information processing”, all of which were also involved in cancer (microRNAs in cancer, choline metabolism in cancer, gastric cancer, breast cancer), signal transduction (mTOR, Hippo, sphingolipid, and phosphatidylinositol signaling), immune system (T cell receptor signaling pathway), etc. Detailed information is shown in Fig. 5D.

## Discussion

Prostatitis seriously affects men’s health, and the malignant development of prostate tissue cells may further transform into prostate cancer. Even though it is one of the most prevalent prostate disorders in the world, CNP is still debatable in terms of its genesis. The current knowledge on its pathogenesis mainly involves pathogen infection, inflammation, immunity, heredity, and oxidative stress.<sup>30–32</sup> However, accumulated evidence has indicated that TCM has amassed rich experience in clinical practice and achieved certain curative effects in the treatment of prostate diseases. Due to the disadvantages of poor water solubility and low bioavailability of artemisinin, DHA, an important derivative of artemisinin, exhibits better bioavailability and increased anti-malarial effects compared to artemisinin. In addition, DHA also has anti-inflammatory and anti-tumor activity, among other pharmacological effects. Herein, we examined how DHA affected mice with prostatitis caused by the administration of prostate tissue and complete Freund’s adjuvant. The EAP model is straightforward to construct and has a high success rate. The modeled

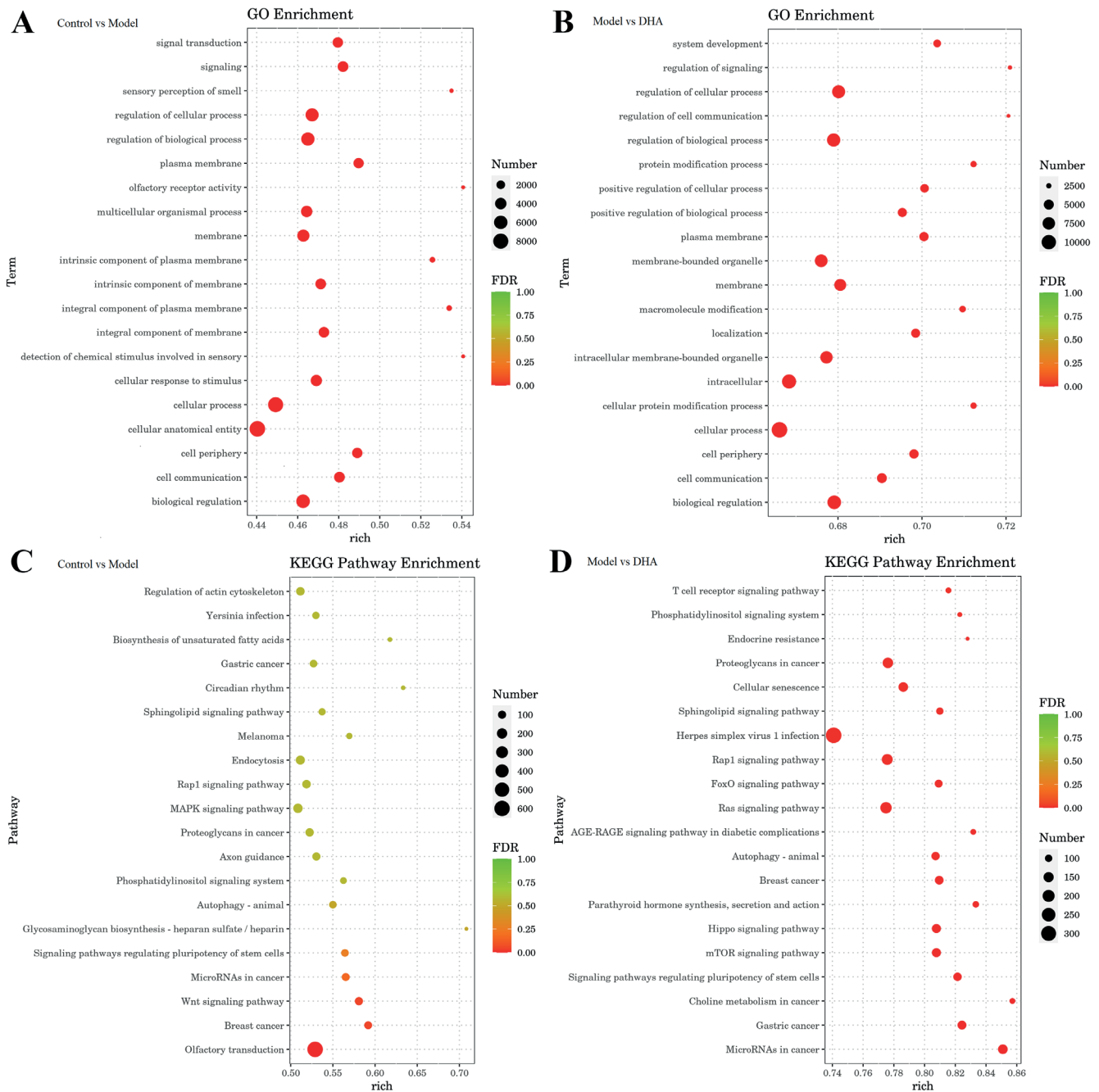


**Fig. 5.** Function and pathway analysis of the target genes of differentially expressed miRNAs (DEMs). A. Gene Ontology (GO) enrichment analysis between the control and model groups; B. GO enrichment analysis between the model and dihydroartemisinin (DHA) group; C. Kyoto Encyclopedia of Genes and Genomes (KEGG) enrichment analysis between the control and model group; D. KEGG enrichment analysis between the model and DHA group. The false discovery rate (FDR) value ranges from 0 to 1, with the values closer to 0 indicating a more substantial enrichment

CNP, which has been widely used, may cause a significant inflammatory response in the prostate gland with strong pathological specificity, prolonged model duration, and pathological changes similar to clinical manifestations. In this study, the results showed that DHA significantly improved CNP. Dihydroartemisinin reduced the frequency of pain responses, improved the epithelial cells and glandular ducts of the prostate tissue, reduced inflammatory infiltration, and decreased the prostate index. Simultaneously, DHA significantly

reduced apoptosis and the inflammatory response in prostate tissue.

Previous investigations have demonstrated that cytokines and inflammation are key factors in the development of CNP.<sup>33</sup> When the prostate is stimulated, it produces a wide range of host defense and inflammatory factors.<sup>34</sup> The IL-1 $\beta$  is a critical pro-inflammatory factor that leads to the occurrence and persistence of inflammation. The release of caspase-1 induced by NOD-like receptor protein 3 (NLRP3) inflammasome and the downstream

cytokine IL-1 $\beta$  may be one of the pathogenic mechanisms of prostatitis.<sup>35,36</sup> The IL-6 is an important pro-inflammatory interleukin, and the level of IL-6 in CNP has been strongly correlated to the intensity of patients' clinical symptoms.<sup>37</sup> The IL-6 is a pleiotropic cytokine that regulates T cell migration and chronic immune responses and is strongly linked to prostate cell growth and death.<sup>38</sup> In addition, IL-6 may regulate the occurrence and development of CNP by regulating cellular autophagy.<sup>39</sup> The TNF- $\alpha$  is a major pro-inflammatory cytokine that is involved in the induction of inflammatory responses as well as the regulation of immune responses.<sup>33</sup> Furthermore, TNF- $\alpha$  can increase the production of cytokines, including IL-1, IL-6 and IL-8, by neutrophils and mononuclear macrophages, which stimulates the inflammatory cascade and exacerbates the inflammatory response.<sup>40</sup> In addition to inflammatory factors, MCP-1 is used as an inflammatory biomarker to identify the response of CNP patients to treatment.<sup>38</sup> Research has revealed that MCP-1 activates monocytes and macrophages and is involved in chemotaxis.<sup>41</sup> It promoted the production of pro-inflammatory cytokines, which in turn boosted the inflammatory response in the CNP pathological conditions. Our previous clinical study showed that reducing prostate inflammatory levels was effective in relieving urinary tract infections in prostate cancer patients.<sup>42</sup> In the current investigation, CNP had elevated levels of IL-1 $\beta$ , TNF- $\alpha$  and IL-6, while DHA markedly decreased these, as well as suppressed MCP-1 levels in prostate tissue. Therefore, DHA may be beneficial for preventing the development of CNP by downregulating inflammatory factors and inflammatory mediators.

Changes in miRNA expression profiles are currently the subject of substantial research in conditions like prostate cancer, but studies in CNP are still relatively sparse. We used small RNA sequencing and real-time PCR to evaluate and validate the abnormally expressed miRNAs in order to further clarify the mechanism underlying DHA's impact on the miRNA expression profile in CNP mice. Small RNA is a key regulator of biological processes, including the control of gene expression, biological maturation, metabolism, and the emergence of illness, and CNP pathogenesis is accompanied by abnormal miRNA expression.<sup>43</sup> We found 48 target gene miRNAs, indicating that DHA has a powerful role in altering prostate miRNA expression. The RNA sequencing results showed that 4 miRNAs (*miR-467a-5p*, *miR-467b-5p*, *miR-335-3p*, *miR-669c-5p*) were dramatically diminished in the model group and substantially elevated after DHA treatment. Meanwhile, 2 miRNAs (*miR-490-3p*, *miR-672-5p*) were elevated in the CNP mice and depressed after DHA treatment. Previous investigations have reported that *miR-467a-5p* reduced inflammation and elevated blood glucose and insulin levels to prevent insulin resistance.<sup>44</sup> The *miR-335-3p* was involved in regulating the inflammatory response in myocardial infarction, ulcerative colitis and Parkinson's

disease.<sup>45–47</sup> The *miR-669c-5p* has been reported to be differentially expressed in mouse spermatocyte-derived GC-2 cells and may affect male reproductive function.<sup>48</sup> The *miR-490-3p* was elevated in the reproductive organs of male rats induced by a high cholesterol diet,<sup>49</sup> while *miR-672-5p* was shown to be altered in the kidney of urolithiasis rats.<sup>50</sup> Therefore, these genes have the potential to become novel biomarkers and therapeutic targets for CNP. In this study, we performed a preliminary investigation of DEMs in CNP, and the relationship of these miRNAs with inflammatory, immune, metabolic and other signaling pathways and their mechanisms need to be further examined.

The KEGG pathway analysis of miRNA expression profile in the CNP mice revealed several signaling pathways related to the pathogenesis of CNP. These included the phosphatidylinositol signaling system, Wnt, MAPK, Rap1, and sphingolipid signaling pathway, and there is a clear correlation between some signaling pathways. However, the role of miRNAs and related signal transduction pathways in CNP occurrence and development needs further investigation. Of note, the development of DHA therapy for CNP involves several signaling pathways, including the mTOR, Hippo, sphingolipid, phosphatidylinositol, and T cell receptor signaling pathways. As expected, we found that all these pathways are involved in inflammatory and immune responses, suggesting a key regulatory role for inflammation and the immune system in initiating and progressing CNP. For example, Akt-mTOR could modulate the immune response and prevent Th17 cell over-activation in order to improve chronic prostatitis and chronic pelvic pain syndrome (CP/CPPS).<sup>51</sup> Jiedu Huoxue decoction was found to inhibit apoptosis and activate the Wnt/GSK-3 $\beta$ / $\beta$ -catenin signaling pathway to treat CP/CPPS.<sup>52</sup> In addition, inflammatory factors could reduce CP/CPPS by downregulating NF- $\kappa$ B and JNK/MAPK pathway to alleviate prostatitis pain.<sup>53</sup> In this study, DHA has demonstrated a powerful therapeutic effect for CNP. However, the role of DHA in the CNP by regulating miRNA profiles acting on inflammatory, immune and apoptotic pathways deserves further exploration.

## Limitations

In this study, we screened some DEMs by transcriptomics, but the role of these miRNAs in prostatitis mice remains to be further investigated. Meanwhile, we found that inflammation and the immune system play a key regulatory role in the CNP, but the exact mechanism still needs to be examined.

## Conclusions

This study explored the effectiveness and mechanism of DHA in the treatment of CNP. We found considerable improvement in the pathogenic condition following

DHA administration in a CNP mouse model. The development of biomarkers associated with CNP will be based on the detection of miRNA expression profiles in prostate tissues, which will aid in the early detection, diagnosis and treatment of CNP diseases. This work added to the body of knowledge on the mechanism of DHA in the treatment of CNP and may offer a fresh approach to its prevention and management.

## Supplementary data

The Supplementary materials are available at <https://zenodo.org/record/8327619>. The package contains the following files:

Supplementary Table 1. The normality test and statistical analysis of multiple dependent variable of Fig. 1.

Supplementary Table 2. The normality test and statistical analysis of multiple dependent variable of Fig. 2.

Supplementary Table 3. The normality test and statistical analysis of multiple dependent variable of Fig. 4.

## ORCID iDs

Jie Hu  <https://orcid.org/0009-0009-5906-0837>  
 Yan Zhou  <https://orcid.org/0009-0007-1095-4739>  
 Junhao Wang  <https://orcid.org/0009-0002-6243-8908>  
 Jianpeng Han  <https://orcid.org/0009-0002-4045-2039>  
 Jianyong Feng  <https://orcid.org/0009-0003-2306-6416>  
 Wenbin Chen  <https://orcid.org/0009-0008-1601-6935>  
 Kuo Guo  <https://orcid.org/0009-0006-9360-5464>  
 Yongzhang Li  <https://orcid.org/0000-0002-6249-5198>

## References

- Fuentes IM, Jones BM, Brake AD, et al. Voluntary wheel running improves outcomes in an early life stress-induced model of urologic chronic pelvic pain syndrome in male mice. *Pain*. 2021;162(6):1681–1691. doi:10.1097/j.pain.0000000000002178
- Liu H, Wang Z, Xie Q, et al. Ningmitai capsules have anti-inflammatory and pain-relieving effects in the chronic prostatitis/chronic pelvic pain syndrome mouse model through systemic immunity. *Front Pharmacol*. 2022;13:949316. doi:10.3389/fphar.2022.949316
- Zang L, Tian F, Yao Y, et al. Qianliexin capsule exerts anti-inflammatory activity in chronic non-bacterial prostatitis and benign prostatic hyperplasia via NF- $\kappa$ B and inflammasome. *J Cell Mol Med*. 2021;25(12):5753–5768. doi:10.1111/jcmm.16599
- Zeng F, Chen H, Yang J, et al. Development and validation of an animal model of prostate inflammation-induced chronic pelvic pain: Evaluating from inflammation of the prostate to pain behavioral modifications. *PLoS One*. 2014;9(5):e96824. doi:10.1371/journal.pone.0096824
- Pontari MA. Etiology of chronic prostatitis/chronic pelvic pain syndrome: Psychoimmunoneuroendocrine dysfunction (PINE syndrome) or just a really bad infection? *World J Urol*. 2013;31(4):725–732. doi:10.1007/s00345-013-1061-z
- Zhang Y, Li X, Zhou K, et al. Influence of experimental autoimmune prostatitis on sexual function and the anti-inflammatory efficacy of celecoxib in a rat model. *Front Immunol*. 2020;11:574212. doi:10.3389/fimmu.2020.574212
- Lee G. Chronic prostatitis: A possible cause of hematospermia. *World J Mens Health*. 2015;33(2):103. doi:10.5534/wjmh.2015.33.2.103
- Almeer RS, Muhammad NAE, Othman MS, Aref AM, Elgamel B, Moneim AEA. The potential protective effect of orange peel and selenium against 17 $\beta$ -estradiol-induced chronic non-bacterial prostatitis in rats. *Anticancer Agents Med Chem*. 2020;20(9):1061–1071. doi:10.2174/1871520620666200331102609
- Isik A, Wysocki AP, Memiş U, Sezgin E, Yezhikova A, Islambekov Y. Factors associated with the occurrence and healing of umbilical pilonidal sinus: A rare clinical entity. *Adv Skin Wound Care*. 2022;35(8):1–4. doi:10.1097/01.ASW.0000833608.27136.d1
- Isik A, Soran A, Grasi A, Barry N, Sezgin E. Lymphedema after sentinel lymph node biopsy: Who is at risk? *Lymph Res Biol*. 2022;20(2):160–163. doi:10.1089/lrb.2020.0093
- Doiron RC, Nickel JC. Management of chronic prostatitis/chronic pelvic pain syndrome. *Can Urol Assoc J*. 2018;12(6 Suppl 3):S161–S163. doi:10.5489/cuaj.5325
- Holt JD, Garrett WA, McCurry TK, Teichman JMH. Common questions about chronic prostatitis. *Am Fam Physician*. 2016;93(4):290–296. PMID:26926816.
- Yi J, Pan J, Zhang S, et al. Improvement of chronic non-bacterial prostatitis by Jiedu Huoxue decoction through inhibiting TGF- $\beta$ /SMAD signaling pathway. *Biomed Pharmacother*. 2022;152:113193. doi:10.1016/j.biopha.2022.113193
- Chen JX, Hu LS. Traditional Chinese Medicine for the treatment of chronic prostatitis in China: A systematic review and meta-analysis. *J Altern Complement Med*. 2006;12(8):763–769. doi:10.1089/acm.2006.12.763
- Dai X, Zhang X, Chen W, et al. Dihydroartemisinin: A potential natural anticancer drug. *Int J Biol Sci*. 2021;17(2):603–622. doi:10.7150/ijbs.50364
- Klayman DL. Qinghaosu (artemisinin): An antimalarial drug from China. *Science*. 1985;228(4703):1049–1055. doi:10.1126/science.3887571
- Luo XD, Shen CC. The chemistry, pharmacology, and clinical applications of Qinghaosu (artemisinin) and its derivatives. *Med Res Rev*. 1987;7(1):29–52. doi:10.1002/med.2610070103
- Van Agtmael M. Artemisinin drugs in the treatment of malaria: From medicinal herb to registered medication. *Trends Pharmacol Sci*. 1999;20(5):199–205. doi:10.1016/S0165-6147(99)01302-4
- Yu R, Jin G, Fujimoto M. Dihydroartemisinin: A potential drug for the treatment of malignancies and inflammatory diseases. *Front Oncol*. 2021;11:722331. doi:10.3389/fonc.2021.722331
- Gutman J, Kovacs S, Dorsey G, Stergachis A, Ter Kuile FO. Safety, tolerability, and efficacy of repeated doses of dihydroartemisinin-piper-quine for prevention and treatment of malaria: A systematic review and meta-analysis. *Lancet Infect Dis*. 2017;17(2):184–193. doi:10.1016/S1473-3099(16)30378-4
- Ho WE, Peh HY, Chan TK, Wong WSF. Artemisinins: Pharmacological actions beyond anti-malarial. *Pharmacol Ther*. 2014;142(1):126–139. doi:10.1016/j.pharmthera.2013.12.001
- Li WD, Dong YY, Tu YY, Lin ZB. Dihydroartemisinin ameliorates lupus symptom of BXSB mice by inhibiting production of TNF-alpha and blocking the signaling pathway NF-kappa B translocation. *Int Immunopharmacol*. 2006;6(8):1243–1250. doi:10.1016/j.intimp.2006.03.004
- Yang B, Gao X, Sun Y, et al. Dihydroartemisinin alleviates high glucose-induced vascular smooth muscle cells proliferation and inflammation by depressing the miR-376b-3p/KLF15 pathway. *Biochem Biophys Res Commun*. 2020;530(3):574–580. doi:10.1016/j.bbrc.2020.07.095
- Zhou Y, Wang JH, Han JP, et al. Dihydroartemisinin ameliorates chronic nonbacterial prostatitis and epithelial cellular inflammation by blocking the E2F7/HIF1 $\alpha$  pathway. *Inflamm Res*. 2022;71(4):449–460. doi:10.1007/s00011-022-01544-8
- Chen H, Zhang Z. A miRNA-driven inference model to construct potential drug-disease associations for drug repositioning. *Biomed Res Int*. 2015;2015:406463. doi:10.1155/2015/406463
- Gee LE, Chen N, Ramirez-Zamora A, Shin DS, Piliitsis JG. The effects of subthalamic deep brain stimulation on mechanical and thermal thresholds in 6OHDA-lesioned rats. *Eur J Neurosci*. 2015;42(4):2061–2069. doi:10.1111/ejn.12992
- Schaeffer EM. Re: Th1–Th17 cells contribute to the development of uropathogenic *Escherichia coli*-induced chronic pelvic pain. *J Urol*. 2014;191(6):1808–1809. doi:10.1016/j.juro.2014.03.029
- Choi YJ, Lee JI, Fan M, et al. Metabolomic analysis of *Morus cultivar* root extracts and their ameliorative effect on testosterone-induced prostate enlargement in Sprague Dawley rats. *Int J Mol Sci*. 2020;21(4):1435. doi:10.3390/ijms21041435
- Wang YL, Zhang Y, Cai DS. Hepatoprotective effects of sevoflurane against hepatic ischemia–reperfusion injury by regulating microRNA-124-3p-mediated TRAF3/CREB axis. *Cell Death Discov*. 2022;8(1):105. doi:10.1038/s41420-021-00784-7

30. Zhang M, Liu Y, Chen J, et al. Single-cell multi-omics analysis presents the landscape of peripheral blood T-cell subsets in human chronic prostatitis/chronic pelvic pain syndrome. *J Cell Mol Med.* 2020; 24(23):14099–14109. doi:10.1111/jcmm.16021
31. Sfanos KS, De Marzo AM. Prostate cancer and inflammation: The evidence. *Histopathology.* 2012;60(1):199–215. doi:10.1111/j.1365-2559.2011.04033.x
32. Wang GC, Huang TR, Hu YY, et al. Corpus cavernosum smooth muscle cell dysfunction and phenotype transformation are related to erectile dysfunction in prostatitis rats with chronic prostatitis/chronic pelvic pain syndrome. *J Inflamm.* 2020;17(1):2. doi:10.1186/s12950-019-0233-z
33. Kang SW, Park JH, Seok H, et al. The effects of Korea Red Ginseng on inflammatory cytokines and apoptosis in rat model with chronic nonbacterial prostatitis. *Biomed Res Int.* 2019;2019:2462561. doi:10.1155/2019/2462561
34. Castiglione R, Salemi M, Vicari LO, Vicari E. Relationship of semen hyperviscosity with IL-6, TNF- $\alpha$ , IL-10 and ROS production in seminal plasma of infertile patients with prostatitis and prostatic vesiculitis. *Andrologia.* 2014;46(10):1148–1155. doi:10.1111/and.12207
35. Zhou R, Yazdi AS, Menu P, Tschopp J. A role for mitochondria in NLRP3 inflammasome activation. *Nature.* 2011;469(7329):221–225. doi:10.1038/nature09663
36. McGettrick AF, O'Neill LAJ. How metabolism generates signals during innate immunity and inflammation. *J Biol Chem.* 2013;288(32):22893–22898. doi:10.1074/jbc.R113.486464
37. Stancik I, Plas E, Juza J, Pflüger H. Effect of antibiotic therapy on interleukin-6 in fresh semen and postmasturbation urine samples of patients with chronic prostatitis/chronic pelvic pain syndrome. *Urology.* 2008; 72(2):336–339. doi:10.1016/j.urology.2008.04.005
38. Xiong Y, Zhou L, Qiu X, Miao C. Anti-inflammatory and anti-hyperplastic effect of Bazhengsan in a male rat model of chronic nonbacterial prostatitis. *J Pharmacol Sci.* 2019;139(3):201–208. doi:10.1016/j.jphs.2019.01.007
39. Santarelli R, Gonnella R, Di Giovenale G, et al. STAT3 activation by KSHV correlates with IL-10, IL-6 and IL-23 release and an autophagic block in dendritic cells. *Sci Rep.* 2014;4(1):4241. doi:10.1038/srep04241
40. Jang TL, Schaeffer AJ. The role of cytokines in prostatitis. *World J Urol.* 2003;21(2):95–99. doi:10.1007/s00345-003-0335-2
41. Singh S, Anshita D, Ravichandiran V. MCP-1: Function, regulation, and involvement in disease. *Int Immunopharmacol.* 2021;101:107598. doi:10.1016/j.intimp.2021.107598
42. Wang J, Han J, Feng J, et al. Effect of Bushen Huoxue decoction combined with moxibustion on inflammation and urinary symptoms in patients with prostate cancer. *Am J Transl Res.* 2022;14(12):8991–9000.
43. Chen Y, Chen S, Zhang J, et al. Expression profile of microRNAs in expressed prostatic secretion of healthy men and patients with IIIA chronic prostatitis/chronic pelvic pain syndrome. *Oncotarget.* 2018; 9(15):12186–12200. doi:10.18632/oncotarget.24069
44. Gajeton J, Krukovets I, Yendamuri R, et al. miR-467 regulates inflammation and blood insulin and glucose. *J Cell Mol Med.* 2021;25(5): 2549–2562. doi:10.1111/jcmm.16224
45. Oliveira SR, Dionísio PA, Correia Guedes L, et al. Circulating inflammatory miRNAs associated with Parkinson's disease pathophysiology. *Biomolecules.* 2020;10(6):945. doi:10.3390/biom10060945
46. Ranjha R, Aggarwal S, Bopanna S, Ahuja V, Paul J. Site-specific microRNA expression may lead to different subtypes in ulcerative colitis. *PLoS One.* 2015;10(11):e0142869. doi:10.1371/journal.pone.0142869
47. Bakhshi A, Khani M, Alipour Parsa S, et al. Investigating the expression level of miR-17-3p, miR-101-3p, miR-335-3p, and miR-296-3p in the peripheral blood of patients with acute myocardial infarction [published online ahead of print on May 24, 2023]. *Mol Cell Biochem.* 2023. doi:10.1007/s11010-023-04766-4
48. Liu Y, Liu WB, Liu KJ, et al. Extremely low-frequency electromagnetic fields affect the miRNA-mediated regulation of signaling pathways in the GC-2 cell line. *PLoS ONE.* 2015;10(10):e0139949. doi:10.1371/journal.pone.0139949
49. Lim W, Bae H, Song G. Differential expression of apolipoprotein D in male reproductive system of rats by high-fat diet. *Andrology.* 2016; 4(6):1115–1122. doi:10.1111/andr.12250
50. Cao Y, Gao X, Yang Y, Ye Z, Wang E, Dong Z. Changing expression profiles of long non-coding RNAs, mRNAs and circular RNAs in ethylene glycol-induced kidney calculi rats. *BMC Genomics.* 2018;19(1):660. doi:10.1186/s12864-018-5052-8
51. Zhan C, Chen J, Chen J, et al. CaMK4-dependent phosphorylation of Akt/mTOR underlies Th17 excessive activation in experimental autoimmune prostatitis. *FASEB J.* 2020;34(10):14006–14023. doi:10.1096/fj.201902910RRR
52. Yi J, Pan J, Zhang S, et al. Jiedu Huoxue decoction improves chronic abacterial prostatitis/chronic pelvic pain syndrome through activating Wnt/GSK $\beta$ / $\beta$ -catenin signaling pathway and alleviating apoptosis. *Biomed Pharmacother.* 2022;149:112830. doi:10.1016/j.biopha.2022.112830
53. Liu H, Zhu X, Cao X, et al. IL-1 $\beta$ -primed mesenchymal stromal cells exert enhanced therapeutic effects to alleviate chronic prostatitis/chronic pelvic pain syndrome through systemic immunity. *Stem Cell Res Ther.* 2021;12(1):514. doi:10.1186/s13287-021-02579-0



# CTRP3/AMPK pathway plays a key role in the anti-hypertrophic effects of cyanidin-3-O-glucoside by inhibiting the inflammatory response

Xueli Zhang<sup>1,A–F</sup>, Xiaoyi Qin<sup>1,B,C</sup>

Department of Geriatrics, Ganzhou People's Hospital, China

A – research concept and design; B – collection and/or assembly of data; C – data analysis and interpretation; D – writing the article; E – critical revision of the article; F – final approval of the article

Advances in Clinical and Experimental Medicine, ISSN 1899–5276 (print), ISSN 2451–2680 (online)

*Adv Clin Exp Med.* 2024;33(8):831–841

## Address for correspondence

Xueli Zhang  
E-mail: aareufa\_zxlll21@sohu.com

## Funding sources

None declared

## Conflict of interest

None declared

Received on April 29, 2023  
Reviewed on June 11, 2023  
Accepted on September 19, 2023

Published online on November 14, 2023

## Abstract

**Background.** Cardiac hypertrophy can be a pathological process that impairs heart function. Anthocyanins are a well-characterized type of natural antioxidant, and recent studies have shown that this type of compound has potential cardioprotective effects against different disorders, such as cardiac hypertrophy.

**Objectives.** We assessed the anti-hypertrophy potential of cyanidin-3-O-glucoside (C3G) and the mechanism associated with any observed effects.

**Materials and methods.** Hypertrophy symptoms were induced using the transverse aortic constriction (TAC) operation in vivo and angiotensin II (Ang II) in vitro. The effect of C3G on the development of hypertrophic symptoms was then determined. Moreover, we examined the influence of CTRP3 inhibition on the anti-hypertrophy function of C3G.

**Results.** The TAC operation induced cardiac fibrosis and heart weight increase, which was associated with increased production of cytokines and suppressed activity of the CTRP3/AMPK pathway. The impairments of heart structure and function were attenuated by C3G. Angiotensin II induced size increases of neonatal rat cardiomyocytes (NRCMs) in vitro, and this effect was inhibited by C3G. Furthermore, the inhibition of CTRP3 counteracted the function of C3G by promoting NRCM hyperplasia and inflammation.

**Conclusions.** The results of the current study showed that the activation of CTRP3 contributed to the anti-hypertrophy effects of C3G.

**Key words:** inflammation, AMPK, cyanidin-3-O-glucoside, cardiac fibrosis, CTRP3

## Cite as

Zhang X, Qin X. CTRP3/AMPK pathway plays a key role in the anti-hypertrophic effects of cyanidin-3-O-glucoside by inhibiting the inflammatory response. *Adv Clin Exp Med.* 2024;33(8):831–841. doi:10.17219/acem/172546

## DOI

10.17219/acem/172546

## Copyright

Copyright by Author(s)  
This is an article distributed under the terms of the Creative Commons Attribution 3.0 Unported (CC BY 3.0) (<https://creativecommons.org/licenses/by/3.0/>)

## Background

Cardiovascular diseases are the primary cause of mortality in affluent countries and have gradually replaced smoking as the leading cause of death in underdeveloped countries.<sup>1</sup> Cardiac hypertrophy, an adaptive reaction of the heart, is common to several cardiovascular diseases.<sup>2</sup> Long-term myocardial hypertrophy predisposes the heart to damage by ischemia, arrhythmias, heart failure, and sudden death. As a result, early management of ventricular hypertrophy has garnered increased interest in recent years.

In developed countries, the use of diets for the treatment of chronic health issues has recently gained popularity. Anthocyanins are a subclass of flavonoids found in foods, such as fruits and vegetables, and are one of the most well-known functional chemicals.<sup>3</sup> These substances have anti-oxidative and anti-inflammatory characteristics, with several positive effects on human health.<sup>3</sup> Aloud et al. demonstrated that cyanidin-3-O-glucoside (C3G) has protective effects in cardiac diseases as it reduced the development of unfavorable ventricular hypertrophy in a hypertensive rat model,<sup>4</sup> confirming the anti-hypertrophy potential of anthocyanins.

Additionally, emerging evidence has demonstrated that the chronic inflammatory response plays a significant role in the pathogenesis of myocardial hypertrophy.<sup>5,6</sup> This notion is supported by the finding that individuals with heart failure have higher plasma levels of oxidative and pro-inflammatory cytokines.<sup>7,8</sup> For example, the development of cardiac hypertrophy is linked to the activation of pro-inflammatory transcription factors, including nuclear factor kappa B (NF- $\kappa$ B).<sup>9</sup> Given that anthocyanins are well-characterized anti-inflammatory agents, their ability to prevent hypertrophy may also be attributed to their anti-inflammatory effects.

There has been recent interest in the ability of certain natural compounds to affect upstream signaling pathways that modulate the immune response, and hence potentially prevent cardiac hypertrophy.<sup>10,11</sup> The CTRP3 is a member of C1q/tumor necrosis factor (TNF)-related proteins and is widely expressed in different tissues, such as white adipose tissue, fibroblasts, chondrocytes, and monocytes.<sup>12,13</sup> It possesses multiple biological functions, such as regulating adipokine secretion,<sup>14</sup> promoting cell proliferation,<sup>15</sup> regulating hepatic lipid metabolism,<sup>16</sup> and inhibiting the inflammatory response.<sup>17</sup> The activation of CTRP3 can reduce post-infarct cardiac fibrosis by activating Smad3 and preventing myofibroblast differentiation,<sup>18</sup> and the activity of the factor can be modulated by different natural compounds such as astragaloside IV and glycine monoester.<sup>19,20</sup> However, it is unclear whether the anti-inflammatory function of CTRP3 also contributes to the therapeutic mechanism of anthocyanins in the treatment of cardiac fibrosis and hypertrophy.

## Objectives

In this study, we performed a preliminary investigation regarding the anti-hypertrophy effects of C3G by focusing on the inflammation-related CTRP3 pathway. The hypertrophic symptoms were induced in vivo using the transverse aortic constriction (TAC) method and in vitro using angiotensin II (Ang II). Then, the symptoms were treated with C3G, and the effects were analyzed using a series of assays to reveal the role of CTRP3-mediated anti-inflammatory effects in the anti-hypertrophy function of C3G.

## Materials and methods

### Establishment of transverse aortic constriction model

Eight-week-old male Sprague Dawley rats (approximate weight: 200 g) were bought from Huafukang Bioscience Co. Inc. (Beijing, China) and housed at 22°C with free access to food and water under a 12:12 h light–dark cycle. The Ganzhou People's Hospital Ethics Committee approved the animal experiments (approval No. 2020AN077). The study was performed following the ARRIVE (Animal Research: Reporting of In Vivo Experiments) recommendations for animal studies. All animal experiments were carried out following the ethical standards of the 1964 Declaration of Helsinki and its later amendments.

For all rats in the TAC and treatment groups, surgery was carried out to induce cardiac hypertrophy. Briefly, a 27-gauge needle was positioned next to the aorta between the right and left carotid arteries. After placing the ligature, the needle was removed, resulting in a ligation of 60–75% of the vessel diameter. To assess the effects of C3G on the progression of cardiac hypertrophy, 30 rats were randomly divided into 5 groups. The sham group was subjected to TAC surgery without constriction of the aorta and then administered normal saline (1 mL/day) via gavage for 8 weeks. In the TAC group, rats were subjected to TAC surgery and then gavaged with normal saline (1 mL/day) for 8 weeks. In the TAC+L group, rats were subjected to TAC surgery and then gavaged with 50 mg/kg body weight of C3G for 8 weeks.<sup>21</sup> Finally, the TAC+H group rats were subjected to TAC surgery and then administered C3G (100 mg/kg body weight) via gavage for 8 weeks.<sup>21</sup>

### Cardiac function measurement

Upon completion of the experiment, the cardiac function of rats in different groups was assessed based on left ventricular end-systolic pressure (LVESP) and left ventricular end-diastolic pressure (LVEDP) while the rats were awake using a noninvasive blood pressure system (XBP 1000; Kent Scientific, Torrington, USA). The fractional shortening of rats was measured using a Philips SON05500



system (Philips Ultrasound, Bothell, USA). Thereafter, cardiac tissues were obtained after the rats were euthanized with an overdose of pentobarbital sodium (200 mg/kg). The ratio of heart weight to body weight was measured. The cardiac tissues were transected, fixed with 10% neutral formalin, and preserved at  $-80^{\circ}\text{C}$  for subsequent assays.

## Masson staining

To evaluate collagen deposition, tissues were extracted from the ventricles and exposed to Masson's trichrome analysis. Briefly, the sections were dehydrated using different concentrations of alcohol and embedded in paraffin. Three distinct dyes were used to distinguish between cells and the extracellular matrix. Tissues were incubated with hematoxylin solution for 6 min, ponceau and acid fuchsin solution for 1 min and phosphomolybdic acid solution for 5 min. Then, the tissues were re-stained with aniline blue solution for 5 min. The fibrotic area was determined using images obtained with a microscope (BX53; Olympus Corp., Tokyo, Japan) at  $\times 200$  magnification. With this staining, collagens stain blue and muscle fibers stain red.

## Detection of cytokine production

The levels of cytokines, including interleukin (IL)-6 (H007; Nanjing Jiancheng Bioengineering Institute, Nanjing, China), IL-1 $\beta$  (H002; Nanjing Jiancheng Bioengineering Institute) and TNF- $\alpha$  (H052; Nanjing Jiancheng Bioengineering Institute) were measured using the corresponding enzyme-linked immunosorbent assay (ELISA) kits following the manufacturer's instructions. Tissues or cells were homogenized, and 20  $\mu\text{L}$  of the sample was incubated with 80  $\mu\text{L}$  of a particular detecting solution at  $37^{\circ}\text{C}$  for 2 h. Thereafter, the supernatant was removed, and the mixture was incubated with 100  $\mu\text{L}$  of horseradish peroxidase (HRP)-labeled streptavidin at  $37^{\circ}\text{C}$  for another 45 min. The cytokine levels were measured using the optical density (OD) values at 450 nm and 570 nm.

## Western blotting

Myocardial tissues or neonatal rat cardiomyocytes (NRCMs) were homogenized using a lysis buffer to collect the total proteins. The protein concentration was determined using a bicinchoninic acid (BCA) protein concentration detection kit (ST506; Beyotime Biotechnology, Shanghai, China) according to the manufacturer's instructions. Equal quantities of protein (40  $\mu\text{g}$ ) were separated using sodium dodecyl sulfate-polyacrylamide gel electrophoresis (SDS-PAGE) and then transferred to polyvinylidene difluoride (PVDF) membranes. Then, the membranes were incubated with primary antibodies (Supplementary Table 1) at  $4^{\circ}\text{C}$  overnight. Subsequently, secondary goat-anti-rabbit IgG-HRP antibodies (1:5000) (A0208; Beyotime Technology) were added to the membranes. The membranes were

incubated at  $37^{\circ}\text{C}$  for 45 min. Following the visualization of protein bands using the BeyoECL Plus reagent (Beyotime Technology), the integral OD of the bands was recorded using the Gel-Pro-Analyzer (Media Cybernetics, Silver Spring, USA). The relative expression levels of the proteins were calculated with reference to the control group.

## Preparation of neonatal rat cardiac myocytes and grouping

Neonatal Sprague Dawley rats (1–3 days old) were euthanized using pentobarbital sodium. The primary culture of NRCMs was performed according to the previously published method.<sup>22</sup> The cells were seeded at a density of  $5 \times 10^6$  cells/mL in Dulbecco's modified Eagle's medium (DMEM) supplemented with 10% fetal bovine serum (FBS) and 0.1 mM 5-bromodeoxyuridine. To determine the role of CTRP3 in the anti-hypertrophy effect of C3G, NRCMs were classified into 4 groups. These included the control group, with normal NRCMs, the Ang II group, in which NRCMs were incubated with Ang II (1  $\mu\text{mol/L}$ ) for 48 h to induce hypertrophy, the Ang II + C3G group, in which NRCMs were pre-treated with 20  $\mu\text{M}$  C3G 30 min before Ang II administration, and the Ang II + C3G + siRNA group, in which NRCMs were transfected with CTRP3 siRNA (Guangzhou RiboBio Company, Guangzhou, China) for 48 h before C3G and Ang II treatments.

## Cell viability and surface area measurement

Following the Ang II administration, the supernatant of cultures was discarded. The NRCMs were incubated with the DMEM medium containing 10  $\mu\text{L}$  Cell Counting Kit-8 (CCK-8) (HY-K0301, MedChem Express (MCE), USA) at  $37^{\circ}\text{C}$  for 1 h. The OD 450 value was detected using a microplate reader (ELX-800; BioTek, Santa Clara, USA) and used to indicate the cell viability. To investigate the development of hypertrophy, the cell surface area was evaluated under a microscope (BX53; Olympus Corp.) at a magnification of  $\times 400$ .

## Statistical analyses

Data are expressed as mean  $\pm$  standard deviation ( $M \pm SD$ ). One-way analysis of variance (ANOVA) and post-hoc Tukey's test were performed. The normality and homogeneity of variance of different datasets were assessed with the Shapiro test and Levene's test, respectively, and the detailed results are shown in Supplementary Tables 2–19. Based on these analyses, all data met the normality and homogeneity of variance prerequisite for ANOVA. The significance level was set at  $<0.05$  (two-tailed p-value). GraphPad Prism v. 6.0 (GraphPad Software, Inc., San Diego, USA) was used to perform statistical analyses and present histograms.

## Results

### C3G reduced the heart weight and improved the cardiac structure in TAC rats

The TAC method was used to induce hypertrophic cardiac symptoms. The successful establishment of the model was verified based on the increased values of LVEDP and reduced values of the LVESP and fractional shortening (FS) (Supplementary Fig. 1, Supplementary Table 1), which represented the characteristic features of hypertrophic hearts. Moreover, compared to the control and healthy groups, the TAC surgery significantly increased the ratio of heart weight to body weight (Fig. 1A, Table 1), confirming the hyperplasia of cardiac tissues. Furthermore, the changes in cardiac function and weight were related to the progression of fibrosis in heart tissues, where collagens were stained blue and muscle fibers were stained red (Fig. 1B). The collagen level was significantly higher in the heart tissues of the TAC group than in the control and sham groups. For rats administered with different doses of C3G, the heart weight to body weight ratio, as well as collagen deposition, was reduced (Fig. 1, Table 1). However, C3G treatment did not affect the hemodynamic parameters, irrespective of the dose used (Supplementary Fig. 1, Supplementary Table 20).

### C3G inhibited the inflammatory response in TAC rats

The development of cardiac hypertrophy was significantly correlated with the inflammatory response, as evidenced by the increased production of IL-6, IL-1 $\beta$  and TNF- $\alpha$  (Fig. 2, Table 2). Moreover, the levels of cytokines were decreased after C3G treatment. Additionally, C3G had a dose-dependent effect on cytokine levels; treatment with 100 mg/kg body weight was associated with a higher anti-inflammatory effect than treatment with 50 mg/kg body weight (Fig. 2, Table 2).

### C3G activated the CTRP3/AMPK pathway in TAC rats

The activity of the CTRP3/AMPK pathway was detected in rats with cardiac hypertrophy. The CTRP3

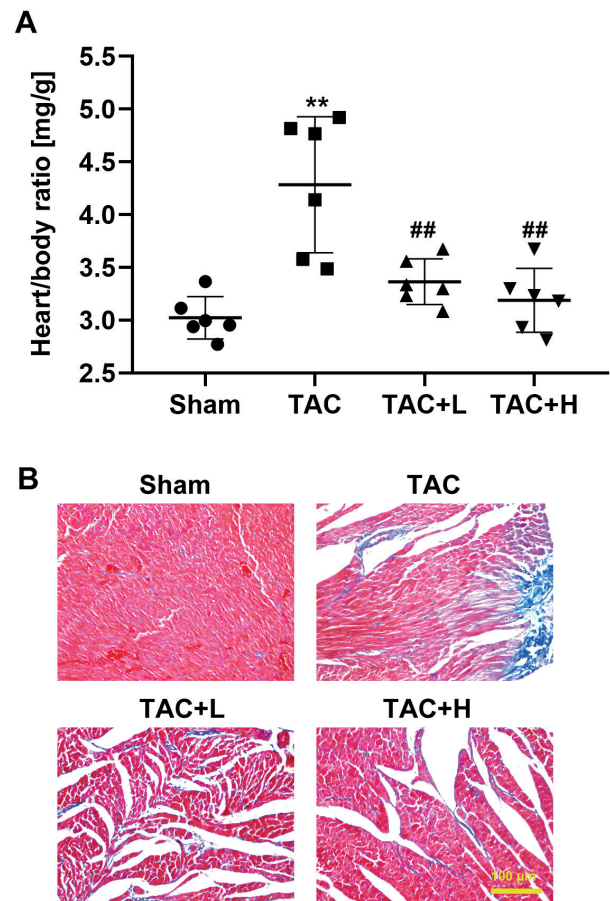


Fig. 1. Effects of cyanidin-3-O-glucoside (C3G) on heart weight and fibrosis in transverse aortic constriction (TAC) rats. Rats were subjected to TAC surgery to induce hypertrophy and then administered 2 doses of C3G (50 and 100 mg/kg body weight). A. Analysis results of heart/body ratio: C3G administrations decreased heart/body ratio; B. Masson staining of the collagen deposition: C3G administrations attenuated deposition of collagens; \*\* $p < 0.01$  compared with the sham group; ## $p < 0.01$  compared with the TAC group. In the sham group, rats were subjected to TAC surgery without constriction of the aorta and then gavaged with normal saline (1 mL/day) for 8 weeks. In the TAC group, rats were subjected to TAC surgery and then gavaged with normal saline (1 mL/day) for 8 weeks. In the TAC+L group, rats were subjected to TAC surgery and then gavaged with 50 mg/kg body weight of C3G for 8 weeks. In the TAC+H group, rats were subjected to TAC surgery and then gavaged with 100 mg/kg body weight of C3G for 8 weeks

and p-AMPK/AMPK ratio levels in cardiac tissues were significantly lower after the TAC operation compared to the sham group (Fig. 3, Table 3). The changes in CTRP3/AMPK activity were restored by C3G administration.

Table 1. Effects of C3G on heart/body ratio

Group	Mean	SD	ANOVA with GLM		Tukey's test (p-value, q value)		
			p-value	F value	TAC	TAC+L	TAC+H
Sham	3.02	0.20	–	–	<0.0001, 8.02	0.4365, 2.17	0.8774, 1.06
TAC	4.28	0.64	–	–	–	0.0027, 5.85	0.0004, 6.97
TAC+L	3.36	0.22	–	–	–	–	0.8585, 1.12
TAC+H	3.19	0.30	<0.0001	12.84	–	–	–

C3G – cyanidin-3-O-glucoside; ANOVA – analysis of variance; TAC – transverse aortic constriction; L – low concentration; H – high concentration; SD – standard deviation; GLM – General Linear Model.

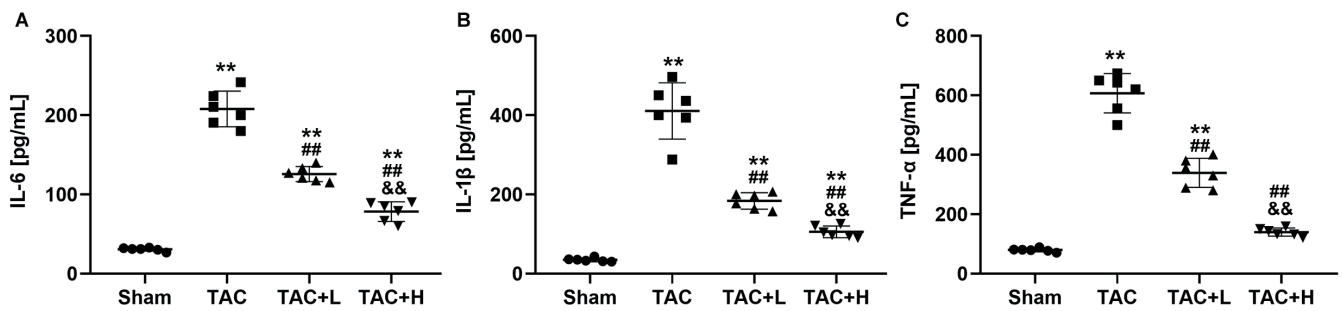


Fig. 2. Effects of cyanidin-3-O-glucoside (C3G) on cytokine production in myocardial tissues of transverse aortic constriction (TAC) rats. Rats were subjected to TAC surgery to induce hypertrophy and then administered 2 doses of C3G (50 and 100 mg/kg body weight). A. Analysis results of enzyme-linked immunosorbent assay (ELISA) detection of interleukin (IL)-6: C3G administrations decreased IL-6 level; B. Analysis results of ELISA detection of IL-1β: C3G administrations decreased IL-1β level; C. Analysis results of ELISA detection of tumor necrosis factor alpha (TNF-α): C3G administrations decreased TNF-α level; \*\*p < 0.01 compared with the sham group; #p < 0.01 compared with the TAC group; &p < 0.01 compared with the TAC+L group. In the sham group, rats were subjected to TAC surgery without constriction of the aorta and then gavaged with normal saline (1 mL/day) for 8 weeks. In the TAC group, rats were subjected to TAC surgery and then gavaged with normal saline (1 mL/day) for 8 weeks. In the TAC+L group, rats were subjected to TAC surgery and then gavaged with 50 mg/kg body weight of C3G for 8 weeks. In the TAC+H group, rats were subjected to TAC surgery and then gavaged with 100 mg/kg body weight of C3G for 8 weeks

Table 2. Effects of C3G on the production of cytokines in myocardial tissues

Parameter	Group	Mean [pg/mL]	SD	ANOVA with GLM		Tukey's test (p-value, q value)		
				p-value	F value	TAC	TAC+L	TAC+H
IL-6	sham	30.6	2.2	-	-	<0.0001, 31.54	<0.0001, 16.90	<0.0001, 8.49
	TAC	207.8	22.5	-	-	-	<0.0001, 14.64	<0.0001, 23.05
	TAC+L	125.6	9.5	-	-	-	-	<0.0001, 8.411
	TAC+H	78.3	12.4	<0.0001	180.7	-	-	-
IL-1β	sham	34.6	4.7	-	-	<0.0001, 24.44	<0.0001, 9.678	0.0089, 5.409
	TAC	410.8	70.8	-	-	-	<0.0001, 14.77	<0.0001, 19.84
	TAC+L	183.6	20.6	-	-	-	-	0.0092, 5.07
	TAC+H	105.5	14.7	<0.0001	112.5	-	-	-
TNF-α	sham	79.4	6.2	-	-	<0.0001, 30.99	<0.0001, 15.26	0.0895, 3.54
	TAC	607.3	66.1	-	-	-	<0.0001, 15.73	<0.0001, 27.45
	TAC+L	339.3	48.7	-	-	-	-	<0.0001, 11.71
	TAC+H	139.8	13.7	<0.0001	195.3	-	-	-

C3G – cyanidin-3-O-glucoside; IL – interleukin; TNF-α – tumor necrosis factor alpha; TAC – transverse aortic constriction; L – low concentration; H – high concentration; SD – standard deviation; GLM – General Linear Model.

Table 3. Effects of C3G on the expressions of proteins in CTRP3/AMPK pathway in myocardial tissues

Parameter	Group	Mean (IOD)	SD	ANOVA with GLM		Tukey's test (p-value, q value)		
				p-value	F value	TAC	TAC+L	TAC+H
CTRP3	sham	3148	38.5	-	-	<0.0001, 17.11	0.0003, 10.51	0.0082, 6.42
	TAC	1342	190.2	-	-	-	0.0082, 6.59	0.0070, 10.39
	TAC+L	2038	227.8	-	-	-	-	0.0773, 4.09
	TAC+H	2470	210.0	<0.0001	51.58	-	-	-
AMPK	sham	2819	115.8	-	-	0.0013, 8.668	0.0032, 7.49	0.0364, 4.85
	TAC	1729	106.6	-	-	-	0.8371, 1.18	0.1015, 3.82
	TAC+L	1676	78.1	-	-	-	-	0.3128, 2.64
	TAC+H	2134	87.5	0.0013	14.81	-	-	-
p-AMPK	sham	4018	161.0	-	-	<0.0001, 50.61	<0.0001, 48.97	<0.0001, 33.72
	TAC	1618	20.1	-	-	-	0.6656, 1.64	<0.0001, 16.89
	TAC+L	1696	22.3	-	-	-	-	<0.0001, 15.25
	TAC+H	2419	13.8	<0.0001	551.5	-	-	-

C3G – cyanidin-3-O-glucoside; IOD – integrated optical density; TAC – transverse aortic constriction; L – low concentration; H – high concentration; SD – standard deviation; GLM – General Linear Model.

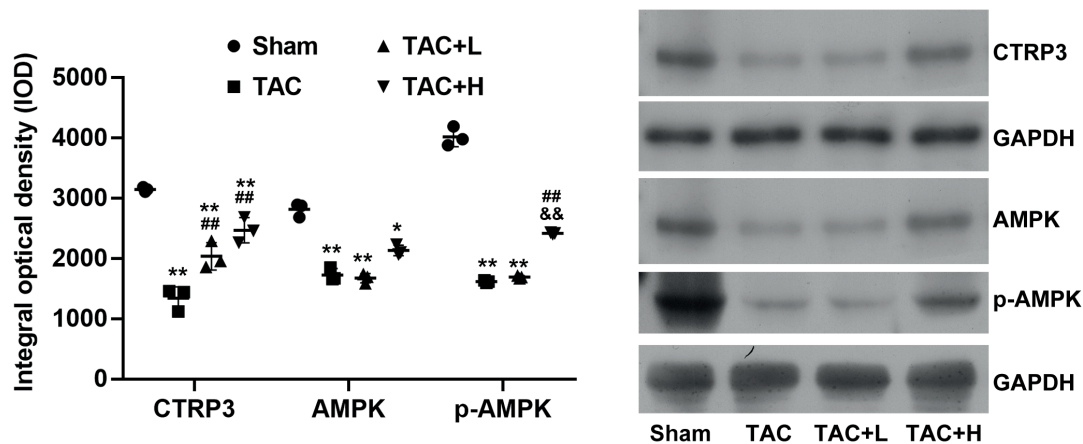


**Fig. 3.** Effects of cyanidin-3-O-glucoside (C3G) on the CTRP3/AMPK pathway in myocardial tissues in transverse aortic constriction (TAC) rats. Rats were subjected to TAC surgery to induce hypertrophy and then administered 2 doses of C3G (50 and 100 mg/kg body weight). Analysis results and images of western blotting detection of CTRP3, p-AMPK and AMPK levels: C3G administrations increased CTRP3 and p-AMPK levels; \* $p < 0.01$  compared with the sham group, \*\* $p < 0.01$  compared with the sham group; ## $p < 0.01$  compared with the TAC group; &p  $p < 0.01$  compared with the TAC+L group. In the sham group, rats were subjected to TAC surgery without constriction of the aorta and then gavaged with normal saline (1 mL/day) for 8 weeks. In the TAC group, rats were subjected to TAC surgery and then gavaged with normal saline (1 mL/day) for 8 weeks. In the TAC+L group, rats were subjected to TAC surgery and then gavaged with 50 mg/kg body weight of C3G for 8 weeks. In the TAC+H group, rats were subjected to TAC surgery and then gavaged with 100 mg/kg body weight of C3G for 8 weeks

Moreover, the levels of CTRP3 and p-AMPK/AMPK ratio were higher in the treatment groups compared to the TAC group (Fig. 3, Table 3). Finally, the effect on the CTRP3/AMPK pathway was exerted in a dose-dependent manner.

### C3G exerted anti-hypertrophy effects in NRCMs that were mediated via CTRP3 activation

To explore the mechanistic role of the CTRP3/AMPK axis in the anti-hypertrophy effects of C3G, the expression

of CTRP3 in NRCMs was attenuated using siRNA (Fig. 4A, Table 4). Then, Ang II and C3G were administered in CTRP3-knockdown NRCMs. When compared to NRCMs transfected with NC siRNA, CTRP3 knockdown reduced the p-AMPK/AMPK ratio (Fig. 4A, Table 4) and the anti-hypertrophy effects of C3G were attenuated by alterations in CTRP3/AMPK pathway activity. Angiotensin II increased the proliferation potential and cell surface area (Fig. 4B,C; Table 5,6), as well as cytokine production in NRCMs, representing enhanced fibrosis (Fig. 4D–F, Table 7). In NRCMs co-treated with both Ang II and C3G, the proliferation potential and cytokine levels of NRCMs

**Table 4.** Effects of C3G on the expressions of proteins in CTRP3/AMPK pathway in NRCMs

Parameter	Group	Mean (IOD)	SD	ANOVA with GLM		Tukey's test (p-value, q value)		
				p-value	F value	Ang II	Ang II+C3G	Ang II+C3G+siRNA
CTRP3	control	4148	38.5	–	–	<0.0001, 81.61	<0.0001, 40.00	<0.0001, 57.35
	Ang II	1476	41.9	–	–	–	<0.0001, 41.62	<0.0001, 24.26
	Ang II+C3G	2838	37.5	–	–	–	–	<0.0001, 17.35
	Ang II+C3G+siRNA	2270	90.6	<0.0001	1181	–	–	–
AMPK	control	3880	100.0	–	–	<0.0001, 20.92	<0.0001, 13.06	<0.0001, 26.67
	Ang II	2677	121.9	–	–	–	0.0024, 7.86	0.0152, 5.95
	Ang II+C3G	3129	40.4	–	–	–	–	<0.0001, 13.61
	Ang II+C3G+siRNA	2346	115.0	<0.0001	133.3	–	–	–
p-AMPK	control	3106	85.4	–	–	0.0020, 8.09	0.0481, 4.57	0.9940, 0.36
	Ang II	2484	87.3	–	–	–	<0.0001, 12.66	0.0015, 8.45
	Ang II+C3G	3457	219.1	–	–	–	–	0.0686, 4.21
	Ang II+C3G+siRNA	3133	86.7	0.0001	28.0	–	–	–

ANOVA – analysis of variance; NRCMs – neonatal rat cardiac myocytes; Ang II – angiotensin II; C3G – cyanidin-3-O-glucoside; IOD – integrated optical density; GLM – General Linear Model.

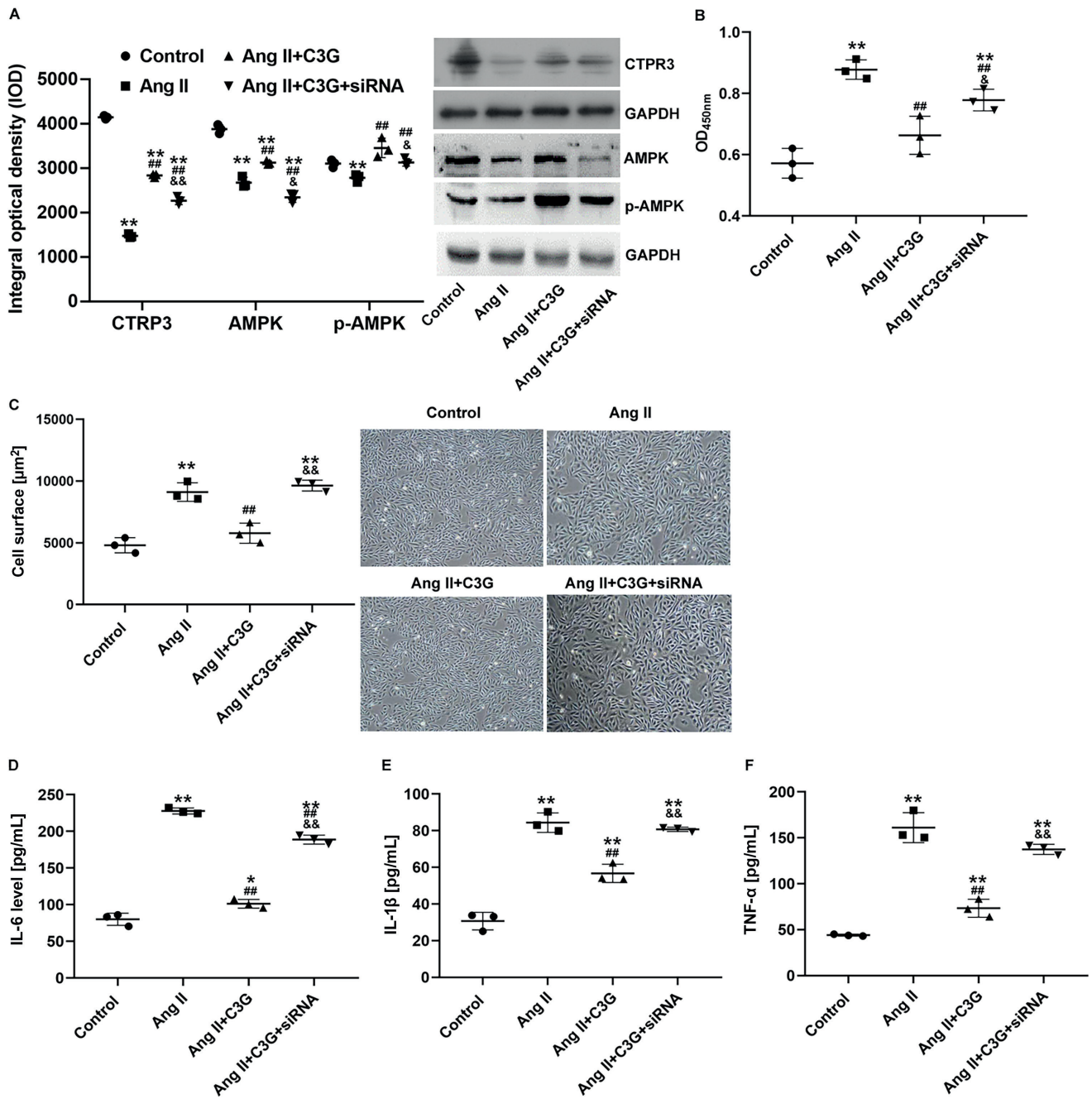


**Fig. 4.** Effects of CTRP3 inhibition on the anti-hypertrophy function of cyanidin-3-O-glucoside (C3G) in neonatal rat cardiac myocytes (NRCMs). NRCMs with CTRP3 inhibition were subjected to angiotensin II (Ang II) and C3G treatments. **A.** Analysis results and images of western blotting detection of CTRP3, p-AMPK and AMPK levels: inhibition of CTRP3 restored the level of p-AMPK even under C3G treatment; **B.** Analysis results of Cell Counting Kit-8 (CCK-8) detection of cell viability: inhibition of CTRP3 restored the viability of NRCMs even under C3G treatment; **C.** Analysis results of cell surface: inhibition of CTRP3 restored the surface area of NRCMs even under C3G treatment; **D.** Analysis results of enzyme-linked immunosorbent assay (ELISA) detection of interleukin (IL)-6: inhibition of CTRP3 restored IL-6 in NRCMs even under C3G treatment; **E.** Analysis results of ELISA detection of IL-1β: inhibition of CTRP3 restored IL-1β in NRCMs even under C3G treatment; **F.** Analysis results of ELISA detection of tumor necrosis factor alpha (TNF-α): inhibition of CTRP3 restored TNF-α in NRCMs even under C3G treatment; \*p < 0.05 compared with the control group; \*\*p < 0.01 compared with the control group; ##p < 0.01 compared with the Ang II group; &p < 0.05 compared with the Ang II + C3G group; &p < 0.01 compared with the Ang II + C3G group. Control group, normal NRCMs; Ang II group, in which NRCMs were incubated with Ang II (1 µmol/L) for 48 h to induce hypertrophy; Ang II + C3G group, in which NRCMs were pre-treated with 20 µM C3G 30 min before Ang II administration; Ang II + C3G + siRNA group, in which NRCMs were transfected with CTRP3 siRNA for 48 h before C3G and Ang II treatments

were suppressed, further confirming the anti-fibrotic effects of C3G. Finally, the cell viability and cytokine levels in NRCMs were increased by CTRP3 inhibition, suggesting that C3G exerted anti-hypertrophy effects through CTRP3 activation.

## Discussion

In this study, we demonstrated that long-term ingestion of C3G can reduce cardiac hypertrophy by delaying the fibrotic process and reducing inflammatory responses both

**Table 5.** Effects of C3G on the cell viability in NRCMs

Group	Mean (OD450)	SD	ANOVA with GLM		Tukey's test (p-value, q value)		
			p-value	F value	Ang II	Ang II+C3G	Ang II+C3G+siRNA
Control	0.572	0.05	–	–	0.0002, 11.51	0.1481, 3.43	0.0026, 7.76
Ang II	0.878	0.03	–	–	–	0.0020, 8.077	0.1087, 3.75
Ang II+C3G	0.663	0.06	–	–	–	–	0.0111, 5.327
Ang II+C3G+siRNA	0.778	0.03	0.0002	25.22	–	–	–

ANOVA – analysis of variance; NRCMs – neonatal rat cardiac myocytes; Ang II – angiotensin II; C3G – cyanidin-3-O-glucoside; SD – standard deviation; GLM – General Linear Model.

**Table 6.** Effects of C3G on the cell surface area in NRCMs

Group	Mean [ $\mu\text{m}^2$ ]	SD	ANOVA with GLM		Tukey's test (p-value, q value)		
			p-value	F value	Ang II	Ang II+C3G	Ang II+C3G+siRNA
Control	4803	613	–	–	0.0002, 11.11	0.3433, 2.53	<0.0001, 12.47
Ang II	9105	752	–	–	–	0.0014, 8.58	0.7763, 1.35
Ang II+C3G	5783	816	–	–	–	–	0.0005, 9.93
Ang II+C3G+siRNA	9629	434	<0.0001	38.29	–	–	–

ANOVA – analysis of variance; NRCMs – neonatal rat cardiac myocytes; Ang II – angiotensin II; C3G – cyanidin-3-O-glucoside; SD – standard deviation; GLM – General Linear Model.

**Table 7.** Effects of C3G on the production of cytokines in NRCMs

Parameter	Group	Mean [pg/mL]	SD	ANOVA with GLM		Tukey's test (p-value, q value)		
				p-value	F value	Ang II	Ang II+C3G	Ang II+C3G+siRNA
IL-6	control	80.0	8.3	–	–	<0.0001, 40.38	0.0145, 5.80	<0.0001, 29.73
	Ang II	227.8	4.2	–	–	–	<0.0001, 34.58	0.0003, 10.65
	Ang II+C3G	101.3	6.1	–	–	–	–	<0.0001, 23.93
	Ang II+C3G+siRNA	188.8	6.1	<0.0001	369.2	–	–	–
IL-1 $\beta$	control	30.7	4.8	–	–	<0.0001, 21.08	0.0004, 10.20	<0.0001, 19.63
	Ang II	84.4	5.3	–	–	–	0.0003, 10.88	0.7403, 1.45
	Ang II+C3G	56.7	5.0	–	–	–	–	0.0007, 9.43
	Ang II+C3G+siRNA	80.7	1.2	<0.0001	95.24	–	–	–
TNF- $\alpha$	control	44.0	1.0	–	–	<0.0001, 20.46	0.0278, 5.125	<0.0001, 16.32
	Ang II	161.1	16.4	–	–	–	<0.0001, 15.33	0.0736, 4.142
	Ang II+C3G	73.3	9.7	–	–	–	–	0.0002, 11.19
	Ang II+C3G+siRNA	137.4	5.5	<0.0001	90.72	–	–	–

ANOVA – analysis of variance; IL – interleukin; TNF- $\alpha$  – tumor necrosis factor alpha; NRCMs – neonatal rat cardiac myocytes; Ang II – angiotensin II; C3G – cyanidin-3-O-glucoside; GLM – General Linear Model.

in vivo and in vitro. The anti-hypertrophy effects of C3G were attenuated by inhibiting the CTRP3/AMPK pathway because these effects are linked to CTRP3/AMPK pathway activation. The study results support the anti-hypertrophy effects of C3G, which are also supported by the findings of Aloud et al.<sup>4</sup> Moreover, the study provided an alternate explanation of the protective benefits of C3G against cardiac hypertrophy, which has long been overlooked. The establishment of the link between the anti-hypertrophy effects of C3G and the function of the CTRP3/AMPK axis forms the basis for the future development of adjuvant therapies and food items, based on the positive effects of C3G on improving cardiac hypertrophy.

The mechanistic role of CTRP3/AMPK to drive the effects of C3G also explains the other biological activities of C3G and other anthocyanins. However, further studies are needed to explore this role.

Anthocyanins are a common class of water-soluble pigments that are characterized by their antioxidant,<sup>23</sup> anti-inflammatory,<sup>24</sup> neuroprotective,<sup>25</sup> and anti-diabetic properties.<sup>26</sup> With regard to the effects on the cardiovascular system, Liu et al. demonstrated that anthocyanin (C3G) protects against diabetes-related endothelial cell dysfunction by increasing adiponectin secretion.<sup>27</sup> Furthermore, Wang et al. demonstrated that C3G attenuates inflammation and apoptosis associated with endothelial

cell dysfunction by inhibiting the miR-204-5p/SIRT1 pathway.<sup>21</sup> Additionally, anthocyanins, such as C3G, have shown cardioprotective properties. Aloud et al. demonstrated that C3G can prevent hypertensive rats from developing maladaptive ventricular hypertrophy.<sup>4</sup> By administering C3G to Ang II-treated NRCMs and TAC rats, our study further confirmed its anti-hypertrophy effect. We demonstrated that C3G administration reduced inflammation and fibrosis, which are manifestations of cardiac hypertrophy. For the attenuation of other symptoms, such as cytokine production in myocardial tissues, the protective effects of C3G showed a dose-dependent effect. However, C3G had only a minor effect on hemodynamic parameters. Although our study used a prolonged treatment course and a high C3G treatment dose (up to 100 mg/kg), it is possible that the dose or duration of C3G treatment was insufficient to normalize the hemodynamic parameters. Additionally, because C3G is an active compound widely distributed in fruits, its effects may not be strong enough to induce significant functional changes in the heart, and this should be the focus of future investigations.

The results of the present and previous studies suggest that the anti-hypertrophy effects of C3G are closely related to its anti-inflammatory properties. In hypertrophic cardiac tissues, macrophage infiltration and inflammatory cytokine production are common.<sup>28,29</sup> Thus, anti-inflammatory medications can successfully reduce cardiac hypertrophy. For instance, astragaloside IV reduces the inflammatory response produced by the TLR4/NF- $\kappa$ B signaling pathway, which in turn reduces the myocardial hypertrophy caused by isoproterenol.<sup>30</sup> Yu et al. demonstrated that miR-143-3p inhibition ameliorates myocardial hypertrophy by inhibiting the inflammatory response.<sup>31</sup> As a well-characterized anti-inflammatory agent, anthocyanins, such as C3G, have positive effects on a variety of tissues, including the liver, gut and eyes. Our results support the previous findings that suggest that C3G can reduce inflammation in the heart.

Furthermore, the current study evaluated the alterations in the activity of the CTRP3/AMPK pathway to further explore whether the anti-inflammatory effects of C3G contribute to its anti-hypertrophy effect. The CTRP3 is a member of the CTRP family and is abundantly expressed in adipose tissue, heart and liver.<sup>32</sup> The CTRP3 can inhibit the inflammatory responses via several different mechanisms.<sup>33,34</sup> In the current study, we focused on changes in the CTRP3/AMPK pathway. The activation of the AMPK signaling transduction by CTRP3 can reduce cardiac dysfunction, inflammation, oxidative stress, and cell death in rats with diabetic cardiomyopathy.<sup>18</sup> Therefore, establishing the connection between C3G and CTRP3/AMPK may provide a preliminary explanation for the compound's anti-hypertrophy properties. Transverse aortic constriction and Ang II treatment reduced the CTRP3 level and p-AMPK/AMPK ratio, whereas C3G restored

these levels both in vivo and in vitro, linking the reduction of hypertrophic symptoms to CTRP3/AMPK activation. Further evidence that the anti-hypertrophy effects of C3G are mediated by the activation of the CTRP3-mediated pathway was provided by the finding that inhibition of CTRP3 counteracted the function of C3G in NRCMs. As a result, the proliferation and inflammatory response were restored even under C3G treatment, which exacerbated the myocardial hypertrophy.

## Limitations

The current study had certain limitations. First, the data only provided a preliminary explanation regarding the potential protective effects of anthocyanins against cardiac diseases. Second, the effects of C3G against cardiac hypertrophy were assessed using only a few assays, and a comprehensive analysis of the anti-hypertrophy effects was not performed. Thus, further studies are needed to investigate the potential effects of C3G and other anthocyanins against cardiac diseases.

## Supplementary data

The supplementary materials are available at <https://doi.org/10.5281/zenodo.8385561>. The package contains the following files:

Supplementary Fig. 1. Effects of C3G on hemodynamics parameters in TAC rats. Rats were subjected to TAC surgery to induce hypertrophy, and then handled with C3G of 2 doses. A. Analysis results of LVEDP; B. Analysis results of LVESP; C. Analysis results of FS. “\*\*”  $p < 0.01$  compared to sham group.

Supplementary Table 1. Antibody information.

Supplementary Table 2. Results of Shapiro test and Levene's test of heart/body ratio.

Supplementary Table 3. Results of Shapiro test and Levene's test of LVEDP.

Supplementary Table 4. Results of Shapiro test and Levene's test of LVESP.

Supplementary Table 5. Results of Shapiro test and Levene's test of FS.

Supplementary Table 6. Results of Shapiro test and Levene's test of IL-6 level in myocardial tissues.

Supplementary Table 7. Results of Shapiro test and Levene's test of IL-1 $\beta$  level in myocardial tissues.

Supplementary Table 8. Results of Shapiro test and Levene's test of TNF- $\alpha$  level in myocardial tissues.

Supplementary Table 9. Results of Shapiro test and Levene's test of CTRP3 level in myocardial tissues.

Supplementary Table 10. Results of Shapiro test and Levene's test of p-AMPK level in myocardial tissues.

Supplementary Table 11. Results of Shapiro test and Levene's test of AMPK level in myocardial tissues.

Supplementary Table 12. Results of Shapiro test and Levene's test of CTRP3 level in cells.

Supplementary Table 13. Results of Shapiro test and Levene's test of p-AMPK level in cells.

Supplementary Table 14. Results of Shapiro test and Levene's test of AMPK level in cells.

Supplementary Table 15. Results of Shapiro test and Levene's test of cell viability.

Supplementary Table 16. Results of Shapiro test and Levene's test of cell area.

Supplementary Table 17. Results of Shapiro test and Levene's test of IL-6 in cells.

Supplementary Table 18. Results of Shapiro test and Levene's test of IL-1 $\beta$  in cells.

Supplementary Table 19. Results of Shapiro test and Levene's test of TNF- $\alpha$  in cells.

Supplementary Table 20. Effects of C3G on hemodynamic parameters.

## Conclusions

Our results support the hypothesis that C3G possesses anti-hypertrophy properties and could inhibit fibrosis and inflammation both in vitro and in vivo. This effect depends on the activation of the CTRP3/AMPK pathway. Our results add to the existing knowledge regarding the use of anthocyanins in functional diets or as an adjunctive treatment to reduce cardiac hypertrophy.

### ORCID iDs

Xueli Zhang  <https://orcid.org/0000-0002-3279-0399>

Xiaoyi Qin  <https://orcid.org/0009-0004-0314-7769>

### References

- Greene SJ, Bauersachs J, Brugts JJ, et al. Worsening heart failure: Nomenclature, epidemiology, and future directions. *J Am Coll Cardiol*. 2023;81(4):413–424. doi:10.1016/j.jacc.2022.11.023
- Martin TG, Juarros MA, Leinwand LA. Regression of cardiac hypertrophy in health and disease: Mechanisms and therapeutic potential. *Nat Rev Cardiol*. 2023;20(5):347–363. doi:10.1038/s41569-022-00806-6
- Sandoval-Ramírez BA, Catalán Ú, Fernández-Castillejo S, Rubió L, Macià A, Solà R. Anthocyanin tissue bioavailability in animals: Possible implications for human health. A systematic review. *J Agric Food Chem*. 2018;66(44):11531–11543. doi:10.1021/acs.jafc.8b04014
- Aloud BM, Raj P, McCallum J, et al. Cyanidin 3-O-glucoside prevents the development of maladaptive cardiac hypertrophy and diastolic heart dysfunction in 20-week-old spontaneously hypertensive rats. *Food Funct*. 2018;9(6):3466–3480. doi:10.1039/C8FO00730F
- Besse S, Nadaud S, Balse E, Pavoine C. Early protective role of inflammation in cardiac remodeling and heart failure: Focus on TNF $\alpha$  and resident macrophages. *Cells*. 2022;11(7):1249. doi:10.3390/cells11071249
- Harding D, Chong MHA, Lahoti N, et al. Dilated cardiomyopathy and chronic cardiac inflammation: Pathogenesis, diagnosis and therapy. *J Intern Med*. 2023;293(1):23–47. doi:10.1111/joim.13556
- He J, Xu D, Wang L, Yu X. Ferrerol prevents angiotensin II-induced cardiac remodeling in vivo and in vitro. *Front Pharmacol*. 2023;13:1079251. doi:10.3389/fphar.2022.1079251
- Higashikuni Y, Liu W, Numata G, et al. NLRP3 inflammasome activation through heart-brain interaction initiates cardiac inflammation and hypertrophy during pressure overload. *Circulation*. 2023;147(4):338–355. doi:10.1161/CIRCULATIONAHA.122.060860
- Shen S, Wu G, Luo W, et al. Leonurine attenuates angiotensin II-induced cardiac injury and dysfunction via inhibiting MAPK and NF- $\kappa$ B pathway. *Phytomedicine*. 2023;108:154519. doi:10.1016/j.phymed.2022.154519
- Chang C, Cheng H, Chou W, et al. Sesamin suppresses angiotensin-II-enhanced oxidative stress and hypertrophic markers in H9c2 cells. *Environ Toxicol*. 2023;38(9):2165–2172. doi:10.1002/tox.23853
- Li Y, He B, Zhang C, He Y, Xia T, Zeng C. Naringenin attenuates isoprenaline-induced cardiac hypertrophy by suppressing oxidative stress through the AMPK/NOX2/MAPK signaling pathway. *Nutrients*. 2023;15(6):1340. doi:10.3390/nu15061340
- Wang Y, Li H, Yu XH, Tang CK. CTRP1: A novel player in cardiovascular and metabolic diseases. *Cytokine*. 2023;164:156162. doi:10.1016/j.cyt.2023.156162
- Kong M, Gao Y, Guo X, Xie Y, Yu Y. Role of the CTRP family in tumor development and progression (review). *Oncol Lett*. 2021;22(4):723. doi:10.3892/ol.2021.12984
- Wölfling B, Buechler C, Weigert J, et al. Effects of the new C1q/TNF-related protein (CTRP-3) "cartonectin" on the adipocytic secretion of adipokines. *Obesity (Silver Spring)*. 2008;16(7):1481–1486. doi:10.1038/oby.2008.206
- Maeda T, Wakisaka S. CTRP3/cartducin is induced by transforming growth factor- $\beta$ 1 and promotes vascular smooth muscle cell proliferation. *Cell Biol Int*. 2010;34(3):261–266. doi:10.1042/CBI20090043
- Peterson JM, Seldin MM, Wei Z, Aja S, Wong GW. CTRP3 attenuates diet-induced hepatic steatosis by regulating triglyceride metabolism. *Am J Physiol Gastrointest Liver Physiol*. 2013;305(3):G214–G224. doi:10.1152/ajpgi.00102.2013
- Hofmann C, Chen N, Obermeier F, et al. C1q/TNF-related protein-3 (CTRP-3) is secreted by visceral adipose tissue and exerts anti-inflammatory and antifibrotic effects in primary human colonic fibroblasts. *Inflamm Bowel Dis*. 2011;17(12):2462–2471. doi:10.1002/ibd.21647
- Wu D, Lei H, Wang JY, et al. CTRP3 attenuates post-infarct cardiac fibrosis by targeting Smad3 activation and inhibiting myofibroblast differentiation. *J Mol Med*. 2015;93(12):1311–1325. doi:10.1007/s00109-015-1309-8
- Zhang Y, Xu G, Huang B, Chen D, Ye R. Astragaloside IV regulates insulin resistance and inflammatory response of adipocytes via modulating CTRP3 and PI3K/AKT signaling. *Diabetes Ther*. 2022;13(11–12):1823–1834. doi:10.1007/s13300-022-01312-1
- Koldemir Gündüz M. BGM, a newly synthesised boron compound, induces apoptosis and reduces oxidative stress by inhibiting lipogenesis in 3T3-L1 adipocytes via PPAR $\gamma$  and CTRP3. *Biol Trace Elem Res*. 2022;200(11):4807–4816. doi:10.1007/s12011-022-03261-z
- Wang Z, Zhang M, Wang Z, Guo Z, Wang Z, Chen Q. Cyanidin-3-O-glucoside attenuates endothelial cell dysfunction by modulating miR-204-5p/SIRT1-mediated inflammation and apoptosis. *BioFactors*. 2020;46(5):803–812. doi:10.1002/biof.1660
- Xu FP, Chen MS, Wang YZ, et al. Leptin induces hypertrophy via endothelin-1-reactive oxygen species pathway in cultured neonatal rat cardiomyocytes. *Circulation*. 2004;110(10):1269–1275. doi:10.1161/01.CIR.0000140766.52771.6D
- Frountzas M, Karanikli E, Toutouza O, et al. Exploring the impact of cyanidin-3-glucoside on inflammatory bowel diseases: Investigating new mechanisms for emerging interventions. *Int J Mol Sci*. 2023;24(11):9399. doi:10.3390/ijms24119399
- Pereira SR, Pereira R, Figueiredo I, Freitas V, Dinis TCP, Almeida LM. Comparison of anti-inflammatory activities of an anthocyanin-rich fraction from Portuguese blueberries (*Vaccinium corymbosum* L.) and 5-aminosalicylic acid in a TNBS-induced colitis rat model. *PLoS One*. 2017;12(3):e0174116. doi:10.1371/journal.pone.0174116
- Shah SA, Amin FU, Khan M, et al. Anthocyanins abrogate glutamate-induced AMPK activation, oxidative stress, neuroinflammation, and neurodegeneration in postnatal rat brain. *J Neuroinflammation*. 2016;13(1):286. doi:10.1186/s12974-016-0752-y
- Takikawa M, Inoue S, Horio F, Tsuda T. Dietary anthocyanin-rich bilberry extract ameliorates hyperglycemia and insulin sensitivity via activation of AMP-activated protein kinase in diabetic mice. *J Nutr*. 2010;140(3):527–533. doi:10.3945/jn.109.118216
- Liu Y, Li D, Zhang Y, Sun R, Xia M. Anthocyanin increases adiponectin secretion and protects against diabetes-related endothelial dysfunction. *Am J Physiol Endocrinol Metab*. 2014;306(8):E975–E988. doi:10.1152/ajpendo.00699.2013
- Zhang Y, Wu J, Dong E, Wang Z, Xiao H. Toll-like receptors in cardiac hypertrophy. *Front Cardiovasc Med*. 2023;10:1143583. doi:10.3389/fcvm.2023.1143583



29. ElKhatib MAW, Isse FA, El-Kadi AOS. Effect of inflammation on cytochrome P450-mediated arachidonic acid metabolism and the consequences on cardiac hypertrophy. *Drug Metab Rev.* 2023;55(1–2): 50–74. doi:10.1080/03602532.2022.2162075
30. Yang J, Wang HX, Zhang YJ, et al. Astragaloside IV attenuates inflammatory cytokines by inhibiting TLR4/NF- $\kappa$ B signaling pathway in isoproterenol-induced myocardial hypertrophy. *J Ethnopharmacol.* 2013;150(3):1062–1070. doi:10.1016/j.jep.2013.10.017
31. Yu B, Zhao Y, Zhang H, Xie D, Nie W, Shi K. Inhibition of microRNA-143-3p attenuates myocardial hypertrophy by inhibiting inflammatory response. *Cell Biol Int.* 2018;42(11):1584–1593. doi:10.1002/cbin.11053
32. Yi W, Sun Y, Yuan Y, et al. C1q/tumor necrosis factor-related protein-3, a newly identified adipokine, is a novel antiapoptotic, proangiogenic, and cardioprotective molecule in the ischemic mouse heart. *Circulation.* 2012;125(25):3159–3169. doi:10.1161/CIRCULATIONAHA.112.099937
33. Petersen PS, Wolf RM, Lei X, Peterson JM, Wong GW. Immunomodulatory roles of CTRP3 in endotoxemia and metabolic stress. *Physiol Rep.* 2016;4(5):e12735. doi:10.14814/phy2.12735
34. Schmid A, Kopp A, Hanses F, Karrasch T, Schäffler A. C1q/TNF-related protein-3 (CTRP-3) attenuates lipopolysaccharide (LPS)-induced systemic inflammation and adipose tissue Erk-1/-2 phosphorylation in mice in vivo. *Biochem Biophys Res Commun.* 2014;452(1):8–13. doi:10.1016/j.bbrc.2014.06.054



# Identification and verification on prognostic index of glioblastoma immune-related lncRNAs

Guofu Zheng<sup>1,A–F</sup>, Qingsong Jiang<sup>1,C,E</sup>, Cai Jiang<sup>1,B,C</sup>, Xingxin Zhu<sup>2,A,B,D,E</sup>, Yongjie Wang<sup>3,A,E,F</sup>

<sup>1</sup> Department of Neurosurgery, Kecheng People's Hospital, Quzhou, China

<sup>2</sup> Department of Thoracic Surgery, The First Affiliated Hospital of Zhejiang University, School of Medicine, Hangzhou, China

<sup>3</sup> Department of Neurosurgery, The Second Affiliated Hospital of Zhejiang University, School of Medicine, Hangzhou, China

A – research concept and design; B – collection and/or assembly of data; C – data analysis and interpretation;

D – writing the article; E – critical revision of the article; F – final approval of the article

Advances in Clinical and Experimental Medicine, ISSN 1899–5276 (print), ISSN 2451–2680 (online)

*Adv Clin Exp Med.* 2024;33(8):843–856

## Address for correspondence

Yongjie Wang

E-mail: 11018196@zju.edu.cn

## Funding sources

Guiding Science and Technology Project of Quzhou City (grant No. 2021092).

## Conflict of interest

None declared

Received on September 29, 2022

Reviewed on February 8, 2023

Accepted on September 20, 2023

Published online on February 20, 2024

## Abstract

**Background.** Glioblastoma (GBM) is the most common cause of primary brain malignancy. Recently, many immune-related long noncoding ribonucleic acids (ir-lncRNAs) are indicated to be closely related to the regulation of the immune microenvironment and immune cell infiltration of GBM.

**Objectives.** Through the joint analysis of multiple public databases, key ir-lncRNAs in GBM were screened. The ir-lncRNAs were used to construct risk-scoring models and promote the development of novel GBM biomarkers.

**Materials and methods.** In this study, we performed a three-way Venn analysis combined with a least absolute shrinkage and selection operator (LASSO) regression analysis on all lncRNAs in The Cancer Genome Atlas (TCGA), the Chinese Glioma Genome Atlas (CGGA) and Imm-Lnc datasets, and identified 10 ir-lncRNAs. Multivariate Cox analysis was used to calculate the coefficient and construct a risk-scoring model.

**Results.** By plotting calibration curves and receiver operating characteristic (ROC) curves, the model showed excellent prediction results. Based on the Tumor Immune Estimation Resource (TIMER) database, the correlation analysis showed that 10 ir-lncRNAs risk scores were related to immune cell infiltration. The enrichment analysis was subsequently performed, which showed that these ir-lncRNAs played an important role in the progression of GBM. Among the 10 lncRNAs, we found that *AL354993.1* was highly expressed in GBM, had not been reported, and was shown to be closely related to GBM progression.

**Conclusions.** In conclusion, the 10 ir-lncRNAs have the potential to predict the prognosis of GBM patients and may play a vital role in the progression of the disease.

**Key words:** immunity, lncRNA, prognostic model, glioblastoma, gene function enrichment analysis

## Cite as

Zheng G, Jiang Q, Jiang C, Zhu X, Wang Y. Identification and verification on prognostic index of glioblastoma immune-related lncRNAs. *Adv Clin Exp Med.* 2024;33(8):843–856. doi:10.17219/acem/172576

## DOI

10.17219/acem/172576

## Copyright

Copyright by Author(s)

This is an article distributed under the terms of the Creative Commons Attribution 3.0 Unported (CC BY 3.0) (<https://creativecommons.org/licenses/by/3.0/>)

## Background

The most aggressive primary brain malignancy originates from oligodendrocyte or astrocyte precursor cells and is known as glioblastoma (GBM). Although accurate surgical resection, radiation and adjuvant chemotherapy are now the conventional treatments for GBM, the prognosis is still poor, and the median survival is just 8–15 months.<sup>1</sup> Immunomodulatory therapy is a new and effective treatment option.<sup>2</sup> The stemness features of GBM are strictly connected to immune infiltration,<sup>3</sup> meaning neoadjuvant anti-programmed cell death protein 1 (PD-1) checkpoint blocking immunotherapy might improve the prognosis of properly selected GBM patients.<sup>4</sup> However, GBM often exhibits severe local immunosuppression, which limits the efficacy of immunotherapy strategies.<sup>5</sup> To further explain the mechanisms of immune regulation in GBM and offer a theoretical basis for GBM immunological treatment, we evaluated effective immune-related prognostic factors and constructed a prognostic model for GBM patients.

Long noncoding ribonucleic acids (lncRNAs) are a group of transcripts with a length of more than 200 nt that primarily function as regulators rather than protein-coding genes.<sup>6</sup> The lncRNAs perform their biological functions in a variety of ways, including alternative splicing, transcription regulation, messenger RNA (mRNA) stability maintenance, chromatin modification, functional micropeptides, and interaction with proteins or small RNAs.<sup>7–9</sup> The lncRNAs are also crucial for GBM progression. The lncRNA HNF1A-AS1 was shown to drive GBM progression through the microRNA (miR)-22-3p/alpha-enolase 1 (ENO1) axis.<sup>10</sup> Indeed, lncRNA miR155HG has been shown to promote GBM progression by upregulating annexin A2 (*ANXA2*) as a competing endogenous RNA (ceRNA) of the tumor suppressor miR-185.<sup>11</sup>

Immune-related lncRNAs (ir-lncRNAs) are involved in regulating the GBM immune microenvironment and have unique prognostic value. According to reports, lncRNA AC003092.1 is connected to the immunosuppressive environment in GBM.<sup>12</sup> Moreover, maternally expressed 3 (MEG3) levels are negatively associated with dendritic cell infiltration and positively correlated with infiltrating CD8<sup>+</sup> T cells. The survival of GBM patients was also significantly correlated with the degree of MEG3 variation in copies.<sup>13</sup> The heat shock protein family A member 7 (HSPA7) lncRNA was found to promote macrophage recruitment to the GBM tumor microenvironment and had a great prognostic value.<sup>14</sup> However, few investigations have established prognostic models based on the identification of ir-lncRNAs in GBM.

## Objectives

The ir-lncRNAs obtained from the Chinese Glioma Genome Atlas (CGGA; <http://www.cgga.org.cn/>) and The Cancer Genome Atlas (TCGA; <https://www.cancer.gov/ccg/research/genome-sequencing/tcga>) were examined. The clinical

prognostic model of GBM was developed after the least absolute shrinkage and selection operator (LASSO) algorithm identified the most critical lncRNAs. Additionally, the underlying pathway of ir-lncRNAs in GBM was investigated.

## Materials and methods

### Data and resources

Both TCGA-GBM (n = 166) and CGGA cohorts (n = 140) were used as public transcriptome datasets in our analysis.<sup>15</sup> Any case with a survival information null value was eliminated. The UCSC Xena database was used to retrieve the clinical information and fragments per kilobase per million (FPKM) data for the TCGA-GBM cohort (<https://xenabrowser.net/>). Transcripts per kilobase million (TPM) values were obtained from all FPKM data. The RNA-sequencing (RNA-seq) data of 140 specimens were retrieved from the CGGA data collection in addition to the clinical data for use as a validation set. The TCGA database provided gene mutation data (MAF files) for the TCGA-GBM group. The proportional hazards assumption test, linearity assumption test and multicollinearity test assessed the TCGA and CGGA cohorts (Supplementary Fig. 1–3).

### Detection of immune-related lncRNA prognostic signature

The ImmLnc database (<http://bio-bigdata.hrbmu.edu.cn/ImmReg/index.jsp>) has collected 3115 GBM ir-lncRNAs.<sup>16</sup> By evaluating the intersection of lncRNAs among the TCGA, CGGA and ImmLNC datasets, we selected ir-lncRNAs. To prevent overfitting and examine the ideal ir-lncRNA signature for estimating the overall survival of GBM individuals, the LASSO was selected. The LASSO regression analysis was performed using the “glmnet” R program. Every sample's risk score was determined from the formula: risk score = expression value of lncRNA 1 × coefficient + expression value of lncRNA 2 × coefficient + ... + expression value of lncRNA n × coefficient. Then, depending on the middle threshold of the risk score, GBM patients were allocated into elevated- and reduced-risk cohorts. The “Survival” program of R software's area under the curve (AUC) function was employed to verify the specificity and sensitivity of the immune-related signature.

### Nomogram

To anticipate the 1-, 2- and 3-year survival rates, a nomogram was developed after the independent prognostic parameters were identified. Receiver operating characteristic (ROC) curves were employed to assess the effectiveness of the model. Additionally, calibration plots were shown utilizing the rms tool to compare the model-predicted survival with the actual survival probability.

## Gene set enrichment analysis

Kyoto Encyclopedia of Genes and Genomes (KEGG; <https://www.genome.jp/kegg/>) and Gene Ontology (GO; <https://geneontology.org/>) mechanisms that positively related to elevated- or reduced-risk scores were investigated using gene set enrichment analysis (GSEA; <https://www.gsea-msigdb.org/gsea/index.jsp>). Molecular Signatures Database gene sets were obtained. Typically, 1000 permutations were used in the analysis, and pathways with a false discovery rate (FDR) of less than 0.25 were detected.

## Estimation of cancer immune microenvironment

The Tumor Immune Estimation Resource (TIMER) ([timer.cistrome.org/](http://timer.cistrome.org/)) platform<sup>17</sup> was employed to investigate the connections between risk score and immune infiltrates, such as B cells, CD8<sup>+</sup> T cells, CD4<sup>+</sup> T cells, macrophages, neutrophils, and dendritic cells, as demonstrated by the purity-corrected partial Spearman approach. Depending on gene expression patterns, the Estimation of STromal and Immune Cells in MAlignant Tumor tissues using Expression data (ESTIMATE) program evaluated the stromal scores and immune scores.<sup>18</sup> In addition, we utilized the tumor immune dysfunction and exclusion (TIDE algorithm; <http://tide.dfci.harvard.edu/>) to evaluate each participant's potential reaction to immune checkpoint inhibitor (ICI) treatment.<sup>19</sup>

## Statistical analyses

The TCGA-GBM cohort contains 166 tumor samples from patients with GBM, while the CGGA cohort includes 140 tumor samples from patients with GBM and normal tissue from 20 patients. For the TCGA-GBM cohort, we divided patients into 2 groups based on the risk score: high-risk group (n = 83) and low-risk group (n = 83). In addition, we used the TIDE algorithm to predict the responsiveness of patients in the TCGA-GBM cohort to immunotherapy, with 48 patients evaluated as responders and 120 evaluated as non-responders. According to isocitrate dehydrogenase 1 (*IDH1*) mutation status, patients in the CGGA cohort were divided into 2 groups: wild-type (wt) group (n = 100) and mutant (mut) group (n = 40). Based on the co-deletion status of x1p19q, patients in the CGGA cohort were divided into 2 groups: Non\_codel group (n = 128) and codel group (n = 12). Additionally, patients in the CGGA cohort were divided into 2 groups based on the expression level of *AL354993.1*: low-expression group (n = 70) and high-expression group (n = 70).

Continuous variables were tested for normality using Kolmogorov–Smirnov or Shapiro–Wilk tests. When the sample size was  $\leq 50$ , the Shapiro–Wilk test was employed. Otherwise, the Kolmogorov–Smirnov test was used. The variables were considered to conform to a normal

distribution when  $p > 0.05$ . When performing a difference analysis for 2 sets of variables, an F-test was used to evaluate the homogeneity of variance between the 2 groups. The variance between the 2 variables was considered equal when  $p > 0.05$ . The results of the tests assessing the assumptions are provided in Supplementary Tables.

When the variables conformed to a normal distribution and the variance was equal, Student's t-test was used to compare between-group differences. If at least one of the assumptions was violated, the Mann–Whitney U test was used to compare the differences between the groups. For Student's t-test, we also calculated the test values and degrees of freedom (df). For the Mann–Whitney U test, we calculated the U and Z values. The  $\chi^2$  or Fisher's exact tests were used to compare the differences between the groups for categorical variables. When the total sample size was  $>40$  and the minimum theoretical frequency was  $>5$ , the  $\chi^2$  test was used. When the total sample size was  $>40$  and  $5 >$ , and the minimum theoretical frequency was  $>1$ , the corrected  $\chi^2$  test was used. If the total sample size was  $<40$  or the minimum theoretical frequency was  $<1$ , Fisher's exact test was used. The results of tests assessing the differences between the groups are presented in tabular form and illustrated using box-and-whisker plots, which contain 5 lines representing the estimated maximum upper quartile ( $Q_U$ ), median lower quartile ( $Q_L$ ), and estimated minimum of the data from top to bottom. Outliers were defined as a value greater than  $Q_U + 1.5 \times QR$  or less than  $Q_L - 1.5QR$ , where  $QR = Q_U - Q_L$ .

The Cox proportional hazards model was used to evaluate the impact of clinical parameters on patient survival time. In terms of parameter selection, we evaluated the clinical parameters common to both TCGA and CGGA cohorts, and age and gender were included in both. Therefore, we included 3 parameters: patient age, gender and the risk score calculated using the Cox regression model. First, we performed the proportional hazards assumption test on all 3 parameters (Supplementary Fig. 1). When the Schoenfeld individual test p-value was less than 0.05, the proportional hazards assumption was considered valid. For the continuous parameters, age and risk score, we performed a linearity assumption test (Supplementary Fig. 2) and a multicollinearity test (Supplementary Fig. 3). When the fitted curve was approximately linear, the linearity assumption was considered valid. When the p-value of the correlation was less than 0.05, these 2 parameters were considered to have no multicollinearity. For each Cox regression result, we calculated Harrell's compliance index as the goodness-of-fit.

The sample size is labeled in the figure legends. The Kaplan–Meier technique (R package survival) was employed to create overall survival (OS) curves, and the log-rank test was used to assess alterations between the curves. This study used  $p < 0.05$  as a statistically significant criterion. Statistical analyses employed R 3.6.2 (R Foundation for Statistical Computing, Vienna, Austria) and IBM SPSS v. 26.0 for Windows (IBM Corp., Armonk, USA).

## Results

### Determination of ten survival-related ir-lncRNAs in GBM

There were 14,038 lncRNAs in the TCGA-GBM database, 1,082 lncRNAs in the CGGA database and 3,175 ir-lncRNAs in the ImmLnc database. After three-way Venn analysis, 276 ir-lncRNAs that coexisted in all 3 databases were identified (Fig. 1A). To further screen for effective prognostic markers, we used LASSO regression to finally select 10 ir-lncRNAs associated with GBM prognosis, namely *CHRM3-AS2*, *LEF1-AS1*, *AL354993.1*, *AC034243.1*, *LINC00452*, *NDUFB2-AS1*, *LINC00571*, *UNC5B-AS1*, *AC009093.1*, and *HOXC-AS2* (Fig. 1B,C).

The Kaplan–Meier examination indicated that elevated expression of each ir-lncRNA was substantially related to poorer OS in the TCGA database, except for *NDUFB2-AS1* and *LINC00571* (Fig. 1C).

### Progression and validation of the ten survival-related ir-lncRNA signatures for survival anticipation

Based on the multivariate Cox regression model, the above 10 ir-lncRNAs were integrated to create a risk score model in the TCGA database. In the TCGA, the Kaplan–Meier examination revealed that OS was considerably poorer in raised-risk participants than in decreased-risk individuals ( $p < 0.0001$ , Fig. 2A). The risk scores and

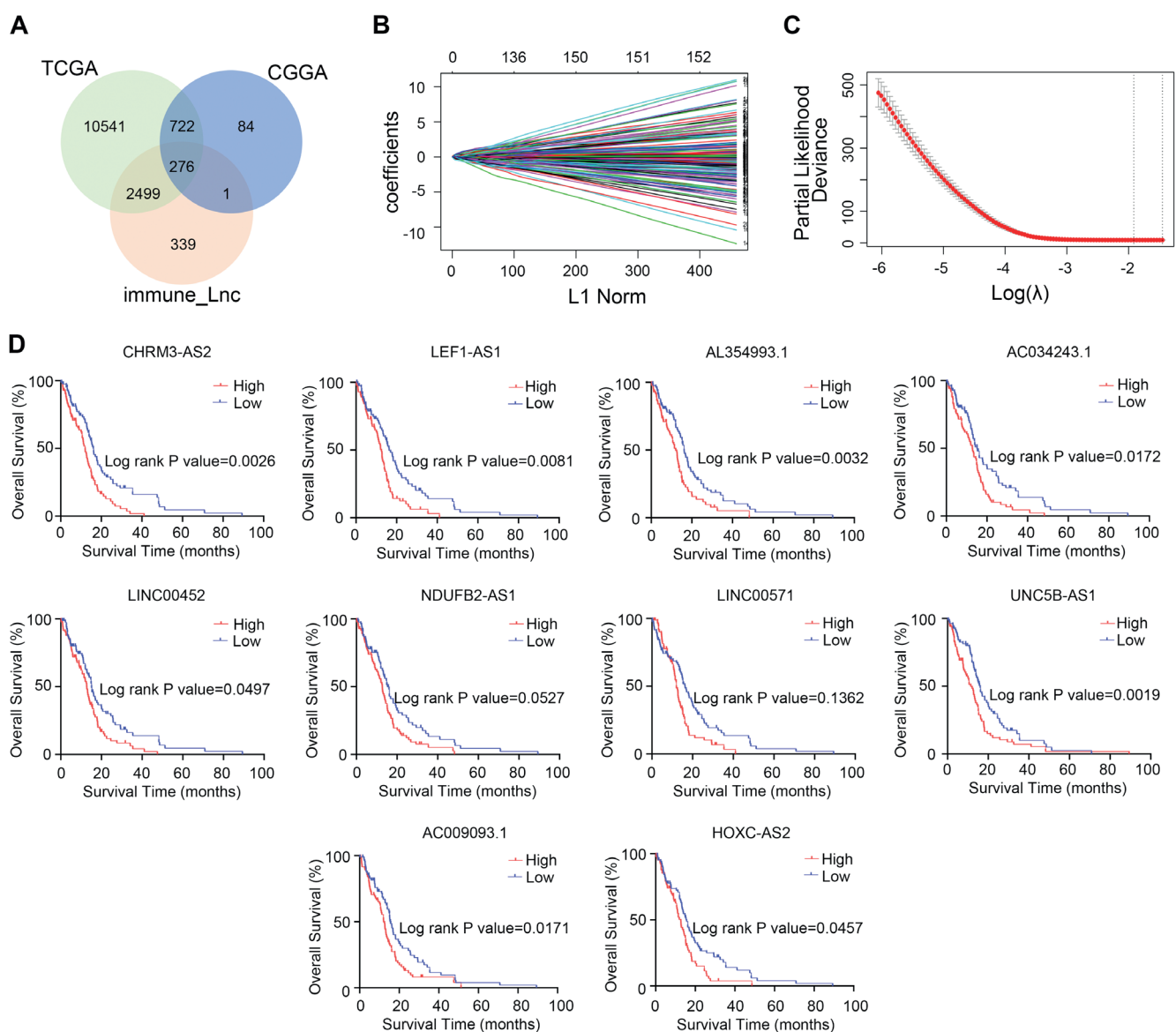


**Fig. 1.** Identification of 10 survival-related immune long noncoding ribonucleic acids (lncRNAs) in glioblastoma. **A.** Venn diagram illustrates that 276 lncRNAs were shared among 3 datasets; **B.** Distribution of least absolute shrinkage and selection operator (LASSO) coefficients for 276 immune-related lncRNAs; **C.** Partial likelihood deviation of the LASSO coefficient distribution. Vertical dashed lines indicate lambda.min and lambda.lse; **D.** The Kaplan–Meier survival curves comparing overall (OS) survival between high- and low-expression groups of the selected immune-related lncRNAs in The Cancer Genome Atlas (TCGA) dataset CGGA – Chinese Glioma Genome Atlas.

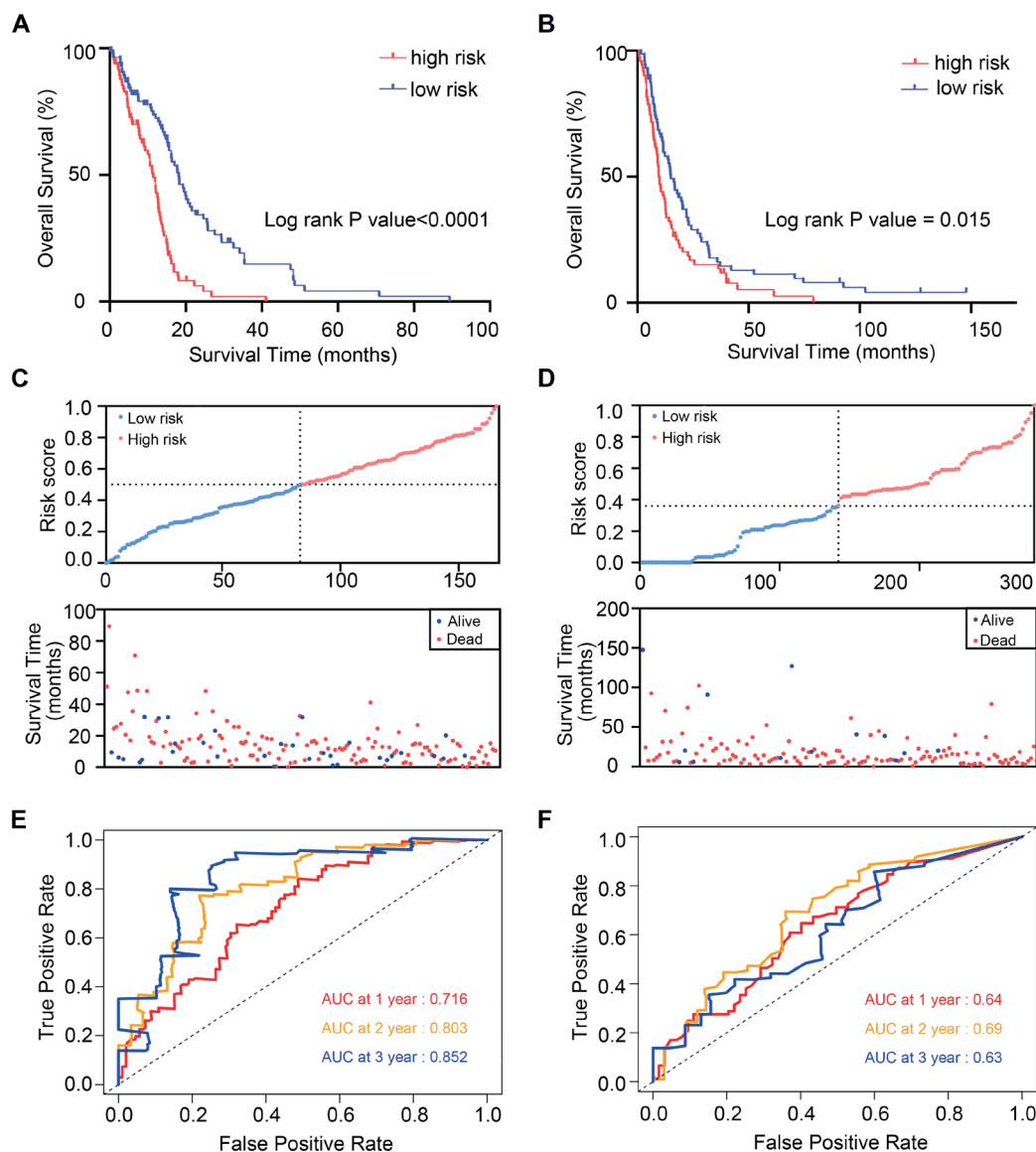


**Fig. 2.** Development and validation of 10 survival-related immune long noncoding ribonucleic acids (lncRNA) signatures for survival prediction. The Kaplan–Meier survival analysis of high-risk and low-risk patients divided by the medium value in The Cancer Genome Atlas (TCGA) (A) and Chinese Glioma Genome Atlas (CGGA) (B) datasets. The distribution of risk scores, survival time and status of patients in TCGA (C) and CGGA (D) datasets. Receiver operating characteristic (ROC) analysis of the prognostic signatures to predict 1-, 2- and 3-year overall survival (OS) in TCGA (E) and CGGA (F) datasets

survival status of every GBM specimen were represented by the risk curve and scatterplot, respectively. The samples in the elevated-risk group had greater risk ratings and mortality rates than those in the reduced-risk cohort (Fig. 2C).

The ROC analysis revealed that the AUC for 1-, 2- and 3-year survival were 0.716, 0.803 and 0.852, respectively (Fig. 2E). Therefore, the risk score model constructed using the 10 ir-lncRNAs was effective in predicting GBM prognosis. Additionally, we developed and assessed the risk score model using the CGGA database as the validation set and acquired comparable outcomes (Fig. 2B,D,F).

### Establishment and evaluation of nomograms by the risk scores and the prognostic value of medical variables

A univariate Cox regression examination was conducted to determine whether the risk score model for the 10 ir-lncRNAs and GBM-related clinical variables

were prognostic factors. The results indicated that risk scores ( $p < 0.001$ ; hazard ratio (HR) = 13.68) and patient age ( $p < 0.001$ ; HR = 1.02) were strongly correlated with OS in the TCGA database (Fig. 3A). The CGGA database was also used as a validation set for univariate Cox regression analysis, and the ir-lncRNA model was found to be a substantial risk factor for GBM individuals (Fig. 3B).

The nomogram with age, gender and risk score was developed for the prediction of patient prognosis in the TCGA dataset. We collected survival information from all patients to anticipate the 1-, 2- and 3-year OS (Fig. 3C). The calibration curve of the 1-, 2- and 3-year OS showed that the nomogram had excellent prognostic value (Fig. 3E). The AUC of the 1-, 2- and 3-year OS were 0.79, 0.82 and 0.91, respectively, according to the ROC curve analysis (Fig. 3F). Similar prediction outcomes were achieved in the CGGA validation set, supporting the nomogram’s effective prediction ability over the risk score model (Fig. 3D,G,H).

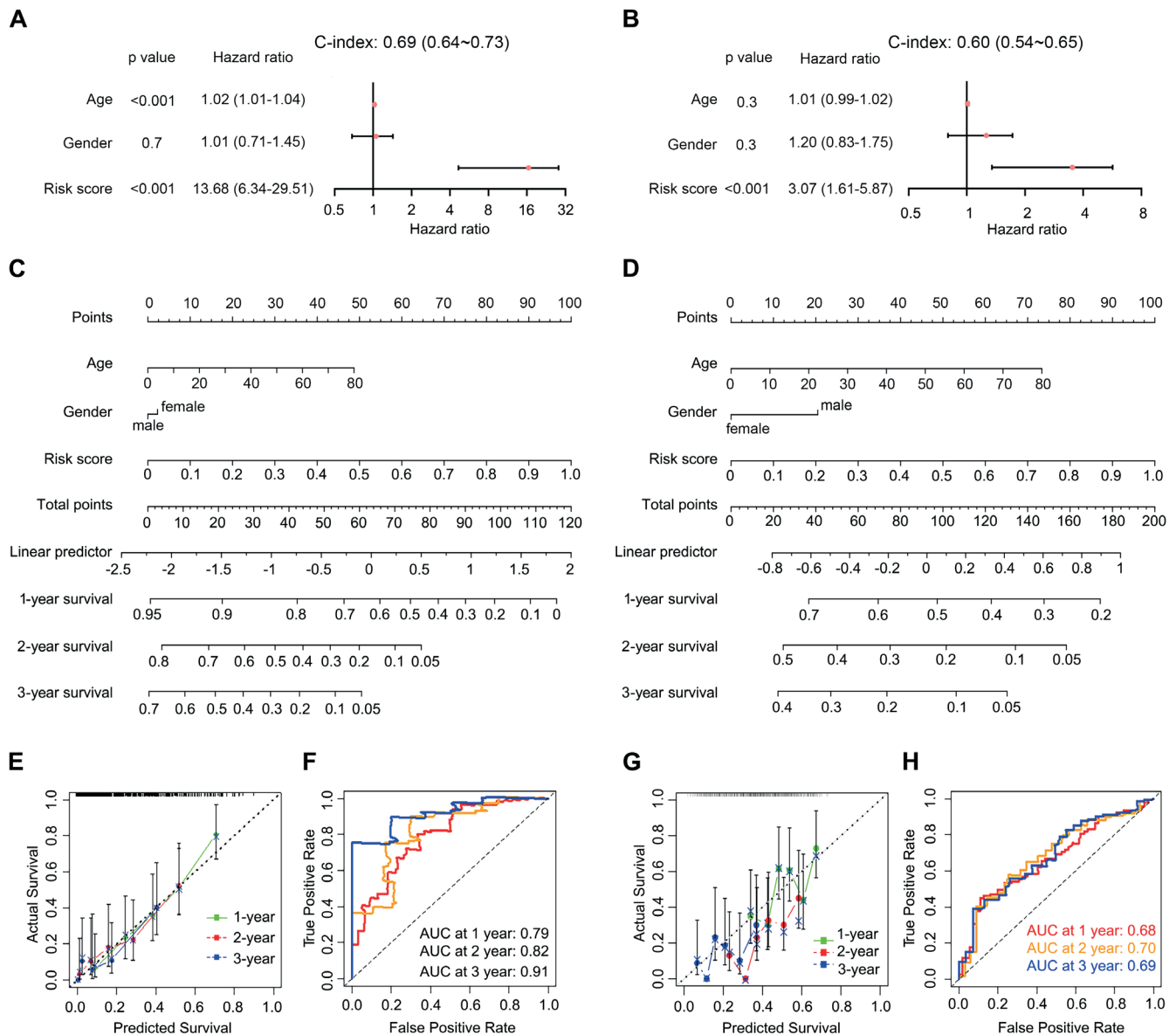


**Fig. 3.** Establishment and evaluation of nomograms using risk scores and the prognostic value of clinical variables. **A.** Univariate Cox analysis showed that risk scores and age were significantly related to overall survival (OS) in The Cancer Genome Atlas (TCGA) dataset using Harrell's compliance index (C-index) as the goodness-of-fit. For the TCGA cohort, the C-index was 0.69 (95% confidence interval (95% CI): of 0.64–0.73), and for the Chinese Glioma Genome Atlas (CGGA cohort), the C-index was 0.6 (95% CI: 0.54–0.65); **B.** Univariate Cox analysis showed that risk scores and age were significantly related to OS in the CGGA dataset; **C.** Development of the nomograms for the prediction of patient prognosis in the TCGA dataset; **D.** Development of the nomograms for the prediction of patient prognosis in the CGGA dataset; **E.** The calibration curve for 1-, 2- and 3-year OS of the nomogram in the TCGA dataset; **F.** Receiver operating characteristic (ROC) curves displayed the area under the curve (AUC) for 1-, 2- and 3-year OS in the TCGA dataset; **G.** The calibration curve for 1-, 2- and 3-year OS of the nomogram in the CGGA dataset; **H.** ROC curves displayed the AUC of 1-, 2- and 3-year OS in the CGGA dataset

## Enrichment analysis identified ir-lncRNA-related biological functions and signaling pathways in GBM

Based on the risk score, GBM participants in the TCGA were separated into elevated- and reduced-risk cohorts. Gene ontology and KEGG enrichment analysis were then performed on the genes that were differently expressed between the 2 groups. The outcomes of KEGG enrichment investigations revealed that the differentially expressed

genes were primarily related to the activation of innate immune response, cellular responses to chemokines, collagen binding, cytokine secretion, humoral immune responses, the Janus kinase (JAK)-signal transducer and activator transcription (STAT) cascade, leukocyte migration, macrophage activation, modulation of lymphocyte activity, and T cell activation (Fig. 4A). According to the outcomes of the GO enrichment analysis, these genes primarily participated in the signaling pathways for cell adhesion molecules, chemokine signaling, cytokine–cytokine



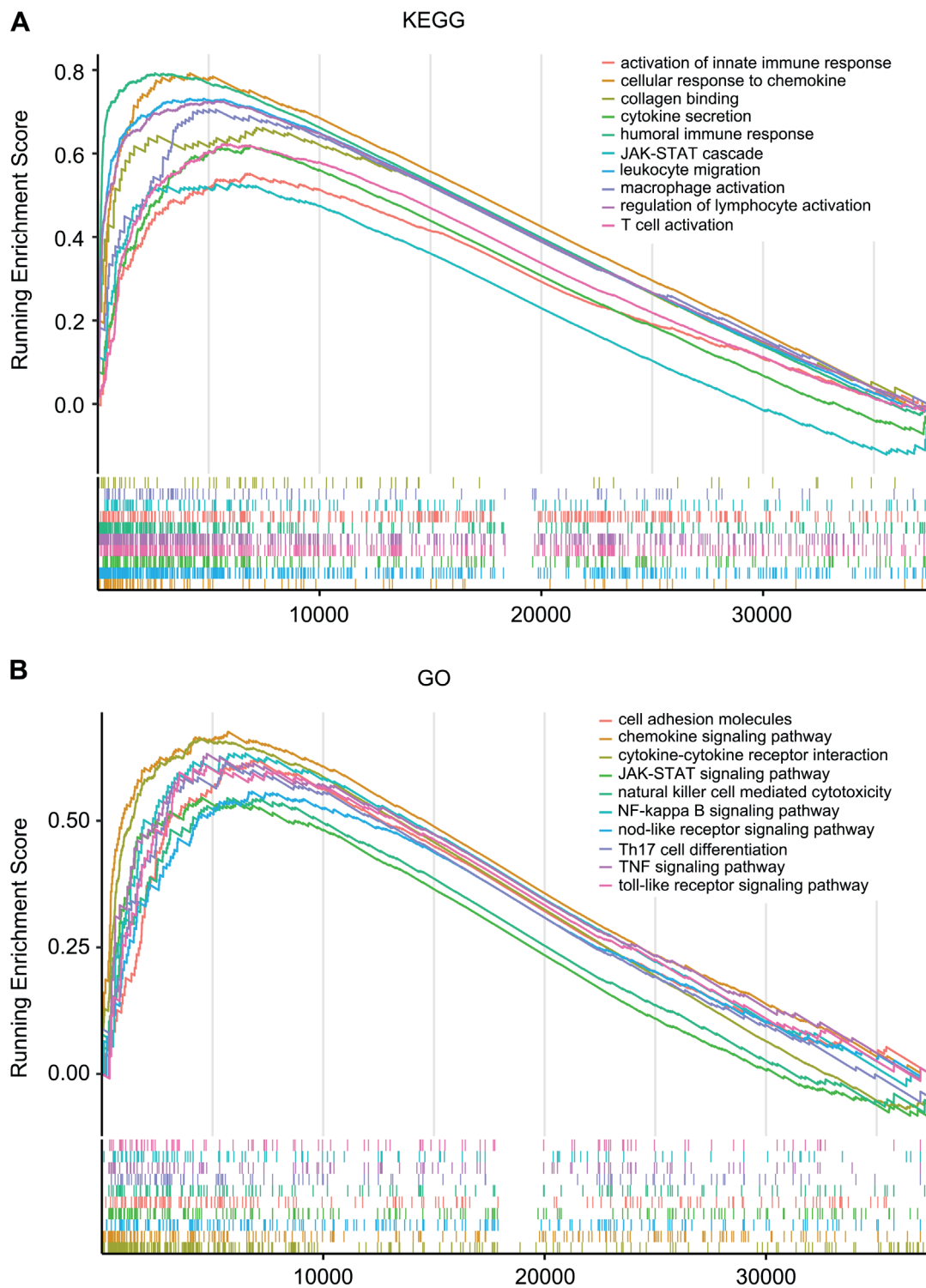


Fig. 4. Gene set enrichment analysis between high-risk and low-risk groups in the Kyoto Encyclopedia of Genes and Genomes (KEGG) and gene ontology (GO) datasets

receptor interactions, JAK-STAT signaling, natural killer cell-mediated cytotoxicity, nuclear factor-kappa B (NF-κB) signaling, nod-like receptor signaling, T helper (Th)17 cell differentiation, tumor necrosis factor (TNF) signaling, and toll-like receptor signaling (Fig. 4B). The knowledge of the underlying pathways involving these ir-lncRNAs in the development and progression of GBM was deepened by these enriched biological processes and signaling mechanisms.

### The ir-lncRNAs-related risk score was correlated with the GBM immune microenvironment

To additionally explore the function of the 10 ir-lncRNAs in the immune microenvironment, the TIMER database was used to examine the connection between the risk score and various infiltrating immune cell subpopulations in GBM. It was shown that the risk score

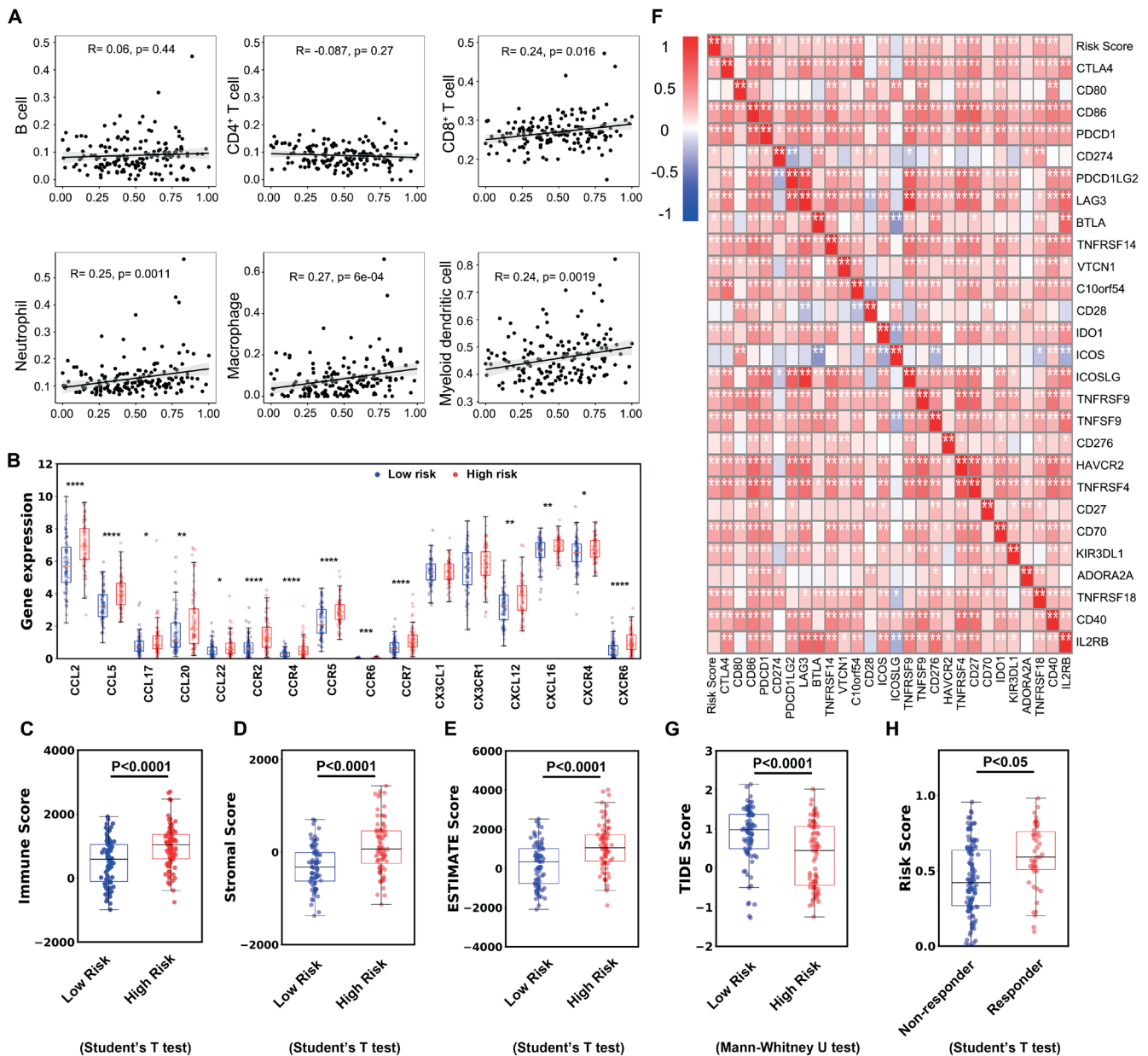


Fig. 5. The immune risk score was correlated with the tumor immune microenvironment. A. The correlation between risk score and immune cell infiltration; B. The expression of chemokines between low- ( $n = 83$ ) and high-risk groups ( $n = 83$ ) (parametric test and the Mann–Whitney U test). The difference in immune score (parametric test) (C), stromal score (parametric test) (D), and Estimation of STromal and Immune Cells in Malignant Tumor tissues using Expression data (ESTIMATE) score (Mann–Whitney U test) (E) between low- ( $n = 83$ ) and high-risk groups ( $n = 83$ ); F. Assessment of associations between risk scores and commonly used immunological checkpoints; G. Tumor immune dysfunction and exclusion (TIDE) scores between high- ( $n = 83$ ) and low-risk group ( $n = 83$ ); H. Comparison of the risk scores between immunotherapy responders ( $n = 48$ ) and non-responders ( $n = 118$ ) predicted with TIDE (parametric test)

was closely related to the infiltration of CD8<sup>+</sup> T cells, neutrophils, macrophages, and myeloid dendritic cells, with correlation coefficients of 0.24, 0.25, 0.27, and 0.24, respectively (Fig. 5A). It is well-known that chemokines efficiently control immune cell infiltration in malignancies. The expression of 16 immune-related chemokines recognized to be linked with GBM development was compared in elevated- and low-risk tissues to further examine the relationship between risk scores and chemokine secretion. The outcomes demonstrated that 14 chemokines were differentially expressed (chemokine ligand (CCL)2, CCL5, CCL17, CCL20, CCL22, CCR2, CCR4, CCR5, CCR6, CCR7,

CXC motif chemokine ligand (CXCL)12, CXCL16, CXC motif chemokine receptor (CXCR)4, and CXCR6) (Fig. 5B, Table 1 and Supplementary Table 1).

Further calculations of the GBM patients' immunological, stromal and ESTIMATE scores in the TCGA dataset indicated that the immune score of the reduced-risk cohort was much less than that of the elevated-risk cohort (Fig. 5C–E, Table 2 and Supplementary Table 2). A strong association between the risk score and commonly employed immunological checkpoints was determined using Pearson's correlation analysis, indicating that the risk score may have implications for immunotherapy (Fig. 5F).

**Table 1.** The expression of chemokines between low- and high-risk groups

Gene	Gene expression		p-value
	low risk (n = 83)	high risk (n = 83)	
<i>CCL2</i>	5.84 ±1.66	6.96 ±1.46	<b>9.00E-06</b>
<i>CCL5</i>	3.33 ±1.02	4.06 ±1.01	<b>9.00E-06</b>
<i>CCL17</i>	0.83 ±0.60	1.10 ±0.95	<b>2.80E-02</b>
<i>CCL20</i>	1.58 ±1.25	2.34 ±1.73	<b>1.40E-03</b>
<i>CCL22</i>	0.54 ±0.39	0.74 ±0.63	<b>1.40E-02</b>
<i>CCR2</i>	0.74 ±0.57	1.44 ±0.97	<b>7.34E-08</b>
<i>CCR4</i>	0.29 ±0.22	0.59 ±0.54	<b>7.00E-06</b>
<i>CCR5</i>	2.31 ±0.97	2.92 ±0.79	<b>1.60E-05</b>
<i>CCR6</i>	0.02 ±0.02	0.03 ±0.04	<b>8.16E-04</b>
<i>CCR7</i>	0.73 ±0.44	1.17 ±0.70	<b>4.00E-06</b>
<i>CXCL1</i>	5.35 ±0.83	5.31 ±0.72	7.28E-01
<i>CX3CR1</i>	5.45 ±1.41	5.76 ±1.21	1.28E-01
<i>CXCL12</i>	3.24 ±1.10	3.82 ±1.19	<b>1.11E-03</b>
<i>CXCL16</i>	6.60 ±0.86	6.94 ±0.57	<b>2.97E-03</b>
<i>CXCR4</i>	6.48 ±0.97	6.74 ±0.75	<b>4.79E-02</b>
<i>CXCR6</i>	0.59 ±0.50	1.03 ±0.65	<b>3.00E-06</b>

Values in bold are statistically significant.

**Table 2.** The difference of immune score, stromal score, ESTIMATE score, and TIDE score

Score items	Value		p-value
	low risk (n = 83)	high risk (n = 83)	
Immune score	-318.36 ±453.26	113.18 ±556.25	6.00E-06
Stromal score	499.02 ±700.96	993.86 ±659.55	1.58E-07
ESTIMATE score	180.66 ±1107.5	1107.04 ±1171.6	5.00E-07
TIDE score	1.06 ±0.46	0.09 ±0.83	3.33E-16

ESTIMATE – Estimation of STromal and Immune Cells in Malignant Tumor tissues using Expression data; TIDE – tumor immune dysfunction and exclusion.

To further anticipate the reaction of GBM to immunotherapy, we used the TIDE algorithm. A high TIDE score means that the likelihood of responding to immunotherapy is low. According to the findings, individuals with elevated-risk GBM had reduced TIDE scores and were more likely to react to immunotherapy (Fig. 5G,H, Table 2,3 and Supplementary Table 2). The previous findings demonstrated that the risk score associated with ir-lncRNAs was strongly connected to the GBM immune microenvironment, and it was anticipated that this relationship might be helpful in targeting future GBM immunotherapy.

### Alterations in the mutation landscape between elevated- and low-risk groups

Tumor somatic mutation of commonly mutated genes was profiled in GBM elevated-risk and reduced-risk cohorts. Most mutated genes, including *TP53*, *PTEN*, *TTN*,

**Table 3.** Comparison of the risk scores between immunotherapy responders (n = 48) and non-responders (n = 118) predicted with TIDE

Score items	Status	Risk score	p-value
TIDE score	non-responder (n = 118)	0.44 ±0.23	1.10E-02
	responder (n = 48)	0.61 ±0.22	

TIDE – tumor immune dysfunction and exclusion.

**Table 4.** Different risk scores divided by *IDH1* mutation and 1p/19q codeletion

Mutation	Status	Risk score	p-value
<i>IDH1</i> mutation	wt (n = 100)	0.45 ±0.24	8.29E-09
	mut (n = 40)	0.17 ±0.22	
1p/19q codeletion	Non_Codel (n = 128)	0.38 ±0.26	2.23E-02
	Codel (n = 12)	0.20 ±0.24	

wt – wild type; mut – mutant.

*EGFR*, *MUC16*, *SPTA1*, *NF1*, *RYR2*, and *FLG*, had high rates of somatic mutations in both raised- and reduced-risk groups. In particular, somatic mutation rates for *RBI*, *HYDIN*, *ATRX*, and *IDH1* were greater in the low-risk cohort (Fig. 6A,B). Notably, *ATRX* and *IDH1* did not have somatic mutations in the raised-risk cohort in the TCGA dataset (Fig. 6C,D). In the CGGA dataset, the patterns of risk scores for *IDH1* mutation and 1p/19q codeletion stats were identified. According to the findings, those with *IDH1* mutations had considerably lower risk scores than individuals with *IDH1* wild type (Fig. 6E, Table 4 and Supplementary Table 4). Participants who had a 1p/19q codeletion also had a lower risk score than patients who did not have a codeletion (Fig. 6F, Table 4 and Supplementary Table 5).

**Table 5.** The expression of immune-related lncRNAs between normal and tumor samples in the CGGA dataset

Gene	Gene expression		p-value
	normal (n = 20)	tumor (n = 140)	
<i>IEF1-AS1</i>	0.126 ±0.131	1.008 ±1.196	<b>3.20E-14</b>
<i>HOXC-AS2</i>	0.011 ±0.036	0.335 ±0.630	<b>1.63E-08</b>
<i>AL354993.1</i>	0.601 ±0.463	1.717 ±2.179	<b>5.86E-07</b>
<i>NDUFB2-AS1</i>	0.491 ±0.171	0.570 ±0.320	9.70E-01
<i>AC034243.1</i>	0.372 ±0.683	0.438 ±0.726	6.99E-01
<i>UNCSB-AS1</i>	0.877 ±0.567	0.529 ±0.693	4.82E-02
<i>LINC00571</i>	0.158 ±0.253	0.238 ±0.379	2.37E-01
<i>CHRM3-AS2</i>	0.062 ±0.060	0.086 ±0.111	1.44E-01
<i>LINC00452</i>	0.020 ±0.025	0.094 ±0.247	4.17E-02
<i>AC009093.1</i>	0.037 ±0.030	0.052 ±0.065	7.99E-02

lncRNAs – long noncoding ribonucleic acids; CGGA – Chinese Glioma Genome Atlas. Values in bold are statistically significant.

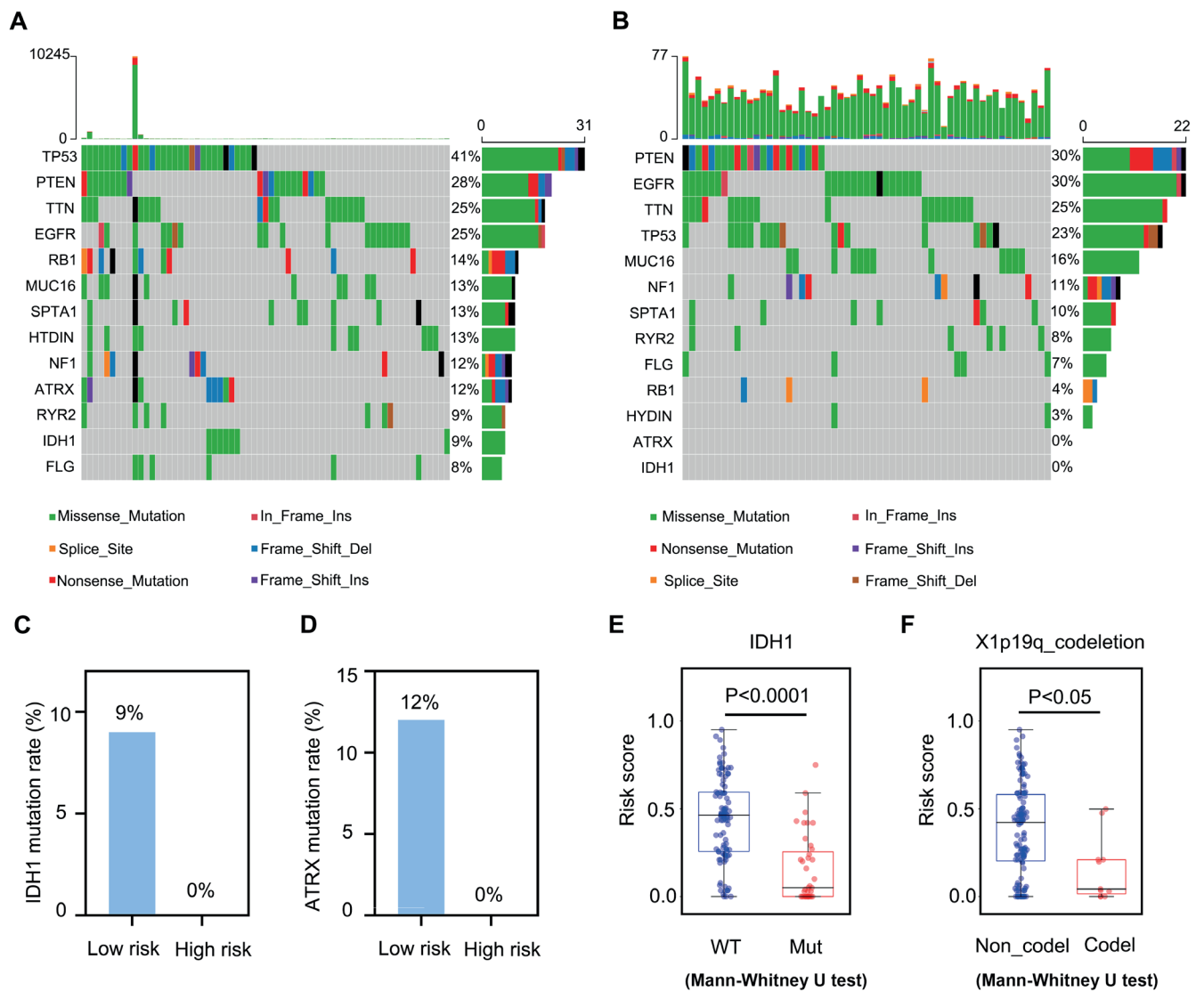


**Fig. 6.** Differences in the mutation landscape between high- and low-risk groups. **A.** Oncoplots of tumor somatic mutations of frequently mutated genes in the low-risk group; **B.** Oncoplots of tumor somatic mutations of frequently mutated genes in the high-risk group. Mutation rates of *IDH1* (**C**) and *ATRX* (**D**) were compared between low- and high-risk groups in The Cancer Genome Atlas (TCGA) dataset; **E.** The distribution of risk score between *IDH1*-wild type (wt) ( $n = 100$ ) and *IDH1*-mutation (Mut) ( $n = 40$ ) patients in the Chinese Glioma Genome Atlas (CGGA) dataset (Mann-Whitney U test); **F.** The distribution of risk score between *1p/19q*-codeleted ( $n = 12$ ) and *1p/19q*-noncodeleted ( $n = 128$ ) patients in the CGGA dataset (Mann-Whitney U test)

## *AL354993.1* was recognized as a potential marker for GBM

The expression of 10 ir-lncRNAs was compared between normal and tumor samples in the CGGA dataset. The *LEF1-AS1*, *HOXC-AS2* and *AL354993.1* were found to be significantly overexpressed in GBM ( $p < 0.0001$ ), among which *AL354993.1* has not been reported (Fig. 7A, Table 5 and Supplementary Table 6). The overexpression of *AL354993.1* suggested a worse GBM prognosis ( $p = 0.029$ ) (Fig. 7B). Furthermore, the expression of *AL354993.1* was lower in GBM tissues with *IDH1* but not with *1p/19q* mutations (Fig. 7C,D, Table 6 and Supplementary Table 7,8). To discover the biological function of *AL354993.1*, GBM subjects in the CGGA dataset were allocated into 2 cohorts with raised and decreased *AL354993.1* expression, and a differential gene

analysis combined with GSEA enrichment was conducted. The outcomes indicated that raised *AL354993.1* expression might indicate the activation of the JAK-STAT pathway, the extracellular matrix (ECM) receptor interaction pathway, chemokine signaling mechanisms, and cytokine-cytokine receptor interaction mechanisms (Fig. 7E). Hence,

**Table 6.** The different expression of *AL354993.1* divided by *IDH1* mutation and *1p/19q* codeletion

Mutation	Status	Risk score	p-value
<i>IDH1</i> mutation	wt ( $n = 100$ )	$1.32 \pm 0.96$	3.00E-05
	mut ( $n = 40$ )	$0.72 \pm 0.62$	
<i>1p/19q</i> codeletion	Non_Codel ( $n = 128$ )	$1.17 \pm 0.91$	1.93E-01
	Codel ( $n = 12$ )	$0.99 \pm 0.98$	

wt – wild type; mut – mutant.

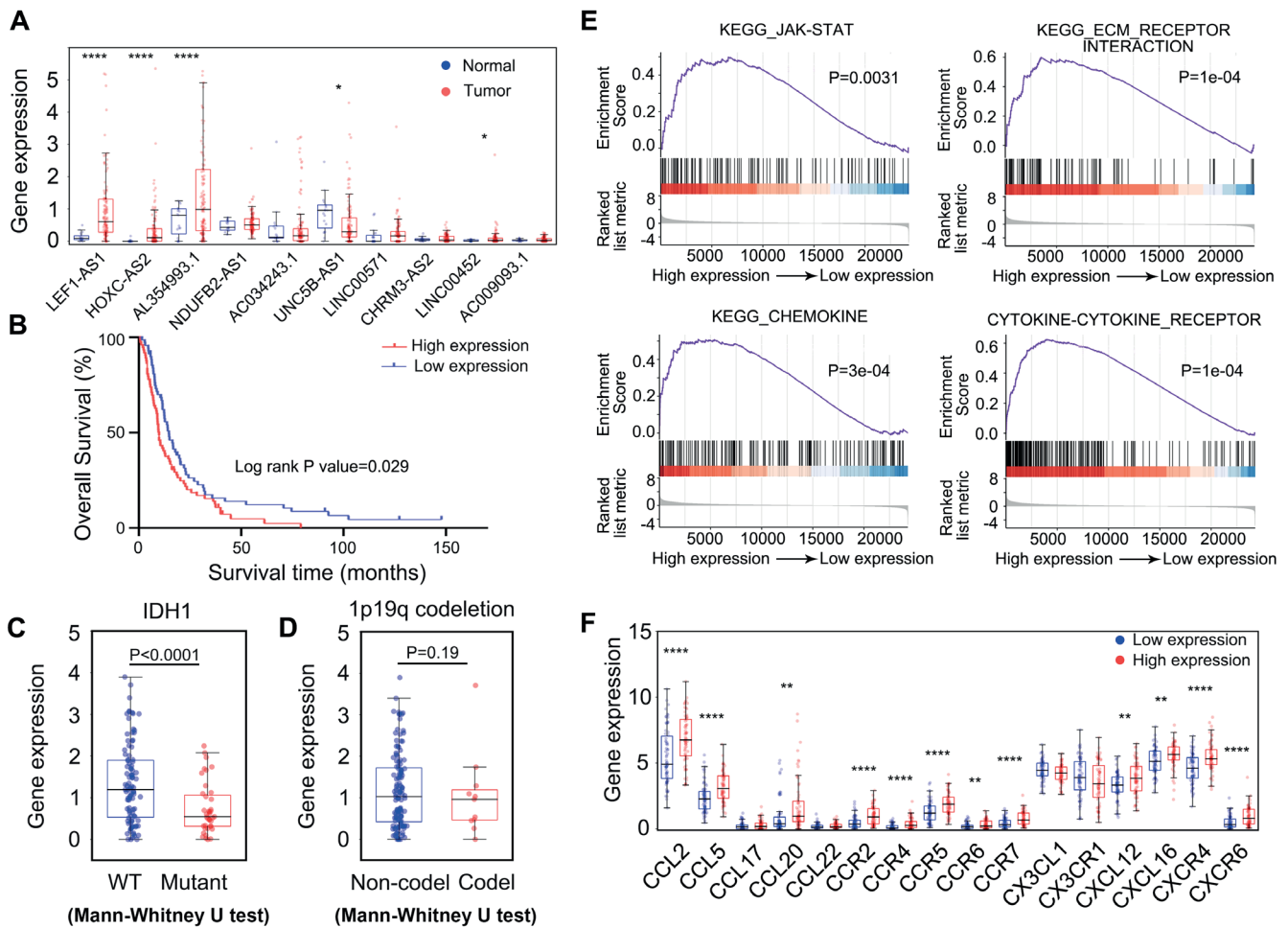


**Fig. 7.** Identification of *AL354993.1* as a potential biomarker for glioblastoma. **A.** The expression of immune-related long noncoding ribonucleic acids (ir-lncRNAs) between normal (n = 20) and tumor samples (n = 140) in the Chinese Glioma Genome Atlas (CGGA) dataset (parametric test and the Mann–Whitney U test); **B.** Survival analysis of patients divided by low and high *AL354993.1* expression in the CGGA dataset; **C.** The expression of *AL354993.1* between *IDH1*-wild type (wt) (n = 100) and *IDH1*-mutation (Mut) (n = 40) patients in the CGGA dataset (Mann–Whitney U test). **D.** The expression of *AL354993.1* between *1p/19q*-codeleted (n = 12) and *1p/19q*-noncodeleted (n = 128) patients in the CGGA dataset (Mann–Whitney U test); **E.** Gene set enrichment analysis between low and high *AL354993.1* expression group in the CGGA dataset; **F.** The expression of chemokines between low (n = 70) and high (n = 70) *AL354993.1* expression group (parametric test and Mann–Whitney U test)

the relationship between *AL354993.1* expression and chemokine secretion were further explored. The expression of 16 chemokines known to be associated with GBM progression was examined in reduced- and elevated-expression groups. The results showed that 13 chemokines were differentially expressed (*CCL2*, *CCL5*, *CCL17*, *CCL20*, *CCR2*, *CCR4*, *CCR5*, *CCR6*, *CCR7*, *CXCL12*, *CXCL16*, *CXCR4*, *CXCR6*) (Fig. 7E, Table 7 and Supplementary Table 9). These outcomes indicate that *AL354993.1* is related to GBM progression and might be a potential GBM biomarker.

## Discussion

Glioblastoma multiforme is one of the most common primary brain tumors, and survival rates are low despite extensive treatment options (surgical resection, radiotherapy and adjuvant chemotherapy).<sup>20</sup> In recent years, many studies carried out on immunotherapy for GBM

have failed to achieve ideal results due to the heterogeneity of GBM and the cancer immunosuppressive micro-environment.<sup>21,22</sup> Numerous investigations have verified that lncRNAs have a function in the modulation of GBM. Several ir-lncRNAs have also been shown to be strongly linked to the modulation of the immunological milieu in GBM and the infiltration of immune cells.<sup>7,16</sup> Therefore, we created a medical prediction model using the TCGA and CGGA datasets and evaluated the lncRNAs most relevant to GBM to further examine the function of lncRNAs in GBM prognosis.

In this investigation, we conducted a three-way Venn examination of all lncRNAs in the TCGA, CGGA and ImmLnc datasets and found that 276 lncRNAs coexisted. The LASSO regression analysis further identified 10 key ir-lncRNAs, with the Kaplan–Meier analysis suggesting that 8 of the 10 were prognostic risk factors for GBM (*CHRM3-AS2*, *LEF1-AS1*, *AL354993.1*, *AC034243.1*, *LINC00452*, *UNC5B-AS1*, *AC009093.1*, and *HOXC-AS2*). Among

**Table 7.** The expression of chemokines between low- and high-AL354993.1 expression groups

Gene	Gene expression		p-value
	low expression (n = 70)	high expression (n = 70)	
<i>cCL2</i>	5.46 ±2.11	6.82 ±1.87	<b>9.74E-05</b>
<i>CCL5</i>	2.35 ±1.10	3.18 ±1.15	<b>2.58E-05</b>
<i>CCL17</i>	0.21 ±0.27	0.28 ±0.35	1.56E-01
<i>CCL20</i>	0.91 ±1.29	1.70 ±1.95	<b>5.45E-03</b>
<i>CCL22</i>	0.20 ±0.19	0.24 ±0.21	2.49E-01
<i>CCR2</i>	0.49 ±0.47	0.98 ±0.69	<b>2.76E-06</b>
<i>CCR4</i>	0.16 ±0.19	0.40 ±0.42	<b>1.95E-05</b>
<i>CCR5</i>	1.28 ±0.78	1.89 ±0.84	<b>1.31E-05</b>
<i>CCR6</i>	0.21 ±0.22	0.34 ±0.33	<b>4.99E-03</b>
<i>CCR7</i>	0.43 ±0.36	0.80 ±0.51	<b>2.94E-06</b>
<i>CX3CL1</i>	4.44 ±0.79	4.20 ±0.71	5.55E-02
<i>CX3CR1</i>	3.94 ±1.49	3.49 ±1.57	8.56E-02
<i>CXCL12</i>	3.28 ±0.99	3.86 ±1.24	<b>2.61E-03</b>
<i>CXCL16</i>	5.13 ±1.03	5.57 ±0.96	<b>9.31E-03</b>
<i>CXCR4</i>	4.58 ±1.16	5.48 ±1.09	<b>6.21E-06</b>
<i>CXCR6</i>	0.49 ±0.48	0.95 ±0.72	<b>2.17E-05</b>

Values in bold are statistically significant.

these, *LEF1-AS1* was found to be related to the malignant growth of GBM through increased EN2 by mir-543 via sponge absorption.<sup>23</sup> Besides, *CHRM3-AS2*, an immune-associated lncRNA, has been recognized as a prognostic risk factor for ovarian cancer and cholangiocarcinoma.<sup>24,25</sup> The *LINC00452* has been shown to promote ovarian cancer by inhibiting ubiquitin-mediated degradation through sponge absorption of mir-501-3p, thereby increasing *ROCK1*.<sup>26</sup> Meanwhile, *UNC5B-AS1* is involved in liver malignancy, prostate tumors and colorectal malignancy.<sup>27,28</sup> By mixing with *HOXC13*, *HOXC-AS2* regulates the growth, cell death and migration of non-small cell lung tumors.<sup>29</sup> The roles of these ir-lncRNAs in GBM are worthy of further investigation.

The coefficient was determined by employing multivariate Cox analysis, and a risk score model was developed to categorize GBM individuals into high- and reduced-risk cohorts. We discovered that the elevated-risk cohort had a lower OS rate and that the risk score model was beneficial in anticipating GBM prognosis. We also developed a nomogram that included sex, age and risk score. The nomogram demonstrated excellent predictive performance when calibration and ROC curves were plotted. Since these ir-lncRNAs have independent prognostic value in GBM OS, the risk prediction model constructed by these ir-lncRNAs also showed strong prognostic value. Therefore, we believe that monitoring these ir-lncRNAs by liquid biopsy or tumor tissue collection for GBM risk and prognosis assessment is a promising strategy.

Functional enrichment analysis was conducted to investigate the probable function and role of the 10 lncRNAs in GBM formation. They were shown to be connected with immune-related activities, including chemokine-related mechanisms, the JAK-STAT signaling pathway, cytokine-related mechanisms, and immune cell activation-related pathways, according to GO and KEGG enrichment assessment. Additionally, they were connected to the stimulation of immune-related mechanisms, such as the Toll-like receptor pathway, the TNF signaling pathway and NF-κB signaling. To further explore the potential impact of the 10 ir-lncRNAs on GBM immunity, we examined the relationship between risk score and immune cell infiltration in GBM tissues. The outcomes demonstrated that CD8<sup>+</sup> T cells, neutrophils, macrophages and myeloid dendritic cells were substantially positively correlated with the risk score. The relationship between risk scores and chemokines was also investigated, with the raised-risk cohort related to a higher chemokine expression.

Immunological checkpoint blocking has become one of the frontiers of cancer immunotherapy,<sup>30</sup> and we discovered that the risk score was substantially associated with immunological checkpoint expression. The ESTIMATE and TIDE scores also verified the relationship between risk score and immune microenvironment. Mutations in the *IDH1* gene are commonly found in GBM, with the product of this mutated enzyme having a novel ability to catalyze the production of 2-hydroxyglutarate, while *IDH1* mutations are shown to be associated with more favorable survival outcomes.<sup>31</sup> In addition, *1p/19q* codeletion suggested a better prognosis.<sup>32</sup> We found higher rates of *IDH1* mutation and *1p/19q* codeletion in GBM individuals with reduced risk scores, while no mutations were found in the raised-risk cohort. These results may be the reason underlying the prognostic value of risk scores. Furthermore, investigation is still required to fully understand the precise pathway of the 10 ir-lncRNAs in GBM.

Among the 10 lncRNAs, we found that only 2 were significantly highly expressed in GBM compared with normal controls, namely *LEF1-AS1* and *AL354993.1*, of which *AL354993.1* has not been reported. We found that *AL354993.1* had significant prognostic value in GBM and was also associated with the tumor immune microenvironment. In addition, *AL354993.1* was closely related to *IDH1* mutation and other clinicopathological factors. Gene enrichment results suggested that *AL354993.1* may promote GBM progression through the JAK-STAT pathway, the ECM interaction pathway, chemokine pathways, and cytokine receptor binding pathways.

## Limitations

There were some restrictions to this analysis since it was retrospective and dependent on open-access databases. Thus, more prospective clinical data are required for

validation and future clinical applications. On the other hand, the effect of *AL354993.1* was only analyzed using a database and should be verified by a series of wet experiments in the future.

## Conclusions

Through the joint analysis of multiple public databases, we screened 10 key ir-lncRNAs in GBM and used them to construct risk-scoring models and promote the development of novel GBM biomarkers. In conclusion, the 10 ir-lncRNAs have the potential to predict the GBM prognosis and may play a vital role in the progression of GBM.

## Supplementary data

The supplementary materials are available at <https://doi.org/10.5281/zenodo.8311458>. The package includes the following files:

Supplementary Fig. 1. Proportional hazards assumption test for age, gender and risk score of TCGA-GBM (A) and CGGA (B) cohort.

Supplementary Fig. 2. A,B. Linearity assumption test for age of TCGA-GBM and CGGA cohort; C,D. Linearity assumption test for the risk score of TCGA-GBM and CGGA cohort.

Supplementary Fig. 3. Multicollinearity test for age and risk score of TCGA-GBM (A) and CGGA (B) cohort.

Supplementary Table 1. The expression of chemokines between low- and high-risk groups (Fig. 5B).

Supplementary Table 2. The difference of immune score, stromal score, ESTIMATE score, and TIDE score between high- and low-risk groups (Fig. 5C–E,G).

Supplementary Table 3. Comparison of the risk scores between immunotherapy responders (n = 48) and non-responders (n = 118) predicted with TIDE (Fig. 5H).

Supplementary Table 4. The distribution of risk score between IDH1-wild type (n = 100) and IDH1-mutation (n = 40) patients in the CGGA dataset (Fig. 6E).

Supplementary Table 5. The distribution of risk score between 1p/19q-codeleted and 1p/19q-noncodeleted patients in the CGGA dataset (Fig. 6F).

Supplementary Table 6. The expression of immune-related lncRNAs between normal and tumor samples in the CGGA dataset (Fig. 7A).

Supplementary Table 7. The expression of *AL354993.1* between IDH1-wild type and IDH1-mutation patients in the CGGA dataset (Fig. 7C).

Supplementary Table 8. The expression of *AL354993.1* between 1p/19q-codeleted (n = 12) and 1p/19q-noncodeleted (n = 128) patients in the CGGA dataset (Fig. 7D).

Supplementary Table 9. The expression of chemokines between low and high *AL354993.1* expression group (Fig. 7F).

## Data availability

The datasets generated and/or analyzed during the current study are available from the corresponding author on reasonable request.

## Consent for publication

Not applicable.

## ORCID iDs

Yongjie Wang  <https://orcid.org/0000-0003-1640-6868>

## References

- Aldape K, Zadeh G, Mansouri S, Reifenberger G, Von Deimling A. Glioblastoma: Pathology, molecular mechanisms and markers. *Acta Neuropathol.* 2015;129(6):829–848. doi:10.1007/s00401-015-1432-1
- Himes BT, Geiger PA, Ayasoufi K, Bhargav AG, Brown DA, Parney IF. Immunosuppression in glioblastoma: Current understanding and therapeutic implications. *Front Oncol.* 2021;11:770561. doi:10.3389/fonc.2021.770561
- Warrier NM, Agarwal P, Kumar P. Integrative analysis to identify genes associated with stemness and immunosuppression in glioblastoma. *Cells.* 2021;10(10):2765. doi:10.3390/cells10102765
- Sun L, Lai TJ, Prins RM. Is there a role for neoadjuvant anti-PD-1 therapies in glioma? *Curr Opin Neurol.* 2021;34(6):834–839. doi:10.1097/WCO.0000000000000992
- Ayasoufi K, Pfaller CK, Evgin L, et al. Brain cancer induces systemic immunosuppression through release of non-steroid soluble mediators. *Brain.* 2020;143(12):3629–3652. doi:10.1093/brain/awaa343
- Gandhi M, Groß M, Holler JM, et al. The lncRNA lincNMR regulates nucleotide metabolism via a YBX1–RRM2 axis in cancer. *Nat Commun.* 2020;11(1):3214. doi:10.1038/s41467-020-17007-9
- Jin X, Ge LP, Li DQ, et al. LncRNA TROJAN promotes proliferation and resistance to CDK4/6 inhibitor via CDK2 transcriptional activation in ER+ breast cancer. *Mol Cancer.* 2020;19(1):87. doi:10.1186/s12943-020-01210-9
- Liu J, Liu ZX, Wu QN, et al. Long noncoding RNA AGPG regulates PFKFB3-mediated tumor glycolytic reprogramming. *Nat Commun.* 2020;11(1):1507. doi:10.1038/s41467-020-15112-3
- Zheng S, Yang L, Zou Y, et al. Long non-coding RNA HUMT hypomethylation promotes lymphangiogenesis and metastasis via activating FOXC1 transcription in triple-negative breast cancer. *J Hematol Oncol.* 2020;13(1):17. doi:10.1186/s13045-020-00852-y
- Ma C, Wang H, Zong G, et al. EGR1 modulated lncRNA HNF1A-AS1 drives glioblastoma progression via miR-22-3p/ENO1 axis. *Cell Death Discov.* 2021;7(1):350. doi:10.1038/s41420-021-00734-3
- Wu W, Yu T, Wu Y, Tian W, Zhang J, Wang Y. The miR155HG/miR-185/ANXA2 loop contributes to glioblastoma growth and progression. *J Exp Clin Cancer Res.* 2019;38(1):133. doi:10.1186/s13046-019-1132-0
- Guo XY, Zhong S, Wang ZN, et al. Immunogenomic profiling demonstrate AC003092.1 as an immune-related eRNA in glioblastoma multiforme. *Front Genet.* 2021;12:633812. doi:10.3389/fgene.2021.633812
- Xu X, Zhong Z, Shao Y, Yi Y. Prognostic value of MEG3 and its correlation with immune infiltrates in gliomas. *Front Genet.* 2021;12:679097. doi:10.3389/fgene.2021.679097
- Zhao R, Li B, Zhang S, et al. The N6-methyladenosine-modified pseudogene HSPA7 correlates with the tumor microenvironment and predicts the response to immune checkpoint therapy in glioblastoma. *Front Immunol.* 2021;12:653711. doi:10.3389/fimmu.2021.653711
- Zhao Z, Zhang KN, Wang Q, et al. Chinese Glioma Genome Atlas (CGGA): A comprehensive resource with functional genomic data from Chinese glioma patients. *Genomics Proteomics Bioinformatics.* 2021;19(1):1–12. doi:10.1016/j.gpb.2020.10.005
- Li Y, Jiang T, Zhou W, et al. Pan-cancer characterization of immune-related lncRNAs identifies potential oncogenic biomarkers. *Nat Commun.* 2020;11(1):1000. doi:10.1038/s41467-020-14802-2

17. Li T, Fu J, Zeng Z, et al. TIMER2.0 for analysis of tumor-infiltrating immune cells. *Nucleic Acids Res.* 2020;48(W1):W509–W514. doi:10.1093/nar/gkaa407
18. Yoshihara K, Shahmoradgoli M, Martínez E, et al. Inferring tumour purity and stromal and immune cell admixture from expression data. *Nat Commun.* 2013;4(1):2612. doi:10.1038/ncomms3612
19. Jiang P, Gu S, Pan D, et al. Signatures of T cell dysfunction and exclusion predict cancer immunotherapy response. *Nat Med.* 2018;24(10):1550–1558. doi:10.1038/s41591-018-0136-1
20. Badillo-Martinez D, Nicotera N, Bodnar RJ. Onset of pain threshold changes induced by neonatal monosodium glutamate. *Int J Neurosci.* 1984;24(3–4):275–279. doi:10.3109/00207458409089816
21. Patel AP, Tirosh I, Trombetta JJ, et al. Single-cell RNA-seq highlights intratumoral heterogeneity in primary glioblastoma. *Science.* 2014;344(6190):1396–1401. doi:10.1126/science.1254257
22. Moserle L, Casanovas O. Anti-angiogenesis and metastasis: A tumour and stromal cell alliance. *J Intern Med.* 2013;273(2):128–137. doi:10.1111/joim.12018
23. Zeng S, Zhou C, Yang DH, et al. LEF1-AS1 is implicated in the malignant development of glioblastoma via sponging miR-543 to upregulate EN2. *Brain Res.* 2020;1736:146781. doi:10.1016/j.brainres.2020.146781
24. Li Y, Huo FF, Wen YY, Jiang M. Screening and identification of an immune-associated lncRNA prognostic signature in ovarian carcinoma: Evidence from bioinformatic analysis. *Biomed Res Int.* 2021;2021:6680036. doi:10.1155/2021/6680036
25. Liu YJ, Hounye AH, Wang Z, Liu X, Yi J, Qi M. Identification and validation of three autophagy-related long noncoding RNAs as prognostic signature in cholangiocarcinoma. *Front Oncol.* 2021;11:780601. doi:10.3389/fonc.2021.780601
26. Yang J, Wang WG, Zhang KQ. LINC00452 promotes ovarian carcinogenesis through increasing ROCK1 by sponging miR-501-3p and suppressing ubiquitin-mediated degradation. *Aging.* 2020;12(21):21129–21146. doi:10.18632/aging.103758
27. Wilkie ND. The search for the practical. *J Prosthet Dent.* 1974;32(3):251–255. doi:10.1016/0022-3913(74)90026-2
28. Tan SF, Ni JX, Xiong H. lncRNA UNC5B-AS1 promotes malignant progression of prostate cancer by competitive binding to caspase-9. *Eur Rev Med Pharmacol Sci.* 2020;24(5):2271–2280. doi:10.26355/eur-rev\_202003\_20493
29. Liu B, Li J, Li JM, Liu GY, Wang YS. HOXC-AS2 mediates the proliferation, apoptosis, and migration of non-small cell lung cancer by combining with *HOXC13* gene. *Cell Cycle.* 2021;20(2):236–246. doi:10.1080/15384101.2020.1868161
30. Galluzzi L, Humeau J, Buqué A, Zitvogel L, Kroemer G. Immunostimulation with chemotherapy in the era of immune checkpoint inhibitors. *Nat Rev Clin Oncol.* 2020;17(12):725–741. doi:10.1038/s41571-020-0413-z
31. Seyfried TN, Shivane AG, Kalamian M, Maroon JC, Mukherjee P, Zuccoli G. Ketogenic metabolic therapy, without chemo or radiation, for the long-term management of IDH1-mutant glioblastoma: An 80-month follow-up case report. *Front Nutr.* 2021;8:682243. doi:10.3389/fnut.2021.682243
32. Kebir S, Weber M, Lazaridis L, et al. Hybrid 11C-MET PET/MRI combined with “machine learning” in glioma diagnosis according to the revised glioma WHO classification 2016. *Clin Nucl Med.* 2019;44(3):214–220. doi:10.1097/RLU.0000000000002398



# Combined bioinformatics and machine learning methodologies reveal prognosis-related ceRNA network and propose *ABCA8*, *CAT*, and *CXCL12* as independent protective factors against osteosarcoma

\*Jiaqi Fan<sup>1,A,C,E,F</sup>, \*Jianhong Liao<sup>2,A–D</sup>, Yuwen Huang<sup>3,B,D</sup>

<sup>1</sup> Department of Orthopaedics, Capital Medical University Affiliated FuXing Hospital, Beijing, China

<sup>2</sup> Department of Otolaryngology Head and Neck Surgery, Beijing Tongren Hospital, Capital Medical University, China

<sup>3</sup> Department of Gastrointestinal and Hepatology, Beijing Youan Hospital, Capital Medical University, China

A – research concept and design; B – collection and/or assembly of data; C – data analysis and interpretation;

D – writing the article; E – critical revision of the article; F – final approval of the article

Advances in Clinical and Experimental Medicine, ISSN 1899–5276 (print), ISSN 2451–2680 (online)

*Adv Clin Exp Med.* 2024;33(8):857–868

## Address for correspondence

Jiaqi Fan

E-mail: fanjiaqi1985@mail.ccmu.edu.cn

## Funding sources

None declared

## Conflict of interest

None declared

## Acknowledgements

The authors would like to express their sincere gratitude to the Biotrainee team ([www.biotrainee.com](http://www.biotrainee.com)) for their valuable guidance regarding code analysis.

\*Jiaqi Fan and Jianhong Liao contributed equally to this work.

Received on December 16, 2022

Reviewed on July 30, 2023

Accepted on September 20, 2023

Published online on February 5, 2024

## Cite as

Fan J, Liao J, Huang Y. Combined bioinformatics and machine learning methodologies reveal prognosis-related ceRNA network and propose *ABCA8*, *CAT*, and *CXCL12* as independent protective factors against osteosarcoma. *Adv Clin Exp Med.* 2024;33(8):857–868. doi:10.17219/acem/172663

## DOI

10.17219/acem/172663

## Copyright

Copyright by Author(s)

This is an article distributed under the terms of the Creative Commons Attribution 3.0 Unported (CC BY 3.0) (<https://creativecommons.org/licenses/by/3.0/>)

## Abstract

**Background.** Aberrant circular RNA (circRNA) acts as an oncogene or suppressor during neoplasm initiation and development. However, the functions of most circRNAs in osteosarcoma (OS) remain unclear.

**Objectives.** We aimed to investigate the expression, molecular functions and mechanisms underlying circRNAs in OS.

**Materials and methods.** Network interaction, pathway enrichment and regression analyses were performed to determine differentially expressed (DE) circRNAs, microRNAs (miRNAs) and messenger RNAs (mRNAs). We constructed competitive endogenous RcodeNA (ceRNA) networks and integrated patient clinical data to analyze the relationship between the networks and prognosis. The circRNA, miRNA and mRNA data were retrieved from Gene Expression Omnibus (GEO) microarray datasets. A circRNA-miRNA-mRNA interaction network was established and visualized using miRNet. Protein interactions were investigated using STRING and Cytoscape, and hub genes were identified using the MCODE plug-in. Gene Ontology, Kyoto Encyclopedia of Genes and Genomes (KEGG) and Reactome pathway analyses were performed to determine the DEmRNAs. LIMMA and RobustRankAggreg were used to screen for DERNAs. Node genes in the interaction network were analyzed using least absolute shrinkage and selection operator (LASSO) and Cox regression to obtain OS-related ceRNA networks.

**Results.** We identified 9 DEcircRNAs, 243 DEmiRNAs and 211 DEmRNAs. We found that a ceRNA subnetwork, based on 1 circRNA, 1 miRNA and 8 mRNAs, was closely associated with OS prognosis. Integrating the proportional hazards model and survival analysis revealed 3 independent protective factors: adenosine triphosphate (ATP)-binding cassette sub-family A member 8 (*ABCA8*), catalase (*CAT*) and C-X-C motif chemokine ligand 12 (*CXCL12*).

**Conclusions.** Our study provides novel insights into circRNA-related ceRNA networks and identifies potential prognostic biomarkers of OS.

**Key words:** prognosis, microRNA, osteosarcoma, circular RNA, competitive endogenous RNA

## Background

Osteosarcoma (OS) is a common malignant bone tumor that occurs in children and adolescents,<sup>1</sup> with its occurrence rate reaching a 2<sup>nd</sup> peak in individuals aged over 60.<sup>2,3</sup> With the emergence of neoadjuvant chemotherapy, patient survival rates have greatly improved over the past 40 years. However, because chemotherapy causes high treatment resistance in OS, the 5-year overall survival rate is still lower than 80%.<sup>2,4</sup> Therefore, identifying molecular markers is important for OS prognosis and treatment.

Circular ribonucleic acids (circRNAs) belong to a class of circular noncoding RNAs with continuous and covalently closed structures that modulate protein expression by acting as microRNAs (miRNAs) or protein inhibitor sponges.<sup>5</sup> With the discovery of circRNA functions, they are increasingly becoming important in understanding disease pathology and treatment. Their biological functions exhibit 5 characteristics: sponge effect, rolling circle translation, circRNA-derived pseudogenes, post-transcriptional regulation, and splicing interference.<sup>6</sup> In recent years, increasing focus has been directed toward understanding the relationship between circRNA and tumor occurrence and metastasis. Multiple circRNAs have been implicated in the development, migration, invasion, and metastasis of OS.<sup>7-9</sup> As such, identifying more unknown circRNAs that may be involved in cancerization and cancer development is critical, especially in malignant tumors such as OS.

The miRNAs are small noncoding RNAs that are 20–24 nucleotides in length.<sup>10</sup> Similar to classic noncoding RNAs, many miRNAs play vital roles in almost all aspects of tumorigenesis and tumor occurrence and development, including invasion, angiogenesis, proliferation, and apoptosis.<sup>11-13</sup> An in-depth understanding of their roles in the development of diseases, especially tumors, is required. Furthermore, miRNAs are attractive tools and potential targets for developing new treatment modalities.<sup>14,15</sup>

Overall, regulatory networks based on the composition of circRNAs, miRNAs and messenger RNAs (mRNAs) play a crucial role in tumor development and prognosis. Nonetheless, further research is imperative to thoroughly analyze the competing endogenous RNA (ceRNA) foundation of OS. In the present study, the Gene Expression Omnibus (GEO) database ([www.ncbi.nlm.nih.gov/geo](http://www.ncbi.nlm.nih.gov/geo)) was investigated, and prognosis-related ceRNA networks were constructed by validating the clinical information from the TARGET (Therapeutically Applicable Research to Generate Effective Treatments; [www.cancer.gov/ccg/research/genome-sequencing/target](http://www.cancer.gov/ccg/research/genome-sequencing/target)) database. The results may provide valuable insights that could facilitate diagnosis, monitoring and prediction of prognosis and circRNA research in primary OS patients (Fig. 1).

## Objectives

We investigated the GEO database to screen for RNAs associated with OS occurrence. By validating clinical information in the TARGET database, we constructed a prognosis-related ceRNA network, which may further enable OS diagnosis, monitoring and prognosis, and facilitate research on circRNAs in primary OS (Fig. 1).

## Materials and methods

### Study design

The GEO and TARGET databases were used to identify differentially expressed miRNAs (DEmiRNAs) and DEMRNAs associated with OS prognosis. A ceRNA network and protein-protein interaction (PPI) network were constructed to discern the interactions between mRNAs. Statistical and survival analyses were performed using the Cox model.

### Setting

#### Data acquisition and processing

According to the data upload description file, the included datasets encompass gene sequencing results from tumor tissue and paracancerous tissue. We downloaded 6 expression profiles from the GEO database: 4 mRNA datasets (GSE28425 (GPL13376, 7 OS and 4 control), GSE99671 (GPL20148, 18 OS and 18 control), GSE36004 (GPL6102, 7 OS and 4 control), and GSE126209 (GPL20301, 6 OS and 5 control)), 1 miRNA expression profile (GSE28425 (GPL8227, 7 OS and 4 control)) and 1 circRNA expression profile (GSE140256 (GPL27741, 3 OS and 3 control)). In relation to prognostic outcomes, we used a GSE79181 profile (GPL15497, 25 patients with OS) and the TARGET database (172 available patients with OS) to identify OS prognosis-associated miRNA and mRNA. The basic traits of these 7 microarray datasets (GSE28425, GSE36004, GSE99671, GSE126209, GSE140256, GSE79181, and TARGET) are listed in Supplementary Table 1. Ethical approval or informed consent was not required for this data as they are publicly available in the GEO and TARGET databases.

## Variables and data measurement

### Identification of circRNA, miRNA, and mRNA

We selected datasets that were investigated using cancerous compared to pan-cancerous tissues through next-generation sequencing. All the datasets were normalized or log<sub>2</sub>-transformed. The circRNA and miRNA were identified using linear models for microarray data in LIMMA

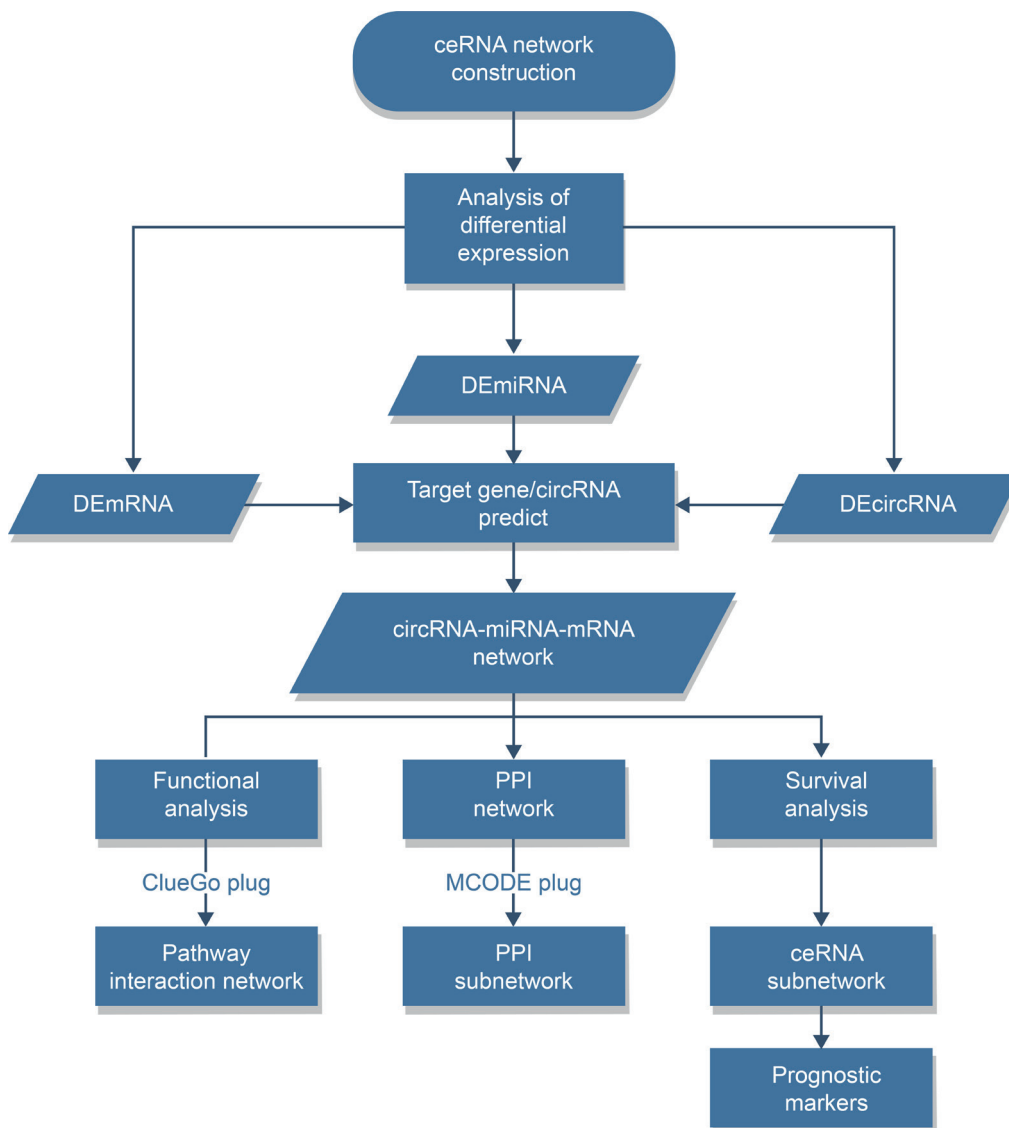


**Fig. 1.** Flowchart of the competitive endogenous RNA network analysis. circRNA, differentially expressed circular RNAs; miRNA, differentially expressed microRNAs; mRNA, differentially expressed messenger RNAs; PPI network, protein-protein interaction network; ceRNA network, competitive endogenous RNA network

v. 3.42.2, an R package that processes normalized data and analyzes the differential expression of genes (<https://bioconductor.org/packages/release/bioc/html/limma.html>). Key mRNAs with common differential expression in the 4 datasets were screened using the RobustRankAggreg package v. 1.1 (<https://cran.r-project.org/web/packages/RobustRankAggreg/index.html>). A p-value < 0.05 and a  $\log_2$  fold change (FC) >1 were considered the cutoff values in the differential expression of genes.

### Construction of a ceRNA network

Using miRNet ([www.mirnet.ca](http://www.mirnet.ca)), a network visual analytics platform based on 11 different miRNA databases, we predicted target genes and circRNAs. Interaction networks were visualized using Cytoscape v. 3.7.1 (<http://cytoscape.org/>).

### Construction of a PPI network and module analysis

To discern the interactions between mRNA involved in the ceRNA network, we established a PPI network using an online database search tool for the retrieval of interacting genes (STRING; <https://string-db.org/>). Cytoscape was used for visualization. The molecular complex detection (MCODE) plug-in was used to extract the subnetwork from the PPI network.

### Functional and pathway enrichment analyses

To elucidate the mRNA-associated mechanisms in OS, Gene Ontology (GO), Kyoto Encyclopedia of Genes and Genomes (KEGG) and Reactome pathway enrichment analyses of mRNAs were performed using ClueGO v. 2.5.6, based on Cytoscape. A p-value <0.05 indicated statistical significance in enrichment.

## Statistical methods and quantitative variables

### Statistical and survival analyses

The GSE79181 miRNA expression profile (25 samples), which is based on GPL15497 (TaqMan array human miRNA cards (A+B Card Set v3); Applied Biosystems, Foster City, USA), was downloaded from the GEO database. The mRNA expression profile and clinical information of 172 primary OS samples were downloaded from the TARGET database. Of these, 63 patients with mRNA expression profiles were selected as the discovery dataset, whereas 109 patients with basic information were used as the testing dataset. We applied the proportional hazard model (least absolute shrinkage and selection operator (LASSO) and multivariate Cox regression analyses) and performed multivariate Cox regression analysis between the time-to-survival and RNA expression in the ceRNA network using the data of 63 patients from the TARGET database and 25 patients from GSE79181. To verify the prediction efficiency of the Cox model, we used the index of concordance (C-index), time-dependent receiver-operating characteristic (ROC) curve, Kaplan–Meier (K–M) survival curves, and log-rank tests to compare the survival rates between high- and low-risk groups. The R v. 3.1-11 packages survival ROC v. 1.0.3 and Survminer v. 0.4.6 ([www.cran.r-project.org/web/packages/survivalROC/survivalROC.pdf](http://www.cran.r-project.org/web/packages/survivalROC/survivalROC.pdf), <https://cran.r-project.org/web/packages/survminer/index.html>) were used to analyze and visualize the overall survival of circRNA, miRNA and mRNA. Genes absent from half of the samples were not considered during these analyses.

## Results

### Identification of circRNAs, miRNAs and mRNAs

We identified 9 circRNAs (Supplementary Table 2), 243 miRNAs and 211 mRNAs in the datasets. Of the 243 miRNAs, 128 were upregulated and 115 were downregulated (Fig. 2A). Three of the 9 circRNAs were upregulated and the remaining 6 were downregulated (Fig. 2B). Lastly, of the 211 mRNAs, 103 were upregulated and 108 were downregulated (Fig. 2C).

### Construction of the ceRNA network

Based on miRNet, we screened 8 targeted circRNAs from 8,975 miRNA/mRNA using overlapping circRNA. We identified 119 of 13,473 targeted mRNAs based on 65,227 pairs of interactions between miRNAs and mRNAs. Using Cytoscape, we constructed a circRNA-miRNA-mRNA network based on the circRNA–DEmiRNA

and DEmiRNA–DEmRNA interactions. Accordingly, we identified 6 circRNAs, 92 miRNAs and 119 mRNAs in the ceRNA network (Supplementary Fig. 1A). Of the 119 mRNAs, 69 were upregulated and 50 were downregulated. Using MCODE in Cytoscape, we recognized 2 subnetworks in which hsa-mir-20a-5p and Ras association domain family member 2 (*RASSF2*) were identified as key nodes, indicating that they may play a critical role in the OS development (Supplementary Fig. 1B,C).

### Construction of the PPI network

We constructed a PPI network with the 119 mRNAs that participated in the ceRNA network (Supplementary Fig. 2A). Using MCODE, we identified 4 significant modules. The 1<sup>st</sup> module consisted of 6 target genes: *CD14*, *IGSF6*, *CIQA*, *GIMAP4*, *CIQB*, and *FGL2* (Supplementary Fig. 2B). The 2<sup>nd</sup> module consisted of 5 target genes: *SEC61G*, *RPL7*, *MRPL13*, *RPL6*, and *RPS28* (Supplementary Fig. 2C). The 3<sup>rd</sup> module comprised 4 target genes: *CDH2*, *TF*, *APOE*, and *SERPINA1* (Supplementary Fig. 2D), while the 4<sup>th</sup> module consisted of 3 target genes: *PTGES3*, *PTGS1*, and *TBXAS1* (Supplementary Fig. 2E). Notably, we identified *CD14*, *SEC61G*, and *PTGES3* as the key genes in the 1<sup>st</sup>, 2<sup>nd</sup> and 4<sup>th</sup> modules, respectively.

### Gene Ontology and pathway enrichment analyses

We identified 67 functional enrichment terms from GO, including 56 biological processes and 11 cellular components. The top 5 biological processes were “xenobiotic metabolic process,” “response to progesterone,” “antigen processing and presentation of exogenous peptide antigen via major histocompatibility complex class I,” “response to electrical stimulus,” and “regulation of telomerase activity.” The top 5 cellular components were “cytosolic large ribosomal subunit,” “tertiary granule lumen,” “ficolin-1-rich granule,” “ficolin-1-rich granule lumen,” and “luminal side of membrane” (Fig. 3). Nineteen KEGG and Reactome pathways were notably enriched. Major pathways enriched in OS were the “signaling by erb-b2 receptor tyrosine kinase 4 (*ERBB4*),” “nuclear signaling by *ERBB4*” and “gelatin degradation by matrix metalloproteinases (MMP) 1, 2, 3, 7, 8, 9, 12, and 13” (Fig. 4).

### Statistical and survival analyses

Twenty-one RNAs were derived from the ceRNA network, with  $\text{coef/se}(\text{coef}) < 0.01$  and  $p > 0.05$ . To find optimal prognostic biomarkers among 3 specific RNAs, we performed a multivariate Cox regression analysis of the RNA expression profiles, clinical traits of 63 patients and other clinical information for 109 patients (Fig. 5A). The predictive potency of adenosine triphosphate (ATP)-binding cassette sub-family A member 8 (*ABCA8*), C-X-C motif

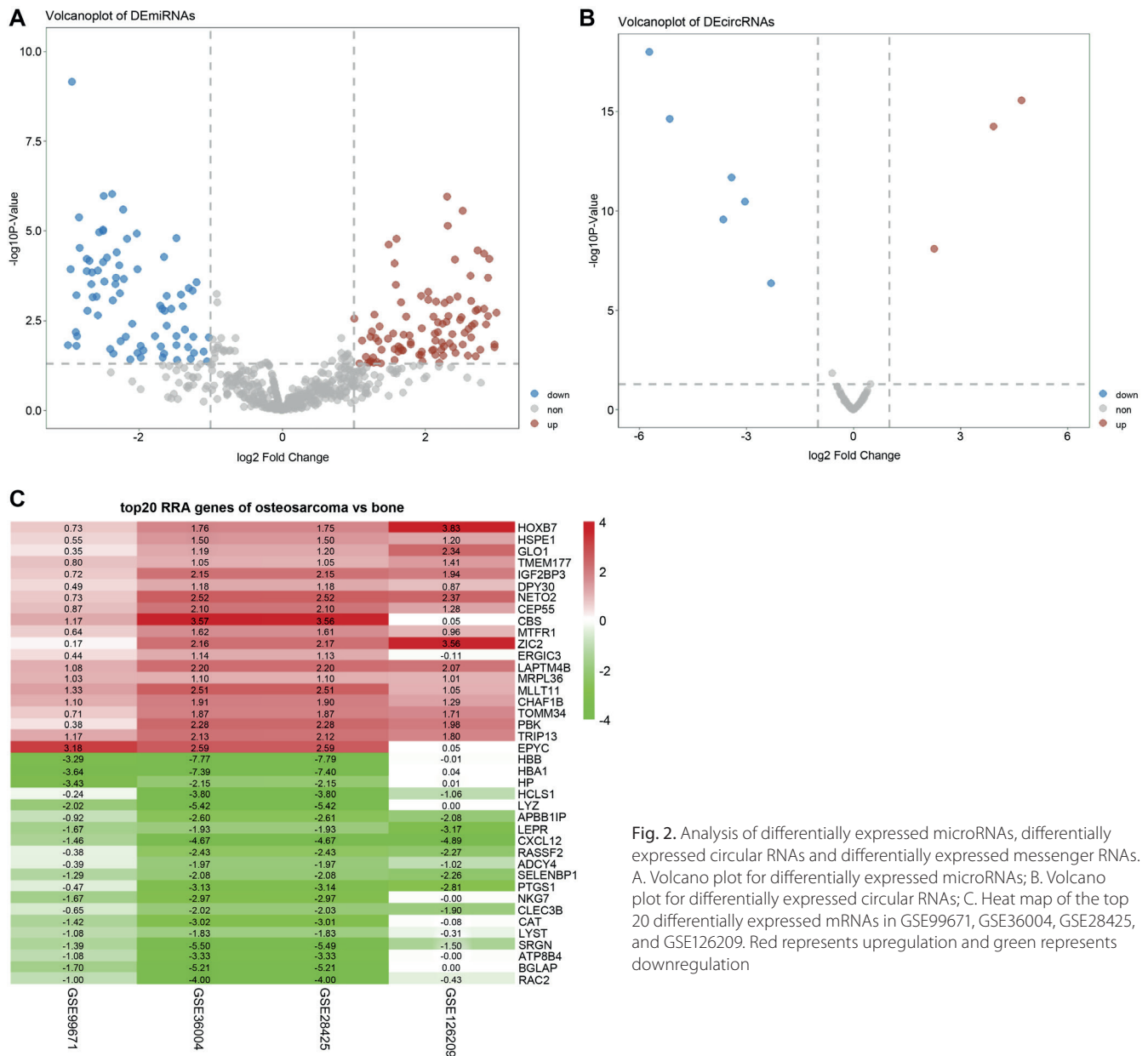


Fig. 2. Analysis of differentially expressed microRNAs, differentially expressed circular RNAs and differentially expressed messenger RNAs. A. Volcano plot for differentially expressed microRNAs; B. Volcano plot for differentially expressed circular RNAs; C. Heat map of the top 20 differentially expressed mRNAs in GSE99671, GSE36004, GSE28425, and GSE126209. Red represents upregulation and green represents downregulation

chemokine ligand 12 (*CXCL12*) and catalase (*CAT*) in OS was mutually independent (Fig. 5B). We calculated the correlation and variance inflation factor of these RNAs. The variance inflation factor was <1.1 and the correlation of each pair was <0.5, indicating no multicollinearity between independent variables (Supplementary Table 3). We made proportional hazard assumptions for the model (Supplementary Table 4 and Supplementary Fig. 3), with results showing that the model and the factors are proportional over time. Linear assumption showed that 3 predictors were linearly correlated with hazard function (Supplementary Fig. 3). Utilizing the same TARGET patient data, we noticed that the area under the curve (AUC) of 5-year overall survival for the module was 0.9, which is close to the C-index of 0.87, thus demonstrating a stable predictive effect (Fig. 5C). We grouped the discovery dataset using the 5-year risk score and used the K–M survival curves and log-rank tests to compare survival

rates between the high- (n = 22) and low-risk (n = 39) groups (Fig. 5D). To investigate associations among the risk scores, OS and biomarkers, we ranked patients according to their risk scores and displayed their clinical information and gene expression on the same abscissa (Fig. 6). The high-risk group corresponded to a poor prognosis, with the 3 genes demonstrating great consistency with patient outcomes. To verify the reliability of this model, we calculated the C-index of *ABCA8*, *CXCL12* and *CAT*, and confirmed the reliability of the prediction (Supplementary Table 3). The RobustRankAggreg analysis for the 3 mRNAs is shown in Supplementary Table 5.

We applied a K–M one-way survival analysis for patients with OS and grouped them by median values. Of the 8 circRNAs, a low expression of *hsa\_circFADS2\_007* was associated with improved survival (Supplementary Fig. 4A), and a high expression of *hsa-mir-335-5p* correlated with improved prognosis (Supplementary Fig. 4B).



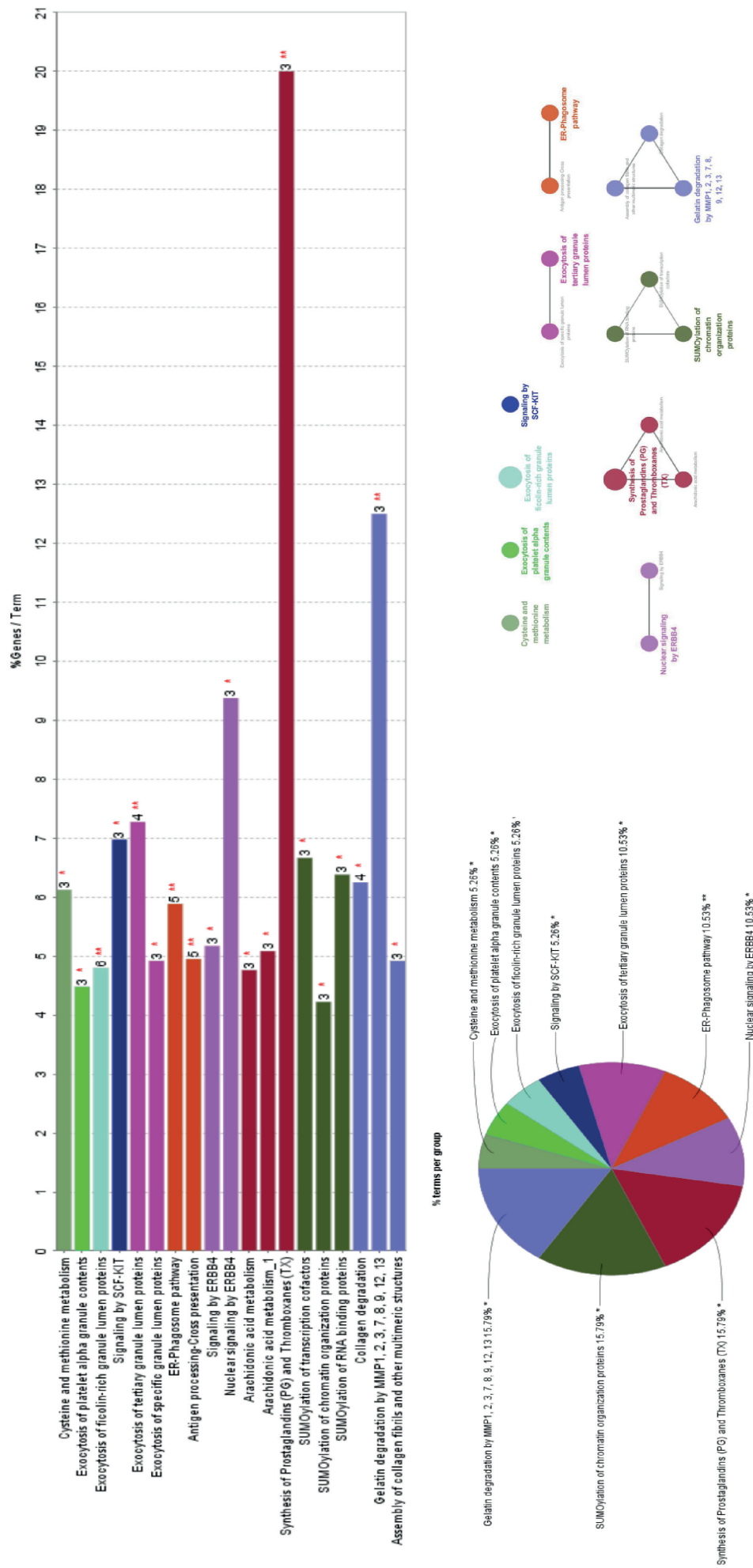


Fig. 4. Pathway enrichment analyses of the target genes involved in the competitive endogenous RNA network of osteosarcoma. Bar graphs show the proportion of genes enriched in the pathway analyses. The pie chart shows the proportion of pathways in each group

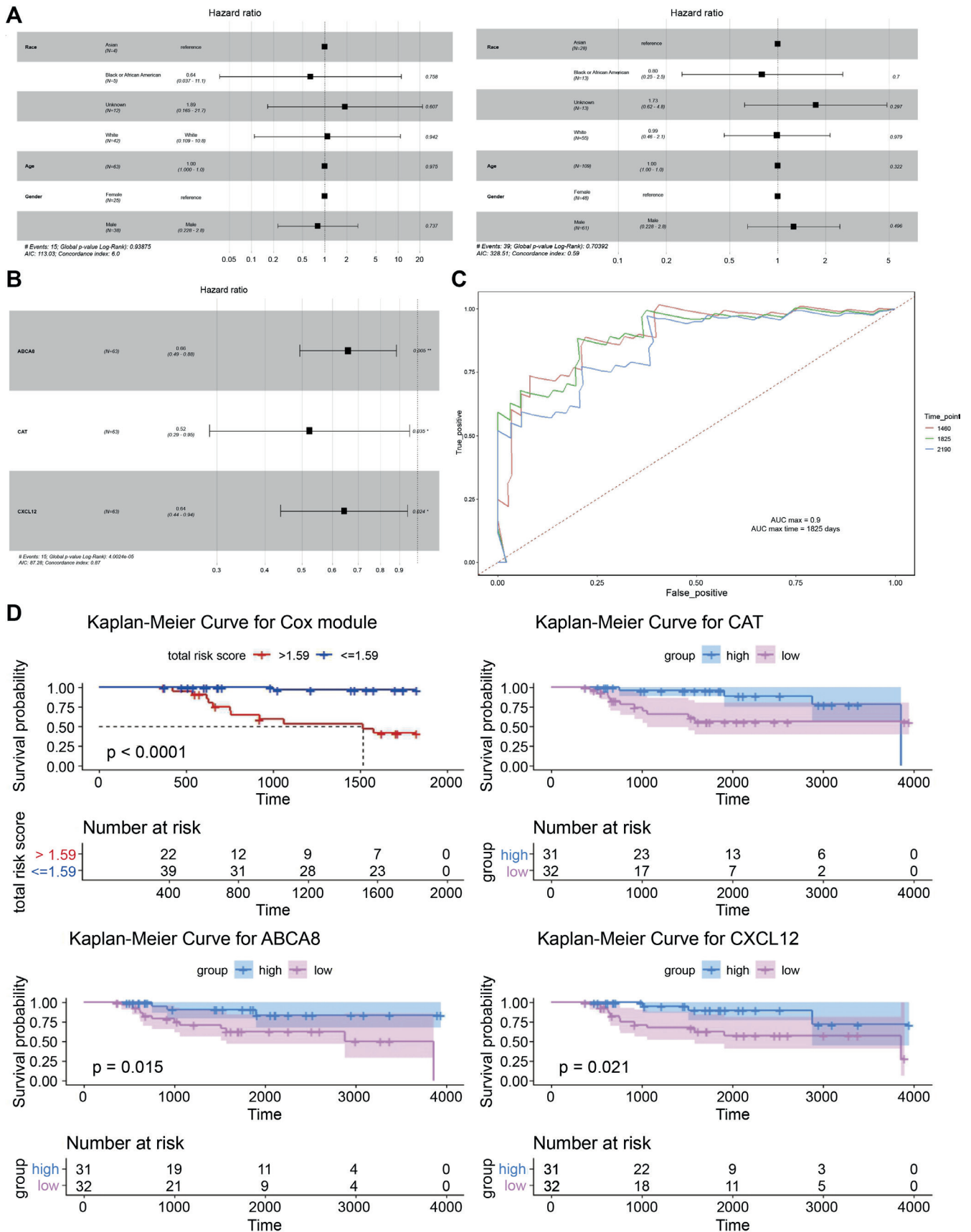


Fig. 5. Multivariate Cox regression analysis. A. Forest plot of risk factors in testing (left) and discovery (right) datasets; B. Visualization of Cox regression; C. The receiver operating characteristic (ROC) curve for 4-, 5- and 6-year survival; D. Kaplan-Meier survival analysis of the module and RNAs



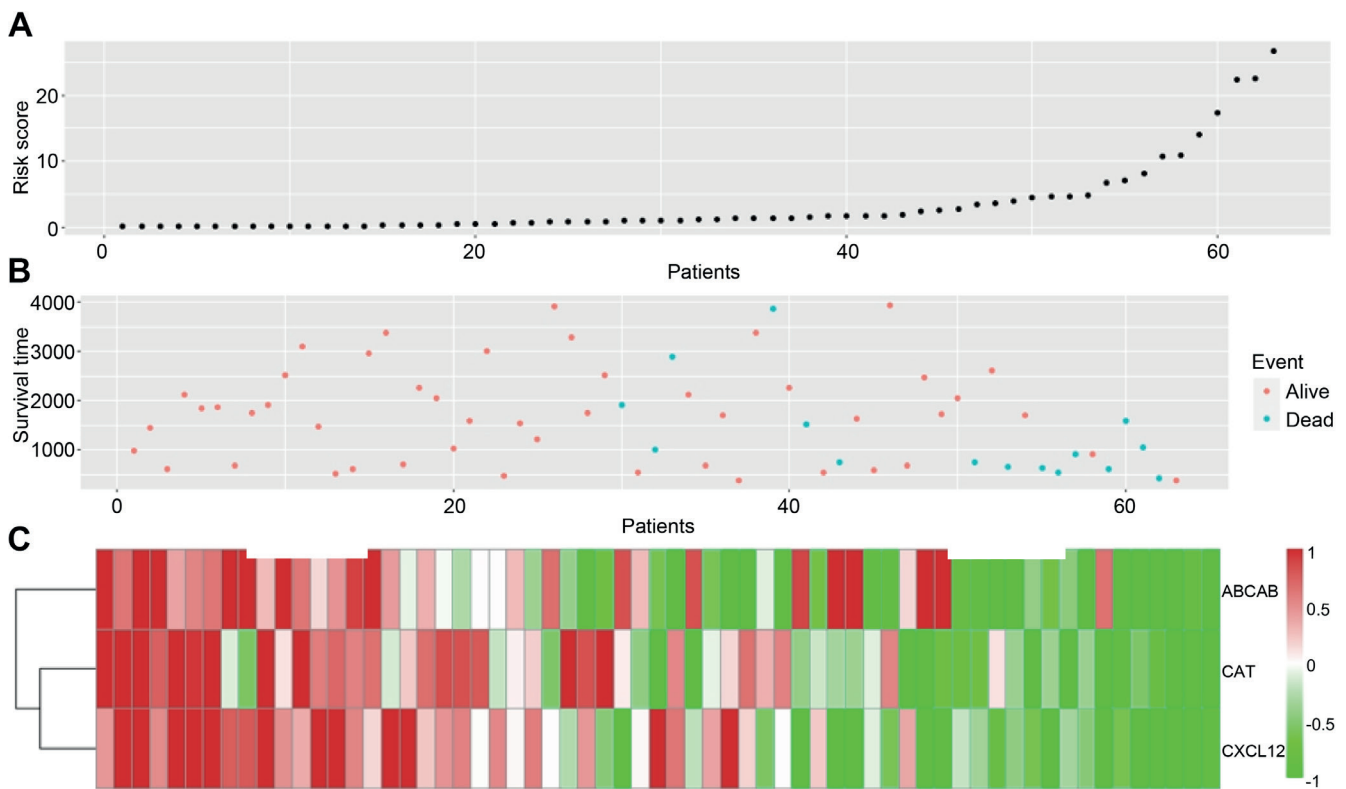


Fig. 6. Characteristics of the prognostic signature in the discovery dataset. A. Sorting of the patients in ascending order of risk score; B. Association of clinical characteristics with risk scores; C. Heatmap of *ABCA8*, *CAT* and *CSCL12* in high- and low-risk groups

Eight mRNAs, including 7 upregulated mRNAs (*ABCA8*, *ACSL5*, *FABP4*, *FGL2*, *LAPTM5*, *SLC38A2*, and *VNN2*) and 1 downregulated DEmRNA (*FADS1*), correlated with improved prognosis (Supplementary Fig. 4C,D). The high expression of *ABCA8*, *FABP4* and *VNN2* was significant for improved OS and event-free survival. We constructed a prognosis-related subnetwork based on 1 circRNA (*hsa\_circFADS2\_007*), 1 miRNA (*hsa-mir-335-5p*) and 8 mRNAs (*ABCA8*, *ACSL5*, *FABP4*, *FADS1*, *FGL2*, *LAPTM5*, *SLC38A2*, and *VNN2*). A high expression of all RNAs, except for *hsa\_circFADS2\_007* and *FADS1*, was associated with improved OS prognosis (Fig. 7).

## Discussion

Although OS is a rare malignant tumor, its characteristics, i.e., rapid invasion and ease of metastasis in vivo, lead to the development of metastases during treatment and follow-up in 30–40% of patients, making ideal treatment difficult.<sup>4</sup> Osteosarcoma treatment primarily involves surgery and chemotherapy; however, the prognosis for patients remains unsatisfactory.<sup>16</sup>

To elucidate the mechanisms underlying RNAs in OS, we constructed a ceRNA network based on differences between primary OS and controls. The GO enrichment analysis revealed that genes participating in the ceRNA network were mainly enriched in the positive regulation

of protein processing and regulation of bone remodeling-related pathways, such as “bone remodeling,” “regulation of vascular permeability” and “regulation of bone resorption.” The ability to deregulate bone remodeling is one of the main characteristics of OS, inducing an increase in factors initially trapped in the bone matrix, such as transforming growth factor- $\beta$ , to promote tumor progression.<sup>17</sup>

Exosomes are important for vascular permeability dysregulation and OS development, and a difference in miRNA content was confirmed between metastatic and nonmetastatic OS-derived exosomes.<sup>18</sup> The *MMPs* are overexpressed in OS and facilitate the survival, growth and metastasis of OS cells; thus, their expression is associated with a shorter survival time in OS patients.<sup>19</sup> SUMOylation is the post-translational modification of proteins whose disorders are believed to be related to malignant transformation in normal cells, cancer progression and the abnormal expression of oncogenes.<sup>20</sup> Prostaglandin promotes cell migration and invasion in different tumors, including OS, by increasing survivin expression and focal adhesion kinase phosphorylation and enhancing cell adhesion and migration.<sup>21</sup> Thus, ceRNA networks play critical roles in OS occurrence and progression.

To further investigate potential prognostic markers in the ceRNA network, we analyzed the correlation between 219 RNAs and OS or event-free survival. The *hsa-mir-335-5p*-related ceRNA subnetwork was significantly

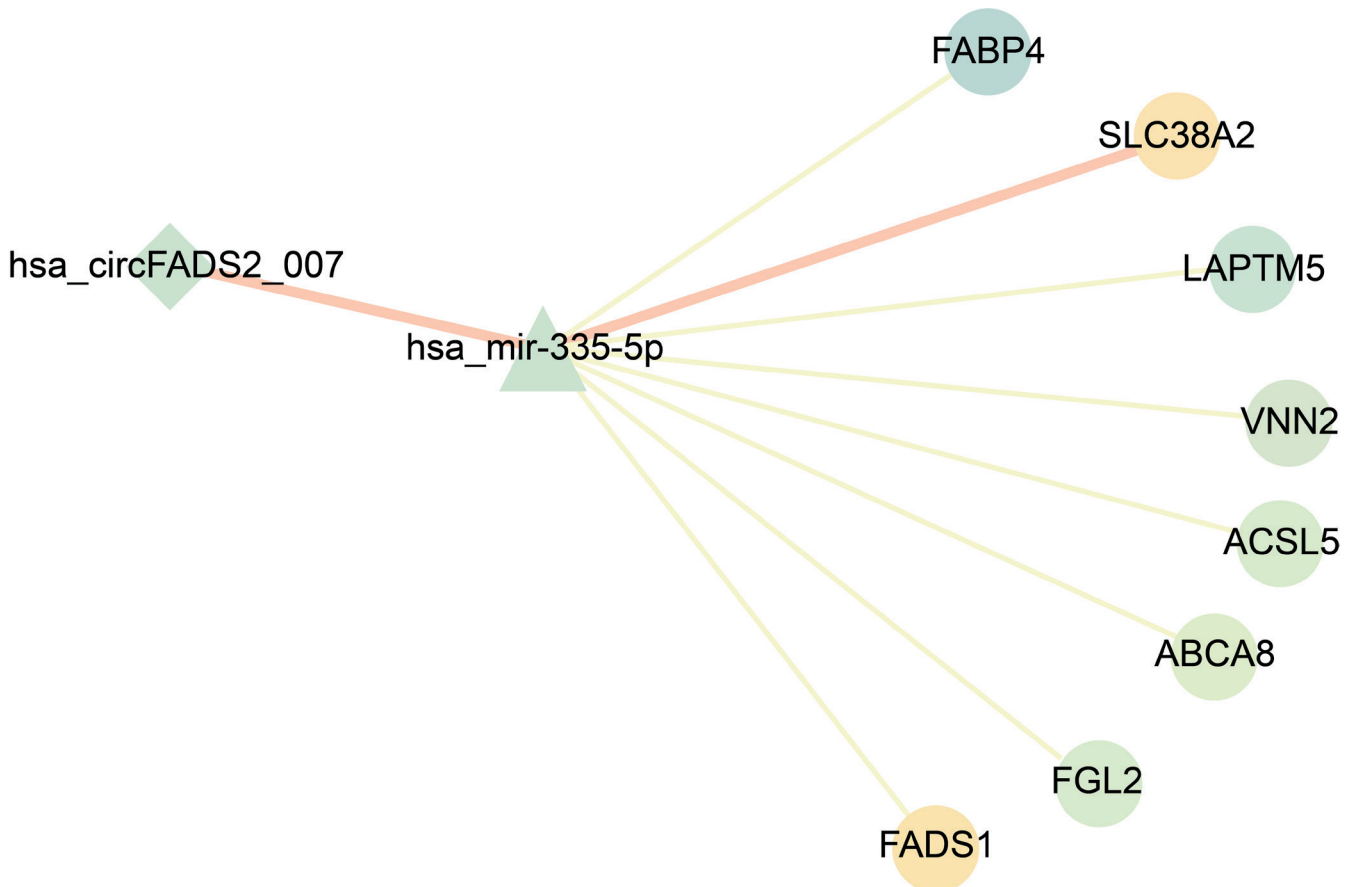


Fig. 7. Survival-related competitive endogenous RNA network. The light color indicates increased RNA expression, whereas the dark color indicates decreased RNA expression. Diamonds indicate circular RNAs, rectangles indicate microRNAs and circles indicate messenger RNAs

correlated with OS prognosis. In particular, we identified 1 circRNA (*hsa\_circFADS2\_007*), 1 miRNA (*hsa-mir-335-5p*) and 8 mRNAs (*ABCA8*, *ACSL5*, *FABP4*, *FADS1*, *FGL2*, *LAPT5*, *SLC38A2*, and *VNN2*) in this subnetwork. Previous studies revealed that these RNAs were involved in tumor progression. A large-scale genetic study found that *FADS1* and *FADS2* (11q12. 2) fatty acid metabolism-related genes were associated with colorectal cancer risk.<sup>22</sup> Meanwhile, *hsa-mir-335-5p* affected the recurrence and prognosis of OS by regulating 2 potential modules.<sup>23</sup> *ABCA8* was reportedly underexpressed in 3 cases of pre-invasive breast cancer but not in invasive cases.<sup>24</sup> The high-level expression of the adenosine triphosphate (ATP)-binding cassette transporters for the “A” subfamily in patients with serous ovarian cancer was significantly associated with a poor survival rate.<sup>25</sup> In patients with colorectal cancer, *ACSL5* is closely related to tumor occurrence and prognosis.<sup>26</sup> Overexpression of miRNA-106a reportedly inhibits the effect of *VNN2* and leads to the invasion, proliferation and migration of OS cells.<sup>21</sup> Furthermore, the dysregulation of *FABP4*, *FGL2*, *LAPT5*, and *SLC38A2* is identified in multiple cancers, such as colorectal, lung, ovarian, and breast.<sup>27–30</sup>

The high expression of *ABCA8*, *CAT* and *CXCL12* is significantly associated with survival time, and also serves

as an independent protective factor in patients with OS. In our study, *CAT* was enriched in the “cyclooxygenase pathway” and “neutral lipid metabolic process,” biological process (BP) pathways, and the “ficolin-1 rich granule” and “exocytosis of ficolin-rich granule lumen proteins,” cellular component (CC) pathways, which are considered closely related to the hypoxia induction and abnormal proliferation of cells. The *CAT* plays a critical role in cellular resistance to oxidative stress, and its downregulation promotes the occurrence of tumors by increasing the level of reactive oxygen species (ROS) in transformed cells.<sup>31</sup> The Cox regression model showed that a high *CAT* expression in OS was associated with better prognoses. Analogously, a local increase in the *CAT* level is a feasible method to reverse or treat tumor cells and thus has attracted increasing attention.<sup>32</sup> Our results are consistent with those from previous studies showing that the hypoxpressive chemokine *CXCL12* controls metastasis and immune responses in OS, supporting that therapies targeting *CXCL12* have a potential for therapeutic intervention.<sup>33</sup> *CXCL12* reportedly induces the constitutive expression and activity of *CAT* by activating downstream p38, Akt and extracellular signal-regulated kinase, which are essential for protecting  $\beta$  cells from DNA damage caused by hydrogen peroxide ( $H_2O_2$ ).<sup>34</sup> This may explain the consistency

in the expression of *CAT* and *CXCL2*. Moreover, *ABCA8*, *CAT* and *CXCL12* may complement the current prognostic gene signatures.

We focused on investigating the circRNAs, miRNAs and mRNAs between primary OS and normal bone or adjacent tissues to identify factors for improved tissue specificity. Although the circRNA-miRNA-mRNA network was built based on GEO data and verified using the TARGET database, the results require further experimental verification.

## Limitations

We used reliable statistical methods to explore the dysregulated ceRNA network in OS. Given the current scarcity of studies on gene sequencing in OS, it is imperative that our findings be corroborated through larger sample sizes and additional experimentation.

## Conclusions

Our findings provide new insights into the molecular mechanisms of OS and reveal potential targets for its diagnosis, monitoring and therapy. Using bioinformatics, we identified 3 independent protective factors in OS. No dataset suitable for Cox model validation was found in the public database to verify their applicability; hence, further experimentation is needed.

## Supplementary data

The Supplementary materials are available at <https://doi.org/10.5281/zenodo.10184102>. The package includes the following files:

Supplementary Table 1. Basic traits of the seven microarray datasets from the GEO and TCGA.

Supplementary Table 2. Basic characteristics of the 9 differentially expressed circRNAs.

Supplementary Table 3. Index of concordance (C-index) and variance inflation factor (VIF) of *ABCA8*, *CXCL12* and *CAT*.

Supplementary Table 4. LASSO and Cox regression analysis of ceRNA with  $\text{coef}/\text{se}(\text{coef}) < 0.01$  and p-value of proportional hazards assumption (PH)  $> 0.05$ .

Supplementary Table 5. Robust rank aggregation analysis of *ABCA8*, *CXCL12* and *CAT*. LogFC in the 4 datasets and RRA score of the three RNAs.

Supplementary Fig. 1. Competitive endogenous RNA in osteosarcoma.

Supplementary Fig. 2. Protein–protein interaction (PPI) network of genes in the competitive endogenous RNA network.

Supplementary Fig. 3. Proportional hazards assumption (left) and linearity assumption (right).

Supplementary Fig. 4. Survival analysis for competitive endogenous RNA in osteosarcoma.

## ORCID iDs

Jiaqi Fan  <https://orcid.org/0000-0003-0270-0900>

Jianhong Liao  <https://orcid.org/0000-0003-2465-3850>

Yuwen Huang  <https://orcid.org/0009-0007-3726-4340>

## References

- Gao F, Zuo Q, Jiang T, Song H, Zhou J. A newly synthesized oleanolic acid derivative inhibits the growth of osteosarcoma cells in vitro and in vivo by decreasing c-MYC-dependent glycolysis. *J Cell Biochem*. 2019;120(6):9264–9276. doi:10.1002/jcb.28202
- Mirabello L, Troisi RJ, Savage SA. Osteosarcoma incidence and survival rates from 1973 to 2004: Data from the Surveillance, Epidemiology, and End Results Program. *Cancer*. 2009;115(7):1531–1543. doi:10.1002/cncr.24121
- Ottaviani G, Jaffe N. The epidemiology of osteosarcoma. In: Jaffe N, Bruland OS, Bielack S, eds. *Pediatric and Adolescent Osteosarcoma*. Cancer Treatment and Research. Vol. 152. Boston, USA: Springer US; 2009:3–13. doi:10.1007/978-1-4419-0284-9\_1
- Smith MA, Altekruze SF, Adamson PC, Reaman GH, Seibel NL. Declining childhood and adolescent cancer mortality. *Cancer*. 2014;120(16):2497–2506. doi:10.1002/cncr.28748
- Kristensen LS, Andersen MS, Stagsted LVW, Ebbesen KK, Hansen TB, Kjems J. The biogenesis, biology and characterization of circular RNAs. *Nat Rev Genet*. 2019;20(11):675–691. doi:10.1038/s41576-019-0158-7
- Liu J, Liu T, Wang X, He A. Circles reshaping the RNA world: From waste to treasure. *Mol Cancer*. 2017;16(1):58. doi:10.1186/s12943-017-0630-y
- Xi Y, Fowdur M, Liu Y, Wu H, He M, Zhao J. Differential expression and bioinformatics analysis of circRNA in osteosarcoma. *Biosci Rep*. 2019;39(5):BSR20181514. doi:10.1042/BSR20181514
- Wu Y, Xie Z, Chen J, et al. Circular RNA circTADA2A promotes osteosarcoma progression and metastasis by sponging miR-203a-3p and regulating CREB3 expression. *Mol Cancer*. 2019;18(1):73. doi:10.1186/s12943-019-1007-1
- Song YZ, Li JF. Circular RNA hsa\_circ\_0001564 regulates osteosarcoma proliferation and apoptosis by acting miRNA sponge. *Biochem Biophys Res Commun*. 2018;495(3):2369–2375. doi:10.1016/j.bbrc.2017.12.050
- Esquela-Kerscher A, Slack FJ. Oncomirs: MicroRNAs with a role in cancer. *Nat Rev Cancer*. 2006;6(4):259–269. doi:10.1038/nrc1840
- Lee YS, Dutta A. MicroRNAs in cancer. *Annu Rev Pathol Mech Dis*. 2009;4(1):199–227. doi:10.1146/annurev.pathol.4.110807.092222
- Sandiford OA, Moore CA, Du J, et al. Human aging and cancer: Role of miRNA in tumor microenvironment. *Adv Exp Med Biol*. 2018;1056:137–152. doi:10.1007/978-3-319-74470-4\_9
- Saliminejad K, Khorram Khorshid HR, Soleymani Fard S, Ghaffari SH. An overview of microRNAs: Biology, functions, therapeutics, and analysis methods. *J Cell Physiol*. 2019;234(5):5451–5465. doi:10.1002/jcp.27486
- Rupaimoole R, Slack FJ. MicroRNA therapeutics: Towards a new era for the management of cancer and other diseases. *Nat Rev Drug Discov*. 2017;16(3):203–222. doi:10.1038/nrd.2016.246
- Mishra S, Yadav T, Rani V. Exploring miRNA based approaches in cancer diagnostics and therapeutics. *Crit Rev Oncol Hematol*. 2016;98:12–23. doi:10.1016/j.critrevonc.2015.10.003
- Moore DD, Luu HH. Osteosarcoma. *Cancer Treat Res*. 2014;162:65–92. doi:10.1007/978-3-319-07323-1\_4
- Lamora A, Talbot J, Mullard J, Brounais-Le Royer B, Redini F, Verrecchia F. TGF- $\beta$  signaling in bone remodeling and osteosarcoma progression. *J Clin Med*. 2016;5(11):96. doi:10.3390/jcm5110096
- Chicón-Bosch M, Tirado OM. Exosomes in bone sarcomas: Key players in metastasis. *Cells*. 2020;9(1):241. doi:10.3390/cells9010241
- Hadjimichael AC, Foukas AF, Savvidou OD, Mavrogenis AF, Psyrri AK, Papagelopoulos PJ. The anti-neoplastic effect of doxycycline in osteosarcoma as a metalloproteinase (MMP) inhibitor: A systematic review. *Clin Sarcoma Res*. 2020;10(1):7. doi:10.1186/s13569-020-00128-6
- Vlachostergios PJ, Papandreou CN. The role of the small ubiquitin-related modifier (SUMO) pathway in prostate cancer. *Biomolecules*. 2012;2(2):240–255. doi:10.3390/biom2020240
- Niu JC, Ma N, Liu W, Wang PJ. EP1 receptor is involved in prostaglandin E2-induced osteosarcoma growth. *Bosn J Basic Med Sci*. 2019;19(3):265–273. doi:10.17305/bjbm.2019.4177

22. Zhang B, Jia WH, Matsuda K, et al. Large-scale genetic study in East Asians identifies six new loci associated with colorectal cancer risk. *Nat Genet.* 2014;46(6):533–542. doi:10.1038/ng.2985
23. Chen Y, Chen Q, Zou J, Zhang Y, Bi Z. Construction and analysis of a ceRNA-ceRNA network reveals two potential prognostic modules regulated by hsa-miR-335-5p in osteosarcoma. *Int J Mol Med.* 2018;42(3):1237–1246. doi:10.3892/ijmm.2018.3709
24. Sultan G. Towards the early detection of ductal carcinoma (a common type of breast cancer) using biomarkers linked to the PPAR( $\gamma$ ) signaling pathway. *Bioinformation.* 2019;15(11):799–805. doi:10.6026/97320630015799
25. Hedditch EL, Gao B, Russell AJ, et al. ABCA transporter gene expression and poor outcome in epithelial ovarian cancer. *J Nat Cancer Inst.* 2014;106(7):dju149. doi:10.1093/jnci/dju149
26. Hartmann F, Sparla D, Tute E, et al. Low acyl-CoA synthetase 5 expression in colorectal carcinomas is prognostic for early tumour recurrence. *Pathol Res Pract.* 2017;213(3):261–266. doi:10.1016/j.prp.2016.09.002
27. Chen Y, Huang T, Yang X, et al. MicroRNA-106a regulates the proliferation and invasion of human osteosarcoma cells by targeting VNN2. *Oncol Rep.* 2018;40(4):2251–2259. doi:10.3892/or.2018.6601
28. Zhang Y, Zhao X, Deng L, et al. High expression of FABP4 and FABP6 in patients with colorectal cancer. *World J Surg Onc.* 2019;17(1):171. doi:10.1186/s12957-019-1714-5
29. Nuylan M, Kawano T, Inazawa J, Inoue J. Down-regulation of *LAPTM5* in human cancer cells. *Oncotarget.* 2016;7(19):28320–28328. doi:10.18632/oncotarget.8614
30. Morotti M, Bridges E, Valli A, et al. Hypoxia-induced switch in SNAT2/SLC38A2 regulation generates endocrine resistance in breast cancer. *Proc Natl Acad Sci U S A.* 2019;116(25):12452–12461. doi:10.1073/pnas.1818521116
31. Winternitz MC, Meloy CR. On the occurrence of catalase in human tissues and its variations in diseases. *J Exp Med.* 1908;10(6):759–781. doi:10.1084/jem.10.6.759
32. Hyoudou K, Nishikawa M, Umeyama Y, Kobayashi Y, Yamashita F, Hashida M. Inhibition of metastatic tumor growth in mouse lung by repeated administration of polyethylene glycol-conjugated catalase. *Clin Cancer Res.* 2004;10(22):7685–7691. doi:10.1158/1078-0432.CCR-04-1020
33. Kim SY, Lee CH, Midura BV, et al. Inhibition of the CXCR4/CXCL12 chemokine pathway reduces the development of murine pulmonary metastases. *Clin Exp Metastasis.* 2008;25(3):201–211. doi:10.1007/s10585-007-9133-3
34. Dinić S, Grdović N, Uskoković A, et al. CXCL12 protects pancreatic  $\beta$ -cells from oxidative stress by a Nrf2-induced increase in catalase expression and activity. *Proc Jpn Acad Ser B Phys Biol Sci.* 2016;92(9):436–454. doi:10.2183/pjab.92.436

# Unleashing the power of anti-CD20 immunotherapy: Mitigating multiple sclerosis risk in Epstein–Barr virus latent infections

Reem Hamoud Alrashoudi<sup>A–F</sup>

Department of Clinical Laboratory Sciences, College of Applied Medical Sciences, King Saud University, Riyadh, Saudi Arabia

A – research concept and design; B – collection and/or assembly of data; C – data analysis and interpretation; D – writing the article; E – critical revision of the article; F – final approval of the article

Advances in Clinical and Experimental Medicine, ISSN 1899–5276 (print), ISSN 2451–2680 (online)

*Adv Clin Exp Med.* 2024;33(8):869–880

## Address for correspondence

Reem Hamoud Alrashoudi  
E-mail: ralrashoudi@ksu.edu.sa

## Funding sources

None declared

## Conflict of interest

None declared

## Acknowledgements

I would like to thank Mrs. Hajera Tabassum for her contribution to this article.

Received on May 21, 2023

Reviewed on August 22, 2023

Accepted on September 13, 2023

Published online on December 12, 2023

## Abstract

Multiple sclerosis (MS) is a chronic inflammatory, demyelinating, and neurodegenerative connective tissue disease affecting the central nervous system (CNS). Recently, there has been a dramatic improvement in several vital concepts of immune pathophysiology underlying MS. Notably, one of the prerequisites to MS development is Epstein–Barr virus (EBV) infection. Greater attention has been drawn towards promising, innovative immunotherapies in the management and treatment of MS. Whilst there are numerous immunotherapies currently proposed for MS, the B cell depleting therapy that predominantly uses the anti-CD20 monoclonal antibodies (mAbs) such as rituximab, ocrelizumab, and ofatumumab have demonstrated promising clinical benefits by targeting the memory B cells, which are the primary reservoir of EBV latency. Although mAbs have proved beneficial in the treatment of MS, they pose the risk of potential adverse effects. The current systematic review was undertaken to explore the therapeutic role of anti-CD20 therapy and its downsides in the treatment of MS and EBV infection. Clinical trials and prospective and retrospective studies reporting anti-CD20 therapy were carefully reviewed. The initial sections discuss the clinical features of MS, the probable link between EBV and MS, and the role of B cells in MS pathogenesis. Here, we show the potential role of anti-CD20 therapy more of a boon than a bane as the therapy yields more promising results for MS treatment. Nevertheless, the adverse effects could be minimized following a planned therapeutic regimen for treating MS patients.

**Key words:** Epstein–Barr virus infections, multiple sclerosis, rituximab, ocrelizumab, ofatumumab

## Cite as

Alrashoudi MR. Unleashing the power of anti-CD20 immunotherapy: Mitigating multiple sclerosis risk in Epstein–Barr virus latent infections. *Adv Clin Exp Med.* 2024;33(8):869–880. doi:10.17219/acem/172240

## DOI

10.17219/acem/172240

## Copyright

Copyright by Author(s)

This is an article distributed under the terms of the Creative Commons Attribution 3.0 Unported (CC BY 3.0) (<https://creativecommons.org/licenses/by/3.0/>)

## Introduction

Multiple sclerosis (MS) is an inflammatory, neurodegenerative, and immune-mediated disorder of the central nervous system (CNS), characterized by the formation of inflammatory lesions of the white matter, axonal damage, loss of oligodendrocyte, gliosis, demyelination, and neurodegeneration.<sup>1</sup> The inter-relationship of various immune, genetic, epigenetic, and environmental factors accounts for the development of this disorder.<sup>2</sup> Before understanding the role of anti-CD20 therapy in mitigating the risk of MS, the epidemiology, together with environmental, genetic, and pathophysiological factors of MS, needs to be reviewed. Multiple sclerosis is one of the most prevalent neurological diseases in the world, affecting mainly women, with about 2.8 million cases worldwide.<sup>3–5</sup> Environmental factors, including exposure to viral and bacterial agents such as Epstein–Barr virus (EBV),<sup>6</sup> human herpes virus, mycoplasma pneumonia,<sup>7</sup> smoking,<sup>8</sup> vitamin deficiency,<sup>9</sup> diet,<sup>10</sup> and exposure to UV radiation are associated with the onset of MS.<sup>11</sup>

Multiple sclerosis has a prevalence gradient dependent on latitude, with a higher incidence in the northern latitudes of Europe and North America.<sup>12</sup> Vitamin D deficiency has been considered as a possible etiology for the noted predisposition of the population in higher latitudes being affected.<sup>13</sup> Genetic susceptibility is not inherited since there is no MS-specific gene,<sup>14</sup> although genetic predisposition may be involved in MS<sup>15–18</sup> as there is a high risk of the disease in patients with affected biological relatives. Moreover, genetic studies have shown a connection between first-, second-, and third-degree relatives.<sup>15,16</sup>

While long considered as a T cell-mediated disease, MS is now known to involve other immune cells like B cells. The role of B cells is now increasingly gaining significance in immunotherapy, and the influence of antibodies on tissue damage is actively investigated. Inflammation of the white and grey matter tissues in the CNS due to focal immune cell infiltration and the subsequent release of cytokines are the primary causes of myelin sheath destruction in MS.<sup>19–22</sup>

Multiple sclerosis is characterized by a wide variety of clinical symptoms. Patients exhibit dysfunction in neural communication as a consequence of demyelination and axonal loss. Approximately 85% of MS patients have alternating episodes of neurological disability and recovery that last for many years, termed relapsing-remitting MS (RRMS). About 90% of RRMS patients progress to steady neurological decline within 25 years, termed secondary progressive MS (SPMS). Nearly 10% of MS patients suffer from steady deterioration of neurological functions without recovery, termed primary progressive MS (PPMS).

In addition to the common motor, sensory, visual, and autonomic deficits, cognitive impairment (CI) is also a common symptom,<sup>23</sup> with approx. 43–65% of MS

patients suffering from CI.<sup>24,25</sup> Executive impairment in MS has been related to damage in frontal-subcortical tracts as the prefrontal cortex (PFC) is believed to support executive functions.<sup>26,27</sup> The assessment of PFC function may provide a useful way to assess cognitive changes in executive function in MS patients.

Besides this, behavioral changes with depressive symptoms are among the most common symptoms in MS.<sup>28</sup> Since mood, fatigue, and sleep disorders are widely acknowledged as important contributors to CI in MS, a comprehensive neuropsychological assessment should always include routine monitoring and screening of these factors to assess the patient's psychological state and any arising difficulties.<sup>29</sup> Besides immunological factors, the pathophysiology of MS could also involve oxidative stress that contributes to the disease progression by inducing axonal and neuronal damage.<sup>30</sup> A causal relationship between neurological disorders such as Alzheimer's disease, MS and diabetes is currently researched across the globe due to the role of oxidative stress and redox status on neurological disorders.<sup>31</sup>

Epstein–Barr virus is a human herpesvirus and the causal agent of infectious mononucleosis (IM). Demyelination is understood to be triggered in genetically predisposed individuals by an infectious agent, with EBV being the lead candidate.<sup>6</sup> In the case of post-EBV infection, the virus persists in latent form in B lymphocytes throughout the life of the host, thus posing a major risk in MS development. Epstein–Barr virus is involved in the etiology underlying the pathogenesis of MS and its progressive stages, namely RRMS, PPMS, and SPMS.<sup>32</sup> While EBV involvement in MS pathology has been studied for many years, the rationale underlying the causality remains inconclusive. It is known that patients with a history of IM or with a higher anti-EBV antibody titer are at greater risk of developing MS. Epstein–Barr virus infection is assumed to be a prerequisite in MS owing to the increased prevalence of MS patients with latent EBV infection,<sup>33–38</sup> with EBV-positive individuals being reported to have a 15 times greater risk of MS than EBV-negative individuals.<sup>34</sup> The strongest evidence reporting EBV infection as a critical contributor to MS was reported by Bjornevik et al., who for over 20 years were analyzing a cohort of >10 million people on active duty in the US military. Adults diagnosed with MS were reported positive for EBV serology.<sup>35</sup>

Presently, there is no cure for MS. However, disease-modifying agents (DMA) comprising modulators and cytotoxic compounds are the mainstay of MS treatment. The antiviral drugs or DMA used in the treatment of viral infections are not completely effective in diminishing the viral load and so have limited effect on the progression of MS. The development of therapies that target EBV or B cells that harbor EBV specifically will be instrumental in addressing this question. Monoclonal antibodies (mAbs) are one of the preferred treatments for MS due

to their target specificity and unusually high efficacy. Approximately 18 mAbs have been approved for the treatment of various diseases, such as rheumatoid and psoriatic arthritis, ankylosing spondylitis, ulcerative colitis, plaque psoriasis, and Crohn’s disease.<sup>39</sup> Monoclonal antibodies target the immune system, which plays a key role in the pathophysiology of MS and these diseases.

Depletion of B cells with mAbs targeting CD20 has emerged as one of the most efficacious therapies for MS<sup>6</sup> and is gaining increasing significance in ameliorating the progression of EBV infection to MS.<sup>39–46</sup> For example, an immunosuppressive mAb, ocrelizumab (OCR) is indicated for the treatment of PPMS and ofatumumab (OMB) was recently licensed for the treatment of SPMS.<sup>47,48</sup> In the case of EBV infection, the anti-CD20 therapy could further dampen the cross-reactive immune response by depleting EBV transformed B cells and mitigate relapses in MS.<sup>45</sup> Whilst anti-CD20 therapy has emerged as an efficient therapeutic tool in managing the risk of MS, these antibodies pose the risk of potential adverse effects. Characteristics, drug efficacy, safety, and outlines of the significant findings of a few mAbs used for B cell depletion are listed in Table 1. Whether anti-CD20 therapy is beneficial or harmful to MS patients remains a question, and the efficacy and safety role of these drugs need to be further established. The current review rationalizes the use of anti-CD20 therapy as positive or negative in mitigating the risk of MS in EPV-infected patients.

## Objectives

The current review was undertaken to ascertain the role of anti-CD20 therapy in mitigating the risk of MS in EBV-infected patients and whether the potential benefits of the therapy outweigh the adverse treatment effects.

## Methodology

### Search strategy and study selection

The current review used the PRISMA protocol. A systematic search was conducted for the published articles across different databases, including PubMed, Scopus, and Google Scholar. Studies on observational, cohort, and case studies evaluating the role of anti-CD20 therapy or B cell depletion in mitigating the risk of EBV and MS were included. All articles included in the review were in English language.

### Inclusion and exclusion criteria

Articles were screened based on originality, those falling within the scope of the review question and following the population, intervention, control, and outcome (PICO) guidelines. Furthermore, articles published during the past 5 years were filtered. Articles not adhering to the review question or satisfying the inclusion criteria, and articles with missing information and repeatability were excluded.

### Data extraction process

The study selection process is outlined in Fig. 1. A comprehensive search was performed using PubMed (Medline) and MeSH terms: “Epstein Barr virus infection” AND “EBV” AND “multiple sclerosis” AND “MS” AND “B cell” AND “immunotherapy” AND “B cell depletion” AND “memory B cells” AND “anti-CD20 therapy” AND “rituximab”, “RTX” AND “ocrelizumab”, “OCR” AND “ofatumumab”, “OMB”, “adverse effects”, etc. The method was adopted following guidelines from previously published studies.<sup>49,50</sup> A total of 102 articles were obtained

**Table 1.** Characteristics, drug efficacy, and safety of mAbs used in anti-CD20 therapy

mAbs	Administration (dose)	Efficacy	Important safety issues
Rituximab	intravenous (500–1000 mg, every 6–12 months)	no phase 3 clinical trials	hypogammaglobulinemia, risk of infections, infusion-related reaction, hepatitis reactivation
Ocrelizumab	intravenous (600 mg, every 6 months)	phase 3 clinical trials: OPERA I OPERA II clinical outcomes: ↓ in ARR (annualized relapse rate) by 46–47% ↓ in Gd-enhancing lesions around 94–95%	hypoglobulinemia, infections, malignancies (breast cancer), infusion-related reaction, hepatitis B reactivation
Ublituximab	intravenous (450 mg, every 24 weeks)	phase 3 clinical trials: ULTIMATE I, ULTIMATE II clinical outcomes: • ↓ in ARR (49.1–59.4%) • ↓ in 24-week confirmed; disability progression (34.3%) MRI outcomes: • ↓ in number of Gd-enhancing lesions (96.5–96.7%)	infusion-related reaction, infections, hepatitis B reactivation, hypogammaglobulinemia
Ofatumumab	subcutaneous (20 mg, every 28 days)	phase 3 clinical trials: ASCLEPIOS I, ASCLEPIOS II clinical outcomes: • ↓ in risk of sustained disability progression (32–34%) • ↓ in ARR (50–60%) MRI outcomes • ↓ number of Gd-enhancing lesions (94–97%)	infusion-related reaction, infections, hepatitis B reactivation, hypogammaglobulinemia

mAbs – monoclonal antibodies; ARR – annual relapse rate; Gd – gadolinium; MRI – magnetic resonance imaging.

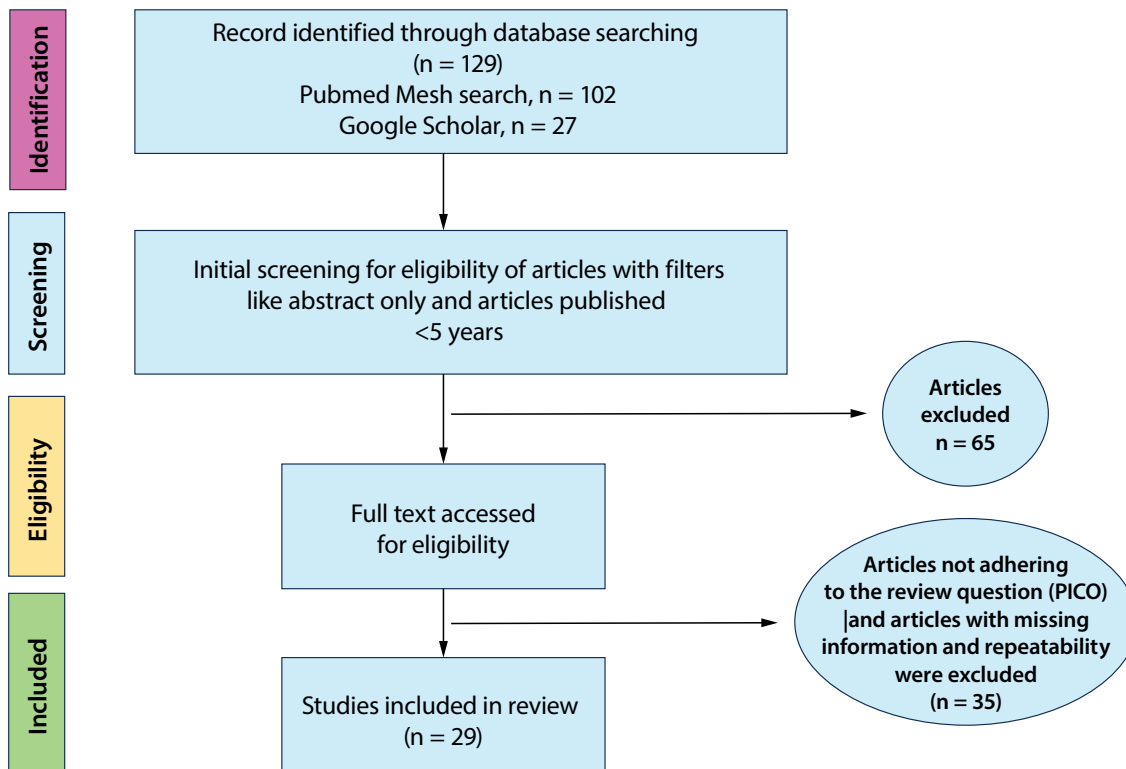


Fig. 1. PRISMA flow diagram showing screening and selection of studies for systematic review

based on the search terms used. An additional 27 articles were also reviewed from a Google search. On applying filters (abstract only and <5 years) and keywords or MeSH used in the review question built on the PICO guidelines, 64 articles were selected. Furthermore, full-text screening of the selected articles resulted in 29 that were reviewed in detail to assess the role of anti-CD20 therapy in treating MS. Articles not adhering to the review question nor meeting the inclusion criteria and articles with missing information and repeatability were excluded. To avoid the risk of bias, 2 reviewers independently evaluated the studies for eligibility and assessed the quality of the included studies. Any conflict between the reviewers was resolved following discussion to reach a common consensus.

## Results

The study selection and data extraction process using the PRISMA protocol are depicted in Fig. 1. The initial screening resulted in the extraction of 64 articles, which was reduced to 29 after full-text screening and inclusion/exclusion criteria. To overcome bias, articles with missing information were removed.

### Risk of bias and quality assessment

The quality of included studies was assessed for risk of bias using the Cochrane risk of bias tool (RoB 2), a revised version<sup>51</sup> consisting of 5 domains, being the selection of the reported result, randomization, intended

interventions, missing outcome data, and outcome measurement (Fig. 2). The risk of bias for a study is determined and categorized as low, high, or some concerns of bias in specific domains. Analysis of domains resulted in raising some concerns that could be due to the following reasons - information on the allocation process used to preserve concealment is not provided in the study, details of intervention in patient information sheet is lacking, and or deviation of the study outcome from intended intervention. Data displayed in Fig. 2 reflect that the study is judged to be at low risk of bias for all domains for this result and ensures the reliability of the included studies.

B cell depleting therapy using anti-CD20 mAbs including rituximab (RTX), ocrelizumab (OCR), and ofatumumab (OMB) has been reported to achieve good efficacy. Rituximab depletes B cells through complement-dependent cytotoxicity<sup>52</sup> and is used as an off-label treatment option for MS and its various progressive forms. In a multi-center retrospective study evaluating the efficacy and safety of RTX in RRMS and PPMS, a significant reduction in annual relapse rate (ARR) following RTX administration in RRMS and SPMS in the 1<sup>st</sup> year of treatment was reported. Three years after RTX treatment, the proportion of patients with the confirmed expanded disability scale (EDSS) progression was 14.6%, 24.7%, and 41.5% in RRMS, SPMS, and PPMS groups, respectively.<sup>53</sup> Infusion-related symptoms were the most prevalent side effects (18.8%), although most were mild. A similar reduction in ARR was observed in a study by Granqvist et al.<sup>54</sup>

Ocrelizumab is the second anti-CD20 humanized mAb and was approved by the US Food and Drug Administration



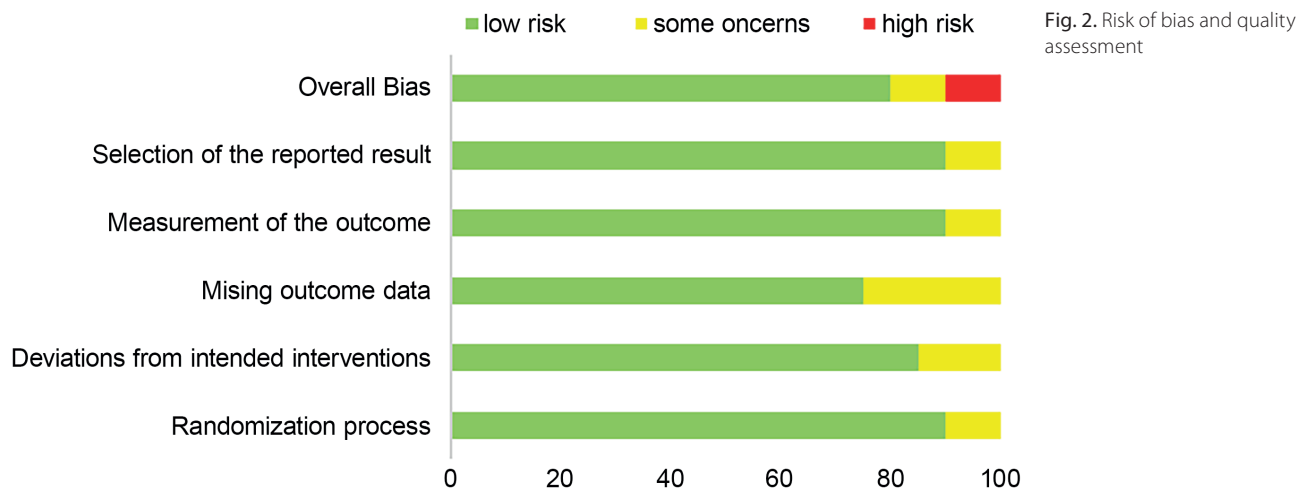


Fig. 2. Risk of bias and quality assessment

(FDA) in March 2017 with proven therapeutic effects reducing disability progression in PPMS. In a clinical trial study by Montalban et al., 732 PPMS patients (ORATORIO trial) received 600 mg of iv. OCR, resulting in a 3.4% decreased brain lesion volume with OCR vs the placebo group.<sup>55</sup> Intriguingly, lower disability progression was observed in the OCR-treated group compared to the placebo group. Other studies evaluating the efficacy of OCR yielded similar findings in mitigating MS risk.<sup>56–58</sup> By week 120, performance on the timed 25-foot walk worsened by 38.9% in the OCR group vs 55.1% in the placebo.<sup>59</sup> In 2 identical phase 3 trials of OCR, lower rates of disease progression were observed compared to the placebo.<sup>55,60</sup> Infections of the upper respiratory tract, nasopharyngitis, and herpes/respiratory viral infections were reported in the treatment of PPMS with OCR in an RCT, although these were mild-to-moderate in severity.<sup>55,60</sup> Cases of tuberculosis or other opportunistic infections were not documented.<sup>60,61</sup> In the ORATORIO trial, of the 11 patients, 2.3% developed breast cancer compared to the placebo group (0.8%).<sup>62</sup> The reported incidence was within expectations based on other epidemiological studies.<sup>63</sup> Compared to RTX, OMB treatment provides effective B cell depletion within lymphoid tissues. Ocrelizumab depletes B cells by antibody-dependent cellular cytotoxicity (ADCC) activity after binding to a CD20 epitope on circulating B cells.<sup>64,65</sup> Annual relapse rate and the number of new magnetic resonance imaging (MRI) lesions were suppressed following the therapy in RRMS patients.<sup>66</sup> The recently reported phase 3 clinical trials, namely ASCLEPIOS I and II, consisting of 1,882 participants with RRMS (94%) and SPMS (5–6%) administered OMB subcutaneously in loading doses of 20 mg on days 1, 7, and 14, followed by 20 mg every 4 weeks while teriflunomide was given orally at 14 mg daily. By using ARR as the primary endpoint, both studies observed significant decreases (51% in ASCLEPIOS I and 58% in ASCLEPIOS II) with OMB therapy.<sup>67</sup>

The efficacy of OMB in MS treatment demonstrated by other clinical studies also yielded satisfactory results. In a clinical trial by Bar-Or et al., 232 patients were

randomized to 3, 30, or 60 mg OMB every 12 weeks, 60 mg every 4 weeks, or placebo for a 24-week treatment period, with a primary endpoint of the cumulative number of new gadolinium-enhancing lesions at week 12. This trial reported a significant reduction in primary endpoint metrics of 65% for all OMB dose groups vs placebo.<sup>68</sup>

Ublituximab (UBX), a newly developed chimeric mAb, is reactive against CD20-positive B lymphocytes, targeting a different epitope on CD20 from that targeted by other CD20 mAbs. Furthermore, it utilizes shorter infusion times and lower doses compared to other anti-CD20 mAbs.<sup>61</sup> In comparison to RTX, UBX has a higher ADCC activity and is 100 times more active on cultured cells from chronic lymphocytic leukemia patients.<sup>69</sup> Following administration, B cell depletion is significant within the first 24 h, reaching approx. 95% within 2 weeks after the 2<sup>nd</sup> dose is administered.<sup>70</sup> Ublituximab has been evaluated in phase 3 trials to test its safety and efficacy as a potential treatment for relapsing MS.<sup>71–74</sup> Recently, Steinman et al. tested the efficacy and safety of UBX against teriflunomide in RRMS patients.<sup>74</sup> In this trial, UBX was administered iv. on day 1, day 15, weeks 24, 48, and 72. Annual relapse rate was considered the primary endpoint, and several gadolinium-enhancing lesions on MRI were scored as the secondary endpoint. The ARR and gadolinium-enhancing lesions were 0.08 and 0.02, respectively in the ULTIMATE I trial, while during the ULTIMATE II trial, ARR and gadolinium-enhancing lesions were 0.09 and 0.01, respectively. These results demonstrate that UBX treatment results in lower ARR and fewer brain lesions on MRI than teriflunomide over 96 weeks. Regarding its safety, in the treated group, it was well tolerated, and infusion-related reactions were observed in 47.7% of the participants. The trial reported approx. 15–17.2% of patients infected with respiratory tract infections, and 52 patients with serious adverse events, including 2 malignancies and 3 deaths due to encephalitis and salpingitis.<sup>74</sup> No cases of PML were reported after RTX therapy. Similarly, in a phase 2 multi-center study by Fox et al., robust B cell depletion and profound reductions in MRI activity and relapses were demonstrated following

UBX treatment. An absence of T1 gadolinium-enhancing lesions was recorded at weeks 24 and 48 of follow-up, and T2 lesion volume decreased by 10%. The ARR was approx. 0.07 and about 74% of patients had no evidence of disease activity (NEDA).<sup>75</sup>

Clinical findings of some studies are outlined in Table 2.<sup>33,53–59,71–75</sup> Overall, the reviewed articles demonstrated the efficacy of anti-CD20 immunotherapy in mitigating the risk of MS in EBV latent infections. Furthermore, they highlight that anti-CD20 therapy is a net benefit to patients and yields promising results for MS treatment. So far, anti-CD20 antibody treatment has been observed to be superior to other treatments, and will likely continue to be utilized until a more comprehensive understanding of the disease develops.

## Discussion

The present review provides evidence from different clinical trials in support of the utility of the therapy in MS management and treatment. B cell depletion via anti-CD20 action is recognized to play a pivotal role in therapeutics for MS. Furthermore, a prophylactic effect may be seen as depletion of infected B cells, which can improve the control of EBV infection and reduce the risk of MS. B cell

depleting therapy using anti-CD20 mAbs has been reported to achieve good efficacy. From the articles reviewed in the current study, anti-CD20 therapy was found effective in treating MS and EBV infections, with few downsides or adverse effects in the treatment. As the immune cells are damaged, the patient is at risk of infections from other disease-causing microorganisms, autoimmune diseases, and cancer. Importantly, the observations reported in the present review are in accordance with the previous studies.<sup>76–78</sup>

In this article, the rationale behind the use of anti-CD20 therapy, and whether this is beneficial or risky to the patients, has been discussed. It is of prime importance to understand the involvement of B cells in EBV infection and MS pathophysiology before the action of anti-CD20 therapy is understood. Epstein–Barr virus, as an essential prerequisite in MS development and action of anti-CD20 therapy, is illustrated in Fig. 3.

Following EBV infection, the EBV-infected or transformed B cells enter the brain through the blood-brain barrier. Here, the B cells differentiate into plasma cells and produce cross-reactive antibodies against myelin antigens, which attack and damage neurons. Further damage to oligodendrocytes, myelin, and neurons occurs by pro-inflammatory cytokines such as IL-2, interferon (IFN)- $\gamma$ , and tumor necrosis factor (TNF)- $\beta$  production,

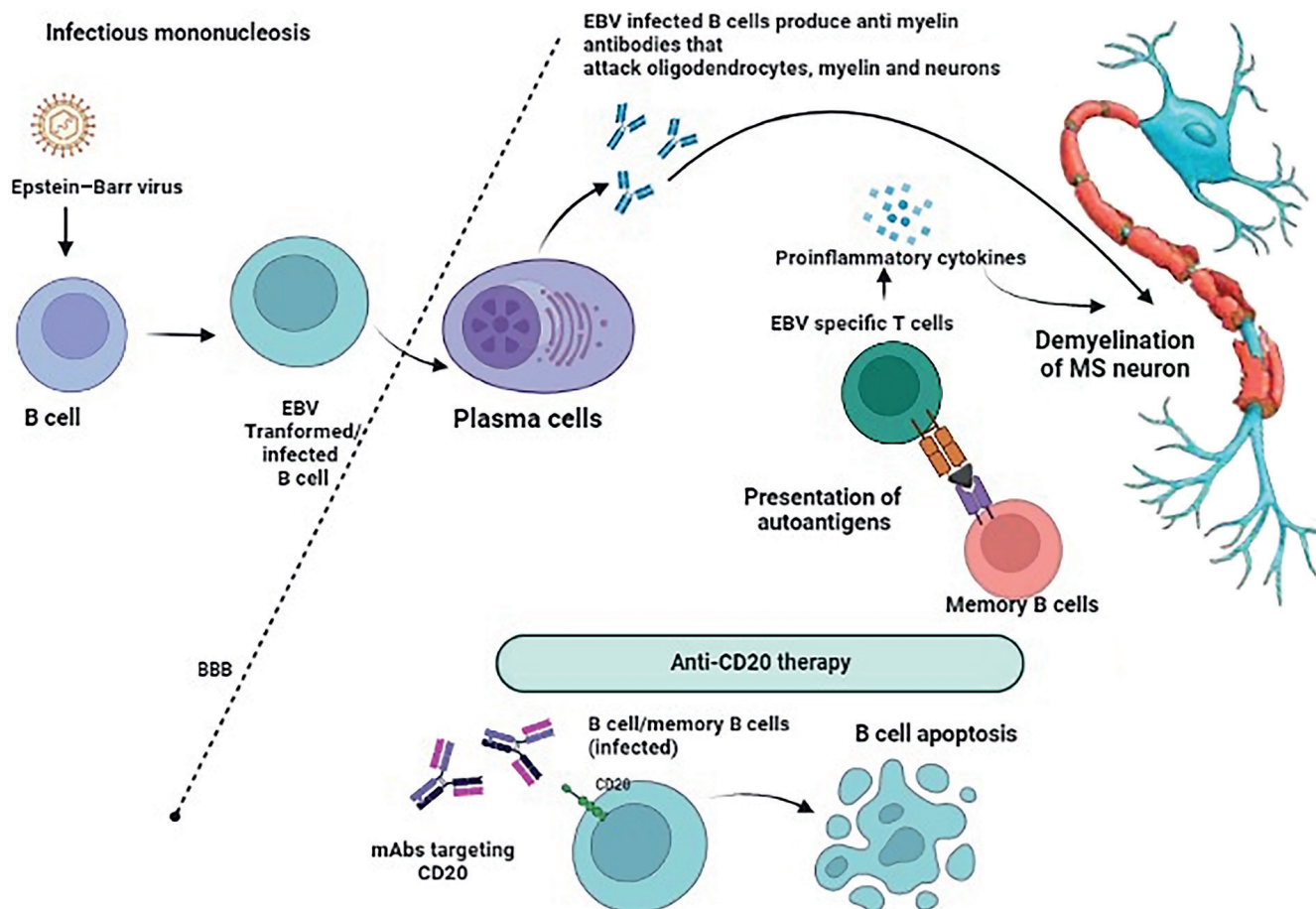


Fig. 3. EBVs association as a prerequisite for MS development and action of anti-CD20 therapy

**Table 2.** Summary of studies assessing anti-CD20 therapy

Author	Type of anti-CD20 therapy	Study design	Major clinical findings	Adverse events
Bar-Or et al. <sup>33</sup>	OMB	phase 2, double-blind, randomized, placebo-controlled study (MIRROR; 48 weeks); number and type of participants: 232 RRMS	stable EDSS in 79% of patients at week 12 and 24	IARs increased in OFT (52%) vs placebo (15%); equivalent infections with OFT and placebo
Zecca et al. <sup>53</sup>	RTX	retrospective, uncontrolled, observational study; number and type of participants: 355 MS (188 RRMS, 43 PPMS, 124 SPMS)	↓ ARR vs 1 year before (RRMS = 0.86 → 0.09 p < 0.001; SPMS = 0.34 → 0.06 p < 0.001; PPMS = 0.12 → 0.07 p = 0.45)	23.7% at least 1 IAR; serious AE (3.1%); death (n = 1) due to mediastinal neoplasm
Granqvist et al. <sup>54</sup>	RTX	retrospective multicenter (follow-up: to 4 years); number and type of participants: 120 RRMS	↓ ARR with RTX vs injectable DMTs (p < 0.01)	absence of serious adverse events with RTX; mild adverse events more common for injectable DMTs vs RTX
Montalban et al. <sup>55</sup>	OCR	phase 3, double-blind, randomized, placebo-controlled, parallel study group (ORATORIO; 120 weeks)	↓ proportion of patients with 3-month CDP (32.9% OCR vs 39.3% placebo, p = 0.03) and 6-month CDP (29.6% vs 35.7%, p = 0.04)	IARs increased with OCR (40%) vs placebo (26%); increased rate of infections with OCR (71.4%) vs placebo (69.9%); increase in upper respiratory tract infections with OCR; no increase in SAE; increase neoplasm with OCR (2.3%) vs placebo (0.8%)
Ellwardt et al. <sup>56</sup>	OCR	retrospective, single-center (median follow-up: 200 days); number and type of participants: 210 MS (155 RRMS/SPMS, 55 PPMS)	relapse rate (13%) and 5% experienced a 12-week CDP	22% AE, 9% IARs: minor infections (8%) and 2 cases of a prolonged herpes labialis; 1 case of toxic drug-induced hepatopathy
Wolinsky et al. <sup>57</sup>	OCR	open-label extension, phase 3 trial (ORATORIO; 144 weeks); number and type of participants: 732 PPMS	↓ proportion of patients with 24 weeks CDP	AE consistent with past reports
Turner et al. <sup>58</sup>	OCR	phase 3, randomized, double-blind, active-controlled, parallel study group (pooled OPERA I and OPERA II; 96 weeks); number and type of participants: 1,656 RRMS	decreased ARR and NEDA-3 re-baselined at week 24 in patients aged < 40 years or with ≥1 Gd <sup>+</sup> lesion at baseline with OCR	–
Hauser et al. <sup>60</sup>	OCR	open-label extension, phase 3 trials (OPERA I and OPERA II); number and type of participants: 702 RRMS	↓ proportion of patients with 6 months CDP (16.1% with OCR/OCR vs 21.3% with IFN-β-1a/OCR at year 5, p = 0.014) NEDA-3 = 65.4% with OCR/OCR vs 55.1% with IFN-β-1a/OCR (p < 0.001)	no new safety signals emerged with prolonged treatment
Sorensen et al. <sup>66</sup>	OMB	phase 2, double-blind, randomized, placebo-controlled study (48 weeks); number and type of participants: 38 RRMS	lower proportion of patients with relapse(s) with OMB compared to placebo (19% vs 25%)	mostly mild-to-moderate severity AEs; 2 patients discontinued for grade-2 (pruritic rash, bronchospasm, cough) and grade-3 (pharyngeal edema, erythema, pruritus) AEs
Alcala et al. <sup>71</sup>	RTX	retrospective single-center; number and type of participants: 90 MS (31 RRMS, 45 SPMS, 14 PPMS)	ARR reduced to 88.4% NEDA-3 at 1 year: all MS = 70% RRMS = 74.2%; PMS = 67%	IAR was 18.8%; 4 SAE (1 agranulocytosis, 3 thrombotic events, 1 death due to pulmonary embolism)
Durozard et al. <sup>72</sup>	RTX	nationwide retrospective multicenter; number and type of participants: 50 RRMS	decrease in ARR	AEs patients = 16; SAEs = 3; discontinuation of treatment due to AE (n = 2)
Honce et al. <sup>73</sup>	RTX	prospective double-blind single center (mean follow-up: 1.5 years); number and type of participants: 55 RRMS	↓ proportion of patients with new T2 lesions (25.9% RTX-GA vs 61.5% placebo-GA, p = 0.009)	IARs increased in RTX; 4 serious AEs in RTX, 5 in placebo
Steinman et al. <sup>74</sup>	UBX	phase 3, double-blind, double-dummy trials (ULTIMATE I and II); number and type of participants: RMS, trial I (n = 549); trial II (n = 545)	trial I: ARR and gadolinium-enhancing lesions were 0.08 and 0.02 trial II: ARR and gadolinium-enhancing lesions were 0.09 and 0.01, respectively	IAR: 47.7%; serious infections: 5.0% in UBX compared to teriflunomide
Fox et al. <sup>75</sup>	UBX	phase 2 placebo-controlled study; number and type of participants: 48 RMS	B cell depletion was >99% by week 4	ARR was 0.07; 93% remained relapse free; 74% had NEDA

OMB – ofatumumab; RTX – rituximab; OCR – ocrelizumab; UBX – ublituximab; MS – multiple sclerosis; RMS – relapsing multiple sclerosis; RRMS – relapsing-remitting multiple sclerosis; SPMS – secondary progressive multiple sclerosis; PMS – progressive multiple sclerosis; PPMS – primary progressive multiple sclerosis; EDSS – expanded disability scale; ARR – annual relapse rate; DMT – disease-modifying therapy; CDP – confirmed disability progression; OCR – ocrelizumab; GA – glatiramer acetate; NEDA – no evidence of disease activity; Gd – gadolinium; AE – adverse event; IAR – infusion-associated reaction; SAE – serious adverse event.

which are released in response to cross-reactive T cells and memory B cells.<sup>40–45</sup> A greater proportion of B cells infected with EBV were found in the post-mortem brain tissue of an RRMS patient.<sup>79</sup> The virus in the infected memory B cells escapes the T cell surveillance by expressing transcription factors EBNA-3A and -3C, which blocks the differentiation of EBV-infected B cells into terminal plasma cells, thereby developing long-term latency in these cells.<sup>80–82</sup>

The use of antiviral drugs, immune modulation via B cell depletion, boosting immune responses, and refining immune surveillance are a few of the effective control measures suggestive of preventing or tackling the increasing risk of MS. Due to the effective treatment against HIV, antiviral compounds like famciclovir, stavudine, zidovudine, abacavir, and raltegravir have been assessed as potential tools in the treatment of MS. However, despite their efficacy against viral infections, therapeutic potential in the case of MS remains unresolved with unsatisfactory results.<sup>82</sup> Besides, anti-herpes viral nucleoside analogs have also received attention as antiviral drugs. Yet, their effect in treating MS was discouraging.<sup>59</sup>

Several anti-CD20 mAbs are beneficial in the treatment of MS via the depletion of CD20<sup>+</sup> B cells.<sup>59,76,83</sup> Recently, Lovett-Racke et al. investigated the role of B cell depletion that could benefit MS patients. In the phase 2 trial of UBX, immune profiles were monitored in 48 patients at 18 time points over a year. Intriguingly, besides CD20<sup>+</sup> B-cells, UBX also depleted CD20 T cells.<sup>84</sup> It is noteworthy that the depletion of T cell subsets adds to the beneficial effects of B-cell depletion therapy. Yet, whether it is the antigen-presenting or antibody-producing property of B-cells targeted in these therapeutics is unclear. The therapeutic efficiency of anti-CD20 B cell mAbs is thus based on the removal of the antigen-presenting capabilities of the B cells.<sup>85</sup> Memory B cells play a key role in EBV infection and progression to MS. The co-receptor used by EBV to infect and immortalize B cells is also expressed by memory B cells (complement C2),<sup>86,87</sup> thus benefitting the virus to establish latency in these cells. Accordingly, memory B cells are recognized as potential targets in ameliorating the progression from EBV infection to MS.<sup>86–88</sup>

A large number of studies have demonstrated a considerable drop in the risk of RRMS and disability with the introduction of anti-CD20 therapy.<sup>39–45</sup> More recently, in a retrospective study conducted at a university hospital in Saudi Arabia to investigate the efficacy of anti-CD20 antibodies (RTX and OCR) in the treatment of RRMS and PPMS,<sup>89</sup> the number of relapses was significantly reduced after 12 months of treatment. Furthermore, a large cohort study testing the efficacy of RTX in different stages of MS, namely RRMS, PPMS, and SPMS, yielded significant diagnostic findings, supporting the use of this therapy in treating MS and likely preventing its transition to secondary progressive forms. A total of 822 RTX-treated patients with MS consisting of 557 RRMS, 198 SPMS, and

67 PPMS were treated with 500 or 1,000 mg of iv. RTX every 6–12 months, with a mean period of 21.8 months. During treatment, the annualized relapse rates (ARR) were 0.044 (RRMS), 0.038 (SPMS), and 0.015 (PPMS), respectively.<sup>81</sup> Similar findings were reported by Zecca et al. with a significant drop in ARR in different stages of MS in a multi-center study.<sup>53</sup> Having known the role of anti-CD20 therapy in effective management in previous sections, it is imperative to judge whether anti-CD20 therapy has drawbacks or is more advantageous.

Notably, the thought of patients living their lives with vastly reduced numbers of B cells is a rather daunting prospect. CD20 is expressed on all stages of B cell development except for early pro-B cells or plasmablasts and plasma cells. Therefore, anti-CD20 therapy comes with a greater concern towards the impact of B cell depletion on total lifelong immunity. A potential problem may be the long-term effects on immunity to new antigens or decreased responses to vaccines. Over the long run, the failure to mount adequate responses to variants of current pathogens or to new pathogens may put chronically B cell-depleted patients at risk of opportunistic infections<sup>68,70,90–99</sup> and a major threat of tumor and secondary autoimmune diseases. Moreover, immunotherapy using mAbs poses a greater risk of infusion-associated reactions (IAR), especially in its early phases.<sup>66</sup>

Few studies reported yielded no neoplastic risk in MS patients on treatment with RTX, others reported a considerable percentage of MS patients to develop cancer.<sup>62</sup> About 0.7% of MS patients develop cancer compared to 0.2% treated with INF- $\beta$ -1a.<sup>100</sup> Conversely, no malignancies were reported in trials in OMB-treated patients.<sup>49</sup> During long-term therapy, serum immunoglobulin (mostly IgM and IgG) levels are greatly reduced. The effects of B cell-depleting therapies on Ig levels, infection risk, long-term immunity, and response to vaccines are important considerations in routine MS disease management. Despite the absence of CD20 in plasma cells, IgG levels are known to decrease following anti-CD20-depleting therapy. It has been reported that serum IgM and IgG decreased following RTX treatment, which can result in hypogammaglobulinemia in long-term treatment.<sup>65</sup> However, a differential effect was observed in the case of OCR. In an RCT, OCR reduced IgM more than IgG, although this result was not supported in either the ASCLEPIOS I and II trials.<sup>49</sup>

Patients treated with anti-CD20 therapy are at higher risk of infections and prone to diseases like HIV and tuberculosis owing to reduced Ig count.<sup>91</sup> Decreases in Ig have been reported in patients receiving long-term therapy with RTX and OCR<sup>92,93</sup> and who were infrequently at risk of severe infections as a result of lymphopenia and neutropenia.<sup>94,95</sup> Parallely, infections in the upper respiratory tract were reported in the treatment of PPMS with OCR in an RCT study.<sup>55</sup> This is together with an increased prevalence of nasopharyngitis and upper respiratory infections being reported in a phase 3 trial following OCR treatment.<sup>60</sup>

In patients with MS and hematological malignancies, a rare but serious viral infection of the brain was reported, termed progressive multifocal leukoencephalopathy (PML), following treatment with OCR and RTX monotherapies, respectively.<sup>96</sup> Moreover, hepatitis B reactivation in patients with prior hepatitis infection and death due to PML on OCR monotherapy is cautioned by the FDA.<sup>97</sup>

Regarding the risk of MS during pregnancy, clinicians have historically discouraged women from conceiving. Yet, this notion changed after the finding by Vukusic et al., who investigated the impact of pregnancy on the clinical course of MS,<sup>101</sup> in which ARR was reported to stay unaltered during pregnancy compared to the pre-pregnancy year. Several studies have assessed the risk of maternal RTX exposure for the fetus. The largest study evaluated 231 pregnancies associated with maternal RTX exposure in lymphoma or autoimmune diseases.<sup>102</sup> Of 153 pregnancies with known outcomes (including 2 patients with MS), nearly 60% resulted in live births, with 24% preterm neonates and only 2.2% of neonates with congenital malformations. However, limited information is available on the use of OCR and OMB during pregnancy. According to the current FDA and European Medicines Agency (EMA) recommendations, OCR should be avoided during pregnancy, and women are recommended to consider pregnancy 6–12 months after the last infusion. This delay could be reduced to 2–3 months for women with active disease as mAbs do not cross the placental barrier during the 1<sup>st</sup> pregnancy trimester.<sup>103</sup>

The data from the current study provide an overview of the potential applications of anti-CD20 therapy in the management of MS and certainly in mitigating the risk of MS in EBV latent infections. The outcome reported herein broadens our understanding of the pivotal role that various immune components play in the immunopathology of MS, together with the role of EBV as a prerequisite in MS development. This would open doors to the development of advanced therapies underlying the ailment and further assist in the initial choice of pharmacological treatment for MS. We hope that these results will assist in shared decision-making between patients, caretakers, and their clinicians. Immunotherapy using T cells is also under development and clinical trials. ATA188 is an off-the-shelf, allogeneic T cell immunotherapy that specifically targets EBV-infected B cells and plasma cells, developed by ATA188 is currently in a phase 2 of randomized, placebo-controlled trial.<sup>104</sup>

The reduction of EBV<sup>+</sup> B cell depletion by anti-CD20 therapy is a promising area of research in MS. While anti-CD20 mAbs have proven efficacy for RRMS treatments, they have failed to prevent long-term disability in SPMS. The most challenging is that the currently available anti-CD20 therapies have little impact on this phase of transitioning MS from RRMS to SPMS. Limited data are available on evidence supporting the efficacy of anti-CD20 therapy in improving the progression of MS by depleting

EBV<sup>+</sup> B cells. In the future, extensive translational research investigating the efficacy of this treatment on progressive stages of MS is warranted for the complete treatment of MS in the advanced stages of the disease.

## Limitations

The current study has some limitations. First, studies reporting data to minimize adverse effects following anti-CD20 therapy are limited, as is the data on the impact of anti-CD20 therapy on the phase transitioning of MS to its progressive stages. The inclusion of such studies and further meta-analysis with statistical evaluation of the main diagnostic findings of the included study would add more information to the outcome of the study and affect the data and future perspectives.

## Conclusions

Data from included studies provides strong evidence in support of anti-CD20 therapy in the management and treatment of EBV infection and MS. Based on the current knowledge of anti-CD20 antibodies, mAbs remain a mainstay in the treatment of MS. Although this therapy has some adverse effects, these can be minimized or managed by timely monitoring of the risk assessment. Thus, it can be justified that anti-CD20 therapy is a net positive in mitigating the risk of MS and EBV infection. Of major concern, the various clinical trials studying the efficacy of different anti-CD20 therapies yielded promising results in treating MS in its early stages. Robust research on the progressive stages of MS is thus needed. Moreover, valuable clues stem from translational research, animal experimentation and other interventional studies on neurodegenerative and neuropsychiatric disorders like those observed in MS. This would further assist in the search for useful biomarkers and exploring novel targets for the treatment of diseases. Several extensive preclinical, clinical, and computational studies are underway for their potential translatability and synthesizability in the search for novel therapeutics for reducing the risk of MS.

## ORCID iDs

Reem Alrashoudi  <https://orcid.org/0000-0002-6842-8893>

## References

1. Ikram MA, Vernooij MW, Roshchupkin GV, et al. Genetic susceptibility to multiple sclerosis: Brain structure and cognitive function in the general population. *Mult Scler*. 2017;23(13):1697–1706. doi:10.1177/1352458516682104
2. Walton C, King R, Rechtman L, et al. Rising prevalence of multiple sclerosis worldwide: Insights from the Atlas of MS, third edition. *Mult Scler*. 2020;26(14):1816–1821. doi:10.1177/1352458520970841
3. Orton SM, Herrera BM, Yee IM, et al. Sex ratio of multiple sclerosis in Canada: A longitudinal study. *Lancet Neurol*. 2006;5(11):932–936. doi:10.1016/S1474-4422(06)70581-6

4. Didonna A, Oksenberg JR. The genetics of multiple sclerosis. In: Zagon IS, McLaughlin PJ, eds. *Multiple Sclerosis: Perspectives in Treatment and Pathogenesis*. Brisbane, Australia: Codon Publications; 2017: 3–16. doi:10.15586/codon.multiplesclerosis.2017.ch1
5. Wallin MT, Culpepper WJ, Coffman P, et al. The Gulf War era multiple sclerosis cohort: Age and incidence rates by race, sex and service. *Brain*. 2012;135(6):1778–1785. doi:10.1093/brain/aws099
6. Guan Y, Jakimovski D, Ramanathan M, Weinstock-Guttman B, Zivadinov R. The role of Epstein–Barr virus in multiple sclerosis: from molecular pathophysiology to in vivo imaging. *Neural Regen Res*. 2019;14(3):373. doi:10.4103/1673-5374.245462
7. Fujinami RS, Von Herrath MG, Christen U, Whitton JL. Molecular mimicry, bystander activation, or viral persistence: Infections and autoimmune disease. *Clin Microbiol Rev*. 2006;19(1):80–94. doi:10.1128/CMR.19.1.80-94.2006
8. Palacios N, Alonso A, Brønnum-Hansen H, Ascherio A. Smoking and increased risk of multiple sclerosis: Parallel trends in the sex ratio reinforce the evidence. *Ann Epidemiol*. 2011;21(7):536–542. doi:10.1016/j.annepidem.2011.03.001
9. Speer G. Impact of vitamin D in neurological diseases and neuro-rehabilitation: From dementia to multiple sclerosis. Part I: the role of vitamin D in the prevention and treatment of multiple sclerosis [in Hungarian]. *Idegygyogy Sz*. 2013;66(9–10):293–303. PMID:24358684.
10. Swank RL, Lerstad O, Strøm A, Backer J. Multiple sclerosis in rural Norway: Its geographic and occupational incidence in relation to nutrition. *N Engl J Med*. 1952;246(19):721–728. doi:10.1056/NEJM195205082461901
11. Sloka S, Silva C, Pryse-Phillips W, Patten S, Metz L, Yong VW. A quantitative analysis of suspected environmental causes of MS. *Can J Neurol Sci*. 2011;38(1):98–105. doi:10.1017/S0317167100011124
12. Simpson S, Blizzard L, Otahal P, Van Der Mei I, Taylor B. Latitude is significantly associated with the prevalence of multiple sclerosis: A meta-analysis. *J Neurol Neurosurg Psychiatry*. 2011;82(10):1132–1141. doi:10.1136/jnnp.2011.240432
13. Sintzel MB, Rametta M, Reder AT. Vitamin D and multiple sclerosis: A comprehensive review. *Neurol Ther*. 2018;7(1):59–85. doi:10.1007/s40120-017-0086-4
14. Miller DH, Leary SM. Primary-progressive multiple sclerosis. *Lancet Neurol*. 2007;6(10):903–912. doi:10.1016/S1474-4422(07)70243-0
15. Ebers GC, Yee IM, Sadovnick AD, Duquette P; Canadian Collaborative Study Group. Conjugal multiple sclerosis: Population-based prevalence and recurrence risks in offspring. *Ann Neurol*. 2000;48(6):927–931. PMID:11117550.
16. Oksenberg JR, Baranzini SE, Sawcer S, Hauser SL. The genetics of multiple sclerosis: SNPs to pathways to pathogenesis. *Nat Rev Genet*. 2008;9(7):516–526. doi:10.1038/nrg2395
17. Quelvennec E, Bera O, Cabre P, et al. Genetic and functional studies in multiple sclerosis patients from Martinique attest for a specific and direct role of the HLA-DR locus in the syndrome. *Tissue Antigens*. 2003;61(2):166–171. doi:10.1046/j.0001-2815.2002.00008.x
18. Alcina A, Abad-Grau MDM, Fedetz M, et al. Multiple sclerosis risk variant HLA-DRB1\*1501 associates with high expression of *DRB1* gene in different human populations. *PLoS One*. 2012;7(1):e29819. doi:10.1371/journal.pone.0029819
19. Lubetzki C, Stankoff B. Demyelination in multiple sclerosis. *Handb Clin Neurol*. 2014;122:89–99. doi:10.1016/B978-0-444-52001-2.00004-2
20. Weiner HL. A shift from adaptive to innate immunity: A potential mechanism of disease progression in multiple sclerosis. *J Neurol*. 2008;255(Suppl 1):3–11. doi:10.1007/s00415-008-1002-8
21. Chunder R, Schropp V, Kuerten S. B cells in multiple sclerosis and virus-induced neuroinflammation. *Front Neurol*. 2020;11:591894. doi:10.3389/fneur.2020.591894
22. Duddy M, Niino M, Adatia F, et al. Distinct effector cytokine profiles of memory and naive human B cell subsets and implication in multiple sclerosis. *J Immunol*. 2007;178(10):6092–6099. doi:10.4049/jimmunol.178.10.6092
23. Läderach F, Münz C. Epstein–Barr virus exploits genetic susceptibility to increase multiple sclerosis risk. *Microorganisms*. 2021;9(11):2191. doi:10.3390/microorganisms9112191
24. Goitia B, Bruno D, Abrevaya S, et al. The relationship between executive functions and fluid intelligence in multiple sclerosis. *PLoS One*. 2020;15(4):e0231868. doi:10.1371/journal.pone.0231868
25. Clough M, Foletta P, Frohman A, et al. Multiple sclerosis: Executive dysfunction, task switching and the role of attention. *Mult Scler J Exp Transl Clin*. 2018;4(2):205521731877178. doi:10.1177/2055217318771781
26. Miller EK, Cohen JD. An integrative theory of prefrontal cortex function. *Annu Rev Neurosci*. 2001;24(1):167–202. doi:10.1146/annurev.neuro.24.1.167
27. Audoin B, Reuter F, Duong M, et al. Efficiency of cognitive control recruitment in the very early stage of multiple sclerosis: A one-year fMRI follow-up study. *Mult Scler*. 2008;14(6):786–792. doi:10.1177/1352458508089360
28. Heldner MR, Kaufmann-Ezra S, Gutbrod K, et al. Behavioral changes in patients with multiple sclerosis. *Front Neurol*. 2017;8:437. doi:10.3389/fneur.2017.00437
29. Portaccio E, Amato MP. Cognitive impairment in multiple sclerosis: An update on assessment and management. *NeuroSci*. 2022;3(4):667–676. doi:10.3390/neurosci3040048
30. Shiri E, Pasbakhsh P, Borhani-Haghighi M, et al. Mesenchymal stem cells ameliorate cuprizone-induced demyelination by targeting oxidative stress and mitochondrial dysfunction. *Cell Mol Neurobiol*. 2021;41(7):1467–1481. doi:10.1007/s10571-020-00910-6
31. Xue H, Zeng L, Liu S. Unraveling the link: Exploring the causal relationship between diabetes, multiple sclerosis, migraine, and Alzheimer's disease through Mendelian randomization. *Front Neurosci*. 2023;17:1233601. doi:10.3389/fnins.2023.1233601
32. Confavreux C, Vukusic S. The clinical course of multiple sclerosis. *Handb Clin Neurol*. 2014;122:343–369. doi:10.1016/B978-0-444-52001-2.00014-5
33. Bar-Or A, Pender MP, Khanna R, et al. Epstein–Barr virus in multiple sclerosis: Theory and emerging immunotherapies. *Trends Mol Med*. 2020;26(3):296–310. doi:10.1016/j.molmed.2019.11.003
34. Ahmed SI, Aziz K, Gul A, Samar SS, Bareeqa SB. Risk of multiple sclerosis in Epstein–Barr virus infection. *Cureus*. 2019;11(9):e5699. doi:10.7759/cureus.5699
35. Bjornevik K, Cortese M, Healy BC, et al. Longitudinal analysis reveals high prevalence of Epstein–Barr virus associated with multiple sclerosis. *Science*. 2022;375(6578):296–301. doi:10.1126/science.abj8222
36. Moreno MA, Or-Geva N, Aftab BT, et al. Molecular signature of Epstein–Barr virus infection in MS brain lesions. *Neural Neuroimmunol Neuroinflamm*. 2018;5(4):e466. doi:10.1212/NXI.0000000000000466
37. Serafini B, Rosicarelli B, Veroni C, Mazzola GA, Aloisi F. Epstein–Barr virus-specific CD8 T cells selectively infiltrate the brain in multiple sclerosis and interact locally with virus-infected cells: Clue for a virus-driven immunopathological mechanism. *J Virol*. 2019;93(24):e00980-19. doi:10.1128/JVI.00980-19
38. Greenfield AL, Hauser SL. B-cell therapy for multiple sclerosis: Entering an era. *Ann Neurol*. 2018;83(1):13–26. doi:10.1002/ana.25119
39. Margoni M, Preziosa P, Filippi M, Rocca MA. Anti-CD20 therapies for multiple sclerosis: Current status and future perspectives. *J Neurol*. 2022;269(3):1316–1334. doi:10.1007/s00415-021-10744-x
40. Bar-Or A, O'Brien SM, Sweeney ML, Fox EJ, Cohen JA. Clinical perspectives on the molecular and pharmacological attributes of anti-CD20 therapies for multiple sclerosis. *CNS Drugs*. 2021;35(9):985–997. doi:10.1007/s40263-021-00843-8
41. Miyazaki Y, Niino M. B-cell depletion therapy for multiple sclerosis. *Immunol Med*. 2022;45(2):54–62. doi:10.1080/25785826.2021.1952543
42. Elsbernd PM, Carter JL. Using monoclonal antibody therapies for multiple sclerosis: A review. *Biol Targets Ther*. 2021;15:255–263. doi:10.2147/BTT.S267273
43. Krajnc N, Bsteh G, Berger T, Mares J, Hartung HP. Monoclonal antibodies in the treatment of relapsing multiple sclerosis: An overview with emphasis on pregnancy, vaccination, and risk management. *Neurotherapeutics*. 2022;19(3):753–773. doi:10.1007/s13311-022-01224-9
44. Läderach F, Münz C. Altered immune response to the Epstein–Barr virus as a prerequisite for multiple sclerosis. *Cells*. 2022;11(17):2757. doi:10.3390/cells11172757
45. Sabatino JJ, Wilson MR, Calabresi PA, Hauser SL, Schneck JP, Zamvil SS. Anti-CD20 therapy depletes activated myelin-specific CD8<sup>+</sup> T cells in multiple sclerosis. *Proc Natl Acad Sci U S A*. 2019;116(51):25800–25807. doi:10.1073/pnas.1915309116
46. Von Essen MR, Ammitzbøll C, Hansen RH, et al. Pro-inflammatory CD20<sup>+</sup> T cells in the pathogenesis of multiple sclerosis. *Brain*. 2019;142(1):120–132. doi:10.1093/brain/awy301

47. Robertson D, Moreo N. Disease-modifying therapies in multiple sclerosis: Overview and treatment considerations. *Fed Pract*. 2016; 33(6):28–34. PMID:30766181. PMID:PMCID:PMC6366576.
48. Hauser SL, Bar-Or A, Cohen JA, et al. Ofatumumab versus teriflunomide in multiple sclerosis. *N Engl J Med*. 2020;383(6):546–557. doi:10.1056/NEJMoa1917246
49. Li H, Hu F, Zhang Y, Li K. Comparative efficacy and acceptability of disease-modifying therapies in patients with relapsing–remitting multiple sclerosis: A systematic review and network meta-analysis. *J Neurol*. 2020;267(12):3489–3498. doi:10.1007/s00415-019-09395-w
50. Eriksen MB, Frandsen TF. The impact of patient, intervention, comparison, outcome (PICO) as a search strategy tool on literature search quality: A systematic review. *J Med Libr Assoc*. 2018;106(4):420–431. doi:10.5195/jmla.2018.345
51. Sterne JAC, Savović J, Page MJ, et al. RoB 2: A revised tool for assessing risk of bias in randomized trials. *BMJ*. 2019;366:l4898. doi:10.1136/bmj.l4898
52. Ganne V, Siddiqi N, Kamaplah B, et al. Humanized anti-CD20 monoclonal antibody (rituximab) treatment for post-transplant lymphoproliferative disorder. *Clin Transplant*. 2003;17(5):417–422. doi:10.1034/j.1399-0012.2003.00054.x
53. Zecca C, Bovis F, Novi G, et al. Treatment of multiple sclerosis with rituximab: A multicentric Italian–Swiss experience. *Mult Scler*. 2020; 26(12):1519–1531. doi:10.1177/1352458519872889
54. Granqvist M, Borealm M, Poorghobad A, et al. Comparative effectiveness of rituximab and other initial treatment choices for multiple sclerosis. *JAMA Neurol*. 2018;75(3):320. doi:10.1001/jamaneurol.2017.4011
55. Montalban X, Hauser SL, Kappos L, et al. Ocrelizumab versus placebo in primary progressive multiple sclerosis. *N Engl J Med*. 2017; 376(3):209–220. doi:10.1056/NEJMoa1606468
56. Ellwardt E, Rolfes L, Klein J, et al. Ocrelizumab initiation in patients with MS: A multicenter observational study. *Neurol Neuroimmunol Neuroinflamm*. 2020;7(4):e719. doi:10.1212/NXI.0000000000000719
57. Wolinsky JS, Arnold DL, Brochet B, et al. Long-term follow-up from the ORATORIO trial of ocrelizumab for primary progressive multiple sclerosis: A post-hoc analysis from the ongoing open-label extension of the randomised, placebo-controlled, phase 3 trial. *Lancet Neurol*. 2020;19(12):998–1009. doi:10.1016/S1474-4422(20)30342-2
58. Turner B, Cree BAC, Kappos L, et al. Ocrelizumab efficacy in subgroups of patients with relapsing multiple sclerosis. *J Neurol*. 2019; 266(5):1182–1193. doi:10.1007/s00415-019-09248-6
59. Drosu NC, Edelman ER, Housman DE. Could antiretrovirals be treating EBV in MS? A case report. *Mult Scler Relat Dis*. 2018;22:19–21. doi:10.1016/j.msard.2018.02.029
60. Hauser SL, Bar-Or A, Comi G, et al. Ocrelizumab versus interferon beta-1a in relapsing multiple sclerosis. *N Engl J Med*. 2017;376(3): 221–234. doi:10.1056/NEJMoa1601277
61. Babiker HM, Glode AE, Cooke LS, Mahadevan D. Ublituximab for the treatment of CD20 positive B-cell malignancies. *Exp Opin Investig Dugs*. 2018;27(4):407–412. doi:10.1080/13543784.2018.1459560
62. Alping P, Askling J, Burman J, et al. Cancer risk for fingolimod, natalizumab, and rituximab in multiple sclerosis patients. *Ann Neurol*. 2020;87(5):688–699. doi:10.1002/ana.25701
63. Gelfand JM, Cree BAC, Hauser SL. Ocrelizumab and other CD20+ B-cell-depleting therapies in multiple sclerosis. *Neurotherapeutics*. 2017;14(4):835–841. doi:10.1007/s13311-017-0557-4
64. Masoud S, McAdoo SP, Bedi R, Cairns TD, Lightstone L. Ofatumumab for B cell depletion in patients with systemic lupus erythematosus who are allergic to rituximab. *Rheumatology (Oxford)*. 2018; 57(7):1156–1161. doi:10.1093/rheumatology/key042
65. Florou D, Katsara M, Feehan J, Dardiotis E, Apostolopoulos V. Anti-CD20 agents for multiple sclerosis: Spotlight on ocrelizumab and ofatumumab. *Brain Sci*. 2020;10(10):758. doi:10.3390/brainsci10100758
66. Sorensen PS, Lisby S, Grove R, et al. Safety and efficacy of ofatumumab in relapsing–remitting multiple sclerosis: A phase 2 study. *Neurology*. 2014;82(7):573–581. doi:10.1212/WNL.000000000000125
67. Salzer J, Svenningsson R, Alping P, et al. Rituximab in multiple sclerosis: A retrospective observational study on safety and efficacy. *Neurology*. 2016;87(20):2074–2081. doi:10.1212/WNL.0000000000003331
68. Bar-Or A, Grove RA, Austin DJ, et al. Subcutaneous ofatumumab in patients with relapsing–remitting multiple sclerosis: The MIRROR study. *Neurology*. 2018;90(20):e1805–e1814. doi:10.1212/WNL.0000000000005516
69. Sharman JP, Farber CM, Mahadevan D, et al. Ublituximab (TG-1101), a novel glycoengineered anti-CD20 antibody, in combination with ibrutinib is safe and highly active in patients with relapsed and/or refractory chronic lymphocytic leukaemia: Results of a phase 2 trial. *Br J Haematol*. 2017;176(3):412–420. doi:10.1111/bjh.14447
70. Fox EJ, Buckle GJ, Singer B, Singh V, Boster A. Lymphopenia and DMTs for relapsing forms of MS: Considerations for the treating neurologist. *Neurol Clin Pract*. 2019;9(1):53–63. doi:10.1212/CPJ.0000000000000567
71. Alcalá C, Gascón F, Pérez-Mirallas F, et al. Efficacy and safety of rituximab in relapsing and progressive multiple sclerosis: A hospital-based study. *J Neurol*. 2018;265(7):1690–1697. doi:10.1007/s00415-018-8899-3
72. Durozard P, Maarouf A, Boutiere C, et al. Efficacy of rituximab in refractory RRMS. *Mult Scler*. 2019;25(6):828–836. doi:10.1177/1352458518772748
73. Honce JM, Nair KV, Sillau S, et al. Rituximab vs placebo induction prior to glatiramer acetate monotherapy in multiple sclerosis. *Neurology*. 2019;92(7):e723–e732. doi:10.1212/WNL.00000000000006916
74. Steinman L, Fox E, Hartung HP, et al. Ublituximab versus teriflunomide in relapsing multiple sclerosis. *N Engl J Med*. 2022;387(8):704–714. doi:10.1056/NEJMoa2201904
75. Fox E, Lovett-Racke AE, Gormley M, et al. A phase 2 multicenter study of ublituximab, a novel glycoengineered anti-CD20 monoclonal antibody, in patients with relapsing forms of multiple sclerosis. *Mult Scler*. 2021;27(3):420–429. doi:10.1177/1352458520918375
76. Bloomgren G, Richman S, Hotermans C, et al. Risk of natalizumab-associated progressive multifocal leukoencephalopathy. *N Engl J Med*. 2012;366(20):1870–1880. doi:10.1056/NEJMoa1107829
77. De Sèze J, Maillart E, Gueguen A, et al. Anti-CD20 therapies in multiple sclerosis: From pathology to the clinic. *Front Immunol*. 2023;14: 1004795. doi:10.3389/fimmu.2023.1004795
78. Serafini B, Scorsi E, Rosicarelli B, Rigau V, Thouvenot E, Aloisi F. Massive intracerebral Epstein–Barr virus reactivation in lethal multiple sclerosis relapse after natalizumab withdrawal. *J Neuroimmunol*. 2017; 307:14–17. doi:10.1016/j.jneuroim.2017.03.013
79. Geginat J, Paroni M, Pagani M, et al. The enigmatic role of viruses in multiple sclerosis: Molecular mimicry or disturbed immune surveillance? *Trends Immunol*. 2017;38(7):498–512. doi:10.1016/j.it.2017. 04.006
80. Tracy SL, Kakalacheva K, Lünemann JD, Luzuriaga K, Middeldorp J, Thorley-Lawson DA. Persistence of Epstein–Barr virus in self-reactive memory B cells. *J Virol*. 2012;86(22):12330–12340. doi:10.1128/ JVI.01699-12
81. Styles CT, Bazot Q, Parker GA, White RE, Paschos K, Allday MJ. EBV epigenetically suppresses the B cell-to-plasma cell differentiation pathway while establishing long-term latency. *PLoS Biol*. 2017;15(8): e2001992. doi:10.1371/journal.pbio.2001992
82. Küry P, Nath A, Créange A, et al. Human endogenous retroviruses in neurological diseases. *Trends Mol Med*. 2018;24(4):379–394. doi:10.1016/j.molmed.2018.02.007
83. Hauser SL, Waubant E, Arnold DL, et al. B-cell depletion with rituximab in relapsing–remitting multiple sclerosis. *N Engl J Med*. 2008;358(7): 676–688. doi:10.1056/NEJMoa0706383
84. Lovett-Racke AE, Yang Y, Liu Y, et al. B cell depletion changes the immune cell profile in multiple sclerosis patients: One-year report. *J Neuroimmunol*. 2021;359:577676. doi:10.1016/j.jneuroim.2021.577676
85. Naismith RT, Piccio L, Lyons JA, et al. Rituximab add-on therapy for breakthrough relapsing multiple sclerosis: A 52-week phase II trial. *Neurology*. 2010;74(23):1860–1867. doi:10.1212/WNL.0b013e3181e24373
86. Fernández-Menéndez S, Fernández-Morán M, Fernández-Vega I, Pérez-Álvarez A, Villafani-Echazú J. Epstein–Barr virus and multiple sclerosis: From evidence to therapeutic strategies. *J Neurol Sci*. 2016;361:213–219. doi:10.1016/j.jns.2016.01.013
87. Ascherio A, Munger KL. EBV and autoimmunity. In: Münz C, ed. *Epstein Barr Virus Volume 1*. Vol. 390. Current Topics in Microbiology and Immunology. Cham, Switzerland: Springer International Publishing; 2015:365–385. doi:10.1007/978-3-319-22822-8\_15
88. Serafini B, Severa M, Columba-Cabezas S, et al. Epstein–Barr virus latent infection and BAFF expression in B cells in the multiple sclerosis brain: Implications for viral persistence and intrathecal B-cell activation. *J Neuropathol Exp Neurol*. 2010;69(7):677–693. doi:10.1097/ NEN.0b013e3181e332ec

89. Bauthman MS. Effectiveness of anti-cluster of differentiation 20 as a disease-modifying therapy in multiple sclerosis across its different phenotypes at the University Hospital of Caen. *Cureus*. 2022; 14(2):e22120. doi:10.7759/cureus.22120
90. Schwab N, Schneider-Hohendorf T, Melzer N, Cutter G, Wiendl H. Natalizumab-associated PML: Challenges with incidence, resulting risk, and risk stratification. *Neurology*. 2017;88(12):1197–1205. doi:10.1212/WNL.0000000000003739
91. Vollmer BL, Wallach AJ, Corboy JR, Dubovskaya K, Alvarez E, Kister I. Serious safety events in rituximab-treated multiple sclerosis and related disorders. *Ann Clin Transl Neurol*. 2020;7(9):1477–1487. doi:10.1002/acn3.51136
92. Roberts DM, Jones RB, Smith RM, et al. Immunoglobulin G replacement for the treatment of infective complications of rituximab-associated hypogammaglobulinemia in autoimmune disease: A case series. *J Autoimmun*. 2015;57:24–29. doi:10.1016/j.jaut.2014.11.004
93. Cohen BA. Late-onset neutropenia following ocrelizumab therapy for multiple sclerosis. *Neurology*. 2019;92(9):435–436. doi:10.1212/WNL.0000000000006924
94. Auer M, Bsteh G, Hegen H, et al. Late-onset neutropenia in a multiple sclerosis patient after first dose of ocrelizumab switched from rituximab. *Mult Scler Relat Dis*. 2020;43:102155. doi:10.1016/j.msard.2020.102155
95. Genentech. RITUXAN® (rituximab) [package insert]. South San Francisco, USA; Genentech; 2020. [https://www.gene.com/download/pdf/rituxan\\_prescribing.pdf](https://www.gene.com/download/pdf/rituxan_prescribing.pdf). Accessed June 3, 2021.
96. Patel A, Sul J, Gordon ML, et al. Progressive multifocal leukoencephalopathy in a patient with progressive multiple sclerosis treated with ocrelizumab monotherapy. *JAMA Neurol*. 2021;78(6):736. doi:10.1001/jamaneurol.2021.0627
97. GlaxoSmithKline plc. ARZERRA® (ofatumumab) [package insert]. London, UK; GlaxoSmithKline plc; 2016. [https://www.accessdata.fda.gov/drugsatfda\\_docs/label/2016/125326s0621b](https://www.accessdata.fda.gov/drugsatfda_docs/label/2016/125326s0621b). Accessed June 3, 2021.
98. Sormani MP, De Rossi N, Schiavetti I, et al. Disease-modifying therapies and coronavirus disease 2019 severity in multiple sclerosis. *Ann Neurol*. 2021;89(4):780–789. doi:10.1002/ana.26028
99. Reder AT, Centonze D, Naylor ML, et al. COVID-19 in patients with multiple sclerosis: Associations with disease-modifying therapies. *CNS Drugs*. 2021;35(3):317–330. doi:10.1007/s40263-021-00804-1
100. Mathias A, Perriard G, Canales M, et al. Increased ex vivo antigen presentation profile of B cells in multiple sclerosis. *Mult Scler*. 2017; 23(6):802–809. doi:10.1177/1352458516664210
101. Vukusic S, Hutchinson M, Hours M, et al. Pregnancy and multiple sclerosis (the PRIMS study): Clinical predictors of post-partum relapse. *Brain*. 2004;127(6):1353–1360. doi:10.1093/brain/awh152
102. Chakravarty EF, Murray ER, Kelman A, Farmer P. Pregnancy outcomes after maternal exposure to rituximab. *Blood*. 2011;117(5):1499–1506. doi:10.1182/blood-2010-07-295444
103. Palmeira P, Quinello C, Silveira-Lessa AL, Zago CA, Carneiro-Sampaio M. IgG placental transfer in healthy and pathological pregnancies. *Clin Dev Immunol*. 2012;2012:985646. doi:10.1155/2012/985646
104. U.S. Food and Drug Administration (FDA). FDA Drug Safety Communication: Boxed Warning and new recommendations to decrease the risk of hepatitis B reactivation with the immune-suppressing and anti-cancer drugs Arzerra (ofatumumab) and Rituxan (rituximab). Silver Spring, USA: U.S. Food and Drug Administration (FDA): September 25, 2013. <http://www.fda.gov/Drugs/DrugSafety/ucm366406.htm>. Accessed November 19, 2018.



# Anterior cervical discectomy and fusion (ACDF) with and without plating: A comparison of radiological and clinical outcomes

\*Adam Bębenek<sup>A–F</sup>, \*Bartosz Godlewski<sup>A–F</sup>

Department of Orthopaedics and Traumatology, with Spinal Surgery Ward. Scanmed – St. Raphael Hospital, Cracow, Poland

A – research concept and design; B – collection and/or assembly of data; C – data analysis and interpretation; D – writing the article; E – critical revision of the article; F – final approval of the article

Advances in Clinical and Experimental Medicine, ISSN 1899–5276 (print), ISSN 2451–2680 (online)

*Adv Clin Exp Med.* 2024;33(8):881–888

## Address for correspondence

Bartosz Godlewski

E-mail: bartoszegodlewski@wp.pl

## Funding sources

None declared

## Conflict of interest

None declared

\* Both authors contributed equally to this work.

Received on June 16, 2023

Reviewed on August 23, 2023

Accepted on September 8, 2023

Published online on September 28, 2023

## Abstract

Treatment for degenerative disc disease of the cervical spine primarily aims to decompress neural structures and preserve the former height of the disc space and foramina. Popular methods include anterior cervical discectomy and fusion (ACDF) using cages with plates or without plates (standalone cages). However, it is still debatable whether a plate is necessary for enhanced treatment outcomes. This paper reviews current literature reports, adding insights from the authors' experience. A literature search was performed with keywords related to ACDF with or without cervical plating. We analyzed the titles and abstracts to identify all potentially relevant studies. Out of these, a total of 28 original research and 5 systematic reviews/meta-analyses met our inclusion criteria. The success of surgery for cervical disc disease depends fundamentally on the appropriate decompression of neural structures. This is the main determinant of postoperative clinical improvement measured according to scales capturing changes in pain intensity and quality of life. An ideal replacement for natural components of the human body does not exist, even though more and more refined solutions are developed every year. A comparison of treatment outcomes using non-plated (standalone) cages and cage + plate systems requires separate analysis of radiological and clinical outcomes. Both methods have their advantages and disadvantages. Radiological outcomes are slightly better with cage + plate systems, and clinical outcomes are comparable.

**Key words:** anterior cervical discectomy and fusion, standalone cervical cages, cervical plates, self-anchoring cervical cages, ACDF outcomes

## Cite as

Bębenek A, Godlewski B. Anterior cervical discectomy and fusion (ACDF) with and without plating:

A comparison of radiological and clinical outcomes.

*Adv Clin Exp Med.* 2024;33(8):881–888.

doi:10.17219/acem/172062

## DOI

10.17219/acem/172062

## Copyright

Copyright by Author(s)

This is an article distributed under the terms of the Creative Commons Attribution 3.0 Unported (CC BY 3.0)

(<https://creativecommons.org/licenses/by/3.0/>)

## Introduction

The cervical segment of the spinal column is a complex anatomical and biomechanical structure. It exhibits the highest degree of mobility among all spinal segments, making it a pivotal component in the preservation of overall sagittal balance and functional integrity. The curvature of the cervical segment is shaped by a range of factors, such as muscle tone distribution in the neck and the shoulder girdle or the shape of the thoracic and lumbosacral segments. The curvatures of individual spinal segments influence each other. Regrettably, similar to other spine regions, the cervical segment is susceptible to degenerative alterations that may necessitate surgical intervention. The primary aim of the treatment for degenerative disc disease of the cervical spine is to decompress neural structures and preserve the former height of the disc space and foramina. Anterior cervical discectomy without the simultaneous insertion of a graft or cage is not recommended because there is a possibility of future instability and kyphotic malalignment of the cervical spine.<sup>1</sup> Anterior cervical discectomy and fusion (ACDF) is currently the gold standard for surgical treatment of degenerative disc disease of the cervical spine. An interbody implant should have a size that produces a tight interference fit and maximizes the dimensions of the graft–vertebral body interface. Popular methods include an ACDF using a standalone cage or a cage with a cervical plate. However, it is still debatable whether a plate is necessary for enhanced treatment outcomes. Both methods have their advantages and disadvantages. Most surgeons believe that plating is not necessary for single-level surgery, but operations on multiple levels require additional strengthening of the fixation obtained using a cervical plate. This paper reviews current literature reports, with insight added from the authors' experience. Anterior cervical plates may increase interbody fusion rates and stability, maintain or improve cervical sagittal alignment, and prevent subsidence, particularly in multiple-level ACDFs. However, anterior plating may also be associated with potential disadvantages and complications. The complications associated with plate fixation consist of esophageal soft tissue damage, neurovascular injuries and dysphagia. The success of surgery for cervical disc disease depends fundamentally on the appropriate decompression of neural structures. This is the main determinant of postoperative clinical improvement measured using scales which show changes in pain intensity and quality of life.

## Objectives

The aim of this study was to compare the clinical and radiological outcomes of ACDF with a standalone cage to ACDF performed with a cage with a cervical plate.

## Materials and methods

This paper reviews current literature reports and also offers insight from the authors' experience. Relevant published studies indexed in MEDLINE were first identified using PubMed and then reviewed by the authors. A literature search was performed with keywords related to ACDF with or without cervical plating, such as "anterior cervical discectomy and fusion", "standalone cages", "cervical plates", "self-anchored cervical cages", "zero-profile cervical cages", "cervical alignment", "subsidence", "fusion rate", and "ACDF outcomes". We studied the titles and abstracts of identified articles and full texts of all potentially meaningful academic papers. Out of these, 28 original research articles and 5 systematic reviews/meta-analyses met our inclusion criteria necessary to compare the radiological and clinical outcomes of surgery for cervical disc disease using standalone cages or cages with cervical plates. Then, we supplemented the analyzed literature with other original contributions, review articles and case reports that do not directly compare ACDF with standalone cages and ACDF with cage + plate, but do describe important aspects of surgery for cervical disc disease such as subsidence, adjacent segment disease (ASD), cervical alignment, types of interbody implants and cervical plates, materials that implants are made of, and complications after ACDF. In our experience, original reports contain more practical advice and information, while meta-analyses/systematic reviews are more mathematical/statistical in nature, analyzing large numbers of cases. Radiological outcome refers to parameters such as fusion rate, IDH, subsidence, and cervical alignment, assessed based on postoperative imaging. Clinical outcome refers to the changes in parameters assessing the quality of life and pain. When comparing the radiological and clinical results of ACDF with standalone cages compared to cage + cervical plating, the type of implant and the technique of implant fixation in the interbody space should also be considered. The recently popular zero-profile implants consisting of a cage fixated to the adjacent vertebral bodies with screws introduced through the implant are usually included in the same group as typical standalone cages, which are placed in the interbody space without using additional fixation. There are, undoubtedly, differences between these 2 types of implants that affect their biomechanics. Nevertheless, to ensure a common methodology and a large number of studies needed to compare treatment outcomes, authors often do not draw finer distinctions concerning the type of interbody implant, the material used to produce the implant, the implant's surface area, the presence or absence of spikes/serration for anchoring in the interbody space, or the presence or absence of a dedicated space to be filled, for example, with fusion-promoting hydroxyapatite. To make a more systematic comparison of individual groups, we grouped reports concerning typical standalone cages and zero-profile cages, also known

as self-anchoring or self-locking cages.<sup>2,3</sup> Similarly, most studies comparing ACDF procedures with standalone cages or cages + plates did not distinguish between the distinct types of plates, i.e., wide plates fixed to each vertebral body with 2 screws or narrower plates fixed to each vertebral body with 1 screw. The most significant difference between traditional cage and plate structures and the zero-profile implant is that the zero-profile implant uses no additional plate fixed to the anterior surface of the vertebral body.

## Results

The ACDF is a commonly used and successful surgical treatment for patients with cervical disc disease. Neural decompression should be combined with interbody stabilization or additional placement of a cervical plate. The neurosurgeon and orthopedist communities have not yet developed an unequivocal position on the necessity of cervical plating with ACDF procedures. It has been questioned whether plate fixation is necessary, especially in single-level fusion, irrespectively of its disadvantages. Most surgeons believe that plating is not necessary for single-level surgery, but operations on multiple levels require additional strengthening of the fixation obtained using a cervical plate. This is not done to prevent spinal instability but to strengthen the cage, expedite fusion and preserve the postoperative height of the disc space near-physiological cervical alignment.<sup>4–7</sup> At the same time, awareness of the postoperative complications believed to be related to the presence of an anterior plate has been contributing to a rising interest in non-plated techniques such as standalone cages. It has been shown that the design of zero-profile implants provides a similar degree of biomechanical stability conferred by anterior plating, simultaneously avoiding increased retraction and anterior bulk connected with plating.

### Cervical cages and plates

At present, the most commonly used interbody cages in cervical spine procedures comprise of polyetheretherketone (PEEK) implants, titanium-coated PEEK cages and titanium implants. Apart from the type of material, the implants are made of, their shape and surface morphology also play an essential role in obtaining fusion.<sup>8</sup> Implant surface morphology can be two-dimensional (2D) or three-dimensional (3D). Most 2D surfaces have irregularities emulating indentations produced by the action of osteoclasts. These indentations generally serve to promote a beneficial response of bone tissue to such morphology.<sup>9,10</sup> For better anchoring in the interbody space, implant manufacturers offer implants with corrugated surfaces and additional protruding titanium spikes placed (immersed) in upper and lower implant surfaces. Furthermore, the so-called

hybrid implants are also available, comprising an interbody cage connected to a plate (cage and plate as one device). In contrast to 2D implants, the porous surfaces of 3D implants are characterized by an interconnected porous spatial network to enhance bone integration and produce mechanical locking (entanglement) of bone and implant surfaces.<sup>11–13</sup> Unlike traditional titanium implants, more recent 3D titanium implants build with porous surfaces produced with laser 3D print technologies are not a source of significant artifacts in postoperative magnetic resonance imaging (MRI) assessment, thus allowing for a detailed postoperative evaluation of the anatomical structures of the cervical spine. The PEEK implants with a porous surface manufactured with 3D technology are relatively new on the market. Laboratory studies have demonstrated that porous PEEK increases osteoblastic differentiation of cells *in vitro* and improves osseointegration *in vivo* compared to both smooth and titanium-coated PEEK. These results have been ascribed to improved mechanical bone locking by the implant's porous spatial surface.<sup>8</sup> A wide variety of plating systems are available. The placement of early devices was associated with piercing the posterior cortex of the vertebral body (bicortical fixation). Contemporary cervical plating systems are designed for uni-cortical placement to avoid posterior bicortical penetration of the cervical vertebra so that neural structures are not injured. New third-generation systems represent dynamic semi-constrained plates designed to prevent stress shielding. Ideally, plates should be available in narrow and wider varieties and they should provide for small increments in plate length. Screws should ideally be marketed in variable lengths and offer variable placement angulation capability, there should be rescue screws matching the corresponding standard screw in length, and the screws should be easy to place with a reliable locking mechanism.<sup>14–15</sup>

### Dysphagia

While the most common complication of ACDF is dysphagia, its mechanism is not fully elucidated, with hypotheses including damage to the esophagus, soft tissue edema, hematoma, and adhesions/scarring around the plate.<sup>16</sup> Most papers indicate a statistically lower rate of dysphagia following non-plated ACDF, with 1 report even showing a link (positive correlation) between cervical plate thickness and dysphagia.<sup>17</sup> Additionally, another study found improvement in the symptoms of dysphagia following the removal of a cervical plate and release of plating-induced adhesions. It reported on a series of 31 patients who had their anterior plates surgically removed due to persistent dysphagia following ACDF. There were extensive adhesions around the periphery of the cervical plate that attached the esophagus to the prevertebral fascia and anterior cervical spine. Surgery brought about a significant improvement to mild or no dysphagia in 27 patients.<sup>18</sup> A few high-quality systematic reviews and meta-analyses

have confirmed that standalone cages are superior to cage + plate systems in reducing the risk of dysphagia.<sup>19–22</sup> The duration of dysphagia symptoms was also longer with plated compared to non-plated cages.<sup>23</sup> In multiple-level procedures, cervical plating requires more extensive surgical access and is associated with more soft tissue injury that may affect clinical status. Another important aspect of cervical plating surgery is the possibility of complications such as loosening or breakage of the screws stabilizing the plate, or plate dislocation. Of further importance is the fact that the use of cervical plates increases the cost of the procedure.<sup>24–28</sup> If a revision procedure is necessary for a patient with a standalone cage, there is obviously no need to remove a previously placed plate, and so the duration of the surgery may be shorter with less blood loss, less retraction of the surrounding tissues, and a reduced risk of postoperative dysphagia.

### Adjacent segment disease (ASD)

A significant aspect of surgery for cervical disc disease is the risk of ASD. Biomechanically, the abolition of mobility within a disc space should lead to the adjacent motion segments below and above the operated segment partly taking over the mobility of the non-mobile segment. Adjacent segment disease is the product of several factors – an accumulated result of natural degeneration and biomechanical changes following fusion within the original motion segment operated on, such as ROM changes of the adjacent segments, changes in the sagittal profile of the spine, and increased intradiscal pressures in the adjacent discs.<sup>29</sup> Symptomatic ASD is the most common underlying cause of revision surgery following ACDF, in up to as many as 47% of patients.<sup>30</sup> The possibility of symptomatic ASD occurrence is higher after single-level fusion than multilevel one, especially if the non-fused segments belong to levels C4–C6. Artificial disc replacement has gained increasing enthusiasm as a motion-sparing alternative to fusion. Nevertheless, despite conducting multiple clinical trials and follow-up studies, the reduction of ASD has not been evidenced when artificial disc replacements are performed instead of fusion. Most of the available published reports indicate a lower risk of ASD with standalone cages than following cage + plate procedures.<sup>16,19,21–23,31–37</sup>

### Subsidence and intervertebral disc height (IDH)

Implant subsidence after ACDF is a widely known, undesirable effect that should be prevented. Reduced disc space height may lead to foraminal stenosis. A review of implant subsidence data in the available literature reveals the superiority of cage + plate procedures over the placement of standalone cages regarding the prevention of this undesirable phenomenon. Subsidence can be reduced if the mechanical properties of vertebral endplates are retained

to the greatest extent possible during the surgery. From a pathophysiological angle, some of the endplates need to be removed so that bone union can occur, but injury to endplates facilitates subsequent sinking of the cage into the vertebral bodies. Cage subsidence occurs more often when endplates are removed. Implant subsidence has been defined in several ways. Two definitions see it as the immersion length of the cage (in millimeters) beyond the borders of the adjacent endplates or as the percentage reduction in interbody space height. The decreased interbody space height may produce foraminal stenosis. The risk of cage subsidence is higher in the presence of a smaller anteroposterior cage diameter, more posterior placement of the cage in relation to the vertebral body, and a smaller cage surface area resulting in endplate coverage.<sup>38</sup> There is a significant relationship between subsidence and a coefficient representing the ratio of the implant surface area to the surface area of bone of the adjacent vertebral bodies: Subsidence is significantly less frequent for coefficient values  $\geq 0.37$ .<sup>39</sup> Cage subsidence may adversely affect spinal biomechanics and alignment, be the cause of segmental kyphosis and contribute to ASD. Additional anterior plate fixation is recommended when endplates are removed.<sup>40</sup>

### Cervical alignment

The normal lordotic alignment of the cervical spine is crucial for ensuring good motion and function of the cervical spine. Alignment in the sagittal plane is important for the distribution of stress across fixation devices. Loss of cervical lordosis theoretically increases the risk of ASD as a kyphotic alignment of the cervical segment accelerates degenerative changes in that segment by augmenting biomechanical stress on the anterior portion of the vertebral bodies of adjacent segments.<sup>41</sup> The most marked alterations in lordosis and intervertebral space height are seen immediately after surgery, with baseline values subsequently usually decreasing gradually over time, but postoperative values at 12 or 24 months are still better than baseline. The curvature of the cervical segment is shaped by a range of factors, such as muscle tone distribution in the neck and the shoulder girdle or the shape of the thoracic and lumbosacral segments. The curvatures of individual spinal segments influence each other. Cervical spine surgery introduces slight modifications to the pre-surgical anatomic relations. Efforts are always made to restore the near-anatomical relationships; however, it is important to note that complete restoration of physiological cervical alignment cannot be guaranteed, and the anatomical changes visible in immediate postoperative radiographs may not be permanent. The preservation of better parameters of cervical alignment following cage + plate procedures is particularly visible after multiple-level surgery, while following single-level surgery, differences between the groups are less evident, or, in some reports, no significant differences are noted.<sup>20,22,23,42–44</sup>

Appropriate rehabilitation appears quite important for maintaining normal spinal curvatures. A meta-analysis by Cheung et al. indicates that cage + plate procedures are associated with better postoperative radiographic appearances, with near-normal values of indices of cervical lordosis and disc space height and lower rates of implant subsidence.<sup>45</sup> Another meta-analysis/systematic review by Liu et al. provided slightly diverging data regarding disc space height as it failed to find a statistically significant difference in disc space height between pre-operative, immediate postoperative and last-follow-up radiographs in patients with non-plated (standalone) compared to plated cages. At the same time, the authors confirmed better preservation of cervical alignment following cage + plate procedures.<sup>23</sup>

## Fusion rate

Regarding the possibility of obtaining better fusion, results vary, but most reports indicate the superiority of cage + plate procedures over the implantation of standalone cages, with fusion occurring earlier following cage + plate surgery than after standalone cage implantation.<sup>46–48</sup> Contrarily, Nabhan et al. in their radiographic analysis of fusion progression following plated compared to non-plated single-level cervical fusion did not reveal any statistical differences between both groups. Three-dimensional analysis of segmental motion (left-right, craniocaudal and posterior-anterior) failed to reveal statistical differences at any postoperative follow-up visits. The results obtained using visual analogue scale (VAS) were also not different between the groups.<sup>24</sup> A biomechanical study of cadavers subjected to 2-level ACDF with either a standalone cage or cage + plate performed by Nayak et al. concluded that a standalone cage confers comparable rigidity/stability to cage + plate.<sup>49</sup> Scholz et al. demonstrated no differences in flexion/extension, lateral bending or axial rotation between the standalone cage and cage + plate groups.<sup>50</sup> The most significant difference when comparing the zero-profile and traditional cage and plate structures is that the zero-profile implant has no additional plate attached to the anterior aspect of the vertebral body. Connecting the anterior plate to adjacent vertebrae with straight locking screws provides a strong anterior tension band and very rigid fixation, whereas only intersegmental fixation is obtained using the zero-profile device. We know from biomechanical studies that the self-locking standalone cage provides less cervical spine stiffness than the locking plate in 2- or 3-level instrumentation.<sup>51,52</sup> Gandhi et al. studied, among others, the degree of fusion in cases when surgery was necessary on account of ASD. Their analysis of such procedures did not detect a substantial difference in fusion at the site of previous surgery between patients bearing standalone cages compared to cage + plate systems.<sup>2</sup> An optimal radiographic outcome following ACDF is defined as complete fusion without implant subsidence.

However, even with implant subsidence, it is still possible for complete fusion at the implant site to occur later. Even if, initially, there is a disruption of endplate continuity and penetration of the implant towards an adjacent vertebral body, it is still possible for complete fusion to occur around the implant. The use of computed tomography (CT) is a reliable, modern approach to evaluating fusion status. The plate curve reduces the likelihood of loss of global cervical lordosis and the fusion segment angle, while also preventing cage subsidence during the fusion process.<sup>53</sup>

## Clinical outcomes

Divergent data are provided in the literature regarding fusion, implant subsidence and cervical alignment, and their direct impact on the patient's clinical status. The success of surgery for cervical disc disease depends mostly on the appropriate decompression of neural structures. This is the main determinant of postoperative clinical improvement measured according to scales capturing changes in pain intensity and quality of life. Subsidence and disruption of the physiological spinal curvatures may contribute to ASD and pain. Some state that complete fusion (arthrodesis) improves the clinical outcome, while others claim that fusion does not correlate with clinical outcomes.<sup>54–57</sup> Karikari et al. reported that the finding of implant subsidence was not directly related to the patient's clinical status or symptoms in most cases.<sup>57</sup> The changes in cervical spine alignment and disc space height are not reflected directly in the quality of life or pain intensity. Surgical outcomes are primarily related to adequate decompression of the spinal cord and nerve roots. The focus for the operating surgeon should be on adequate decompression of neural structures and necessary stabilization, while restoration of ideal physiological cervical alignment should not be attempted as the latter does not contribute decisively or directly to treatment outcomes. Still, it should be borne in mind that when cervical lordosis is restored or maintained, this may reduce the future likelihood of ASD.<sup>58–60</sup>

## Key differences between standalone cage compared to cage + plate procedures

Based on the analyzed literature and our own experience of many years in surgery for cervical disc disease, we summarized the most significant differences between standalone cage and cage + plate procedures, and presented the analyzed information in Table 1.

## Limitations

Including standalone cages and zero-profile cages, also known as self-anchoring or self-locking cages, in one group, despite some differences between them, is not an ideal solution, but it was done intentionally to systematize comparable treatment methods.

**Table 1.** Summary of key differences between standalone cage compared to cage + plate procedures


Criterion	Standalone cage	Cage + plate
Fusion	inferior fusion indices	superior fusion indices
	longer time to fusion	shorter time to fusion
Intervertebral disc height	inferior preservation of disc space height achieved	superior preservation of disc space height achieved
Subsidence	greater risk	lower risk
Cervical alignment (multiple-level surgery)	inferior cervical alignment indices	superior cervical alignment indices
cervical alignment (single-level surgery)	similar cervical alignment indices	similar cervical alignment indices
Dysphagia	lower rates of dysphagia	higher rates of dysphagia
	shorter time to resolution of dysphagia	longer time to resolution of dysphagia
Adjacent segment disease	lower risk	higher risk
Surgery duration	shorter	longer
Cost of surgery	lower	higher
Technical difficulty of revision/repeat surgery	less	more
Clinical outcomes (pain, quality of life)	comparable	comparable

## Conclusions

An ideal replacement for natural components of the human body does not exist, even though increasingly more refined solutions appear every year. A comparison of the outcomes of standalone cage and cage + plate procedures should separately analyze radiological and clinical outcomes. Both methods have their advantages and disadvantages. Overall, radiological outcomes are slightly better following cage + plate procedures, while clinical outcomes are comparable.

### ORCID iDs

Adam Bębenek  <https://orcid.org/0000-0002-6687-1517>

Bartosz Godlewski  <https://orcid.org/0000-0003-0673-1480>

### References

- Pointillart V, Cernier A, Vital JM, Senegas J. Anterior discectomy without interbody fusion for cervical disc herniation. *Eur Spine J.* 1995; 4(1):45–51. doi:10.1007/BF00298418
- Gandhi SD, Fahs AM, Wahlmeier ST, et al. Radiographic fusion rates following a standalone interbody cage versus an anterior plate construct for adjacent segment disease after anterior cervical discectomy and fusion. *Spine (Phila Pa 1976).* 2020;45(11):713–717. doi:10.1097/BRS.0000000000003387
- Sun Z, Liu Z, Hu W, Yang Y, Xiao X, Wang X. Zero-profile versus cage and plate in anterior cervical discectomy and fusion with a minimum 2 years of follow-up: A meta-analysis. *World Neurosurg.* 2018; 120:e551–e561. doi:10.1016/j.wneu.2018.08.128
- McLaughlin MR, Purighalla V, Pizzi FJ. Cost advantages of two-level anterior cervical fusion with rigid internal fixation for radiculopathy and degenerative disease. *Surg Neurol.* 1997;48(6):560–565. doi:10.1016/S0090-3019(97)00366-2
- Schneeberger AG, Boos N, Schwarzenbach O, Aebi M. Anterior cervical interbody fusion with plate fixation for chronic spondylotic radiculopathy: A 2- to 8-year follow-up. *J Spinal Disord.* 1999;12(3):215–220; discussion 221. PMID:10382774.
- Connolly PJ, Esses SI, Kostuik JP. Anterior cervical fusion: Outcome analysis of patients fused with and without anterior cervical plates. *J Spinal Disord.* 1996;9(3):202–206. PMID:8854274.
- Zhang D, Liu B, Zhu J, et al. Comparison of clinical and radiologic outcomes between self-locking standalone cage and cage with anterior plate for multilevel anterior cervical discectomy and fusion: A meta-analysis. *World Neurosurg.* 2019;125:e117–e131. doi:10.1016/j.wneu.2018.12.218
- Godlewski B, Dominiak M. Advantages and disadvantages of the use of various types of interbody implants in cervical spine surgery: Critical review of the literature. *Ortop Traumatol Rehabil.* 2020;22(4):213–222. doi:10.5604/01.3001.0014.3457
- Feighan JE, Goldberg VM, Davy D, Parr JA, Stevenson S. The influence of surface-blasting on the incorporation of titanium-alloy implants in a rabbit intramedullary model. *J Bone Joint Surg.* 1995;77(9): 1380–1395. doi:10.2106/00004623-199509000-00015
- Martin JY, Schwartz Z, Hummert TW, et al. Effect of titanium surface roughness on proliferation, differentiation, and protein synthesis of human osteoblast-like cells (MG63). *J Biomed Mater Res.* 1995;29(3):389–401. doi:10.1002/jbm.820290314
- Wennerberg A, Albrektsson T. Effects of titanium surface topography on bone integration: A systematic review. *Clin Oral Implants Res.* 2009;20:172–184. doi:10.1111/j.1600-0501.2009.01775.x
- Karageorgiou V, Kaplan D. Porosity of 3D biomaterial scaffolds and osteogenesis. *Biomaterials.* 2005;26(27):5474–5491. doi:10.1016/j.biomaterials.2005.02.002
- Converse GL, Conrad TL, Roeder RK. Mechanical properties of hydroxyapatite whisker reinforced polyetherketoneketone composite scaffolds. *J Mech Behav Biomed Mater.* 2009;2(6):627–635. doi:10.1016/j.jmbm.2009.07.002
- Fogel GR, Liu W, Reitman CA, Esses SI. Cervical plates. *Spine J.* 2003; 3(2):118–124. doi:10.1016/S1529-9430(02)00464-3
- Benzel E, Gonugunta V, Krishnaney A. Anterior cervical plating. *Neurol India.* 2005;53(4):424. doi:10.4103/0028-3886.22608
- Ahn SS, Paik HK, Chin DK, Kim SH, Kim DW, Ku MG. The fate of adjacent segments after anterior cervical discectomy and fusion: The influence of an anterior plate system. *World Neurosurg.* 2016;89:42–50. doi:10.1016/j.wneu.2016.01.013
- Lee CH, Hyun SJ, Kim MJ, et al. Comparative analysis of 3 different construct systems for single-level anterior cervical discectomy and fusion: Standalone cage, iliac graft plus plate augmentation, and cage plus plating. *J Spinal Disord Tech.* 2013;26(2):112–118. doi:10.1097/BSD.0b013e318274148e
- Fogel GR, McDonnell MF. Surgical treatment of dysphagia after anterior cervical interbody fusion. *Spine J.* 2005;5(2):140–144. doi:10.1016/j.spinee.2004.06.022
- Chen Y, Chen H, Cao P, Yuan W. Anterior cervical interbody fusion with the zero-P spacer: Mid-term results of two-level fusion. *Eur Spine J.* 2015;24(8):1666–1672. doi:10.1007/s00586-015-3919-9

20. Wang Z, Zhu R, Yang H, et al. Zero-profile implant (Zero-p) versus plate cage benezech implant (PCB) in the treatment of single-level cervical spondylotic myelopathy. *BMC Musculoskelet Disord*. 2015; 16(1):290. doi:10.1186/s12891-015-0746-4
21. Wang ZD, Zhu RF, Yang HL, et al. The application of a zero-profile implant in anterior cervical discectomy and fusion. *J Clin Neurosci*. 2014;21(3):462–466. doi:10.1016/j.jocn.2013.05.019
22. Zhang XB, Yuan WH, An JD, et al. Comparison between zero-profile and cage plate devices in the treatment of single-level cervical spondylosis [published online as ahead of print on June 29, 2021]. *Br J Neurosurg*. 2021. doi:10.1080/02688697.2021.1923654
23. Liu Z, Yang Y, Lan J, Xu H, Zhang Z, Miao J. Changes in cervical alignment of zero-profile device versus conventional cage-plate construct after anterior cervical discectomy and fusion: A meta-analysis. *J Orthop Surg Res*. 2022;17(1):510. doi:10.1186/s13018-022-03400-1
24. Nabhan A, Pape D, Pitzten T, et al. Radiographic analysis of fusion progression following one-level cervical fusion with or without plate fixation. *Zentralbl Neurochir*. 2007;68(3):133–138. doi:10.1055/s-2007-984462
25. Lowery GL, McDonough RF. The significance of hardware failure in anterior cervical plate fixation: Patients with 2- to 7-year follow-up. *Spine (Phila Pa 1976)*. 1998;23(2):181–186. doi:10.1097/00007632-199801150-00006
26. Panjabi MM, Isomi T, Wang JL. Loosening at the screw-vertebra junction in multilevel anterior cervical plate constructs. *Spine (Phila Pa 1976)*. 1999;24(22):2383. doi:10.1097/00007632-199911150-00016
27. Pompili A, Canitano S, Caroli F, et al. Asymptomatic esophageal perforation caused by late screw migration after anterior cervical plating: Report of a case and review of relevant literature. *Spine (Phila Pa 1976)*. 2002;27(23):E499–E502. doi:10.1097/00007632-200212010-00016
28. Yen CP, Hwang TY, Wang CJ, Howng SL. Fracture of anterior cervical plate implant: Report of two cases. *Acta Neurochir (Wien)*. 2005;147(6):665–667. doi:10.1007/s00701-005-0518-2
29. Alhashash M, Shousha M, Boehm H. Adjacent segment disease after cervical spine fusion: Evaluation of a 70 patient long-term follow-up. *Spine (Phila Pa 1976)*. 2018;43(9):605–609. doi:10.1097/BRS.00000000000002377
30. Van Eck CF, Regan C, Donaldson WF, Kang JD, Lee JY. The revision rate and occurrence of adjacent segment disease after anterior cervical discectomy and fusion: A study of 672 consecutive patients. *Spine (Phila Pa 1976)*. 2014;39(26):2143–2147. doi:10.1097/BRS.0000000000000636
31. Lu Y, Bao W, Wang Z, et al. Comparison of the clinical effects of zero-profile anchored spacer (ROI-C) and conventional cage-plate construct for the treatment of noncontiguous bilevel of cervical degenerative disc disease (CDD): A minimum 2-year follow-up. *Medicine (Baltimore)*. 2018;97(5):e9808. doi:10.1097/MD.00000000000009808
32. Chen Y, Lü G, Wang B, Li L, Kuang L. A comparison of anterior cervical discectomy and fusion (ACDF) using self-locking standalone polyetheretherketone (PEEK) cage with ACDF using cage and plate in the treatment of three-level cervical degenerative spondylopathy: A retrospective study with 2-year follow-up. *Eur Spine J*. 2016;25(7):2255–2262. doi:10.1007/s00586-016-4391-x
33. Liu Y, Wang H, Li X, et al. Comparison of a zero-profile anchored spacer (ROI-C) and the polyetheretherketone (PEEK) cages with an anterior plate in anterior cervical discectomy and fusion for multilevel cervical spondylotic myelopathy. *Eur Spine J*. 2016;25(6):1881–1890. doi:10.1007/s00586-016-4500-x
34. Shi S, Zheng S, Li XF, Yang LL, Liu ZD, Yuan W. Comparison of a stand-alone anchored spacer versus plate-cage construct in the treatment of two noncontiguous levels of cervical spondylosis: A preliminary investigation. *World Neurosurg*. 2016;89:285–292. doi:10.1016/j.wneu.2016.02.009
35. Sun B, Shi C, Wu H, et al. Application of zero-profile spacer in the treatment of three-level cervical spondylotic myelopathy: 5-year follow-up results. *Spine (Phila Pa 1976)*. 2020;45(8):504–511. doi:10.1097/BRS.00000000000003312
36. He S, Feng H, Lan Z, et al. A randomized trial comparing clinical outcomes between zero-profile and traditional multilevel anterior cervical discectomy and fusion surgery for cervical myelopathy. *Spine (Phila Pa 1976)*. 2018;43(5):E259–E266. doi:10.1097/BRS.00000000000002323
37. Chen Y, Liu Y, Chen H, Cao P, Yuan W. Comparison of curvature between the zero-P spacer and traditional cage and plate after 3-level anterior cervical discectomy and fusion: Mid-term results. *Clin Spine Surg*. 2017;30(8):E1111–E1116. doi:10.1097/BSD.0000000000000440
38. Yang JJ, Yu CH, Chang BS, Yeom JS, Lee JH, Lee CK. Subsidence and nonunion after anterior cervical interbody fusion using a standalone polyetheretherketone (PEEK) cage. *Clin Orthop Surg*. 2011;3(1):16. doi:10.4055/cios.2011.3.1.16
39. Godlewski B, Bebenek A, Dominiak M, Karpinski G, Cieslik P, Pawelczyk T. Subsidence following cervical discectomy and implant-to-bone ratio. *BMC Musculoskelet Disord*. 2022;23(1):750. doi:10.1186/s12891-022-05698-8
40. Pinder EM, Sharp DJ. Cage subsidence after anterior cervical discectomy and fusion using a cage alone or combined with anterior plate fixation. *J Orthop Surg (Hong Kong)*. 2016;24(1):97–100. doi:10.1177/230949901602400122
41. Kwon WK, Kim PS, Ahn SY, et al. Analysis of associating factors with C2-7 sagittal vertical axis after two-level anterior cervical fusion: Comparison between plate augmentation and standalone cages. *Spine (Phila Pa 1976)*. 2017;42(5):318–325. doi:10.1097/BRS.0000000000001776
42. Lan T, Lin JZ, Hu SY, Yang XJ, Chen Y. Comparison between zero-profile spacer and plate with cage in the treatment of single level cervical spondylosis. *J Back Musculoskelet Rehabil*. 2018;31(2):299–304. doi:10.3233/BMR-169708
43. Li T, Yang JS, Wang XF, et al. Can zero-profile cage maintain the cervical curvature similar to plate-cage construct for single-level anterior cervical discectomy and fusion? *World Neurosurg*. 2020;135:e300–e306. doi:10.1016/j.wneu.2019.11.153
44. Qi M, Chen H, Liu Y, Zhang Y, Liang L, Yuan W. The use of a zero-profile device compared with an anterior plate and cage in the treatment of patients with symptomatic cervical spondylosis: A preliminary clinical investigation. *Bone Joint J*. 2013;95-B(4):543–547. doi:10.1302/0301-620X.95B4.30992
45. Cheung ZB, Gidumal S, White S, et al. Comparison of anterior cervical discectomy and fusion with a standalone interbody cage versus a conventional cage-plate technique: A systematic review and meta-analysis. *Global Spine J*. 2019;9(4):446–455. doi:10.1177/2192568218774576
46. Oliver JD, Goncalves S, Kerezoudis P, et al. Comparison of outcomes for anterior cervical discectomy and fusion with and without anterior plate fixation: A systematic review and meta-analysis. *Spine (Phila Pa 1976)*. 2018;43(7):E413–E422. doi:10.1097/BRS.00000000000002441
47. Yu J, Ha Y, Shin JJ, et al. Influence of plate fixation on cervical height and alignment after one- or two-level anterior cervical discectomy and fusion. *Br J Neurosurg*. 2018;32(2):188–195. doi:10.1080/02688697.2017.1394980
48. Song KJ, Taghavi CE, Hsu MS, Lee KB, Kim GH, Song JH. Plate augmentation in anterior cervical discectomy and fusion with cage for degenerative cervical spinal disorders. *Eur Spine J*. 2010;19(10):1677–1683. doi:10.1007/s00586-010-1283-3
49. Nayak AN, Stein MI, James CR, et al. Biomechanical analysis of an interbody cage with three integrated cancellous lag screws in a two-level cervical spine fusion construct: An in vitro study. *Spine J*. 2014; 14(12):3002–3010. doi:10.1016/j.spinee.2014.06.011
50. Scholz M, Reyes PM, Schleicher P, et al. A new standalone cervical anterior interbody fusion device: Biomechanical comparison with established anterior cervical fixation devices. *Spine (Phila Pa 1976)*. 2009;34(2):156–160. doi:10.1097/BRS.0b013e31818ff9c4
51. Scholz M, Schleicher P, Pabst S, Kandziora F. A zero-profile anchored spacer in multilevel cervical anterior interbody fusion: Biomechanical comparison to established fixation techniques. *Spine (Phila Pa 1976)*. 2015;40(7):E375–E380. doi:10.1097/BRS.0000000000000768
52. Clavenna AL, Beutler WJ, Gudipally M, Moldavsky M, Khalil S. The biomechanical stability of a novel spacer with integrated plate in contiguous two-level and three-level ACDF models: An in vitro cadaveric study. *Spine J*. 2012;12(2):157–163. doi:10.1016/j.spinee.2012.01.011
53. Chung CK, Kim CH. Anterior plating is better than the standalone cage in the restoration of segmental kyphosis. *Spine J*. 2012;12(9):S100. doi:10.1016/j.spinee.2012.08.277
54. Bohlman HH, Emery SE, Goodfellow DB, Jones PK. Robinson anterior cervical discectomy and arthrodesis for cervical radiculopathy: Long-term follow-up of one hundred and twenty-two patients. *J Bone Joint Surg*. 1993;75(9):1298–1307. doi:10.2106/00004623-199309000-00005

55. Phillips FM, Carlson G, Emery SE, Bohlman HH. Anterior cervical pseudarthrosis: Natural history and treatment. *Spine (Phila Pa 1976)*. 1997; 22(14):1585–1589. doi:10.1097/00007632-199707150-00012
56. Shibani E, Nies M, Kogler J, et al. No correlation between radiological and clinical outcome 1 year following cervical arthrodesis. *Acta Neurochir*. 2018;160(4):845–853. doi:10.1007/s00701-018-3495-y
57. Karikari IO, Jain D, Owens TR, et al. Impact of subsidence on clinical outcomes and radiographic fusion rates in anterior cervical discectomy and fusion: A systematic review. *J Spinal Disord Tech*. 2014;27(1):1–10. doi:10.1097/BSD.0b013e31825bd26d
58. Godlewski B, Stachura MK, Czepko RA, Banach M, Czepko R. Analysis of changes in cervical spinal curvature and intervertebral disk space height following ACDF surgery in a group of 100 patients followed up for 12 months. *J Clin Neurosci*. 2018;52:92–99. doi:10.1016/j.jocn.2018.04.005
59. Katsuura A, Hukuda S, Saruhashi Y, Mori K. Kyphotic malalignment after anterior cervical fusion is one of the factors promoting the degenerative process in adjacent intervertebral levels. *Eur Spine J*. 2001; 10(4):320–324. doi:10.1007/s005860000243
60. Wilkinson JS, Mann SA, Stoneham GW, Hentschel S, Fourney DR. Comparison of post-operative lordosis with the PEEK cage and the cervical plate. *Can J Neurol Sci*. 2011;38(1):72–77. doi:10.1017/S0317167100011100



# Expansion of T follicular helper cells is associated with disease progression in rat experimental membranous nephropathy model

Li Deng<sup>1,2,C,D</sup>, Bishun Deng<sup>1,B,C</sup>, Ziling Zhao<sup>1,B</sup>, Huijie Huang<sup>1,C</sup>, Xiaowan Wang<sup>3,4,B</sup>, Ruimin Tian<sup>4,B</sup>, Guohua Li<sup>1,B</sup>, Enyu Liang<sup>1,B</sup>, Anping Peng<sup>1,3,B,C</sup>, Peifeng Ke<sup>1,B</sup>, Peng Xu<sup>3,4,E,F</sup>, Min He<sup>1,3,A,E,F</sup>

<sup>1</sup> Department of Laboratory Medicine, The Second Clinical College of Guangzhou University of Chinese Medicine, China

<sup>2</sup> Department of Laboratory Medicine, Maoming People's Hospital, China

<sup>3</sup> State Key Laboratory of Dampness Syndrome of Chinese Medicine, the Second Affiliated Hospital of Guangzhou University of Chinese Medicine, China

<sup>4</sup> Department of Nephrology, Second Clinical College of Guangzhou University of Chinese Medicine, China

A – research concept and design; B – collection and/or assembly of data; C – data analysis and interpretation;

D – writing the article; E – critical revision of the article; F – final approval of the article

Advances in Clinical and Experimental Medicine, ISSN 1899–5276 (print), ISSN 2451–2680 (online)

Adv Clin Exp Med. 2024;33(8):889–899

## Address for correspondence

Min He

E-mail: minhe@gzucm.edu.cn

## Funding sources

1. State Key Laboratory of Dampness Syndrome of Chinese Medicine grant No. SZ2021ZZ24

2. State Key Laboratory of Dampness Syndrome of Chinese Medicine grant No. SZ2021ZZ11

3. Science and Technology Projects in Guangzhou grant No. 202201020334

4. Science and Technology Projects in Guangzhou grant No. 202201020556

5. Science and Technology Projects in Guangzhou grant No. 202201020487

6. Guangdong Basic and Applied Basic Research Foundation grant No. 2020A1515110329

7. Science and technology research project of traditional Chinese Medicine of Guangdong Provincial Hospital of Chinese Medicine grant No. YN2018ML04

## Conflict of interest

None declared

Received on October 19, 2023

Reviewed on March 1, 2024

Accepted on June 19, 2024

Published online on August 28, 2024

## Cite as

Deng Li, Deng B, Zhao Z, et al. Expansion of T follicular helper cells is associated with disease progression in rat experimental membranous nephropathy model.

Adv Clin Exp Med. 2024;33(8):889–899.

doi:10.17219/acem/189865

## DOI

10.17219/acem/189865

## Copyright

Copyright by Author(s)

This is an article distributed under the terms of the Creative Commons Attribution 3.0 Unported (CC BY 3.0) (<https://creativecommons.org/licenses/by/3.0/>)

## Abstract

**Background.** T follicular helper (Tfh) cells drive humoral immunity by facilitating B cell responses, but the functional role of Tfh cells in the pathogenesis of idiopathic membranous nephropathy (IMN) remains unclear.

**Objectives.** This study aimed to establish a rat experimental membranous nephropathy model, investigate the phenotypic characteristics of Tfh cells, and analyze a clinically significant correlation between Tfh cells.

**Materials and methods.** Passive Heymann nephritis (PHN) rats were induced by immunizing Sprague Dawley rats with anti-Fx1A serum. The frequency of Tfh and B cell subsets was analyzed with flow cytometry (FC). The serum concentration of interleukin-21 (IL-21), the relative mRNA expression levels of IL-21 and B cell lymphoma 6 (Bcl-6) in spleen mononuclear cells (MNCs), and the kidney infiltration of CD4<sup>+</sup> T cells and IL-21 were assessed. The potential correlations among these measures were analyzed.

**Results.** In comparison with the control group, significantly increased percentages of Tfh cells, inducible T cell co-stimulator-positive (ICOS<sup>+</sup>) Tfh cells, and mRNA expression of Bcl-6 were detected in the spleen of PHN rats. Elevated IL-21 expression was detected in the serum and kidneys. Remarkably, the percentage of splenic ICOS<sup>+</sup> Tfh cells was positively correlated with 24 h urine protein concentrations ( $r = 0.676$ ,  $p = 0.011$ ) in PHN rats.

**Conclusions.** These data indicate that ICOS<sup>+</sup> Tfh cells contribute to development of IMN, and they might be potential therapeutic targets for IMN.

**Key words:** B cells, T follicular helper cells, passive Heymann nephritis, interleukin -21, B cell lymphoma 6

## Background

Idiopathic membranous nephropathy (IMN) is a major pathological type of adult nephrotic syndrome.<sup>1,2</sup> Idiopathic membranous nephropathy is now recognized as an autoimmune disease with the identification of the podocyte antigens, which includes thrombospondin type-1 domain-containing 7A (THSD7A) and the M-type receptor for phospholipase A2 (PLA2R).<sup>3</sup> Due to impaired immune tolerance, B cells produce nephritogenic autoantibodies, which bind podocytes to form immune deposits, leading to complement activation and damage to the glomerular basement membrane (GBM), creating a risk of renal failure.<sup>4</sup> In patients with IMN, an increased proportion of circulating plasma cells and oligoclonal expansion of B cells in the renal tissue have been observed.<sup>5,6</sup> These findings, together with the clinical efficacy of B-cell-depleting therapies (rituximab), have highlighted the pathogenic role of B lymphocytes in IMN.<sup>7</sup> Despite these findings, the immunological pathogenesis of IMN has not been fully elucidated.

The germinal center (GC) response is crucial for B cell maturation and the establishment of efficacious protective humoral immunity.<sup>8</sup> T follicular helper (Tfh) cells are a distinct subgroup of T cells, which play an essential role in promoting GC reactions and supporting the differentiation of B cells and antibody production.<sup>9,10</sup> They are characterized by their expression of C-X-C chemokine receptor type 5 (CXCR5), programmed cell death protein 1 (PD-1), inducible T cell co-stimulator (ICOS), and B cell lymphoma 6 (Bcl-6). The ICOS and PD-1 are closely associated with the maintenance and function of Tfh cells.<sup>11</sup> B cell lymphoma 6 is considered the dominant lineage-defining transcription factor for Tfh cells.<sup>12</sup> Additionally, Tfh cells can secrete interleukin (IL)-21, which is a crucial cytokine in the regulation of B cell differentiation, maturation and class switch recombination. Moreover, in addition to lymphoid follicles, resident Tfh cells and circulating Tfh (cTfh) cells have been found in the peripheral blood (PB), and were shown to share functional properties with GC Tfh cells.<sup>13</sup>

Recently, aberrant expression of Tfh cells has been shown to contribute to autoimmune disease development, including multiple sclerosis (MS), systemic lupus erythematosus (SLE) and rheumatoid arthritis (RA).<sup>14–16</sup> A defective Tfh checkpoint profoundly impacts immune responses and promotes pathogenic autoantibody production. Despite the enrichment of Tfh cells reported in the circulation of IMN patients,<sup>17,18</sup> the collaboration between Tfh cells and B cell subsets during the pathogenesis of IMN remains largely unknown.

## Objectives

To gain insights into the phenotypic and functional characteristics of Tfh cells in the pathogenesis of IMN, this study employed the rat model of passive Heymann

nephritis (PHN).<sup>19</sup> The frequencies of Tfh cells and B cell subpopulations were dynamically monitored during PHN induction. Additionally, the correlation between the frequency of Tfh cells with 24 h urine protein was analyzed.

## Materials and methods

### Induction of passive Heymann nephritis

Male Sprague Dawley rats were obtained from the Medical Experimental Animal Center of Guangdong Province (Guangzhou, China). The animals were housed in polypropylene cages under pathogen-free conditions with a 12 h light/dark cycle and free access to standard laboratory chow and sterile water. Animal experiments were approved by the institutional animal use committee of Guangdong Provincial Hospital of Chinese Medicine (Guangzhou, China; approval No. 2021081). Induction of the PHN rat model was performed as previously described.<sup>20</sup> After acclimatization for 3 days, animals were randomly divided into 2 groups: the PHN group and the control group. Passive Heymann nephritis rats were injected with sheep-derived anti-Fx1A antiserum (Probetex, Inc., San Antonio, USA) in the tail vein at a dose of 0.5 mL/100 g. Rats in the control group were given an equivalent volume of saline. The onset of nephritis in the rats was monitored by assessment of 24 h urine protein. Animals were divided into 5 groups according to the number of days after immunization, with 5 rats in each group. All animals were euthanized on day 0, 2, 6, 13, or 20, and urine, peripheral blood, kidney, and spleen specimens were collected.

### Isolation of mononuclear cells from the spleen and peripheral blood

Following euthanasia, blood samples and spleens were harvested from PHN rats and control rats. Blood samples anticoagulated with ethylene diamine tetraacetic acid (EDTA-K2) were collected to separate peripheral blood mononuclear cells (PBMCs). The dissected spleens were homogenized with the tip of a syringe plunger. The homogenates were passed through a 70- $\mu$ m nylon mesh filter (BD Biosciences, Franklin Lakes, USA), and single-cell suspensions were obtained. Mononuclear cells from peripheral blood or spleen were separated using peripheral blood mononuclear cell isolation kits or spleen lymphocyte isolation kits (both from TBD Science, Tianjin, China) for rats, respectively. The isolated mononuclear cells were used for reverse transcription quantitative polymerase chain reaction (RT-qPCR) or flow cytometry (FC) analysis.

### Transmission electron microscopy

Rat renal tissues were fixed with 2.5% glutaraldehyde in 0.1 M sodium cacodylate buffer at 4°C for 2 h. After

washing with the same buffer, renal specimens were post-fixed with 1% osmium tetroxide at 4°C for 2 h, dehydrated through immersion in ascending grades of ethanol, and embedded in Epon 812. Ultrathin sections were stained with uranyl acetate and lead citrate and then examined using transmission electron microscopy (TEM; JEM1400 PLUS; Joel Ltd., Akishima, Tokyo, Japan). The thickness of glomerular basement membrane (GBM) in each ultrathin slice was detected using RADIUS software v. 2.0 (EMSIS, Boston, USA).

## Flow cytometry

For Tfh cell detection, mononuclear cells were incubated with anti-rat-CXCR5 (Abcam, Cambridge, UK; ab254415) at 4°C for 30 min, followed by staining with goat anti-rabbit IgG-Alexa Fluor 488 (Abcam; ab150077), anti-rat-CD4-BV421 (BD Biosciences; 743088), and anti-rat-ICOS-PE (eBioscience, Thermo Fisher Scientific, Waltham, USA; 12994981) for 30 min at 4°C. For B cell subset phenotyping, the cells were first stimulated with Leukocyte Activation Cocktail (BD Bioscience) for 6 h, then stained with anti-rat-CD45R-PE-Cyanine7 (Invitrogen, Waltham, USA; 25046082), anti-rat-CD3-APC (Invitrogen; 17003082) and anti-rat-CD27-PE (Invitrogen; 12027182). After cell surface staining, the cells were fixed, permeabilized and stained with anti-rat-IgG-BV605 (BioLegend, San Diego, USA; 405430). Cells were analyzed with the Agilent NovoCyte flow cytometer, and the data were analyzed with Agilent software v. 1.5.6 (Agilent Technologies, Palo Alto, USA).

## ELISA

Serum concentrations of IL-21 were measured using a rat enzyme-linked immunosorbent assay (ELISA) kit (Cloud-clone SEB688Ra; Cloud-CloneCorp, Wuhan, China) following the manufacturer's instructions.

## Urine analysis

The concentration of urine creatinine and 24 h urine protein was analyzed using Cobas 8000 analyzer (Roche Diagnostics, Mannheim, Germany).

## Immunohistochemistry

For immunohistochemical staining, 3 micrometers of serially sliced kidney tissue were used. Paraffin-embedded sections were first deparaffinized and then hydrated. After antigen retrieval, the activity of endogenous peroxidase and non-specific binding sites were blocked. Incubation with mouse anti-CD4 (Immunoway, Plano, USA) or rabbit anti-IL-21 (Affbiotech, Changzhou, China) overnight at 4°C was then performed. Next, sections were incubated with an horseradish peroxidase (HRP)-labeled secondary antibody (Maxin, Fuzhou, China). Finally, the sections

were developed in diaminobenzidine solution and counterstained with hematoxylin. Immunostained slides were observed under a fluorescence microscope (BX61; Olympus Corp., Tokyo, Japan). The CD4- and IL-21-positive regions were quantitatively detected using ImageJ software (National Institutes of Health, Bethesda, USA), and these values were described as average optical density (AOD).

## Reverse transcription-quantitative PCR

Total RNA from rat spleen mononuclear cells was purified with the Trizol reagent (Invitrogen). After treatment with DNase I, mRNAs were reverse transcribed using Evo M-MLV RT Mix Kit (Accurate Biology, Changsha, China). The PCR was performed with a SYBR Green PCR Kit (Accurate Biology) on the ViiA7 detection system (Applied Biosystems, Darmstadt, Germany). The sequences of the primers were:

$\beta$ -actin forward: 5'-GACATGCCGCCTGGAGAAAC-3';

$\beta$ -actin reverse: 5'-AGCCCAGGATGCCCTTTAGT-3';

IL-21 forward:

5'-GCCAAACTCAAGCCATCAAACACTG-3';

IL-21 reverse: 5'-CTTAGCAGGCAGCCTCCTCCTC-3';

Bcl-6 forward: 5'-TCGAGGTCGTGAGGTTGTGGAG-3';

Bcl-6 reverse: 5'-TCGGATAAGAGGCTGGTGGTGTGTC-3'.

Gene expression was normalized against  $\beta$ -actin, and the relative expression levels were calculated with the  $2^{-\Delta\Delta Ct}$  method.

## Statistical analyses

All statistical analyses were performed with the IBM SPSS v. 20.0 software (IBM Corp., Armonk, USA) and GraphPad Prism v. 9.0 software (GraphPad Software Inc., San Diego, USA). Data were collected from independent samples to examine the differences between PHN rats. All variables were performed using nonparametric tests: the Mann–Whitney U test was used for comparison between the 2 groups, and the Kruskal–Wallis with Bonferroni correction for multiple testing was used for comparisons between 3 or more groups. The data were expressed as median  $\pm$  interquartile range ( $\pm$ IQR), and correlations were determined using Spearman's correlation coefficients. A p-value <0.05 was considered statistically significant.

## Results

### Pathologic changes of nephritic function in PHN rats induced by anti-Fx1A antiserum

Twenty days after administration of the anti-Fx1A antibody, the GBM was irregularly thickened. In addition, subepithelial electron-dense deposits were observed, and characteristic spike-like structures were formed in PHN rats (Fig. 1A). Quantitative analysis of TEM results (Fig. 1B)

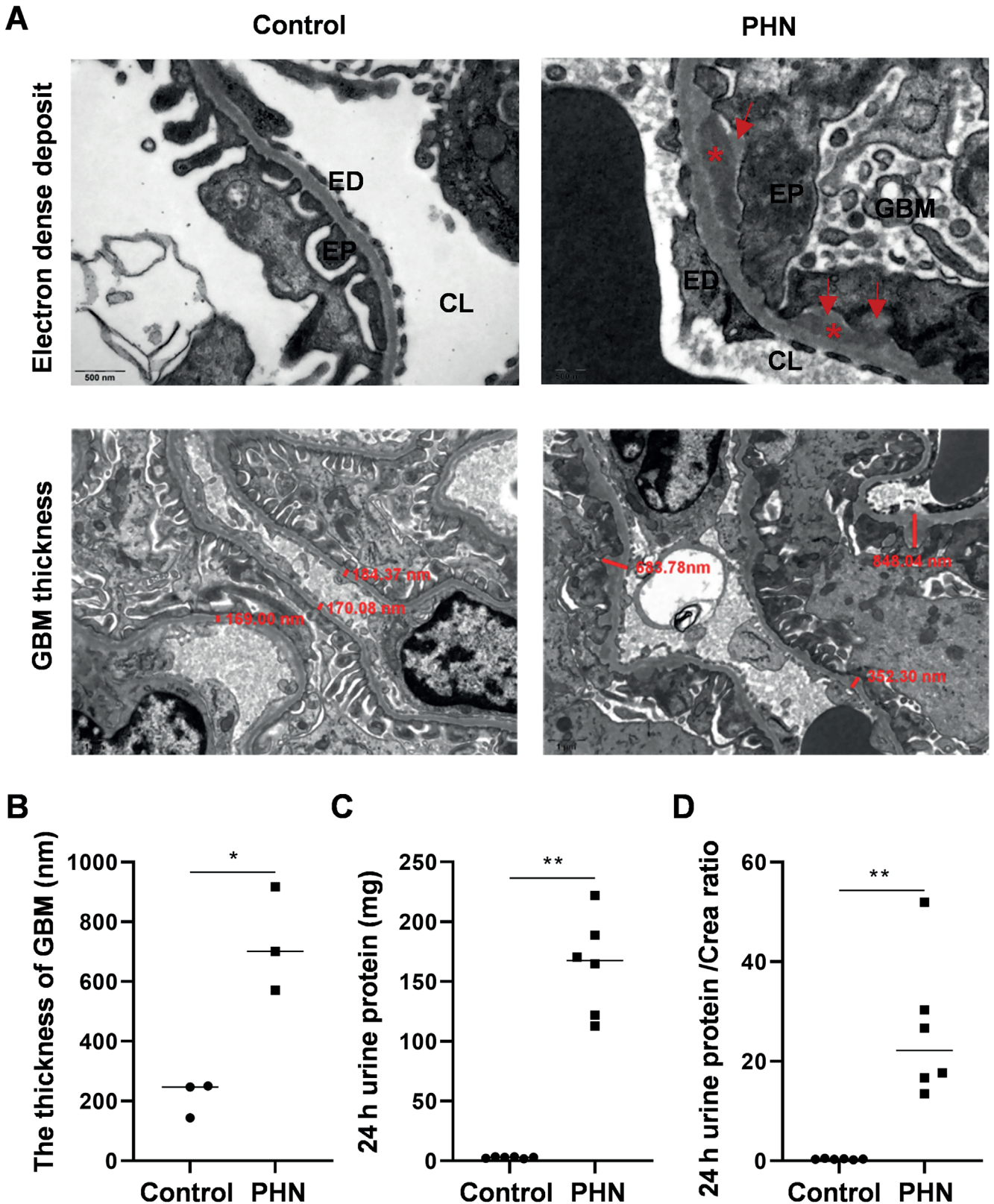


Fig. 1. Pathologic change of nephritic function in passive Heymann nephritis (PHN) rats. The animals were induced with anti-Fx1A antiserum. A. Transmission electron micrograph (TEM) of the glomerular capillary wall from control and PHN rats at 20 days after anti-Fx1A antiserum injection. The red asterisks indicate electron-dense deposits, and the red arrows represent the new basement membrane (TEM  $\times 30,000$  and  $\times 12,000$ , respectively). B. Comparison of semi-quantification of GBM thickness in control and PHN rats ( $n = 3$ ); C,D. Comparison of 24 h urine protein (C) and 24 h urine protein/creatinine ratio (D) in control and PHN rats ( $n = 6$  for each). Horizontal line shows the median. \* $p < 0.05$  and \*\* $p < 0.01$  using Mann-Whitney U test GBM – glomerular basement membrane; EP – epithelial cell; ED – endothelial cell; CL – capillary lumen.

showed the thickness of GBM in PHN rats was significantly greater than in control rats ( $701.6 \pm 172.8$  nm vs  $247.0 \pm 53.4$  nm, Mann–Whitney U test,  $p = 0.05$ ). In addition, PHN rats developed significantly heavier proteinuria, as evidenced by increased 24 h urine protein ( $167.7 \pm 77.4$  mg vs  $3.0 \pm 1.4$  mg, Mann–Whitney U test,  $p = 0.004$ ; Fig. 1C) and the 24 h urine protein/creatinine ratio (Mann–Whitney U test,  $p = 0.004$ ; Fig. 1D). These results suggest that PHN rats developed nephritis after immunization with anti-Fx1A antiserum.

## Tfh cells were expanded and activated in the spleen in PHN rats

We then examined whether Tfh (defined as  $CD4^+CXCR5^+$ ) cells were enriched in the context of rat PHN models. Both circulating and splenic Tfh cells were characterized employing FC analysis. The gating strategy and representative plots are shown in Fig. 2A–C. On day 20 following immunization with anti-Fx1A antibody, phenotypic analysis indicated the percentages of Tfh cells among splenic MNCs (Mann–Whitney U test,  $p = 0.025$ ; Fig. 2D, left) and  $CD4^+$  T cells were significantly higher in PHN rats than the control group (Mann–Whitney U test,  $p = 0.016$ ; Fig. 2E, left). Similarly, an approximately twofold increase in  $ICOS^+$  Tfh cells in splenic  $CD4^+$  T cells was observed in PHN rats as compared to control rats ( $0.34 \pm 0.3\%$  vs  $0.19 \pm 0.08\%$ , Mann–Whitney U test,  $p = 0.016$ ; Fig. 2F, left). However, varying expression patterns were observed concerning circulating Tfh cells, which were considered peripheral memory Tfh cells. Although higher frequencies of circulating Tfh cells among MNCs or  $CD4^+$  T cells were found in PHN rats as compared to the control group, no significant difference was observed (Fig. 2D–F, right). In addition, circulating  $ICOS^+$  Tfh cells were comparable between the 2 groups. Therefore,  $ICOS^+$  Tfh cells were enriched in the spleen but not in the PB of PHN rats.

## Distribution of B cell subsets in PHN rats

To investigate the association between dysregulation of Tfh cells and B cells, we subsequently examined splenic B cell subsets in PHN rats. Among the B cell subsets, total B cells ( $CD3^-CD45R^+$ ), antibody-secreting B cells (ASCs, defined as  $CD3^-CD45R^+IgG^+$ ), and memory B cells ( $CD3^-CD45R^+CD27^+$ ) were evaluated. In agreement with a previous study,<sup>21</sup> no statistical difference in the frequency of total B cells was observed 20 days after immunization (Mann–Whitney U test,  $p = 0.513$ ). However, there was a significant induction of ASCs (Mann–Whitney U test,  $p = 0.05$ ) and a reduction of memory B cells (Mann–Whitney U test,  $p = 0.05$ ) in PHN rats compared to control rats (Fig. 3A–E). Moreover, as shown in Fig. 3F–H, kinetic analysis showed distinct differentiation patterns of B cell subsets over the immunization time. Of note, rapid induction

of total B cells was identified on day 2 (Kruskal–Wallis with Bonferroni correction, day 2 vs day 0,  $p = 0.031$ ) and then gradually decreased. The frequency of  $IgG^+$  ASCs was continually increased, reaching a peak at day 20. Therefore, the B cell subset was found to be altered, which may affect autoantibody production in IMN disease.

## Dynamic changes of Tfh cell frequency in PHN rats and the correlation with disease progression

To obtain a deeper insight into the role of Tfh cells in IMN development, we dynamically monitored the changes in Tfh cells and Bcl-6 expression in the spleen of PHN rats. Consistent with progressive development of nephritis (Fig. 1), the proportion of Tfh cells showed an increasing trend during the development of PHN, which reached a peak at day 13 (Kruskal–Wallis test with Bonferroni correction, day 13 vs day 0,  $p = 0.019$ , Fig. 4A). A rapid induction of  $ICOS^+$  Tfh cells was found on day 2, remaining stable through day 20 (Fig. 4B). Bcl-6 is a key transcription factor for the programming of Tfh cells. The RT-qPCR also confirmed the mRNA level of Bcl-6 in spleen MNCs of PHN rats was elevated (Kruskal–Wallis with Bonferroni correction, day 6 vs day 0,  $p = 0.006$ ; Fig. 4C). In addition, although no significant correlation was found between the frequency of Tfh cells and 24 h urine protein, the percentage of  $ICOS^+$  Tfh cells and Bcl-6 mRNA levels were positively associated with 24 h urine protein levels ( $r = 0.676$ ,  $p = 0.011$ ;  $r = 0.706$ ,  $p = 0.034$ , respectively) (Fig. 4D–F). Taken together, these results suggest that an induction of Tfh cells was accompanied by the progression of PHN.

## The expression of IL-21 was elevated in PHN rats

Interleukin-21 is reported to be the main effector of Tfh cells; thus, we next explored its expression in PHN rats. As shown in Fig. 5A, serum concentrations of IL-21 began to rise on day 2 and peaked on day 13 after immunization (Kruskal–Wallis test with Bonferroni correction, day 13 vs day 0,  $p = 0.041$ ). Consistent with this finding, IL-21 mRNA expression in spleen MNCs was higher, but not significantly, in PHN rats than in control rats (Fig. 5B). Furthermore, IHC was performed to compare expression and localization of  $CD4^+$  and  $IL-17^+$  cells in kidney tissue from PHN and control rats. As shown in Fig. 5C–E, the infiltration of  $IL-21^+$  cells and  $CD4^+$  cells was significantly increased in the kidney tissue of PHN rats than control rats, especially around the kidney tubules (Fig. 5C). Passive Heymann nephritis rats showed a significantly higher AOD value of  $CD4$  ( $0.237 \pm 0.007$  vs  $0.231 \pm 0.009$ , Mann–Whitney U test,  $p = 0.047$ ; Fig. 5D) and  $IL-21$  ( $0.292 \pm 0.008$  vs  $0.287 \pm 0.004$ , Mann–Whitney U test,  $p = 0.047$ ; Fig. 5E). These results confirmed IL-21 was elevated in PHN rats.

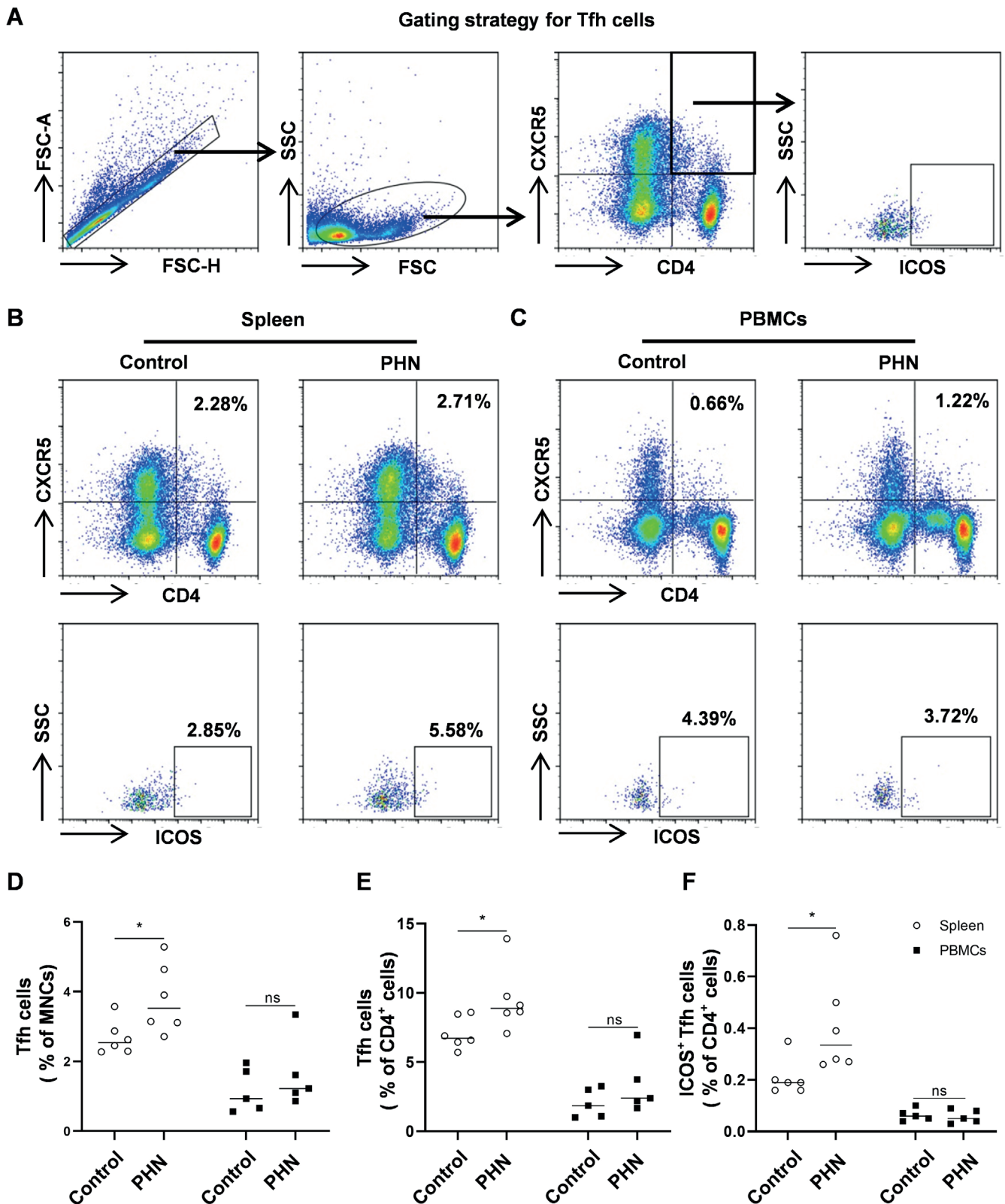


Fig. 2. T follicular helper (Tfh) cells were expanded in the spleen of passive Heymann nephritis (PHN) rats. The PHN and control rats were euthanized on day 20, mononuclear cells (MNCs) were separated from peripheral blood and spleen, and Tfh cell subpopulations were detected using fluorescence activated cell sorting (FACS). A. Gating strategy for Tfh cell subsets; B,C. Representative flow cytometric histograms for inducible T cell co-stimulator-positive (ICOS<sup>+</sup>) Tfh cells in spleen (B) and peripheral blood mononuclear cells (PBMCs) (C) from control and PHN rats; D–F. Statistical analysis of the frequencies of Tfh cells of MNCs (D), Tfh cells of CD4<sup>+</sup> cells (E) and ICOS<sup>+</sup> Tfh cells (F) between control and PHN rats, n = 5 of each. Significant differences were assessed with Mann–Whitney U test

Horizontal line shows median; NS – not significant; \*p < 0.05.

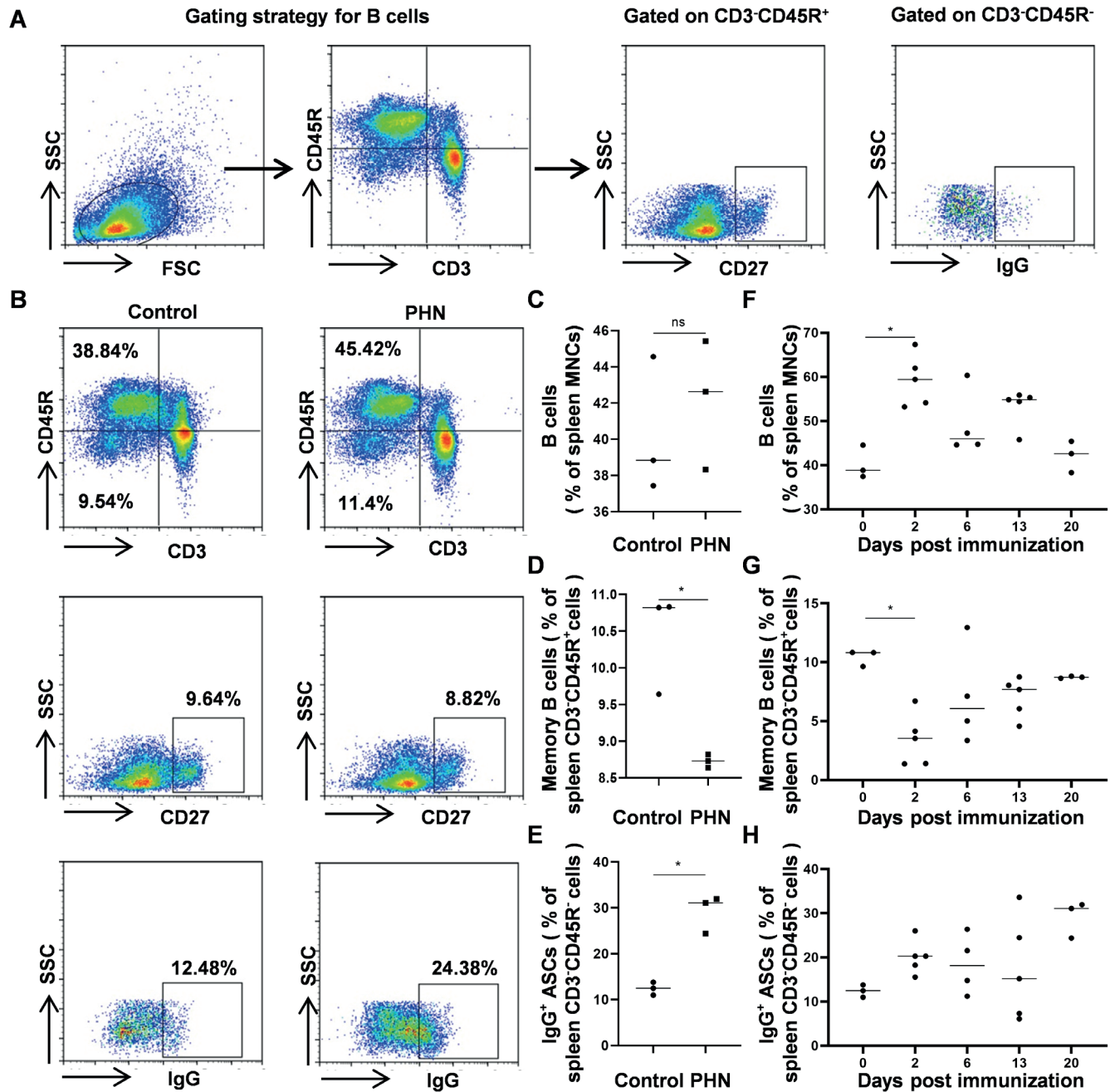


Fig. 3. The frequency of B cells in passive Heymann nephritis (PHN) rats. The B cell subpopulations of control and PHN rats were detected in spleen mononuclear cells (MNCs), and their correlation with different T cell subsets was analyzed. A,B. Gating strategy (A) and representative plots (B) of B cell subpopulations analyzed using fluorescence activated cell sorting (FACS); C–E. Statistical analysis of the percentage of B cells (C), memory B cells (D) and IgG<sup>+</sup> ASCs (E) in control and PHN rats (n = 3 for each). Significant differences were assessed with Mann–Whitney U test. \*p < 0.05 compared with control rats; F–H. The kinetic frequency of B cells (F), memory B cells (G) and IgG<sup>+</sup> ASCs (H) in B cells at indicated times. Significant differences were assessed using Kruskal–Wallis with Bonferroni correction

Horizontal line shows median; \*p < 0.05 compared with PHN rats euthanized on day 0; NS – not significant.

## Discussion

T follicular helper cells are crucial regulators of GC formation, B cell development and long-term memory responses.<sup>22</sup> In this study, we report that Tfh cells are highly enriched and activated in PHN rats, and their frequency is significantly associated with disease severity.

The PHN model is a classical model for investigating the pathogenesis of IMN. In this study, the PHN rats displayed histopathological and laboratory features of IMN, including irregularly thickened GBM, subepithelial spikes on the outer surface of the capillary wall, abnormal proteinuria development, and an elevated 24 h urine protein/creatinine ratio. Dynamic results suggested that splenic

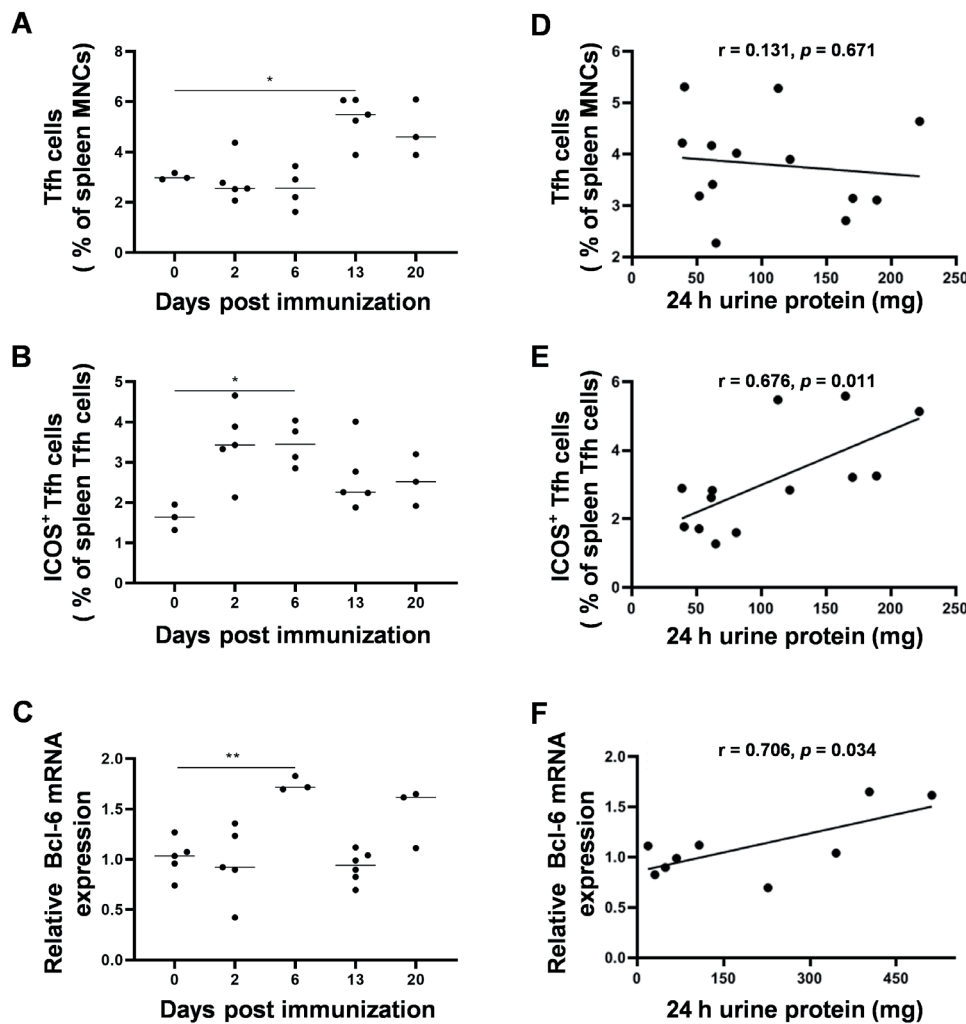


**Fig. 4.** Dynamic changes of activated T cell frequency in passive Heymann nephritis (PHN) rats and correlation with disease progression. Passive Heymann nephritis rats were euthanized on day 0, 2, 6, 13, or 20, and spleen mononuclear cells (MNCs) were separated for fluorescence activated cell sorting (FACS) analysis and reverse transcription quantitative polymerase chain reaction (RT-qPCR), while 24 h urine samples were collected for 24 h urine protein detection. A, B. The kinetic detection of the frequency of T follicular helper (Tfh) cells (A) and inducible T cell co-stimulator-positive (ICOS<sup>+</sup>) Tfh cells (B) at specific days as indicated ( $n \geq 3$  for each); C. Fold change of B cell lymphoma 6 (Bcl-6) mRNA in PHN rats; D–E. Correlation of 24 h urine protein with the frequency of Tfh cells (D) and ICOS<sup>+</sup> Tfh cells (E) in PHN rats ( $n = 13$  for each); F. Association of 24 h urine protein with the fold change of Bcl-6 mRNA ( $n = 9$ ). Horizontal line shows the median, with \* $p < 0.05$ , \*\* $p < 0.01$  using Kruskal–Wallis with multiple comparisons of Bonferroni correction (A–C). Spearman correlation statistics are shown in D–F.

Tfh cells were gradually upregulated after injection with anti-Fx1A antiserum and were significantly higher than in the control group on day 20. Additionally, RT-qPCR results also indicated that Tfh cells upregulated Bcl-6, which is a specific transcription factor for Tfh cell differentiation.<sup>23,24</sup> These findings demonstrated that splenic Tfh cells were mature in PHN rats. It is noteworthy that Zhang et al. previously reported an expansion of cTfh cells in patients with IMN.<sup>17</sup> However, despite higher frequencies of circulating Tfh cells found in PHN rats, no significant difference was found between those and the control group. This discrepancy may be representative of the different stages of disease. In this study, circulating Tfh cells were induced at the onset of disease, which preceded the appearance of proteinuria, whereas in Zhang et al. elevated cTfh cells were found in confirmed IMN patients with kidney injury and high proteinuria. Consistent with our results, the induction of Tfh cells was found in the lymph node biopsies of early RA patients, whereas the frequency of Tfh cells did not differ in the blood between RA patients and controls.<sup>25</sup> In particular, mass cytometric comparison results have suggested that cTfh cells can be generated at the T cell–B cell border, and then travel through efferent

lymph to the blood.<sup>26,27</sup> Overall, these results confirmed that Tfh cells are expanded in the PHN model and the elevation of Tfh cells were first detected in the spleen but not in the PB after immunization.

Splenic Tfh cells from PHN rats expressed higher ICOS than the control group, whereas no significant differences were found in the frequency of circulating ICOS<sup>+</sup> Tfh cells. Interestingly, the correlation analysis indicated that splenic ICOS<sup>+</sup> Tfh cells, together with the Bcl-6 mRNA levels, positively correlated with concentrations of 24 h urine protein, which was the clinical biomarker for monitoring disease severity. In particular, several studies showed an offset between immunologic and clinical remissions that was indicative of the longer timespan needed to form enough deposits to initially induce proteinuria and the time needed to remove subepithelial deposits, repair podocyte and capillary wall damage, and restore glomerular perm selectivity.<sup>28</sup> These data suggested that higher percentages of Tfh cells, especially ICOS<sup>+</sup> Tfh cells, may be considered as a potential biomarker to monitor the disease activity of IMN.

Interleukin-21, a pleiotropic Tfh cell-derived cytokine, has been proven to play a crucial role in the formation and





signals were detected in the same location (Fig. 5C–E). In addition, our previous study confirmed elevated serum IL-21 expression in IMN patients compared to healthy controls.<sup>29</sup> Thus, our data demonstrated that the expression of IL-21 was elevated in PHN rats, which might be a new clinical biomarker for monitoring disease processes.

It is widely accepted that the expansion of Tfh cells leads to perturbations of B cells that could eventually contribute to the development of autoimmune disorders.<sup>30</sup> As such, we take an interest in B cell subset distribution and the association between B cell subsets and Tfh cells in IMN. Interestingly, the distribution of B cell subsets was different. The antibody producing ASCs were expanded, but the memory B cells were decreased in PHN rat spleens compared with the normal group (Fig. 3D,E). Memory B cells are located in the blood, spleen and other lymphoid organs and are a critical reservoir for plasma cell generation in the secondary response.<sup>31</sup> This reduction of memory B cells might be a result of their differentiation into antibody-producing ASCs. Consistent with our results, a reduction of circulating memory B cells in IMN patients has been reported.<sup>21</sup>

## Limitations

The lack of rat antibodies restricted our ability to sort Tfh cells and further characterize the helper function of B cells in PHN rats. Additionally, negative feedback between T and B cells has been reported. In patients with MS, activated memory B cells can suppress the proliferation of Tfh cells.<sup>32</sup> Therefore, further research is required to define the mechanisms of T cells and B cells collaboration in the promotion of disease progression.

## Conclusions

Altogether, our study confirmed that Tfh cells and ASCs were significantly increased in PHN rats. Furthermore, Tfh cells were activated by upregulating ICOS and IL-21 expression, and the frequency of ICOS<sup>+</sup> Tfh cells was positively correlated with 24 h urine protein. These findings document the importance of Tfh cells in the pathogenesis of IMN and provide a potential new therapeutic target.

## Supplementary data

The Supplementary materials are available at <https://doi.org/10.5281/zenodo.11406851>. The package includes the following files:

Supplementary Table 1. Comparing parameters between controls and PHN rats.

Supplementary Fig. 1. Isotype control staining results for IHC.

Supplementary Fig. 2. Statistical analysis for data in PHN rats.











## Data availability

The datasets generated and/or analyzed during the current study are available from the corresponding author on reasonable request.

## Consent for publication

Not applicable.

## ORCID iDs

Li Deng  <https://orcid.org/0000-0002-0873-0388>  
 Bishun Deng  <https://orcid.org/0000-0002-2579-3380>  
 Ziling Zhao  <https://orcid.org/0000-0002-3995-2872>  
 Huijie Huang  <https://orcid.org/0000-0002-1286-2252>  
 Xiaowan Wang  <https://orcid.org/0000-0001-9152-8908>  
 Ruimin Tian  <https://orcid.org/0000-0001-8591-9419>  
 Enyu Liang  <https://orcid.org/0000-0002-3499-503X>  
 Anping Peng  <https://orcid.org/0000-0001-5668-4323>  
 Peng Xu  <https://orcid.org/0000-0003-0048-8723>  
 Min He  <https://orcid.org/0000-0003-0361-8984>

## References

- Ronco P, Debiec H. Molecular pathogenesis of membranous nephropathy. *Ann Rev Pathol Mech Dis.* 2020;15(1):287–313. doi:10.1146/annurev-pathol-020117-043811
- Ronco P, Beck L, Debiec H, et al. Membranous nephropathy. *Nat Rev Dis Primers.* 2021;7(1):69. doi:10.1038/s41572-021-00303-z
- Liu W, Gao C, Dai H, et al. Immunological pathogenesis of membranous nephropathy: Focus on PLA2R1 and its role. *Front Immunol.* 2019;10:1809. doi:10.3389/fimmu.2019.01809
- Lateb M, Ouahmi H, Payré C, et al. Anti-PLA2R1 antibodies containing sera induce in vitro cytotoxicity mediated by complement activation. *J Immunol Res.* 2019;2019:1324804. doi:10.1155/2019/1324804
- Cantarelli C, Jarque M, Angeletti A, et al. A comprehensive phenotypic and functional immune analysis unravels circulating anti-phospholipase A2 receptor antibody secreting cells in membranous nephropathy patients. *Kidney Int Rep.* 2020;5(10):1764–1776. doi:10.1016/j.ekir.2020.07.028
- Kolovou K, Laskari K, Roumelioti M, et al. B-cell oligoclonal expansions in renal tissue of patients with immune-mediated glomerular disease. *Clin Immunol.* 2020;217:108488. doi:10.1016/j.clim.2020.108488
- Fervenza FC, Appel GB, Barbour SJ, et al. Rituximab or cyclosporine in the treatment of membranous nephropathy. *N Engl J Med.* 2019;381(1):36–46. doi:10.1056/NEJMoa1814427
- Olatunde AC, Hale JS, Lamb TJ. Cytokine-skewed Tfh cells: Functional consequences for B cell help. *Trends Immunol.* 2021;42(6):536–550. doi:10.1016/j.it.2021.04.006
- Crotty S. T follicular helper cell differentiation, function, and roles in disease. *Immunity.* 2014;41(4):529–542. doi:10.1016/j.immuni.2014.10.004
- Song W, Craft J. T follicular helper cell heterogeneity: Time, space, and function. *Immunol Rev.* 2019;288(1):85–96. doi:10.1111/imr.12740
- Shi J, Hou S, Fang Q, Liu X, Liu X, Qi H. PD-1 controls follicular T helper cell positioning and function. *Immunity.* 2018;49(2):264–274.e4. doi:10.1016/j.immuni.2018.06.012
- Choi J, Crotty S. Bcl6-mediated transcriptional regulation of follicular helper T cells (TFH). *Trends Immunol.* 2021;42(4):336–349. doi:10.1016/j.it.2021.02.002
- Morita R, Schmitt N, Bentebibel SE, et al. Human blood CXCR5<sup>+</sup>CD4<sup>+</sup> T cells are counterparts of T follicular cells and contain specific subsets that differentially support antibody secretion. *Immunity.* 2011;34(1):108–121. doi:10.1016/j.immuni.2010.12.012
- Rao DA, Gurish MF, Marshall JL, et al. Pathologically expanded peripheral T helper cell subset drives B cells in rheumatoid arthritis. *Nature.* 2017;542(7639):110–114. doi:10.1038/nature20810

15. Zhang X, Ge R, Chen H, et al. Follicular helper CD4<sup>+</sup> T cells, follicular regulatory CD4<sup>+</sup> T cells, and inducible costimulator and their roles in multiple sclerosis and experimental autoimmune encephalomyelitis. *Mediators Inflamm.* 2021;2021:2058964. doi:10.1155/2021/2058964
16. Wei X, Niu X. T follicular helper cells in autoimmune diseases. *J Autoimmun.* 2023;134:102976. doi:10.1016/j.jaut.2022.102976
17. Zhang Z, Shi Y, Yang K, Crew R, Wang H, Jiang Y. Higher frequencies of circulating ICOS<sup>+</sup>, IL-21<sup>+</sup> T follicular helper cells and plasma cells in patients with new-onset membranous nephropathy. *Autoimmunity.* 2017;50(8):458–467. doi:10.1080/08916934.2017.1385775
18. Shi X, Qu Z, Zhang L, et al. Increased ratio of ICOS<sup>+</sup>/PD-1<sup>+</sup> follicular helper T cells positively correlates with the development of human idiopathic membranous nephropathy. *Clin Exp Pharmacol Physiol.* 2016;43(4):410–416. doi:10.1111/1440-1681.12555
19. Jiang H, Feng Z, Zhu Z, et al. Advances of the experimental models of idiopathic membranous nephropathy (Review). *Mol Med Rep.* 2020;21(5):1993–2005. doi:10.3892/mmr.2020.11014
20. Wang X, Liu J, Tian R, et al. Sanqi oral solution mitigates proteinuria in rat passive Heymann nephritis and blocks podocyte apoptosis via Nrf2/HO-1 pathway. *Front Pharmacol.* 2021;12:727874. doi:10.3389/fphar.2021.727874
21. Rosenzweig M, Languille E, Debiec H, et al. B- and T-cell subpopulations in patients with severe idiopathic membranous nephropathy may predict an early response to rituximab. *Kidney Int.* 2017;92(1):227–237. doi:10.1016/j.kint.2017.01.012
22. Crotty S. Follicular Helper CD4 T Cells (T<sub>FH</sub>). *Ann Rev Immunol.* 2011;29(1):621–663. doi:10.1146/annurev-immunol-031210-101400
23. Ciucci T, Vacchio MS, Chen T, et al. Dependence on Bcl6 and Blimp1 drive distinct differentiation of murine memory and follicular helper CD4<sup>+</sup> T cells. *J Exp Med.* 2022;219(1):e20202343. doi:10.1084/jem.20202343
24. Liu D, Yan J, Sun J, et al. BCL6 controls contact-dependent help delivery during follicular T-B cell interactions. *Immunity.* 2021;54(10):2245–2255.e4. doi:10.1016/j.immuni.2021.08.003
25. Anang DC, Ramwadhoebe TH, Hähnlein JS, et al. Increased frequency of CD4<sup>+</sup> follicular helper T and CD8<sup>+</sup> follicular T cells in human lymph node biopsies during the earliest stages of rheumatoid arthritis. *Cells.* 2022;11(7):1104. doi:10.3390/cells11071104
26. Walker LSK. The link between circulating follicular helper T cells and autoimmunity. *Nat Rev Immunol.* 2022;22(9):567–575. doi:10.1038/s41577-022-00693-5
27. Wong MT, Chen J, Narayanan S, et al. Mapping the diversity of follicular helper T cells in human blood and tonsils using high-dimensional mass cytometry analysis. *Cell Rep.* 2015;11(11):1822–1833. doi:10.1016/j.celrep.2015.05.022
28. Francis JM, Beck LH, Salant DJ. Membranous nephropathy: A journey from bench to bedside. *Am J Kidney Dis.* 2016;68(1):138–147. doi:10.1053/j.ajkd.2016.01.030
29. Liu M, Huang D, Liang E, et al. Elevated plasma interleukin 21 is associated with higher probability and severity of idiopathic membranous nephropathy. *J Lab Med.* 2023;47(3):121–127. doi:10.1515/labmed-2022-0149
30. Crotty S. T follicular helper cell biology: A decade of discovery and diseases. *Immunity.* 2019;50(5):1132–1148. doi:10.1016/j.immuni.2019.04.011
31. Inoue T, Moran I, Shinnakasu R, Phan TG, Kurosaki T. Generation of memory B cells and their reactivation. *Immunol Rev.* 2018;283(1):138–149. doi:10.1111/imr.12640
32. Asashima H, Axisa PP, Pham THG, et al. Impaired TIGIT expression on B cells drives circulating follicular helper T cell expansion in multiple sclerosis. *J Clin Invest.* 2022;132(20):e156254. doi:10.1172/JCI156254

